Polymeric Micelles for the Delivery of Poorly Soluble Anti-Cancer Agents

THESIS

Submitted in partial fulfilment

of the requirements for the degree of

DOCTOR OF PHILOSOPHY

by

PREETI KUMARI

ID No. 2013PHXF0013H

Under the supervision of

Dr. SWATI BISWAS

BITS Pilani

Pilani | Dubai | Goa | Hyderabad

BIRLA INSTITUTE OF TECHNOLOGY AND SCIENCE, PILANI

2018

BIRLA INSTITUTE OF TECHNOLOGY AND SCIENCE, PILANI

CERTIFICATE

This is to certify that the thesis entitled "**Polymeric Micelles for the Delivery of Poorly Soluble Anti-cancer Agents**" and submitted by **PREETI KUMARI** ID No. **2013PHXF0013H** for award of Ph.D. of the Institute embodies original work done by her under my supervision.

Signature of the Supervisor:

Name in capital letters: **SWATI BISWAS**

Designation : **Associate Professor**

Date:

ACKNOWLEDGEMENT

This dissertation would not have been possible without the guidance and the help of several individuals who in one way or another contributed and extended their valuable assistance in the preparation and completion of this study.

First and foremost, my utmost gratitude to my esteemed research guide Dr. Swati Biswas, Associate Professor, Department of Pharmacy, BITS Pilani, Hyderabad Campus whose sincerity and encouragement I will never forget. Her wide knowledge and her logical way of thinking have been of great value for me. Her understanding, encouraging and personal guidance have provided a good basis for the present thesis. Her extensive discussions around my work and interesting explorations in operations have been very helpful for this study.

I am deeply grateful to Dr. V. Vamsi Krishna, Department of Pharmacy, BITS Pilani Hyderabad who acted as Doctoral Advisory Committee (DAC) member, for his detailed and constructive comments, and for his important support throughout this work.

I wish to express my warm and sincere thanks to Prof. Punna Rao Ravi, Department of Pharmacy, BITS Pilani Hyderabad who acted as a Doctoral Advisory Committee (DAC) member for his suggestions and invaluable time to review my dissertation report.

I take this opportunity to thank Prof. Souvik Bhattacharyya, Vice Chancellor, Prof. G. Sundar, Director, BITS Pilani, Hyderabad Campus, Prof. S. C. Sivasubramanian, Acting Registrar, Prof. Sanjay Kumar Verma, Dean, Academic Research, Prof. Niranjan Swain, Dean, General Administration and Prof. Vidya Rajesh, Associate Dean, Academic Research (Ph.D. Programme) BITS-Pilani, Hyderabad, for providing excellent working facilities and a fascinating academic environment.

I would like to express my gratitude to Prof. D. Sriram, Head, Department of Pharmacy, BITS Pilani Hyderabad for his support and providing me with all the necessary laboratory facilities.

My sincere thanks to Dr. Balaram Ghosh, Assistant Professor, Department of Pharmacy, BITS Pilani Hyderabad for his invaluable guidance and constant encouragements. His infinite patience, stimulating discussion and friendly critics have been most invaluable to the accomplishment of this thesis.

I owe my most sincere gratitude to all my teachers especially, Prof. P. Yogeeswari, Dr. Shrikant Y. Charde, Prof. A. Sajeli Begum Dr. Onkar Prakash Kulkarni, Dr. Arti Dhar, and other faculty members of BITS-Pilani, Hyderabad campus who gave me untiring help during my difficult moments.

I gratefully acknowledge the financial assistance in form of senior research fellowship under INSPIRE fellowship program, Department of Science & Technology (DST), Government of India, New Delhi.

I am also indebted to my friends Manasa, Priyanka, Pavan, Jutika, Swagatika, Sai, Uday, Karthik, and Kiran not only for all their useful suggestions but also for being there to listen when I needed an ear.

I sincerely admire the contribution of all my lab mates Dr. Omkara Swami Muddineti, Mr. Vishnu, Mrs. Prakruti Trivedi, Mr. Himanshu, Mrs. Anusha, Ms. Yamini, Dr. Praveen, Dr. Suman, Dr. Anup, Ms. Shubhmita, Dr. Sudeep, Ms. Asha, Mr. Lokesh, Mr. Girdhari, and Mr. Deepanjan.

During this work I have collaborated with many colleagues Dr. Shailender, Ms. Rimpy, Mr. Teja, Ms. Avantika, Ms. Ekta Prasanthi, Dr. Hasitha, Mr. Shubham, Ms. Nikhila, Ms. Prasanthi, Mr. Siva Krishna, Ms. Priyanka Reddy, Ms. Jaspreet, Mr. Suresh, Ms. Kalyani, Ms. Kavita, Mr. Santhosh, Ms. Kirti, Ms. Pragya, Dr. Poorna, Dr. Mahibalan, Dr. Rukaiyya S Khan, Dr. Priyanka, Dr. Reshma, Dr. Brindha, Dr. Madhubabu, Ms. Srividya, Mr. Karthik, and Ms. Shreya, for whom I have great regard, and I wish to extend my warmest thanks to all those who have helped me with my work .

I warmly thank staff of BITS Pilani Hyderabad like Ms. Saritha, Mr. Praveen, Ms. Laxmi, Mr. Narendra Verma, Mr. Rajesh, Ms. Rekha, and Ms. Sunitha, for their humble gesture and kind support to me during my project and other college works.

I would like to thank the Indian Council of Medical Research (ICMR) for providing the international travel support grant and giving me an opportunity to present my research work at various conferences.

I owe my loving thanks to my parents without their encouragement and understanding it would have been impossible for me to finish this work. My special gratitude is to my brothers, Arvind and Pradeep for providing me constant encouragement, and supporting me spiritually throughout.

Last but not the least, my family and the one above all of us, the omnipresent God, for answering my prayers for giving me the strength to undertake this research task and enabling me to its completion, thank you so much Lord Krishna and Srimati Radharani.

Preeti Kumari

ABSTRACT

Recently polymeric micelles have been utilized for the delivery of drugs to overcome the limitations of the conventional chemotherapeutics including poor water solubility and improving the targetability through the enhanced permeability and retention (EPR) effect. In comparison to other drug delivery systems, polymeric micelles offers significant advantages for example preventing drugs from unfavorable surrounding environment by encapsulating the drugs in a hydrophobic inner core and can be specifically designed as either pH-sensitive or temperature sensitive nanocarriers.

First, we attempted to synthesize the block co-polymer, methoxy-poly(ethylene glycol)-poly(D,L-Lactide) (mPEG-PLA) by ring opening polymerization reaction. The curcumin (CUR) loaded micelles were prepared by the thin-film hydration technique. The CUR-mPEG-PLA micelles showed low critical micelles concentration (50 µg/mL), confirming the integrity of micelles when they were in contact with body fluids after injection. The *in vitro* release study demonstrated a sustained release of CUR-mPEG-PLA micelles, which enhanced the circulation time in blood. CUR-mPEG-PLA micelles showed significantly higher cellular internalization than free CUR in murine melanoma cells, B16F10 and human breast cancer cells, MDA-MB-231 in dose and time dependent manner. The *in vitro* cytotoxicity assays of CUR-mPEG-PLA micelles on B16F10 and MDA-MB-231 cells showed the higher cell toxicity compared to free CUR. The above results clearly indicated that the developed mPEG-PLA micellar system as a potential carrier for the delivery of the curcumin for cancer therapy.

Targeted delivery approaches are widely used for the site-specific delivery of drugs. Herein, we have explored the possibility of modifying the CUR-loaded mPEG-PLA micelles with transferrin (Tf). Transferrin (Tf), a human serum glycoprotein of molecular weight 80 KDa serves as a cargo for iron, which is needed abundantly by the proliferating cancer cells. The Tf-receptors (TfR) are over-expressed in many tumors, including hepatic, ovarian, and cervical origin. The selective localization of TfR to cancer cells compared to normal cells can be exploited for the purpose of active targeting of nanocarriers to cancer cells. The therapeutic effect of Tf modified CUR-mPEG-PLA (Tf-CUR-mPEG-PLA) micelles was assessed against HeLa, HepG2, and NIH-3T3 cells. This formulation was also tested on HeLa cervical cancer spheroids. The results displayed that the Tf-CUR-mPEG-PLA micelles showed excellent cellular selectivity, and cytotoxicity in the HeLa and HepG2 cancer cells while showing no cytotoxicity to normal NIH3T3 cells. In addition, even though the CUR-mPEG-PLA micelles demonstrated a cytotoxicity against the HeLa and HepG2 cells, the modified Tf-micelles significantly enhanced the cytotoxic effects. The confocal microscopy and flow cytometry showed significantly deeper penetration of Tf-CUR-mPEG-PLA into the HeLa spheroids compared to non-targeted micelles. The above results demonstrate the potential application of Tf-mPEG-PLA micelles in the treatment of cancer overexpressing TfR.

Second, the conjugation of cholesterol to poly(D,L-Lactide) was attempted to the best of our knowledge to improve the biocompatibility of the polymeric micellar system and drug loading. Even though nanocarrier-mediated drug delivery to cancer has proven to be therapeutically effective compared to conventional free drug administration, however, degradation of the nanoparticles are slow leading to residence of the polymer in the system.

In this regard, cell-membrane components-associated nanoparticles are being developed as biomimetic drug delivery system. In this context, development of cholesterol-conjugated drug delivery system for cancer therapy is a rational approach towards improving the biocompatibility of the polymeric system. Cholesterol-modified mPEG-PLA polymer was synthesized, where cholesterol is conjugated to the free hydroxyl group of PLA. The polymer self-assembled efficiently into stable micelles with low CMC. Our result indicated that the newly developed mPEG-PLA-Ch micelles loaded curcumin effectively, delivered it to the B16F10 and MDA-MB-231 cancer cells leading to decreased dose-dependent cell viability, and increased rate of tumor volume of reduction when administered *in vivo* in B16F10-xenografted tumor-bearing mice. The results demonstrate that cholesterol modified mPEG-PLA could serve as a promising nanocarrier to improve the solubility and bioactivity of curcumin.

Third, even though photodynamic therapy (PDT) has emerged as an increasingly recognized alternative for the treatment of cancer compared to conventional chemotherapy and radiotherapy. However, poor water solubility, strong oxygen and light dependence, and limited tissue penetrability of photosensitizers represent major barriers to the clinical application of PDT. In this regard, we developed chlorin e6 loaded methoxy poly(ethylene glycol)-poly(D,L-Lactide) (Ce6-mPEG-PLA) micelles. Our result demonstrated that mPEG-PLA micelles loaded Ce6 effectively, and delivered it to the A549 cancer cells leading to decreased dose-dependent cell viability, induced significant cellular apoptosis and produced strong photo-toxicity in tested A549 3D spheroids. In conclusion, the Chlorin e6-loaded micellar system could be utilized in PDT as an effective treatment modality for solid tumors.

TABLE OF CONTENTS

LIST OF TABLES

LIST OF FIGURES

LIST OF ABBREVIATIONS

µg	Microgram
µL	Microlitre
µM	Micromolar
^{1}H NMR	Proton Nuclear Magnetic Resonance
A549	Human alveolar adenocarcinoma cells
Akt	Protein kinase B
AP-1	Activator protein 1
B16F10	Murine melanoma cells
BCA	Bicinchoninic acid
Ce6	Chlorin e6
Ch	Cholesterol
CMC	Critical micelle concentration
CUR	Curcumin
DAPI	4',6-diamidino-2-phenylindole
DCM	Dichloromethane
DLS	Dynamic Light Scattering
DMA	9,10-dimethylanthracene
DMEM	Dulbecco's modified Eagle's media
DMF	Dimethyl formamide
DMSO	Dimethyl sulphoxide
DSC	Differential scanning calorimetry
EDTA	Ethylene diamine tetra acetic acid
EE	Encapsulation efficiency
EPR	Enhanced Permeability and Retention
FDA	Food and Drug Administration
FITC	Fluorescein isothiocyanate
FREE CUR	Free curcumin
FTIR	Fourier transform infrared spectroscopy

G	Gram
h	Hour
HeLa	Human cervical carcinoma cells
Hep G2	Human hepatoma cells.
HEPES	2-[4-(2-hydroxyethyl)piperazin-1-yl]ethanesulfonic acid
HepG2	Human hepatocellular carcinoma cells
IC_{50}	Half maximal inhibitory concentration
JNK	c-Jun N-terminal kinases
MDA-MB-231	Human breast cancer cells
mg	Milligram
min	Minute
mL	Millilitre
mm	Millimetre
mmol	Millimole
MPA	3-(Maleimido) propionic acid *N*-hydroxysuccinimide ester
mPEG	Methoxy-poly(ethylene glycol)
mPEG-PLA	Methoxy-poly(ethylene glycol)-poly(D,L-Lactide)
MTT	3-[4,5-Dimethylthiazol-2-yl]- 2,5-diphenyltetrazolium bromide
MW	Molecular weight
MWCO	Molecular weight cut-off
NF-κB	Nuclear factor kappa-light-chain-enhancer of activated B cells
NIH-3T3	Mouse embryo fibroblast cells
nm	Nanometre
PBS	Phosphate buffered saline
PDI	Polydispersity index
PDT	Photodynamic therapy
PEG	Poly (ethylene glycol)
PI	Propidium iodide
PLA	Poly(D,L-Lactide)
PS	Photosensitizer
RNO	*N*,*N*-Dimethyl-4-nitrosoaniline

ROS	Reactive oxygen species
rpm	Rotation per minute
RPMI 1640	Roswell Park Memorial Institute 1640 media
RT	Room temperature
SD	Standard deviation
SDS	Sodium dodecyl sulphate
SEM	Standard error of the mean
SOG	Singlet oxygen generation
SOSG	Singlet oxygen sensor green
TEM	Transmission electron microscope
Tf	Transferrin
THF	Tetrahydrofuran
TUNEL	Terminal Deoxynucleotidyl Transferase dUTP nick end labeling
UV	Ultraviolet
λ_{max}	Wavelength maxima for UV-absorbance
^{o}C	Degree centigrade

Chapter 1

Introduction

1.1.Cancer

Cancer remains a leading cause of mortality throughout the world, registering for 8.2 million deaths in 2012. According to the Global Cancer Report reported by World Health Organization (WHO), estimates more than 10 million new cases of cancer annually and over 6 million deaths every year (Stewart and Kleihues 2003). Cancer is a pathophysiologically heterogeneous disease that rapidly progresses to an uncontrollable stage after onset (Ferrari 2005). Even though various treatment modalities, including immuno, photothermal, photodynamic, gene and hormone therapy display promising cancer eradicating potential in pre-clinical studies, however, surgery, radiation therapy, and chemotherapy remains the first line treatment option for most cancers (Jia and Jia 2012). However, these focused treatment strategies fail to control metastatic tumors that has reached in distant organs. Conventional chemotherapy, the next major strategy for cancer treatment is highly non-specific in targeting the drugs to the cancer cells causing undesirable side-effects to the healthy tissues. Even though cytotoxic drugs are commonly utilized for the treatment in recurrent cancers and improved patient's survival, however, they also have several limitations, including poor aqueous solubility, non-specific distribution in the body affecting both normal and cancer cells, severe systemic cytotoxicity, development of drug resistance mechanisms (Stortecky and Suter 2010). Therefore, quest for alternate therapeutic approaches remains as unmet necessity.

Use of nanotechnology in various biomedical applications, including drug delivery has attracted great interest due to their capability to enhance the solubility of hydrophobic drugs, and to alter drug's pharmacokinetics (Nehoff et al. 2014). Nanomedicines render improved solubility of poorly soluble drugs and reduced metabolism by dissolving them in their

hydrophobic or hydrophilic compartment. Nanomedicines have prolonged plasma half-life and different biodistribution profile compared to conventional chemotherapy.

1.2.Chemotherapy

1.2.1. Cell biology of cancer

Cancer is described as a disorder that ascends from number of genetic changes and cellular abnormalities that interfere with the normal balance of the cell cycle due to uncontrolled cell division (Luo, Solimini, and Elledge 2009). The cell cycle divided into four stages, includes normal non dividing cells (G0), growth phase (G1), synthesis phase (S), and growth phase before cell division (G2), and chromosome separation followed by cell division phase (M). In normal circumstances, the daughter cells either continues through the cycle, leave and enter the resting phase (G0) or turn to terminally differentiated at the end of a cell division cycle. However, in cancer, mutation in several genes results in stimulation of cell cycle inappropriately and abnormally high cell proliferation. The genetic mutations are broadly divided into two categories, including dominant mutations where a gene in a pair gets mutated, and recessive mutations where both the genes in the pair get affected. While dominant mutation do not generally affect normal cellular activity due to the expression of the non-mutated intact gene, recessive mutation alters the cellular function as both the genes activity are compromised. For example, recessive mutation in tumor suppressor protein, p53 perturbs its normal function of turning off the cell cycle to control cell growth, which leads to abnormally high rate of cell proliferation leading to the formation of tumor (Floor et al. 2012).

1.2.2. Cytotoxic chemotherapy mechanisms of action

Conventional chemotherapy agents either inhibits the rate of growth or kills the cancerous cells with minimal effect on non-neoplastic host cells. The strategies followed to stop the progress of cancer, includes damaging the DNA of affected tumor cells, inhibiting the synthesis of new DNA strands to halt the cell from replicating, and hindering mitosis or actual splitting of the original cell into two new cells. The mechanism of action of many chemotherapy agents are cell cycle-dependent inhibiting cancer cell growth at specific stages in the cell cycle. These are known as phase-specific drugs whereas alkylating agents are independent of the stages of the cell cycle and are known as cycle-specific drugs (Figure. 1.1).

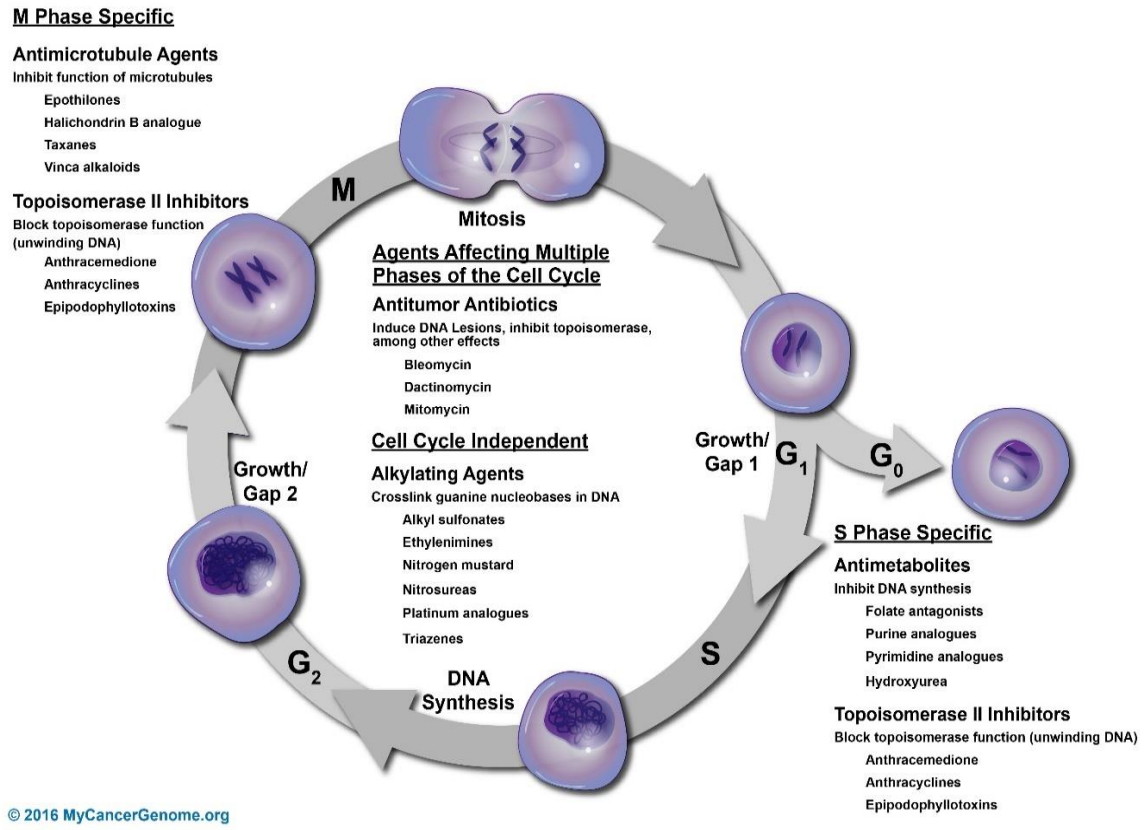

Figure 1.1. Normal cell cycle representing the different phases at which cytotoxic drugs act, such as G1 phase, S phase, G2 phase and M phase. Reproduced from web page https://www.mycancergenome.org/content/molecular-medicine/pathways/cytotoxic-chemotherapy-mechanisms-of-action.

1.2.3. Limitations of conventional chemotherapy

The use of chemical cytotoxic drugs for the treatment of localized and metastasized cancers, mostly administered through IV regimens, referred to as chemotherapy is the primary therapeutic approach. Although widely used in cancer treatment, chemotherapeutic drugs possess limitations as follows.

- The lack of specificity towards neoplastic tissues causes substantial damage to non-cancerous cells leading to severe surplus side effects for example, nausea, suppression of bone marrow activity (immuno and myelosuppression), secondary neoplasms, mucositis, and infertility. In addition, the high distribution volume of cytotoxic drugs renders the non-specific drug delivery to cancer cells resulting in an abnormal concentration of the chemotherapeutics in healthy tissues (Giordano and Jatoi 2005).
- The lack of selectivity in mechanism of action is prominent drawback in conventional chemotherapy. Most chemotherapeutic drugs do not act on intracellular mechanisms unique to cancer cells but on common pathways shared by both malignant and normal cells. (Mays et al. 2010).
- Chemotherapeutic agents induce cytotoxicity due to high pharmacokinetic volume of distribution for low molecular weight drugs. Chemicals of low molecular weight are excreted quickly. For this reason, a higher concentration is required to achieve a therapeutic effect that leads to toxicity. The low therapeutic index of chemotherapeutic

drugs suggests that the needed concentration for the effective treatment is often high leading to systemic dose-dependent side effects (Torchilin 2000).

- Formulating chemotherapeutic drugs is challenging due to their poor aqueous solubility. The low solubility makes preparation of drugs difficult (Gao et al. 2015). Due to poor aqueous solubility and high hydrophobicity, the chemotherapeutic use of paclitaxel has been limited (Lipinski et al. 2012; Lipinski 2000).
- In addition, high degradation rate by the reticuloendothelial system (RES) allows avoiding the use of the formulation for oral administration and suggests administration regimens, not in compliance with the patients such as IV, transdermal and intraperitoneal. Thus, the modification could be done in routes of administration of available chemotherapeutic agents by optimizing drug delivery systems (Langer 1998). The poorly soluble drugs may result in embolization of blood vessels upon intravenous injection due to aggregation of the insoluble drugs, and often lead to local toxicity due to high concentration of drug at the site of deposition. One of the currently available formulation of paclitaxel comprises of Cremophor EL (polyethoxylated castor oil) and dehydrated ethanol. Though, Cremophor EL is toxic and causes serious side effects, including hypersensitivity reactions, cardiotoxicity, and nephrotoxicity (Brannon-Peppas and Blanchette 2012). Alternatively, surfactants has been employed in the formulation to solubilize the drug, however, this may result in precipitation of drug *in vivo*, due to their low critical micelle concentration in physiological fluids (Kim et al. 2006; Torchilin 2002).
- Chemotherapy experience limited efficacy of anticancer drugs due to strong innate or acquired chemoresistance mechanisms (Szakács et al. 2006). The tumor interstitium is

characterized by high hydrostatic pressure, resulting in an outward convective interstitial flow which removes the drug away from the tumor unlike in normal tissues. Moreover, even though drug is delivered successfully to the interstitium of tumor, its efficacy may be restricted if the tumor cells have developed multidrug resistance (MDR) (Brigger, Dubernet, and Couvreur 2002). The characteristic feature of MDR is over-expression of the plasma membrane P-glycoprotein (P-gp), which keeps the drugs away from the cell. Various approaches have been proposed to avoid P-gp-mediated MDR, such as encapsulation of anticancer drugs in nanoparticles and the co-administration of P-gp inhibitors (Krishna and Mayer 2000). Efflux of many lipophilic drugs via drug efflux transporters leading to sub-optimal therapeutic drug concentration at the site of action is considered to be one of the barriers behind the success of chemotherapy (Serpe 2006).

- Conventional chemotherapy encounters challenge during transport of the drugs to the tumor. Physico-chemical characteristics of the drug, including particle size, composition, and surface charge plays major role in the transport (Park et al. 2008). Further hurdles consist in the pathophysiological tumor heterogeneity, which inhibit a uniform drug delivery into the whole tumoral mass. In addition, acidic tumor microenvironment causes degradation of the acid-sensitive drugs (Kumar 2006).

1.2.4. Toxicity of chemotherapy

Toxicities of chemotherapy varies corresponding to the particular drug, dose, and administration route. The side effects of chemotherapy include nausea, vomiting, and acute cholinergic gastrointestinal effects. The most common toxicities arises due to the cytotoxic effects on the normal dividing cells such as anaemia, thrombocytopenia, myelosupression with leucopenia, alopecia, and ulceration of mucous membrane. The late toxicities includes

the congestive cardiomyopathy due to neurotoxicity with platinums, vinca alkaloids and taxanes, high doses of anthracyclines, persistent cytopenias with alkylating agents, and pulmonary fibrosis with bleomycin (Skeel and Khleif 2011).

1.3. Photodynamic therapy

Photodynamic therapy (PDT) recently has become a recognized approach for the treatment of cancer. PDT involves the localization of photosensitizers (PSs) in target region prior to irradiation employing specific wavelength of light. The irradiated PSs generates singlet oxygen species which in turn triggers a cascade of biochemical reactions that destroy the cancer cells directly or by inducing vascular stasis. The PDT has been better tolerated as they destroy primarily cancer cells without affecting the normal cells (Hopper 2000; Oleinick and Evans 1998).

1.3.1. Photosensitizers

A photosensitizer (PS) most commonly a dye can be administered (injected or used topically), gets accumulated in the affected area then, illuminated using specific wavelength of light. Many natural and synthetic photoactive chemicals has shown photosensitizing activity. The examples are quinines, degradation products of chlorophyll, antraquinones, thiopenes, polyacetylenes, and 9-methoxypsoralen (Konopka and Goslinski 2007). Most commonly photosensitizing agents employed clinically includes dyes, chlorins, porphyrins, and furocoumarins. The ideal characteristic of PSs should be non-toxicity, local toxicity after irradiation by specific wavelength of light, short half-life period, maximum accumulation in cancer tissue rapidly, high quantum yield of singlet oxygen generation (SOG) *in vivo,* high aqueous solubility, and rapid clearance from tissues (Konopka and Goslinski 2007).

The photosensitizers are grouped into three generations.

First generation

- Photofrin dihematoporphyrin-ester (DHE)
- Hematoporphyrin derivatives (HPDs).

Second generation

- 5-Aminolevulinic acid (ALA)
- Temoporfin Meta-Tetra-Hydroxy Phenyl Chlorin (mTHPC)
- Foscan (mTHPC)
- Talaporfin sodium (LS11)
- Benzoporphyrin derivative (BPD)

Third generation

The presently existing photosensitizers are altered with monoclonal antibodies or protein carrier, and modification with a radioactive tag. Presently, four photosensitizers are commercially in use, Photofrin, ALA, Visudyne (verteporfin) and Foscan. The first three PSs have been permitted by FDA, whereas all four PSs are used in Europe (Konopka and Goslinski 2007).

1.3.2. Mechanism of action

The photophysical and photochemical of photodynamic therapy have been extensively studied (Ochsner 1997). The photosensitizers upon irradiation reaches to the first excited single state (S1) from the ground state (S0), resulting in conversion to the triplet state (T1) through intersystem crossing. In the triplet state, the excited PS interacts with the surrounding molecules generating cytotoxic species. The excited triplet can undergo reaction in two ways: Type I and Type II reaction as shown in Figure 1.2 (Foote 1991).

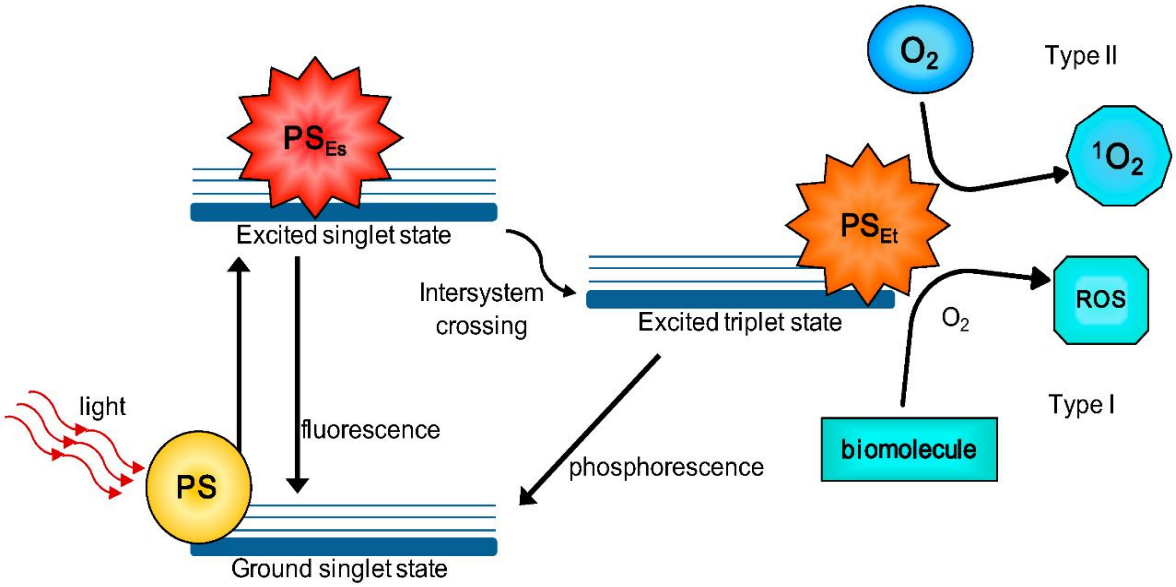

Figure 1.2. Schematic Jablonski's diagram showing Type I and Type II reactions in photodynamic therapy. PS_{Es}: photosensitizer excited singlet state; PS_{Et}: photosensitizer excited triplet state; ROS: reactive oxygen species; $^1O_2$: singlet oxygen. Reproduced from Calixto et al., 2016.

Type I reaction includes electron-transfer reactions or hydrogen-atom abstraction between the excited state of the PS and a substrate (either a solvent, biological, or another sensitizer), to generate free radicals or radical ions. The resulting free radical species being highly reactive interacts with molecular oxygen causing severe biological damage or can generate reactive oxygen species (ROS) such as hydroxyl radicals or superoxide anions. The above reactions cause oxidative damage ultimately stated as biological lesions. However, Type II reaction results from an energy transfer amongst the ground-state molecular oxygen, and excited triplet state of the photosensitizers producing first excited state of oxygen, singlet oxygen. The resulted zwitterionic species reacts fastly with various biological substrates, causing oxidative damage and eventually killing the cell. It has been seen that Type II reaction prevails throughout the photodynamic therapy and singlet oxygen is primarily

considered to be cytotoxic resulting in cellular damage (Fuchs and Thiele 1998; Ito 1978; Weishaupt, Gomer, and Dougherty 1976; Valenzeno 1987) whereas, Type I reaction occurs mainly at low concentration of oxygen or in presence of polar environment (Ochsner 1997; Rosenthal and Ben-Hur 1995). Though, both Type I and Type II reactions results in comparable free radical chain reactions and oxidative damage in the presence of oxygen within the target site causing tumor destruction.

1.3.3. Limitations of photodynamic therapy

The limitations of photodynamic therapy are following (Konopka and Goslinski 2007; Veerendra et al. 2009):

• Specific wavelength of light source is required to trigger the activity of PSs.

• PSs cannot enter ≥1.5 cm of the depth of tissue employing standard lasers or low power light-emitting diode systems, thus limiting its efficacy in treatment of large tumors.

• Patients allergic to porphyrins, cannot be treated by photodynamic therapy.

1.4.Nanoparticle drug delivery systems

Nanoparticles (NPs) have attracted considerable attention over the last decade offering benefits for drug delivery systems in overcoming limitations of conventional chemotherapy (Subbiah, Veerapandian, and S Yun 2010; Koo et al. 2011). NPs are utilized in cancer therapy due to their unique size, i.e. 1–1000 nm, or preferably in the range of 5-200 nm suitable for drug delivery applications. The nanoranged size, large surface-to-volume ratios and its ability for surface functionalization plays a crucial role in its *in vivo* biodistribution. These nanoparticles are formed using different materials such as lipids (e.g. liposomes, solid-lipid nanoparticles), polymers (e.g. biodegradable polymeric nanoparticles, dendrimers), inorganic materials (e.g. quantum dots, metal nanoparticles), and biological

materials (e.g. albumin nanoparticles, viral nanoparticles) (Cho et al. 2008). Additionally, these nanoparticles can be designed to deliver drugs and imaging probes simultaneously for targeting the diseased tissues. The first clinical trial of nanoparticles for anti-cancer drug delivery had been conducted in mid-1980s, and the first nanoformulation liposomes encapsulating doxorubicin was available in clinic in 1995. Subsequently, various nanoparticles for the delivery of chemotherapeutics have been explored owing to its advantage of enhancing solubility and stability of hydrophobic drugs, reducing non-specific uptake, prolonging circulation time, avoiding unwanted off-target and side effects, enhancing cellular internalization, and effective targeting of cancer.

1.4.1. Promises of targeted nanoparticles for cancer therapy

The targeted nanocarriers has received potential attention in improving drug/gene delivery overcoming many problems associated with conventional chemotherapy (Koo et al. 2011; Ali et al. 2011; Heidel and Davis 2011). The passive targeting or active targeting of nanoparticles demonstrated enhanced intracellular uptake of drugs/genes in cancer cells without causing toxicity to normal cells.

In addition, targeted delivery of the chemotherapeutic agent can be achieved by developing multifunctional nanocarrier systems (Larina et al. 2005; Nasongkla et al. 2006). The engineered nanocarriers offer various other advantages compared to free drug administration, such as (i) nanometer size range suitable for tumor targeting via EPR effect, (ii) protective insulation of drug molecules to enhance their stability and minimize their systemic clearance, (iii) ability for surface functionalization, (iv) possibility of multiple drug delivery to achieve synergistic therapeutic response, (v) opportunity for the application of combination therapy by utilizing chemotherapeutic and photothermal effects,

or creating magnetic nanostructures making delivery of NPs easier with the application of an external magnetic field (Jain 1987).

1.4.2. Advantages of nanoparticle drug delivery systems

Nanoparticular drug delivery systems offer distinct advantages for cancer therapy over free drug administration such as:

- improving the therapeutic index of the loaded chemotherapeutic agents compared to the drugs delivered via conventional dosage forms.
- increasing drug efficacy by achieving steady state therapeutic levels of drugs over an extended period.
- lowering drug toxicity due to controlled drug release and improving drug's pharmacokinetics by increasing drug's solubility and stability.

Improvement in drug's pharmacokinetic parameters by the development of nanotechnology based formulations allows resuming investigation of potentially productive new chemical entities that have been hindered during the pre-clinical or clinical development due to their suboptimal pharmacokinetic or biochemical properties.

The parameters such as particle size, conformation, non-covalent interactions and surface adsorption would have remarkable effects and variations on the interaction between the nanoparticles and the biological environment (Moghimi, Hunter, and Murray 2005; Pokropivny and Skorokhod 2008). In addition, surface characteristics of nanocarriers influence their internalization and clearance *in vivo*. Nanoparticles clearance occurs mainly via opsonization and phagocytosis by macrophages following the mechanism of receptor-mediated endocytosis (Serpe 2006; Maeda 2001b). To delay degradation, surface of the NPs has been decorated using a biocompatible and non-immunogenic hydrophilic polymer,

poly(ethylene glycol) (PEG) leading to reduction in binding to opsonins, preventing reticuloendothelial degradation (Owens III and Peppas 2006). Furthermore, nanocarriers encapsulating drugs can minimize chemoresistance to drug action, increasing the selectivity of drugs toward tumor cells while reducing toxicity toward normal cells (Serpe 2006). In addition, the selectivity of nanocarriers toward cancer cells increases by modifying their surface with specific antibodies or Ab-fragments, which recognize specific epitopes of tumor-associated antigens (TAA) and tumor-specific antigens (TSA) (Gullotti and Yeo 2009). After eventual accumulation to the tumor tissues, nanocarriers are accumulated in the tumor interstitium due to their compromised lymphatic clearance at the tumor site (Ozawa et al. 2008).

1.5. Targeted delivery of nanoparticles

The systemically delivered targeted nanoparticles would reach the desired tissue site overcoming the barriers with insignificant loss of volume or activity. After reaching the tumor tissue, drugs should translocate into the cancer cells and produce cytotoxicity (Allen 2002; Ozcelikkale, Ghosh, and Han 2013; Rizzo et al. 2013). The delivery of nanoparticles to the tumor tissue via systemic circulation has been achieved by two targeting strategies, including passive and active targeting.

1.5.1. Passive targeting

Passive targeting involves certain pathophysiological characteristics of targeted tissue that allows the retention of nanocarriers and releases the drug, devoid of any external stimuli or ligands. The Enhanced Permeability and Retention Effect (EPR) effect mediated delivery of nanocarriers has been considered to be the common pathophysiological characteristics in tumors leading to the targeted anticancer therapy shown in Figure 1.3.A (Torchilin 2011).

The Matsumura and Maeda group reported that most of the solid tumors have blood vessels with defective architecture and display enhanced vascular permeability to ensure sufficient supply of nutrients and oxygen to tumor tissues for rapid proliferation. EPR effect enables extravasation of macromolecules larger than 40 KDa from the tumor vessel into the interstitial space resulting in accumulation of macromolecules. However, tight junctions in the normal endothelial cells do not allow such extravasation. Therefore, EPR effect offers tumor targeted drug delivery, which is considered to be a promising paradigm for anticancer drug development (Maeda 2001a; Fang, Sawa, and Maeda 2003; Iyer et al. 2006; Maeda, Bharate, and Daruwalla 2009). One such passive targeted doxorubicin loaded liposomal formulation, Doxil® is in the clinic for the treatment of Kaposi sarcoma and many more nanomedicines relying only on EPR effect for their tumor targeting are in clinical trials and in pre-clinical studies (Barenholz 2012; Maeda, Bharate, and Daruwalla 2009; Torchilin 2011; Torchilin 2010).

Even though EPR effect-based anticancer drug delivery has shown some effect in nanocarrier mediated targeted delivery of chemotherapeutic agents, however, this strategy faces several challenges in delivering drugs to the tumor. Firstly, interstitial fluid pressure creates a considerable barrier preventing the penetration of nanocarriers inside the tissues. Fluid pressure develops with the growth of tumor as the plasma fluids and proteins leak out from the capillaries. The elevated protein content in the interstitial space causes colloidal pressure to develop that prevents the entry of any macromolecules from the blood flow. Secondly, rapidly growing tumor cells compresses the lymphatic vessels causing reduction of interstitial fluid drainage with a net gain of fluid pressure. Third factor arises from the heterogeneity of the tumor tissues. Central part of the tumor comprised of tumor stem cells

show less accumulation of nanocarriers compared to other parts of the tumor. Entry of drug to this necrotic, central part of the tumor is poor via EPR effect as the central part is hypo-vascularized with the consequence of less vascular leakage.

1.5.2. Active targeting

In active targeting, based on molecular recognition processes, the homing moiety, for example a ligand or a monoclonal antibody can be attached, to deliver a drug to desired site or to cross biological barriers shown in Figure 1.3.B (Brigger, Dubernet, and Couvreur 2002; Fenart et al. 1999; Huynh et al. 2009).

Active targeting involves ligand-mediated, or antibody (Ab)-mediated targeting of the nanocarriers to the cancer cells (Torchilin 2010). Ligand mediated targeting of nanocarriers enhances the therapeutic index of the drug by increasing the drug's efficacy and reducing the non-specific toxicity (Malam, Loizidou, and Seifalian 2009; Perumal et al. 2011). A wide range of targeting ligands as nanocarrier-surface modifier, including proteins (antibody or antibody fragments), peptides (arginine-glycine-aspartic acid or RGD), vitamin (folic acid), nucleic acid (aptamer) and glycoprotein (transferrin) are currently being exploited extensively for the development of cancer targeted nanocarriers (Heath et al. 1983; Schiffelers et al. 2003; Rui et al. 1998; Brody and Gold 2000; Juliano and Stamp 1976).

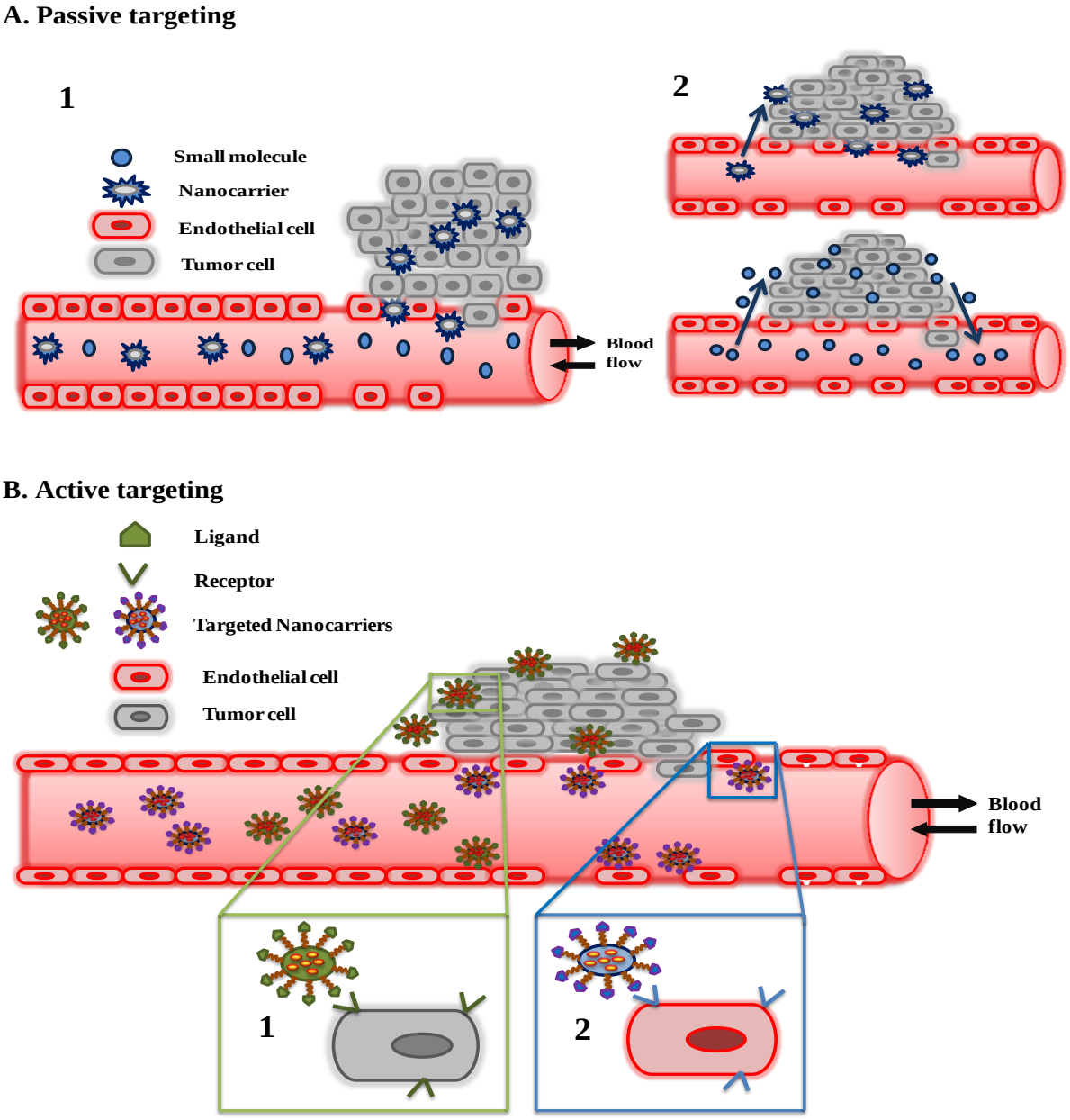

Figure 1.3. Schematic representation of passive targeting (A) and active targeting (B) of the nanocarriers. Reproduced from Biswas Swati et al., 2016.

1.6. Polymeric Micelles as Drug Delivery Systems

Polymeric micelles are self-assembled, monolayer system formed spontaneously under suitable conditions, including the concentrations of amphiphilic surfactants, temperature,

pH, and ionic strength with a hydrophilic shell and a hydrophobic core in the nanometer range. In an aqueous medium, at low concentration the amphiphiles exist as monomers in solution, but when the concentration rises, the amphiphiles self-assembles within a slight concentration range, resulting in formation of micelles shown in Figure 1.4 (Torchilin 2007). The concentration at which micelles are produced is mentioned as the critical micelle concentration (CMC). Above CMC, the constitution of micelles begins due to the dehydration of the hydrophobic tails, resulting in a positive state of entropy. Furthermore, the development of Van der Waals bonds helps the lipophilic polymers to unite and create the micellar core (Torchilin 2007). The subsequent hydrophilic outer shell forms hydrogen bond network with surrounding water. The increase in hydrophobicity and molecular weight of the hydrophobic block results in low CMC (Torchilin 2001; Kabanov, Batrakova, and Alakhov 2002). Polymeric micelles are made up of block-copolymers which can be organized in three ways: diblock copolymer (A-B type), triblock copolymer (A-B-A type), and grafted copolymer (Torchilin 2007; Jones and Leroux 1999).

The selection of polymer for micelles depends on the characteristics of both the hydrophilic and the hydrophobic block copolymer. The outer shell hydrophilic in nature offers steric stability and prevents internalization by RES, leading to extended circulation time in body (Adams, Lavasanifar, and Kwon 2003). Poly(ethylene glycol) (PEG), most commonly used hydrophilic polymer provides desired hydrophilicity to corona thereby improving the biocompatibility of the system (LaPorte 1997). Additionally, non-ionic hydrophilic PEG avoids the adsorption of opsonin and further clearance by the mononuclear phagocyte system. Consequently, prolonging the residence time of the micelles in the circulation, which influences pharmacokinetics and biodistribution of the encapsulated drug (Owens and

Peppas 2006; Vonarbourg et al. 2006). The hydrophobic block copolymer should possess high drug loading, encapsulation efficiency, and excellent compatibility of the hydrophobic core with the loaded drug. Most commonly used hydrophobic polymers are polyesters, polyethers, and polyamino acids (Sutton et al. 2007; Gaucher et al. 2005).

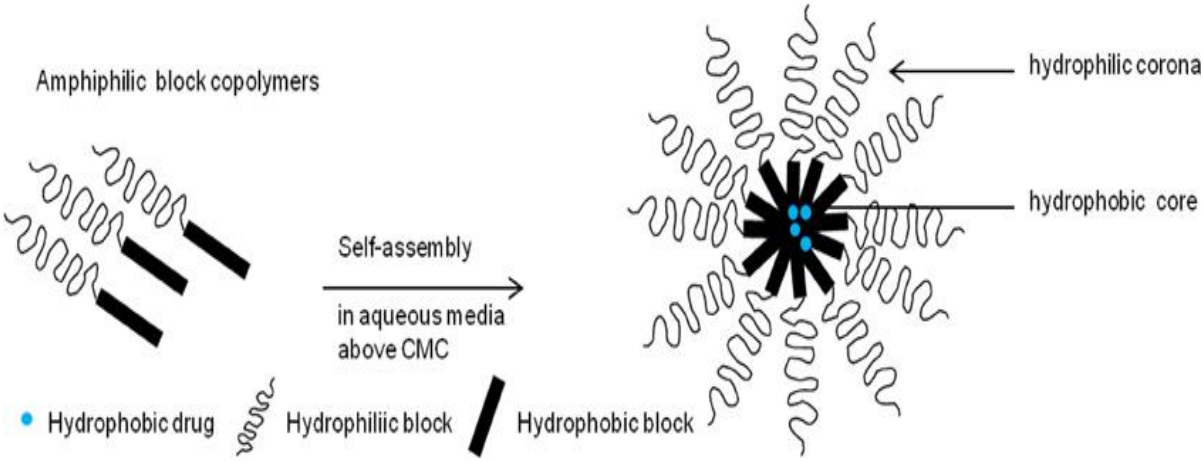

Figure 1.4. Schematic representation of self-assembly of amphiphilic block copolymers forming micelles in aqueous media. Reproduced from Jhaveri, Aditi M et al., 2014.

1.6.1. Curcumin as an anticancer agent

Curcumin is a naturally occurring small molecule that demonstrated powerful anticancer activity in various pre-clinical studies (Naksuriya et al. 2014). CUR, bis(4-hydroxy-3-methoxyphenyl)-1,6-diene-3,5-dione is a polyphenol compound derived from the rhizome of plant *Curcuma longa.* CUR has been reported to having a wide range of pharmacological activities such as anti-microbial, anti-oxidant, anti-inflammatory, anti-parasitic, anti-mutagenic, anti-human immuno-deficiency virus, and anti-cancer with low or no intrinsic toxicity (Srivastava et al. 2011; Kawamori et al. 1999; Anand et al. 2008). CUR could inhibit the generation, vegetation and metastasis of many tumors, including breast, pancreatic, colon, stomach, liver, cervical, and epithelial cell carcinoma (Kim et al. 2011).

Treatment of breast and pancreatic cancers by CUR is in phase I and II of clinical trials, respectively (Dhillon et al. 2008; Mock, Jordan, and Selvam 2015). Despite its pharmacological potentials, the application of CUR in clinic is limited due to its low aqueous solubility (0.6 µg/mL) and rapid degradation in physiological conditions (Wu et al. 2011). Wang and co-workers reported cleavage of the heptadienedione chain of curcumin resulting in vanillin, ferulic acid, and feruloylmethane as minor products (Wang et al. 1997). However, it was found that the major product detected by Wang and co-workers was likely the bicyclopentadione product of autoxidative transformation of curcumin (Griesser et al. 2011). After oral administration, curcumin is metabolized by reduction and conjugation. Consecutive reduction of the double bonds in the heptadienedione chain results in the formation of di-, tetra-, hexa-, and octahydro- curcumin. Reduction can occur in the gut by the NADPH-dependent reductase CurA that has been identified in intestinal Escherichia coli (Tan et al. 2014; Hassaninasab et al. 2011). After systemic absorption, alcohol dehydrogenase reduces curcumin to tetra- and hexahydrocurcumin in the liver, whereas formation of di- and octahydrocurcumin required an unidentified microsomal enzyme (Ireson et al. 2001; Ireson et al. 2002) (Hoehle et al. 2006). The reduced metabolites, especially tetra- and hexahydrocurcumin, represent the largest portion of curcumin metabolites (Pan, Huang, and Lin 1999). With few exceptions their biological activities are strongly reduced compared to those of curcumin (Aggarwal, Deb, and Prasad 2014; Wu et al. 2014). However, because of the several therapeutic activities of curcumin, there has been a continual search for a solution to the above problems. Nanoparticle drug delivery systems are being explored as a potential approach to overcome these limitations (Yallapu et al. 2010; Lin et al. 2012).

1.6.2. Chlorin e6 as a photosensitizer

Among the commercially available photosensitizers, chlorin e6 (Ce6), a chlorophyll derivative is a second-generation photosensitizer with a strong absorption in the red region of the light spectrum. Remarkable clinical benefits have been achieved with Ce6-mediated PDT in the treatment against a broad spectrum of cancers, including melanoma, bladder cancer, and nasopharyngeal cancer (Li et al. 2014). Chlorin e6 has a strong absorption peak at a wavelength of 663 nm, exhibiting deeper penetration of tissue and generating higher reactive oxygen species (ROS) (Zenkevich et al. 1996). The photosensitizers must travel through the blood circulation with high aqueous-stability for efficient photodynamic therapy. However, Chlorin e6 being hydrophobic in nature and insoluble in aqueous medium, which significantly diminishes its PDT effects. To overcome the above limitations, hydrophilic polymers including poly(vinyl pyrrolidone) (PVP), poly(ethylene glycol) and various polypeptides were commonly used to improve the solubility of chlorin e6 (Chin et al. 2008; Li et al. 2013; Lee et al. 2013).

1.7. Objectives

Our objective is to evaluate the therapeutic efficacy of polymeric micelles encapsulating poorly soluble chemotherapeutics against a range of cancer cell types *in vitro* and *in vivo*. Even though nanocarrier-mediated drug delivery to cancer has proven to be therapeutically effective compared to conventional free drug administration, however, degradation of the nanoparticles are slow leading to residence of the polymer in the system.

In this study, we investigated an amphiphilic polymer consisting of poly(ethylene glycol) as hydrophilic chain, and poly(lactic acid) and cholesterol as the hydrophobic moiety to effectively load and deliver hydrophobic anticancer drugs. The conjugation of cholesterol to

poly(lactide) is the first attempt to the best of our knowledge to improve the biocompatibility of the polymeric micellar system and drug loading. The nanocarriers were modified with transferrin for active targeting. In our study, poorly water soluble yet potent anticancer drugs, curcumin and chlorin e6 was used as a model drug.

Objective 1: To develop methoxy-poly(ethylene glycol)-poly(D,L-lactide) (mPEG-PLA) polymeric micelles as drug delivery system for the delivery of curcumin (CUR).

Specific aims:

(i) To synthesize and characterize the mPEG-PLA polymer.

(ii) To prepare and optimize the curcumin loaded micelles.

(iii) To evaluate the cellular uptake and *in vitro* cytotoxicity of the developed micellar formulations against cancer cells.

(iv) To modify the mPEG-PLA micelles with transferrin.

(v) To evaluate the efficacy of the targeted micellar formulations against monolayers cells and 3D spheroids.

Objective 2: To develop cholesterol-conjugated poly(Lactide)-based micelles as a nanocarrier system for the delivery of curcumin (CUR).

Specific aims:

(i) To synthesize and characterize the mPEG-PLA-Ch polymer.

(ii) To prepare and optimize the curcumin loaded micelles.

(iii) To evaluate the cellular uptake and *in vitro* cytotoxicity of the developed micellar formulations against cancer cells.

(iv) To study *in vivo* therapeutic efficacy of the developed formulation.

Objective 3: To develop poly(Lactide)-based polymeric micelles loaded with chlorin e6 for photodynamic therapy.

Specific aims:

(i) To prepare and optimize the Chlorin e6 loaded mPEG-PLA micelles.

(ii) To evaluate the cellular uptake and *in vitro* phototoxicity of the developed micellar formulation against cancer cells.

(iii) To evaluate the efficacy of the micellar formulation against 3D spheroids.

Chapter 2A

Curcumin delivery by poly(Lactide)-based co-polymeric micelles: An *in vitro* anticancer study

ABSTRACT

Even though curcumin (CUR), the naturally occurring anticancer drug is highly effective in inducing apoptosis in multiple cancer cell types and has the ability to kill the cancer cells via several mechanisms, low aqueous solubility and poor bioavailability limit its clinical application. Here, to improve the solubility and bioavailability, CUR was physically entrapped in the newly synthesized block co-polymeric micelles, methoxy-poly(ethylene glycol)-poly(D,L-Lactide) (mPEG-PLA). The block co-polymer of balanced hydrophobicity was prepared using mPEG of molecular weight (MW) 5.0 KDa resulting in the co-polymer mPEG-PLA in the range of MW. 5970 Da as confirmed by gel permeation chromatography. The polymeric micelles displayed low critical micelles concentration (50 µg/mL) determined by pyrene assay, average particle size of 110.79 ± 1.53 nm with polydispersity index of 0.273 ± 0.19 measured by light scattering method and surface charge of -29.17 ± 0.81 mV assessed by the measurement of zeta potential. The micelles loaded hydrophobic CUR efficiently inside the hydrophobic core compartment with encapsulation efficiency (EE) and drug loading (DL) of 91.89 ± 1.27% and 11.06 ± 0.83%, respectively. Differential scanning calorimetry (DSC) analysis indicated that the curcumin in the micellar core remained either in amorphous or in solid dispersion state that would improve the bioavailability of curcumin. Sustained release of CUR from micelles was observed with 9.73% CUR release from micelles compared to 64.24% release of free curcumin in first 6 h under sink condition. The CUR-mPEG-PLA was efficiently taken up by the cancer cells, murine melanoma cells (B16F10) and human breast adenocarcinoma cells (MDA-MB-231) in dose and time dependent manner. The cytotoxic potential of CUR delivered to cancer cells via these polymeric micelles was assessed by following two treatment regimens, in which the cells were subjected to a drug treatment either

for continuous 24 h or 6 h followed by 24 h incubation. CUR-mPEG-PLA dose-dependently induced cytotoxicity. Following 24 h incubation, CUR-mPEG-PLA induced higher cytotoxicity compared to free CUR in MBA-MB-231 cell lines indicating exposure of higher dose of free CUR to cells lead to up-regulation of drug efflux mechanisms leading to decreased cell death in case of free CUR administration. Together, the result clearly indicated that the proposed micellar system has the potential to serve as an efficient carrier for CUR by effectively solubilizing, stabilizing and delivering the drug in a controlled manner to the cancer cells. The proposed nano-formulation holds promise in cancer treatment, especially for the treatment of metastatic breast cancer.

2A.1. INTRODUCTION

Recently, medical applications of polymeric nanoparticles to achieve site-specific drug delivery have attracted growing interest. Especially, polymeric micelles are currently recognized as one of the most promising carriers of drug due to the unique features, including loading of hydrophobic drug, passive targeting capability based on Enhanced Permeability and Retention (EPR) effect, surface functionalizability to endow active cancer targeting, and ease of preparation and scale up (Nishiyama and Kataoka 2006). Polymeric micelles are core/shell structures formed through self-assembly of amphiphilic block copolymers. The most unique aspect of polymeric micelles is the flexibility in modification of both hydrophilic (shell) and hydrophobic (core) block of polymer without affecting one another (Xiong et al. 2008).

Methoxy-poly(ethylene glycol)-poly(D,L-Lactide) (mPEG-PLA) is an amphiphilic copolymer that displays many advantageous features as the building block for the development of micellar structure for drug delivery application. The copolymer, mPEG-PLA is biocompatible, biodegradable, less toxic, and can be produced economically in bulk quantities. Potential advantage is provided by the hydrophilic poly (ethylene glycol) (PEG), which provides desired hydrophilicity in the corona and improve the biocompatibility of the delivery vehicle (LaPorte 1997). Moreover, non-ionic hydrophilic PEG shell suppresses the adsorption of opsonin and subsequent clearance by the mononuclear phagocyte system. As a result, residence time of the micelles in the circulation gets prolonged, which influences pharmacokinetics and biodistribution of the loaded drug (Owens and Peppas 2006; Vonarbourg et al. 2006). On the other hand, the hydrophobic core constituted of PLA solubilizes hydrophobic drugs and protect them from degradation in circulation. Hence, PEG-PLA has been studied widely as a

biomaterial for sustained release of drugs and antigens (Dong and Feng 2004; Yang et al. 2011; Wang et al. 2010).

Among the natural phytochemicals, Curcumin (diferuloyl methane, CUR), a low-molecular-weight, natural polyphenolic compound that is isolated from the rhizome of turmeric (Curcuma longa) has received considerable attention in cancer research, especially in cancer prevention and cancer therapeutics (Aggarwal, Kumar, and Bharti 2003). Even though curcumin has not proven its clinical efficacy yet, however, curcumin has shown myriads pharmacological activity in pre-clinical settings, including anticancer and anti-inflammatory, antioxidant, antimicrobial, anti-depressant, and anti-HIV activities (Anand et al. 2008; Kawamori et al. 1999; Mohanty et al. 2010; Sahu et al. 2011; Aggarwal and Sung 2009). Curcumin has proven to have a diverse range of molecular targets, including various receptors, enzymes, growth factors, transcription factors, cytokines, enzymes, transcription factors and genes regulating cell proliferation and apoptosis (Aggarwal and Sung 2009). In a recent study, administration of curcumin altered the expression of 32 different proteins mainly associated with cell cycle and apoptotic pathway in HepG2 cells (Chen et al. 2015). Additionally, curcumin induced generation of reactive oxygen species resulting in cell cycle arrest. Several studies on curcumin offers insights into the molecular mechanisms by which curcumin modulates cell cycle, apoptotic signals, miRNAs, Wnt/β-catenin signaling, protein kinases, nuclear factor kappaB, epigenetic modulations and reversal of multiple drug resistance (Tuorkey 2014). Moreover, curcumin is safe and well tolerated at high doses (8 g/day orally) in human clinical trials. The high safety profile, low side effects and effectiveness on multiple cancer cell types make CUR a promising candidate for the treatment of several cancers (Martin et al. 2015; Mehmet et al. 2013; Mohanty et al. 2010; Mulik et al. 2012; Raveendran, Bhuvaneshwar, and Sharma 2013; Sahu et al. 2011).

Despite these promising properties, curcumin encounters limited clinical application due to their extremely low solubility in aqueous solution (2.99 X 10^{-8} M) leading to poor bioavailability (Letchford, Liggins, and Burt 2008; Anand et al. 2007). Various attempts have been made over the last few years to improve the bioavailability of CUR by encapsulating it into the nanoparticles, including polymeric micelles, liposomes, polymeric nanoparticles, lipid-based nanoparticles, and hydrogels (Sahu et al. 2008; Ma et al. 2008; Li et al. 2007; Bisht et al. 2007; Sou et al. 2008; Vemula, Li, and John 2006).

In this regard, here, we attempted to develop mPEG-PLA polymeric micellar system as a nanocarrier for curcumin encapsulation with a view to improve the aqueous solubility, stability and controlled delivery of CUR in cancer cells. Following the synthesis of mPEG-PLA copolymer of balanced amphiphilicity, curcumin loaded mPEG-PLA (CUR-mPEG-PLA) micelles were prepared. The therapeutic utility of the newly developed anticancer nano-formulation was determined by registering its drug loading capability, *in vitro* drug release kinetics, interaction with cancer cells, and cytotoxicity in murine melanoma cells (B16F10) and human breast adenocarcinoma cells (MDA-MB-231).

2A.2. MATERIALS AND METHODS

2A.2.1. Materials and cell lines

Methoxy-polyethylene glycol (mPEG, MW 5000 Da), D,L-Lactide, Stannous 2-ethylhexanoate, Curcumin, Tetrahydrofuran (THF), toluene, and pyrene were obtained from Sigma-Aldrich Chemicals (Germany). Dialysis membrane was obtained from Spectrum Laboratories, Inc. (USA). 3-(4,5-dimethylthiazol-2-yl)-2,5-di-phenyltetrazolium bromide (MTT), Trypan blue solution, and Fluoromount-G were purchased from Himedia (Mumbai,

India). All the other chemicals and solvents obtained commercially were of analytical grade or higher.

Dulbecco's modified Eagle's media (DMEM), and Growth medium RPMI-1640, concentrated penicillin/ streptomycin stock solution and heat-inactivated fetal bovine serum (FBS) were obtained from Himedia (Mumbai, India). All other chemical and solvents purchased from Sigma-Aldrich were of analytical grade and used without further purification.

2A.2.2. Cell lines and animals

The murine melanoma cells (B16F10) and human breast adenocarcinoma cells (MDA-MB-231) were purchased from the NCCS (Pune, India). Cells were grown in DMEM and RPMI-1640 medium supplemented with 10% FBS and 1% penicillin-streptomycin solution. Cells were maintained in a humidified atmosphere at 37°C and 5% CO_2.

Pathogen free female C57BL/6 mice of age 6-8 weeks were procured from National Centre for Laboratory Animal Sciences (NCLAS), National Institute of Nutrition (Hyderabad, India). All animal studies were carried out under the guidelines compiled by the Institutional Animal Ethics Committee of the BITS Pilani University. The animals were maintained in a room (23 ± 2°C and 60 ± 10% humidity) under a 12 h light/dark cycle. Food and water were given *ad libitum*.

2A.2.3. Synthesis of mPEG-PLA copolymers

The mPEG-PLA diblock copolymers were synthesized by ring opening polymerization reaction following a previously reported procedure. Briefly, 0.4 g of pure D, L-Lactide and 1 g of mPEG were placed in a dried polymerization tube. Stannous octoate (0.008% w/w) in toluene was added as a catalyst into the reaction mixture (Zhang et al. 2005). The reactants were heated for some time till they turn to liquid. The tube was sealed under vacuum, and the copolymerization

was carried out at 160°C for 6 h (Zhu, Xiangzhou, and Shilin 1990). The crude product was dissolved in THF and then purified by precipitation in ice-cold diethyl ether followed by filtration. The precipitated product was rota-evaporated to remove the solvent. 2-3 mL amount of water was added to perform dialysis against water by using cellulose ester membrane (MWCO 12-14,000 Da). The product was lyophilized for 10-15 h (yield 72.17%). ^{1}H NMR spectra were recorded in 300 MHz Bruker spectrometer (AVANCE model, Germany) at 25°C using deuterated chloroform ($CDCl_3$) as solvent.

2A2.4. Physico-chemical characterization of copolymer micelles

2A.2.4.1. Preparation of mPEG-PLA micelles

mPEG-PLA polymeric micelles were prepared by thin film hydration technique (Dabholkar et al. 2006). Briefly, mPEG-PLA solution in chloroform was evaporated to dryness as a thin film. Phosphate buffered saline (PBS); pH 7.4 at 10 mg mPEG-PLA/mL of PBS was added to hydrate the film and vortexed at room temperature to dissolve the polymeric film.

2A.2.4.2. Encapsulation of CUR in mPEG-PLA micelles

To prepare CUR-loaded mPEG-PLA micelles, previously mentioned thin film hydration technique was followed. Briefly, pre-weighed amount of CUR in solution (0.1% acetic acid methanol solution) and mPEG-PLA copolymer (chloroform solution) were mixed together. The organic solvents were removed by the rotary evaporation and the thin film of drug/polymer mixture was hydrated by using PBS pH 7.4. The suspension was vortexed to disperse the film (Figure. 2A.1). The solution was further centrifuged (13500g, 4°C) and the supernatant was collected.

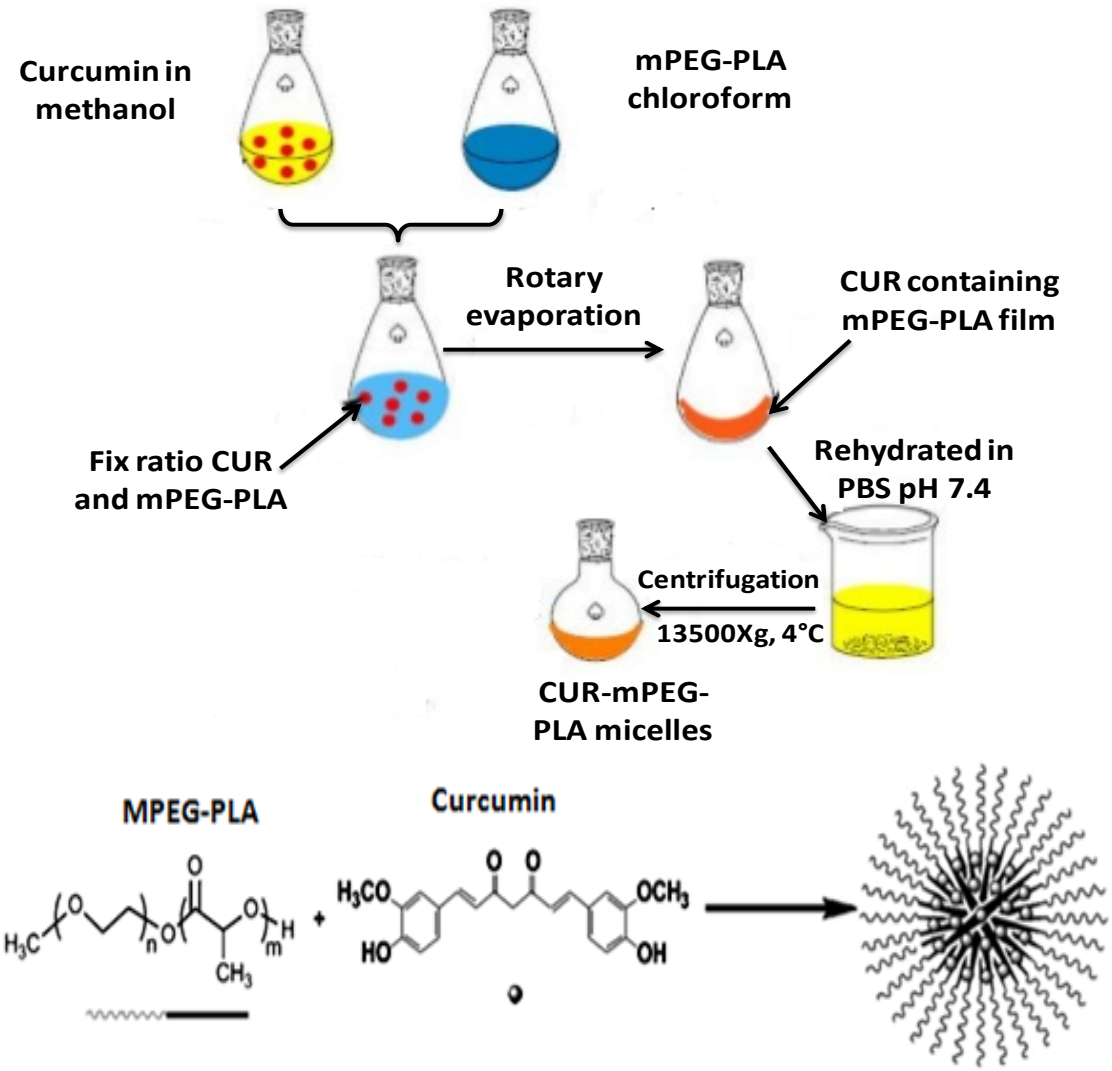

Figure 2A.1. Development of CUR-mPEG-PLA polymeric micelles. CUR-loaded self-assembled polymeric micelles were formed following hydration of the mPEG-PLA and CUR.

2A.2.4.3. Particle size and zeta potential

The mean diameter and zeta potential of the mPEG-PLA and CUR-mPEG-PLA micelles were determined by zetasizer (Nano ZS90, Malvern Instruments Ltd., UK). All the measurements were analyzed in triplicate at 25°C.

2A.2.4.4. Morphology of polymeric micelles

The morphology of the mPEG-PLA and the CUR-mPEG-PLA micelles was observed under transmission electron microscope (TEM, JEM-1200EX, JEOL, Tokyo, Japan). One drop of micelles solution was placed on a film-coated copper grid followed by negative staining with phosphotungstic acid (PTA) for 20s, excess solution was absorbed with filter paper, and samples were naturally dried for observation.

2A.2.4.5. Determination of critical micelles concentrations (CMC)

The CMC of mPEG-PLA micelles was determined using pyrene as a fluorescent probe (Zhang et al. 2004). Pyrene solution (50 µL; 10 mg/mL dissolved in chloroform) was added to 5 mL glass vials. After complete evaporation of the chloroform, a series of concentrations of mPEG−PLA (3.125 to 150 µg/mL) in millipore water was added to the mixture. The mixtures were kept overnight in a shaking incubator at 150 rpm at 25°C. Free pyrene was removed by filtration through polycarbonate membranes with a 0.45 µm pore size. The filtered samples were transferred to a 96-well plate and the fluorescence was measured using a plate reader (Spectramax^{TM} M4, Multi detection Reader) at excitation and emission wavelengths of λex 339 and λem 390 nm, respectively. CMC values were determined from the pyrene fluorescence in solution as a function of conjugate concentration, and corresponded to concentrations at which a sharp increase in the solution fluorescence occurred. The amphiphile poly(ethylene glycol)-distearoylphosphatidylethanolamine (PEG-DSPE) was used as a reference.

2A.2.4.6. Entrapment efficiency (EE) and drug loading (DL)

To determine EE and DL drug loaded micelles were dispersed in PBS and further diluted by 80% (v/v) ethanol to cause breaking of micelles and release of drug. The drug concentration was analysed using UV-Vis spectrophotometer (Spectramax^{TM}, microplate reader, Molecular

Devices, US) at a wavelength of 420 nm. The standard curve of curcumin was set up from 2-20 µg/mL. The EE and DL of curcumin loaded micelles were calculated using following equations,

$$\boldsymbol{EE}\,(\%) = \frac{\boldsymbol{Wentrapped}}{\boldsymbol{Wtotal}}\,\boldsymbol{X}\,\mathbf{100} \qquad (1)$$

$$\boldsymbol{DL}\,(\%) = \frac{\boldsymbol{Wentrapped}}{\boldsymbol{Wentrapped} + \boldsymbol{Wpolymer}}\,\boldsymbol{X}\,\mathbf{100} \qquad (2)$$

In above equation, $W_{entrapped}$ represents the amount of drug (curcumin) entrapped in the micelles, W_{total} represents the total concentration of feeding drug, $W_{polymer}$ represents the weight of polymer.

2A.2.4.7. Storage stability

The CUR-mPEG-PLA micelles were stored at 4°C and 25°C for upto two months. At pre-determined time point (10, 20, 30 and 60 days), the samples were analyzed in terms of particle size, zeta potential, and curcumin content. Further, the stability of the micelles were evaluated serum containing DMEM medium at 37°C for 72 h. Aliquots were removed at 0, 12, 24, 48, and 72 h followed by analysis with UV-Vis spectroscopy.

2A.2.4.8. Differential scanning calorimetry (DSC)

The physical status of Curcumin, pure polymers, and CUR encapsulated in the polymeric matrix of the mPEG-PLA was studied by DSC (DSC 60, Shimadzu, Japan) under nitrogen atmosphere at a flow rate of 20 mL/min. The temperature-rising speed was 10°C /min from 20 to 250°C.

2A.2.5. *In vitro* drug release

To determine the release kinetics of CUR from CUR-mPEG-PLA micelles, 1 mL of CUR-mPEG-PLA micelles solution or 1 mL CUR solution (100 µg/mL in propylene glycol) was placed in a dialysis bag with molecular weight cut off of 2000 Da (Spectrum Laboratories, Inc. USA). Dialysis bags were immersed into 40 mL of phosphate buffer solution (pH 7.4) containing 5% w/w sodium dodecyl sulphate (SDS) at 37 ± 0.5°C with a stirring speed of 300 rpm. At pre-determined time points, 1 mL of incubation medium was taken and replaced with fresh incubation medium. The amount of released drug in the incubation medium was measured by UV-Vis spectrophotometer (Spectramax™ M4, Multi detection Reader, Molecular devices, USA) at 420 nm. The cumulative release percentage was calculated. This study was repeated three times, and the result was expressed as mean value ± SD.

2A.2.6. Cellular uptake of CUR loaded micelles

Cellular uptake of micelles was visualized by using fluorescence microscopy. B16F10 and MDA-MB-231 cells (5 X 10^4 cells/well) were grown in complete media on circular cover glasses placed in 12-well tissue culture plates in complete media. The following day, cells were incubated with free CUR and CUR-mPEG-PLA at a CUR concentration of 50 and 100 µg/mL for 1 and 4 h in serum-free media. After the incubation period, the cells on the cover-slips were treated with Hoechst 33342, 5 µg/mL for 5 min, washed thoroughly with PBS, and fixed with 4% *para*-formaldehyde for 10 min at room temperature. The cover-slips were washed thoroughly with PBS, mounted cell-side down on superfrost microscope slides with fluorescence-free glycerol-based mounting medium (Fluoromount-G; Sigma Aldrich, USA) and viewed under a fluorescence microscope (Olympus IX 53). The images of the cells were

taken using FITC filter (λex 495 nm and λem 520 nm). The LSM picture files were analyzed by using Image J software.

2A.2.7. Quantification of cellular uptake of CUR micelles by flow cytometry

To assess the cellular uptake of Curcumin loaded micelles, a time and concentration dependent flow cytometry analysis was performed. B16F10 and MDA-MB-231 cells were seeded in 6-well tissue culture plates at a density of 4 X 10^5 cells/well. After 24 h, cells were incubated with free CUR, CUR-mPEG-PLA at a CUR concentration of 50 and 100 µg/mL for 1 and 4 h in serum-free media at 37°C. After the incubation, the media were removed; the cells were washed several times, trypsinized, collected in 15 mL tubes and then centrifuged at 1000 rpm for 5 min at 4°C to obtain a cell pellet. The cells were re-suspended in PBS, pH 7.4 (200 µL). Each data point was performed in triplicate. Then, intracellular CUR fluorescence was analyzed by flow cytometer (Amnis Flowsight, United States) after excitation with a 488 nm argon laser. Fluorescence emission at 520-530 nm from 10,000 cells were collected, amplified, and scaled to generate single parameter histogram. The data were analyzed with Image Data Exploration and Analysis Software (Version 6.0).

2A.2.8. *In vitro* cytotoxicity

The *in vitro* cytotoxicity of CUR-loaded micelles was evaluated by the MTT assay. Briefly, B16F10 and MDA-MB-231 cells were seeded into 96-well plates in 100 µL growth medium at a density of 1 X 10^4 cells/well and 5 X 10^3 cells/well, respectively, and incubated overnight. Then, cells were exposed to a series of CUR micelles or free CUR at different concentrations of 0-50 µg/mL for 6 and 24 h, respectively. After incubation for 6 h, media was removed and the cells were incubated for an additional 24 h in fresh complete media. B16F10 and MDA-MB-231 cells without any treatment were used as the control. After the incubation period, the

media was removed and the cells were treated with 3-(4,5-dimethylthiazol-2-yl)-2,5-di-phenyltetrazolium bromide (MTT) solution (50 µL; 5 mg/mL) in serum-free DMEM and RPMI-1640 for 4 h. The solution was removed and 150 µL of dimethyl sulfoxide (DMSO) was added into each well. Then the plate was incubated for 30 min at room temperature. Absorbance intensity was measured by using a microplate reader (Spectramax^{TM}, microplate reader, Molecular Devices, US) at 590 nm with a reference wavelength of 620 nm. Cell viability was expressed by the following equation

$$\text{Cell viability (\%)} = \frac{\text{Abs}_{\text{sample}}}{\text{Abs}_{\text{control}}} \text{ X100}$$

where, Abs_{sample} was the absorbance of the cells treated with free CUR or CUR-mPEG–PLA micelles, while $Abs_{control}$ was the averaged absorbance of the cells without drug treatment. The results were expressed as the mean absorbance ± SD for three replicates.

2A.2.9. Statistical analysis

The data were tested for statistical significance using Student's t-tests. p values, calculated with the Graph Pad prism 5 software (GraphPad Software, Inc, San Diego, CA). All numerical data are expressed as mean ± SD, n = 3 or 4, from 3 different experiments. Any p values less than 0.05 was considered statistically significant. *, **, *** in figures indicated p values <0.05, 0.01 and 0.001, respectively.

2A.3. RESULTS AND DISCUSSION

2A.3.1. Preparation and Characterization of copolymer

The non-ionic amphiphilic block copolymer, mPEG-PLA was synthesized by ring-opening polymerization reaction following a previously reported procedure (Figure.2A.2) (Zhang et al.

2005). The block lengths of mPEG and PLA could be adjusted by changing the molecular weight of mPEG and the molar ratio of LA to mPEG.

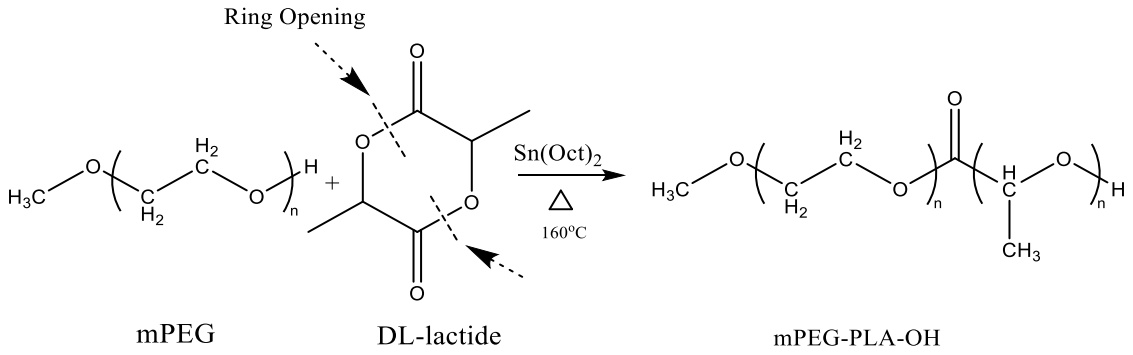

Figure. 2A.2. Synthesis scheme of mPEG-PLA.

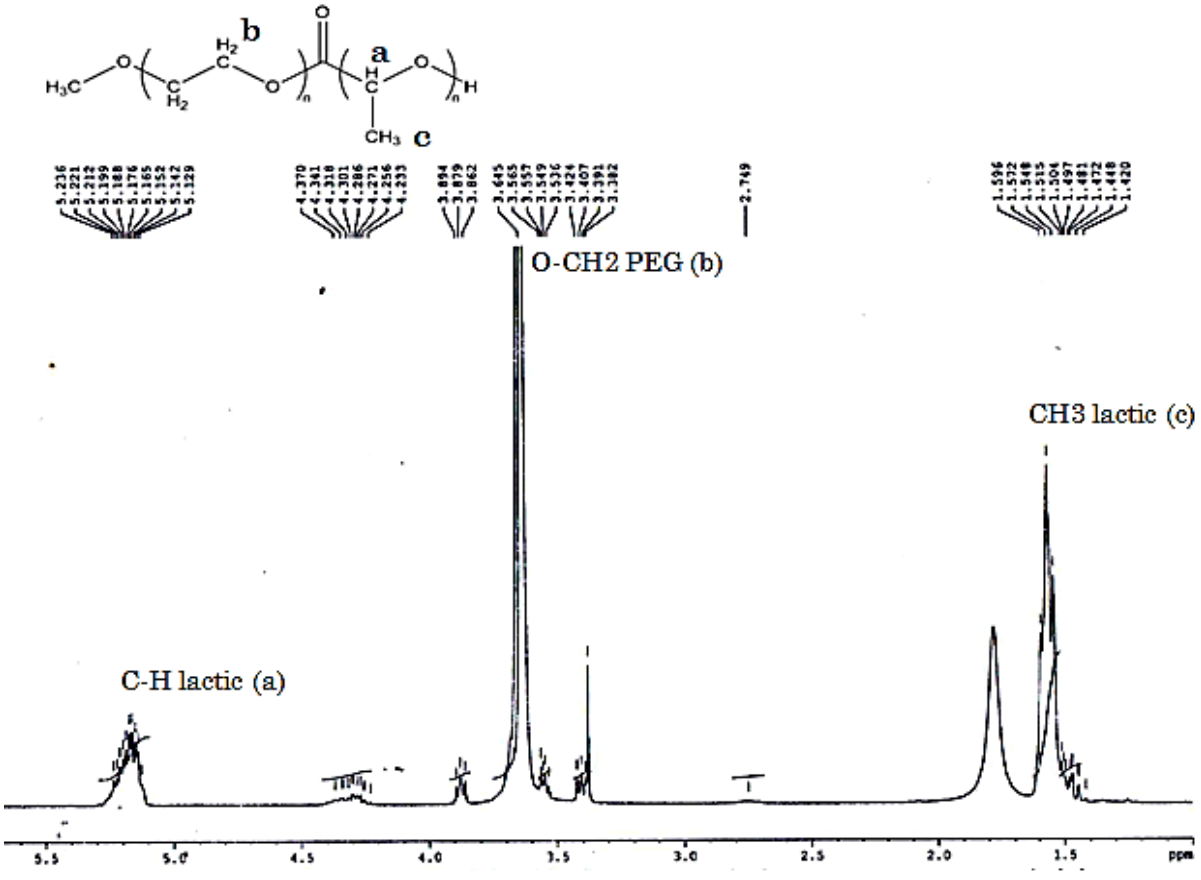

Figure. 2A.3. NMR spectrum of mPEG-PLA.

The gel permeation chromatography performed using mPEG-PLA dissolved in water reported that the molecular weight of the polymer is in the range of 5970 Da. The structure of copolymer

was confirmed by ^{1}H NMR (Figure. 2A.3). The length of the PLA block was calculated by comparing the integrals of the characteristic peaks of mPEG (e.g., the singlet of -CH_2-O- (b) at 3.65 ppm) with that of the characteristic peaks of PLA (e.g., the multiplet of –CH (c) at 1.60 ppm and CH_3-O- (a) at 5.2 ppm) in the ^{1}H NMR spectroscopy.

2A.3.2. Preparation and characterization of polymeric micelles

mPEG-PLA self-assembled into micelles in water at room temperature with mPEG molecular weight as 5000 Da at critical micelles concentration of 50 µg/mL as shown in Figure. 2A.4. The block copolymer PEG-DSPE was used a standard amphiphilic copolymer that showed CMC at 12.5 µg/mL. The low CMC of mPEG-PLA indicated that nanoscale micelles could be formed at a lower copolymer concentration due to the optimal hydrophobic-hydrophilic balance in mPEG-PLA copolymer. The synthesized mPEG-PLA block copolymer of average molecular weight 5970 Da with an attachment of PEG of molecular weight 5000 Da as indicated by gel permeation chromatography (GPC) formed stable polymeric micelles in aqueous solution with low CMC as indicated by pyrene assay (Figure. 2A.4).

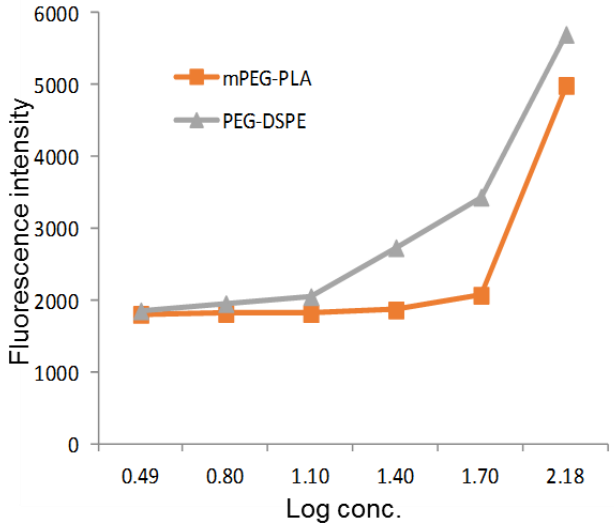

Figure. 2A.4. Critical micelle concentration (CMC) of mPEG-PLA and PEG-DSPE.

Curcumin (Cur) loaded mPEG-PLA micelles (CUR-mPEG-PLA) was prepared using the thin film hydration technique. To optimize the process parameters, we investigated the effect of copolymer to drug ratio in the feed on the properties of the resulting micelles, shown in Table 2A.1. With increase of copolymer/drug ratio in feed, the particle size, and PDI increased, whereas, the EE and stability decreased accordingly. The micelles with a ratio of 7.5:3 (C6) were unstable and aggregated in few minutes. Thus, particle size, PDI, DL, and EE could not be determined. In consideration of drug loading and stability, C3 (9.5:1.5) was chosen for further study and was characterized in detail. The distribution of sizes of optimized CUR-loaded micelles (C3) was shown in Figure. 2A.5A. Micelles had a size less than 200 nm with a PDI of 0.273 ± 0.19 suggesting good polydispersity. The average size of blank and CUR-loaded micelles was 104.65 ± 2.14 nm and 110.79 ± 1.53 nm with rather narrow size distribution patterns, respectively. The zeta potential of mPEG-PLA and CUR-mPEG-PLA was about -25.92 ± 0.29 mV and -29.17 ± 0.81 mV. As shown in Figure. 2A.5B, the morphology of the CUR-loaded micelles observed under TEM was spherical in shape with a smooth surface. The average drug encapsulating efficiency and drug loading were 91.89 ± 1.27% and 11.06 ± 0.83% (w/w), respectively. Here, the samples were analysed by UV-Vis spectrophotometer at 420 nm. The standard curve was set up from 2-20 µg/mL. The standard regression equation obtained was A = 0.03836*B - 0.01184, R^2 = 0.997. The higher ratio of hydrophobic groups (such as D,L-LA) in the core of mPEG-PLA micelles promoted efficient loading of CUR in the hydrophobic PLA compartment of mPEG-PLA polymeric micelles by interaction between CUR and hydrophobic group of mPEG-PLA micelles.

Table 2A.1. Characteristics of curcumin-loaded mPEG-PLA micelles.

Sample	mPEG-PLA/ CUR[a]	Particle Size (mean ± SD)	PDI (mean ± SD)	Zeta Potential (mV) (mean ± SD)	DL (%) (mean ± SD)	EE (%) (mean ± SD)
C1	10:0.5	141.86 ± 0.73	0.275 ± 0.87	-25.88 ± 0.45	9.01 ± 2.93	88.37 ± 0.82
C2	9.5:1	178.54 ± 1.03	0.384 ± 0.76	-20.52 ± 0.59	9.65 ± 1.59	85.28 ± 1.73
C3	9.5:1.5	110.79 ± 1.53	0.273 ± 0.19	-29.17 ± 0.81	11.06 ± 0.83	91.89 ± 1.27
C4	9:2	216.92 ± 1.29	0.436 ± 0.92	-22.05 ± 1.05	8.45 ± 1.45	79.56 ± 2.08
C5	8:2.5	198.41 ± 0.85	0.542 ± 0.38	-21.1 ± 0.74	7.33 ± 0.95	70.23 ± 1.52
C6	7.5:3	b	b	b	b	b

a In feed

b Cannot be determined

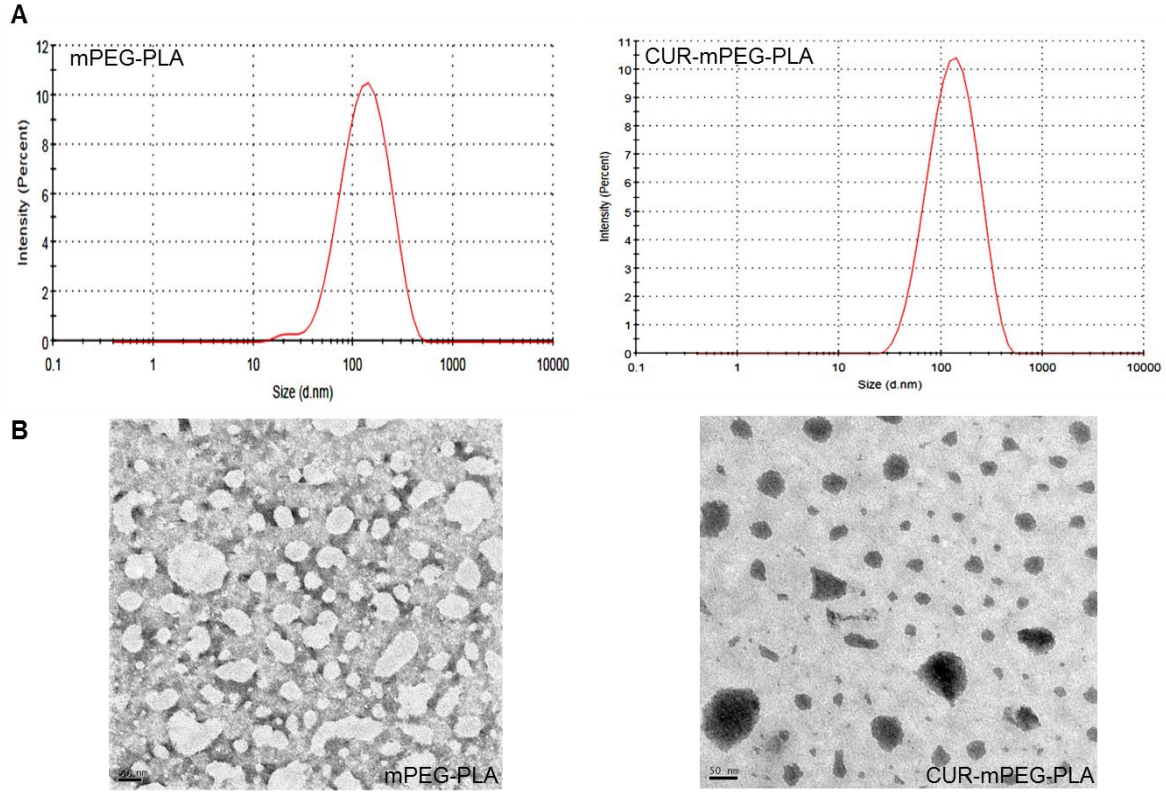

Figure. 2A.5. (A) Particle size distribution of mPEG-PLA and CUR-mPEG-PLA micelles measured by light scattering method. (B) Transmission electron micrograph of mPEG-PLA and CUR-mPEG-PLA micelles.

The physical stability of CUR-mPEG-PLA micelles was evaluated in terms of particle size and zeta potential (Table 2A.2). At the end of two month, CUR-mPEG-PLA micelles maintained colloidal stability and no aggregation was observed. The chemical stability of curcumin in CUR-mPEG-PLA micelles was examined by monitoring the drug content at different time points. For mPEG-PLA-CUR micelles, there was no significant change of curcumin content within two month at 4°C.

The stability of CUR-mPEG-PLA after incubation in DMEM medium at different time points was evaluated shown in Table 2A.3. The particle size of CUR-mPEG-PLA increased from 111.97 ± 3.11 nm (zeta potential: -28.33 ± 1.92) to 127.23 ± 8.23 nm (zeta potential: -23.52 ± 1.16) and 145.06 ± 4.04 nm (zeta potential: -24.52 ± 1.07) after incubation in PBS and DMEM for 72 h, respectively.

The physical form of the drug encapsulated in the polymeric matrix was evaluated by performing DSC analysis. The thermograms of CUR and CUR-mPEG–PLA polymeric micelles are shown in Figure. 2A.6A. Curcumin exhibited an endothermic melting peak at 172.32°C which implied that CUR is in crystal status. Upon encapsulation inside the particles, the melting peak of CUR disappeared. The absence of CUR peak suggested the presence of curcumin in molecular dispersion form in the micellar core compartment (Jain and Jain 2008). The solid dispersion state of the drug inside the polymer promotes its sustained release, which was demonstrated in release study (Bhadra et al. 2003).

Table 2A.2. Stability of curcumin-mPEG-PLA micelles at 4°C and 25°C.

Micelles	Day	Particle Size (mean ± SD)	PDI (mean ± SD)	Zeta Potential (mV) (mean ± SD)	DL (%) (mean ± SD)	EE (%) (mean ± SD)
CUR-mPEG-PLA 4°C	0	110.79 ± 1.53	0.273 ± 0.19	-29.17 ± 0.81	11.06 ± 0.83	91.89 ± 1.27
	10	112.71 ±1.91	0.296 ± 0.25	-21.4 ± 1.24	10.09 ± 1.04	90.24 ± 1.93
	20	113.42 ± 2.44	0.201 ± 0.41	-20.1 ± 1.32	9.91 ± 1.43	89.57 ± 0.74
	30	119.54 ± 2.21	0.367 ± 0.62	-22.8 ± 0.62	9.16 ± 1.04	88.35 ± 2.75
	60	121.82 ± 2.38	0.339 ± 0.17	-21.1 ± 0.74	9.01 ± 0.72	87.54 ± 1.54
CUR-mPEG-PLA 25°C	0	110.79 ± 2.83	0.273 ± 0.19	-29.17 ± 0.81	11.06 ± 0.83	91.89 ± 1.27
	10	180.34 ± 8.40	0.248 ± 1.52	-24.86 ± 1.07	8.94 ± 1.43	80.73 ± 1.04
	20	263.85 ± 4.91	0.443 ± 0.27	-19.24 ± 0.49	5.93 ± 0.25	64.32 ± 1.57
	30	483.42 ± 7.04	0.724 ± 0.88	-13.42 ± 1.30	3.04 ± 1.89	47.68 ± 2.63
	60	-	-	-	-	-

Table 2A.3. Stability of CUR-mPEG-PLA in the presence of DMEM medium containing serum at 37°C.

Time (h)	Particle size (nm)	Zeta-potential (mV)	Encapsulation efficiency (%)
0	111.97 ± 3.11	-28.33 ± 1.92	90.36 ± 1.02
12	112.23 ± 2.81	-29.83 ± 3.24	88.12 ± 2.07
24	113.96 ± 4.97	-25.64 ± 2.82	89.52 ± 1.64
48	117.32 ± 5.86	-26.71 ± 1.94	88.44 ± 1.08
72	125.06 ± 4.04	-28.52 ± 1.07	87.73 ± 2.17

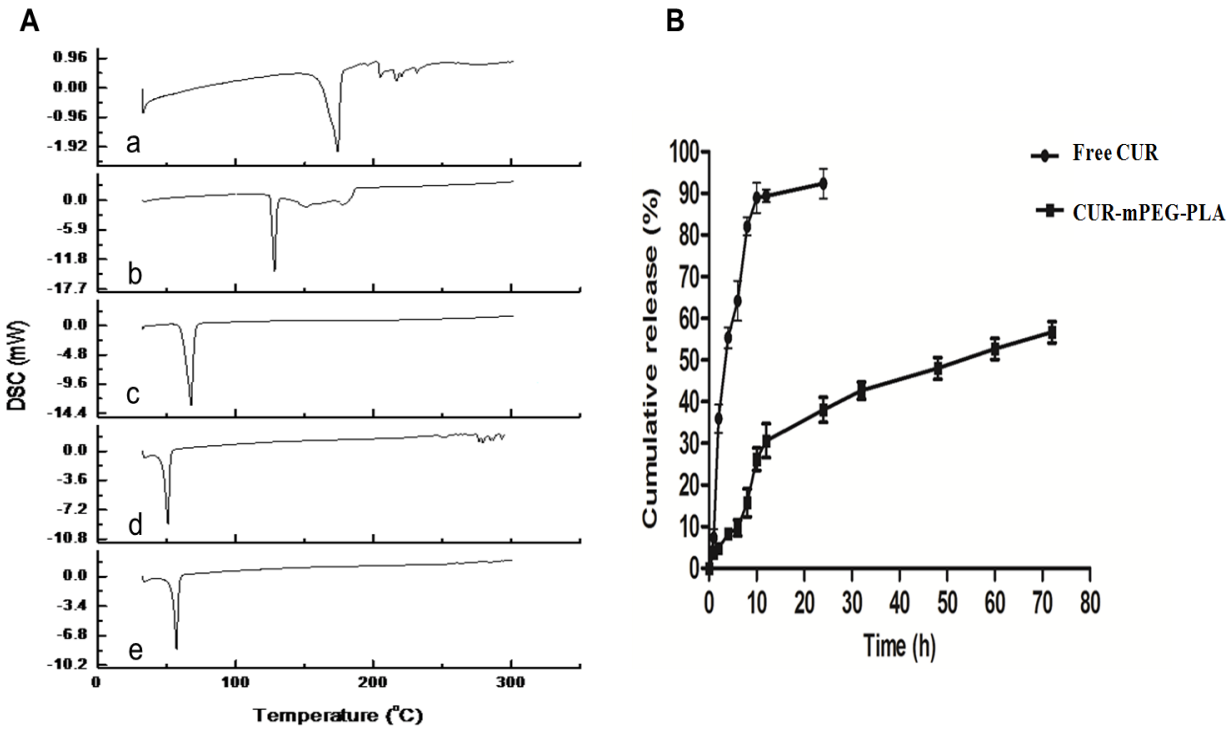

Figure. 2A.6. (A) DSC thermograms of a) Curcumin b) D,L-Lactide c) mPEG-5000 d) mPEG-PLA and e) CUR-mPEG-PLA. (B) Release profiles of CUR from CUR-mPEG-PLA (■) and the free CUR in propylene glycol solution (●) in 5% SDS solution under sink condition at 37°C. Each point represents average ± SD (n = 3).

2A.3.3. *In vitro* release of CUR from micelles

The *in vitro* release of CUR from micelles under sink condition was investigated by dialysis method with 5% SDS solution as release medium. As shown in Figure. 2A.6B, only 9.73% of CUR was released from the CUR-mPEG-PLA micelles within the first 6 h, while about 64.24% of CUR was released from the propylene glycol solution during the same time period. After 72 h, about 45% of the initially incorporated drug still existed in the micelles. To simulate the release process *in vivo*, the release characteristic in *vitro* of CUR-loaded micelles was carried on in physiological saline added with 5% SDS in order to enhance the solubility of CUR. The

release of CUR from micellar system represented sustained release characteristic compared to the relative rapid release in the control group (Figure. 2A.6B). The interaction forces between CUR and carriers made CUR stable in the simulated physiological environment. The results indicated that the micelles showed a sustained-release property for the incorporated CUR, which was similar to the reported studies (Dabholkar et al. 2006).

2A.3.4. Cellular uptake of CUR loaded micelles

The uptake of CUR by murine melanoma cells, B16F10 and human breast adenocarcinoma cells, MDA-MB-231 cells following administration of free CUR and CUR in mPEG-PLA micelles were assessed by visualizing treated cells under fluorescence microscope and by analysing the intensity of CUR-fluorescence in treated cells by flow cytometry. Fluorescence micrograph of B16F10 and MDA-MB-231 cells treated free CUR, and CUR-mPEG-PLA for 1, and 4 h is shown in Figure. 2A.7A and B. No fluorescence was observed in cells treated with blank micelles (data not shown). A negligible increase in fluorescence intensity was observed in cells treated with free CUR (50 and 100 µg/mL) at both the time points of 1 h and 4 h compared to control group. However, CUR-mPEG-PLA could rapidly accumulate in B16F10 and MDA-MB-231 cells even in 1 h, as revealed by the bright green fluorescence. Intensity of fluorescence was further increased significantly following a 4 h treatment with CUR-mPEG-PLA compared to the fluorescence intensity of cells treated for 1 h. The fluorescence intensity was significantly higher in cells treated with 100 µg/mL of CUR in CUR-mPEG-PLA compared to 50 µg/mL of CUR in both the time points of 1 h and 4 h. The dose- and time-dependent increase in the intensity of fluorescence was quantitatively analysed by performing flow cytometry on both, B16F10 and MDA-MB-231 cell lines as shown in Figure. 2A.8A and 8B.

The fluorescence intensity of cells treated with CUR micelles is much stronger than that of free CUR treated cells after incubation for 4 h.

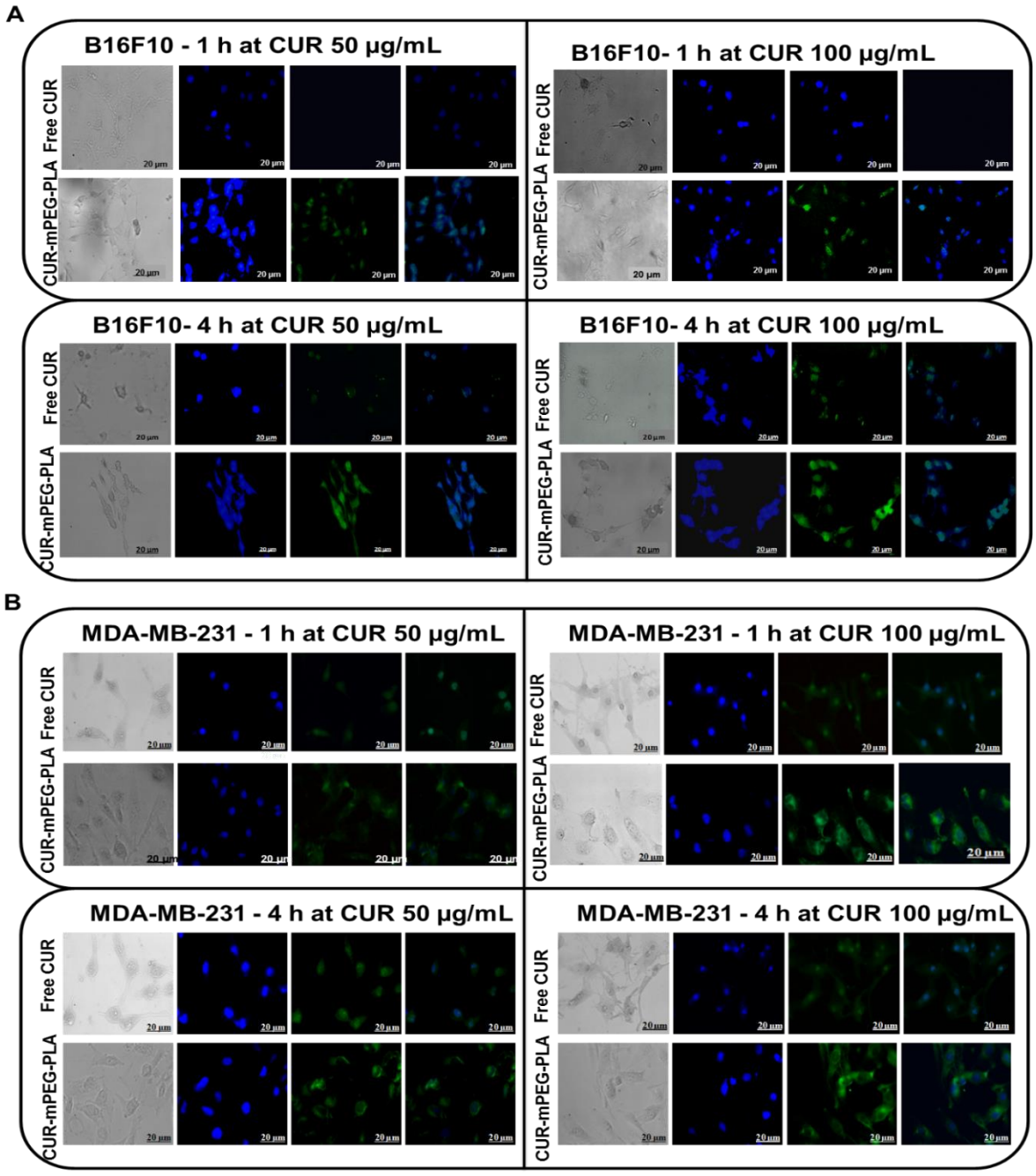

Figure. 2A.7. Fluorescent images of B16F10 (A) and MDA-MB-231 (B) cells incubated with Free CUR (50 and 100 µg/mL) and CUR-mPEG-PLA (50 and 100 µg/mL) for 1 and 4 h respectively. For each panel, the images from left to right showed the bright field image of cells,

cell nuclei stained by using Hoechst 33342 (blue), CUR fluorescence in cells (green) and overlays of both the fluorescence images.

In recent years, several clinical trials have been undergoing utilizing CUR as drug for the treatment of various cancers, including pancreatic cancer, colorectal cancer, and breast cancer (Yang et al. 2013). A randomized, double blind, placebo-controlled clinical trial had been conducted to assess the ability of CUR to reduce severity of dermatitis following radiotherapy for breast cancer (Ryan et al. 2013). To investigate potentiality of the developed formulation for breast cancer treatment, human breast adenocarcinoma cells, MDA-MB-231 had been chosen to assess the cellular uptake and cell viability following treatment with newly developed CUR-loaded nano-formulation. Uptake and viability in a model murine cancer cells (murine melanoma, B16F10) have also been studied parallel. As stated earlier, cells were incubated with 50 and 100 µg/mL free CUR or CUR-mPEG-PLA formulations for 1 and 4 h. These treated cells were evaluated for CUR uptake by flow cytometry visualizing or measuring the CUR fluorescence. Cellular uptake of CUR via CUR-mPEG-PLA formulations was more higher compared to the uptake of free CUR in both the cell lines (Figure. 2A.7A, and B). When treating the cells with blank mPEG-PLA micelles, no fluorescence was detected; however, CUR-mPEG-PLA micelles produced clear fluorescence in the cytoplasm of cells. The major difference between the cellular uptake of free CUR and CUR-mPEG-PLA was that the former located both in the cytoplasm and nucleus, while the latter resided primarily in the cytoplasmic compartment without marked nuclear localization, indicating different internalization mechanisms for both types of curcumin. Similar results were reported using the PEG-polyester micelles and such micelles were often internalized by endocytosis that was time- and concentration-dependent (Shuai et al. 2004; Luo et al. 2002). Once engulfed by the plasma

membrane, the micelles are transported by endosomes and later lysosomes; the acidic endocytic compartments and the presence of large collections of hydrolases facilitate the cleavage of the ester linkage between curcumin and the polymers (Aryal, Hu, and Zhang 2011). The release of lactic acid caused by the degradation of PLA could further lower the environmental pH aiding the release of conjugated curcumin. An excellent model illustrating the difference of cellular internalization of free drug and micelle-incorporated drug was detailed previously (Savić et al. 2003). Yallapu *et al.* demonstrated that the intracellular drug retention of Nano-CUR6 formulation was better than free curcumin (dissolved in DMSO) due to the sustained release of the active (Yallapu et al. 2010). Along with fluorescence micrograph, flow cytometry analysis was performed to quantitatively assess the cellular uptake. The flow cytometry analysis corroborated the results obtained from fluorescence image analysis (Figure. 2A.8A and B).

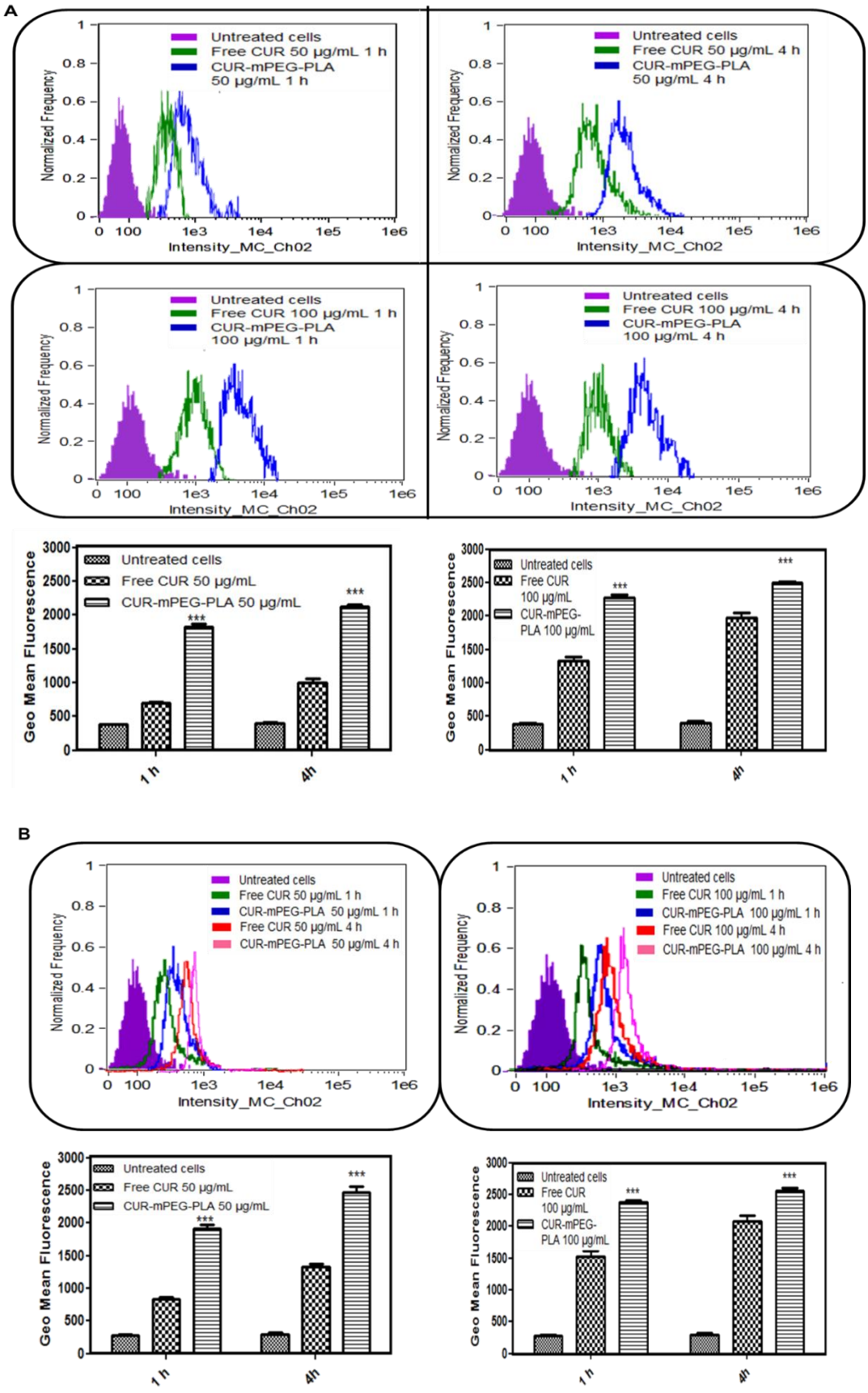
A
Untreated cells
Free CUR 50 µg/mL 1 h
CUR-mPEG-PLA 50 µg/mL 1 h
Free CUR 50 µg/mL 4 h
CUR-mPEG-PLA 50 µg/mL 4 h
Free CUR 100 µg/mL 1 h
CUR-mPEG-PLA 100 µg/mL 1 h
Free CUR 100 µg/mL 4 h
CUR-mPEG-PLA 100 µg/mL 4 h
Normalized Frequency
Intensity_MC_Ch02
Geo Mean Fluorescence
Free CUR 50 µg/mL
CUR-mPEG-PLA 50 µg/mL
Free CUR 100 µg/mL
CUR-mPEG-PLA 100 µg/mL
1 h
4h
***
B
Free CUR 50 µg/mL 1 h
CUR-mPEG-PLA 50 µg/mL 1 h
Free CUR 50 µg/mL 4 h
CUR-mPEG-PLA 50 µg/mL 4 h
Free CUR 100 µg/mL 1 h
CUR-mPEG-PLA 100 µg/mL 1 h
Free CUR 100 µg/mL 4 h
CUR-mPEG-PLA 100 µg/mL 4 h

Figure. 2A.8. Comparison of cellular uptake of Free CUR and CUR-mPEG-PLA micelles by flow cytometry. The B16F10 (A) and MDA-MB-231 (B) cells were incubated with Free CUR and CUR-mPEG-PLA at 50 and 100 µg/mL of CUR for 1 and 4 h, after which the flow cytometry analysis was performed. The cell-associated CUR fluorescence was measured. The representative histogram plot obtained from histogram statistics of the flow cytometry analysis and comparison of the geometric mean of fluorescence of the cells treated with Free CUR or CUR-mPEG-PLA. The data are mean ± SD, averaged from three separate experiments. The significance of difference between the mean was analyzed by Student's t-test, ***$p < 0.001$.

2A.3.5. *In vitro* cytotoxicity

The *in vitro* cytotoxicity of CUR-mPEG-PLA was assessed in both MDA-MB-231 and B16F10 cells. The empty micelles of mPEG-PLA with the same copolymer concentrations as CUR-mPEG-PLA were used as control. CUR in DMSO solution was used to treat the cells of free CUR group. The cells were incubated for either 6 or 24 h in presence of the micelles or free CUR followed by 24 h, and 0 h incubation, respectively and their survival was analyzed using the MTT assay. The viability of MDA-MB-231 and B16F10 cells after incubation with various formulations of CUR and empty micelles was presented in Figure. 2A.9.

Free CUR incubated for 24 h demonstrated higher cytotoxicity in B16F10 cells compared to 6 h treatment. However, time dependent increase in curcumin toxicity was not observed in MDA-MB-231 cell lines. The % cell viability of MDA-MB-231 cells following CUR-mPEG-PLA and free CUR in DMSO solution treatment at CUR-concentration 50 µg/mL for 6 h followed by 24 h incubation were 35.12 ± 8.56%, 65.74 ± 1.09% (Figure. 2A.9C), respectively, while 35.32 ± 6.91%, 76.61 ± 7.83% for B16F10 cells at similar incubation condition (Figure. 2A.9A) (CUR dose of 50 µg/mL at 6 h). Similarly, CUR-mPEG-PLA demonstrated 44.85 ± 3.57% and

32.71 ± 1.08% (Figure. 2A.9D) cell viability compared to 63.35 ± 0.94% and 13.17 ± 0.69% (Figure. 2A.9B) for free CUR at the highest tested CUR dose of 50 µg/mL following 24 h incubation period for MDA-MB-231 and B16F10 cells, respectively. To prove that the cytotoxic effect of CUR-mPEG-PLA micelles is because of the toxicity of CUR, we tested the CUR-free micelles for their effect on cell viability. mPEG-PLA copolymer showed nominal cytotoxicity in highest concentration.

The cytotoxicity of CUR-loaded mPEG-PLA micellar system had been studied in both the cancer cell lines. Two different protocols were followed to determine cell viability following curcumin treatment (Figure. 2A.9). In one study, the cells were treated for 6 h followed by removal of treatment and incubation for 24 h before assessing the cell viability. In the other study, the cells were subjected to CUR-treatment for 24 h before performing cell viability study. Extrapolation of the results obtained following prolonged exposure of cancer cells to a static drug concentration to predict *in vivo* therapeutic efficacy remains questionable as concentration of drug reaching the tumor microenvironment is not static for as long as 24 h. Overall, CUR-mPEG-PLA demonstrated dose-dependent decrease in cell viability. For short term drug treatment (6 h), decreased cell viability of CUR-mPEG-PLA treatment was observed compared to the treatment with free CUR. As free drug gets internalized by simple diffusion process, the internalized drug from the cells is released following removal of the drug from the media. Due to this diffusion, the drug concentration inside the cells was at sub-therapeutic level resulting in minimal cell death in both the cell lines. The CUR loaded in mPEG-PLA micelles were most likely internalized by endocytosis, the common route of internalization for nanocarriers. Cytotoxicity of CUR was higher in mPEG-PLA micelles as micelles delivered CUR in controlled manner, and could not escape out of the cells by diffusion as free drug (Figure. 2A.9A

and C). However, on the contrary in case of 24 h incubation study, the cells were under a static drug concentration, which could allow cells to internalize maximum amount of drugs. Accumulation of drug in presence of unlimited drug supply as free drug would lead to continuous diffusion resulting in higher cell death compared to micellar formulation (considering no complicated mechanism of drug efflux involved), where energy dependent endocytosis could still be a barrier for drug internalization. The cytotoxicity data obtained in B16F10 cells corroborated the prior statement as higher cytotoxicity was observed with free CUR treatment compared to micellar-CUR treatment (Figure. 2A.9D). However, unlike the study with B16F10, MDA-MB-231 cells displayed higher cell death in case of micellar CUR than free curcumin under static drug concentration on cells for 24 h (Figure. 2A.9B). This could be due to the upregulation of multiple drug resistance (MDR) pathways following exposure to high CUR concentration. The internalized free CUR is pumped out constantly by up-regulated MDR-proteins resulting in the lower drug concentration compared to CUR delivered via mPEG-PLA resulting in increased cell viability following free CUR treatment. The finding proved the complexity of pathogenesis in human cancers, and the importance of controlled release of drug in the intracellular compartment which could minimize the rate of over-expression of MDR proteins. In all the cell viability experiments, free mPEG-PLA micelles were analyzed to check their cytotoxicity at the same experimental condition. No marked cytotoxicity was observed following treatment of cells with blank micelles.

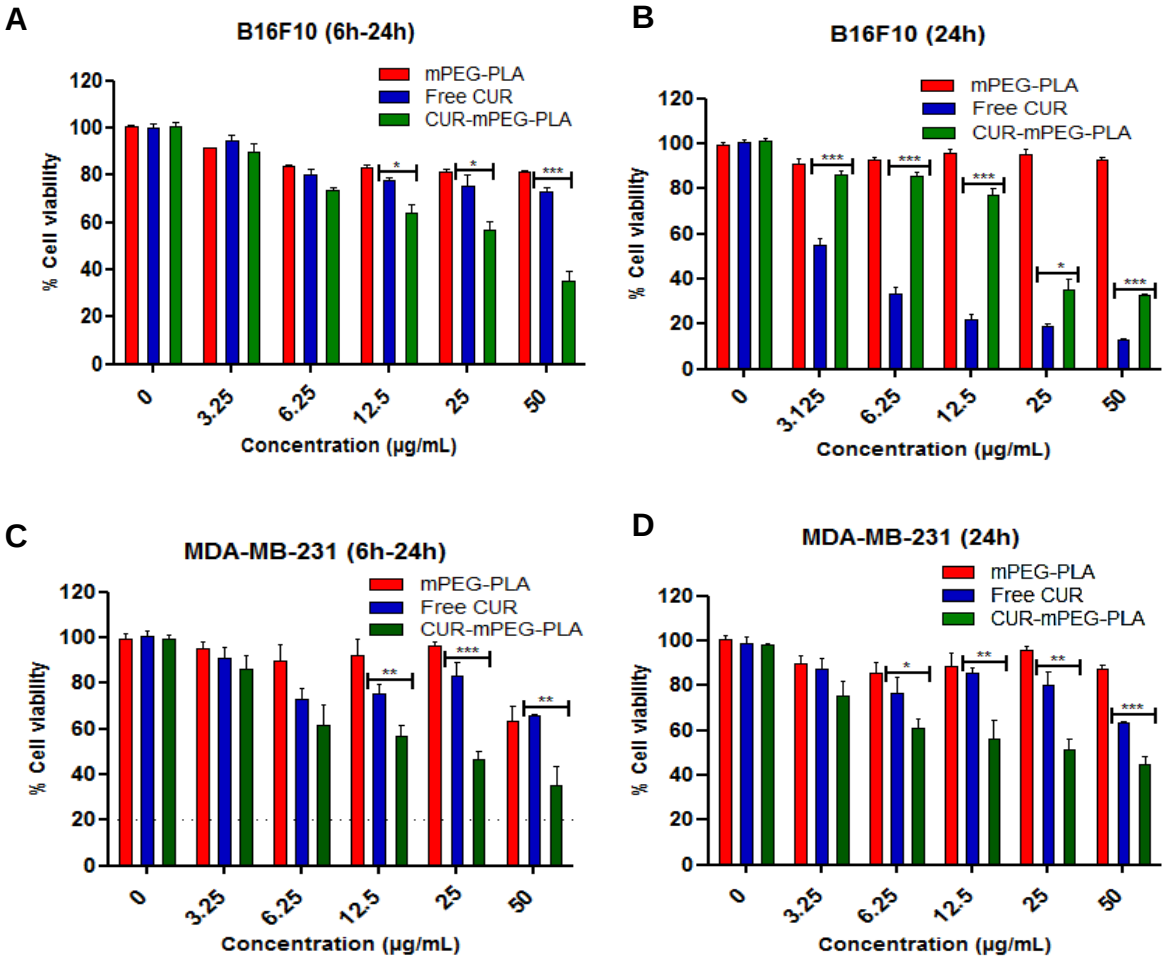

Figure. 2A.9. Assessment of cell viability of B16F10 and MDA-MB-231 cells treated with Free CUR and CUR-loaded micelles at CUR concentration of 0–50 µg/mL for 6 and 24 h. The significance of difference between the mean was analyzed by Student's t-test, *, **, *** indicates <0.05, 0.01 and 0.001, respectively.

2A.4. CONCLUSION

A novel nano-sized polymeric micellar formulation consisting of a block copolymer, methoxy-poly(ethylene glycol)-b-poly(D,L-Lactide) (mPEG-PLA) as a carrier for curcumin has been prepared. As stated earlier, curcumin is a naturally occurring anticancer drug with potential to halt disease progression by several mechanisms. Notably, curcumin has proved to be effective

against wide variety of cancer. However, due to poor solubility and low bioavailability, few curcumin-based formulations have been tested pre-clinically so far. Although nanocarrier-based formulations encapsulating curcumin have been developed in the recent past, their effectiveness has been limited due to their higher particle size and lower penetrating capacity into the cancer cells, resulting in poor therapeutic effects in cancer treatment (Shaikh et al. 2009; Mittal et al. 2007; Anand et al. 2010) The current study demonstrated that the encapsulation of curcumin in mPEG-PLA micelles rendered curcumin completely dispersible in water, thus overcoming the poor water solubility of curcumin. Newly developed CUR-mPEG-PLA micelles have advantages such as small size, narrow size distribution, high encapsulation efficiency, high drug loading, simple preparation method, and good re-solubility. The nanoparticle formulation (CUR-mPEG-PLA) were taken up by the cancer cells efficiently, has shown a greater inhibitory effect on the growth of the metastatic murine (melanoma) and multiple drug resistant human (breast adenocarcinoma) cancers cells compared to free curcumin. In conclusion, the mPEG-PLA polymeric micelles proved to be an efficient carrier for curcumin and the developed curcumin-loaded nano-formulation holds great promise in treatment of metastatic breast cancer.

Chapter 2B

Transferrin-anchored poly(Lactide) based micelles to improve anticancer activity of curcumin in hepatic and cervical cancer cell monolayers and 3D spheroids

ABSTRACT

In recent years, actively targeted drug delivery systems have been utilized in pre-clinical studies for site-specific delivery of drugs, which reduces toxicities associated with chemotherapy. This study reports the preparation of the tumor homing ligand, transferrin (Tf) anchored methoxy-polyethylene glycol-poly(D,L-Lactide) polymeric micelles (Tf-mPEG-PLA). Curcumin which possess wide anti-cancer activity was loaded into the micelles. Tf-CUR-mPEG-PLA with average particle size of 132.16 ± 1.37 nm and encapsulation efficiency of 88.27 ± 2.53% showed a sustained drug release. The efficacy of Tf-CUR-mPEG-PLA was studied *in vitro* in Tf-overexpressing human cervical carcinoma (HeLa) and human hepatoma (HepG2) cells. The mouse embryo fibroblast (NIH-3T3) cells were used as control cells. Tf-CUR-mPEG-PLA showed higher internalization compared to non-targeted micelles (CUR-mPEG-PLA). The curcumin-mediated cytotoxicity increased significantly following Tf-CUR-mPEG-PLA treatment in both the tested cell lines. In NIH-3T3 cells, Tf conjugation did not differ in comparison to the non-targeted micelles. Further, the efficiency of Tf-CUR-mPEG-PLA was studied in three-dimensional (3D) HeLa tumor spheroids. The Tf-CUR-mPEG-PLA was efficiently internalized by the spheroidal structures, causing higher cytotoxicity and apoptosis compared to CUR-mPEG-PLA. These results reveal that the newly developed, Tf-CUR-mPEG-PLA could be employed as an effective chemotherapy in the treatment of Tf- overexpressing cancers.

2B.1. INTRODUCTION

Cancer is a complex disease with multiple pathological hallmarks, which is still a prime cause of mortality worldwide. In spite of our improved knowledge about the disease progression, and invention of newer strategies to combat cancer, eradication of cancer is still elusive. Nanotechnological intervention in the delivery of conventional chemotherapeutic agents holds promise due to various advantages. Nanocarriers encapsulate the non-specifically toxic drugs, thus, reduce their systemic exposure and improve the stability and their biopharmaceutical properties (Peer et al. 2007). Moreover, nanocarriers in the size range of 20-200 nm enters through the leaks in the compromised vasculature and eventually gets accumulated in the tumor microenvironment, and liberate the drugs at the tumor site following enhanced permeation and retention (EPR) phenomena (Matsumura and Maeda 1986; Maeda, Sawa, and Konno 2001; Danhier, Feron, and Préat 2010). However, in order for EPR effect to work, the size and the long circulatory property of the nanocarrier as well as the size of the leaks in the tumor vasculature are primarily important, which could vary significantly among nanocarriers and types of tumors as well (Hillaireau and Couvreur 2009).

Another emerging strategy to improve the targeting of nanocarriers to the cancer cells is by active targeting, i.e., modifying the surface of nanocarriers by tumor homing ligands (Danhier, Feron, and Préat 2010). Transferrin (Tf), a human serum glycoprotein of molecular weight 80 KDa serves as a cargo for iron, which is needed abundantly by the proliferating cancer cells, and therefore, the Tf-receptors (TfR) are over-expressed in many tumors, including hepatic, ovarian, and cervical origins (Muthu et al. 2015; Daniels et al. 2006; Calzolari et al. 2007). The selective localization of TfR to cancer cells compared to normal cells allows development of tumor targeted drug delivery systems, where Tf is anchored on

the surface of the nanocarriers for easy recognition and binding to the TfR (Talekar et al. 2011; Tavano et al. 2013).

Amphiphilic copolymer, methoxy-poly(ethylene glycol)-poly(D,L-Lactide) (mPEG-PLA) have been utilized for the delivery of chemotherapeutic agents by our group and others for cancer treatment (Xiao et al. 2010; Zhan et al. 2010; Kumari et al. 2016). Curcumin, (CUR) a hydrophobic polyphenol derived from *Curcuma longa L*., is a miracle drug with myriads of pharmacological activities, including anticancer, and anti-inflammatory properties. Mechanistically, curcumin inhibits various cell signaling pathways, including NF-κB, Akt, JNK, AP-1 that causes induction of apoptosis in cancer cells. However, curcumin suffers from poor aqueous solubility and bioavailability, which limits its potential application in cancer treatment. (Safavy et al. 2007; Yallapu, Jaggi, and Chauhan 2012; Anand et al. 2007).

Here, we prepared Tf conjugated curcumin-loaded methoxy-poly(ethylene glycol)-poly(D,L-Lactide) micelles (Tf-CUR-mPEG-PLA) to improve the therapeutic efficacy of curcumin for the treatment of cancer. The physicochemical characteristics such as particle diameter, zeta potential, loading capacity, entrapment efficiency, and *in vitro* release of drug from the micelles were investigated. *In vitro* cytotoxicity and cellular association of curcumin-loaded micelles against Human cervical cancer (HeLa) and Human hepatocellular carcinoma (HepG2) cells overexpressing transferrin receptors and mouse embryo fibroblast cells (NIH-3T3, without TfR expression) were assessed using MTT assay and flow cytometry. Further, curcumin-loaded micelles were tested in three dimensional (3D) HeLa spheroids to assess growth inhibition, penetration efficiency and *in vitro* cytotoxicity, live/dead cell assay and apoptosis.

2B.2. MATERIALS AND METHODS

2B.2.1. Materials

Methoxy-poly (ethylene glycol) (MW 5000 Da), 3-(Maleimido) propionic acid N-hydroxysuccinimide ester (MPA), Methoxy-poly (ethylene glycol) amine, D,L-lactide, Curcumin, Transferrin (Tf), tin(II) octoate, 5,5-dithiobis (2-nitrobenzoic acid) (Ellman's reagent), bicinchoninic acid (BCA) kit for protein determination were supplied by Sigma-Aldrich Chemicals (Bangalore, India). Traut's reagent was purchased from Thermo Scientific. Annexin V-FITC Apoptosis analysis Kit and Presto Blue cell viability assay reagent were purchased from Invitrogen (USA). Spectra/Por dialysis membranes (3.5, 12-14, and 100 KDa) were purchased from Spectrum Laboratories, Inc. (USA). Accutase™, Fluoromount-G, and Trypan blue solution and were purchased from Himedia Laboratories (Mumbai, India). All the other chemicals were of analytical reagent grade.

Dulbecco's Modified Eagle Medium (high glucose) cell culture medium, fetal bovine serum (FBS), Penicillin-Streptomycin, trypsin-EDTA, cell culture flasks, and plates were purchased from Himedia Laboratories (Mumbai, India).

2B.2.2. Cell lines

Human hepatocellular carcinoma (HepG2), Human cervical cancer (HeLa) and Mouse embryo fibroblast (NIH-3T3) cells were procured from National Center for Cell Sciences (Pune, India). All media were supplemented with 10% FBS and 1% penicillin-streptomycin solution. Cells were maintained at 37°C in a humidified incubator containing 5% CO_2.

2B.2.3 Synthesis of Tf-modified mPEG-PLA conjugate

2B.2.3.1. Synthesis of mPEG-PLA copolymer

The methoxy-polyethylene glycol-poly(D,L-Lactide) (mPEG-PLA) copolymer was synthesized according to a previously reported method (Kumari et al. 2016). In brief, D,L-Lactide (0.4 g) and methoxy-polyethylene glycol (1 g) were dissolved in toluene (3 mL) in presence of tin(II) octoate (0.008% w/w). The reaction mixture was kept for 6 h at 160°C in oil bath. After 6 h, the crude reaction mixture was dissolved in tetrahydrofuran (THF) and precipitated with diethyl ether (cold). The obtained product was dried at room temperature (RT), dispersed and dialyzed against distilled water for 24 h by using molecular weight cut-off (MWCO: 12-14,000 Da, Spectrum Co. USA) to remove the unreacted materials. The solid mass of mPEG-PLA was obtained by lyophilization and characterized by ^{1}H NMR spectrometer (AVANCE model, Germany) at 300 MHz.

2B.2.3.2. Synthesis of mal-PEG-PLA

The block copolymer maleimide-polyethylene glycol–poly(D,L-Lactide) (mal-PEG-PLA) was synthesized by following a method reported previously (Liu et al. 2010). To prepare amine-polyethylene glycol-poly(D,L-Lactide) (amine-PEG-PLA), 100 mg of amine-polyethylene glycol and 40 mg of D,L-Lactide were heated at 160°C for 6 h in presence of tin(II) octoate (0.008% w/w) in toluene. The obtained reaction mixture was dissolved in THF, and precipitated by diethyl ether (ice-cold). The crude product was dialyzed against water using a regenerated cellulose membrane of MWCO 12-14,000 Da (Spectrum Co. USA). The product was lyophilized to obtain solid mass of amine-PEG-PLA.

Next, amine-PEG-PLA (100 mg) and 3-(Maleimido) propionic acid *N*-hydroxysuccinimide ester (MPA; 17.6 mg) was dissolved in dimethyl formamide (10 mL, DMF), and kept under

magnetic stirring overnight at RT. Finally, the MPA-conjugated product was dialyzed cellulose ester membrane (MWCO: 12-14,000 Da) against water for 2 days. The dialyzed sample was freeze dried to obtain mal-PEG-PLA.

2B.2.3.3. Synthesis of thiolated-Tf

Tf (6.61 mg) was thiolated for 20 min with 2-iminothiolane in sodium borate buffer (150 mM, pH 8.0) in a molar excess of 40:1, supplied with 0.1 mM EDTA. The amount of thiol groups were calculated by Ellmann's Reagent following manufacturer's instruction (Ellman 1959).

2B.2.4. Preparation of curcumin-loaded micelles (CUR-mPEG-PLA and Tf-CUR-mPEG-PLA)

Targeted and non-targeted micelles were prepared using mixture of mPEG-PLA and mal-PEG-PLA via thin film hydration technique. In brief, 1 mg curcumin, 10 mg mPEG-PLA and 0.256 mg mal-PEG-PLA were dissolved in chloroform (1 mL), the reaction mixture was evaporated using rotary evaporated at 37°C. The thin film was hydrated using 400 µL of HEPES (10 mM) buffer. The thiolated Tf was added to the hydrated film and stirred overnight at 4°C. Then, the product was dialyzed against HEPES buffer (10 mM) for 4 h using dialysis bag (MWCO: 100 KDa) to remove the unconjugated Tf. The non-targeted micelles were prepared using mPEG-PLA following the same method except addition of transferrin (CUR-mPEG-PLA). The schematic for synthesis is represented in Figure. 2B.1. The amount of Tf in the Tf-CUR-mPEG-PLA micelles was calculated by bicinchoninic acid (BCA) protein assay using pure transferrin as a standard.

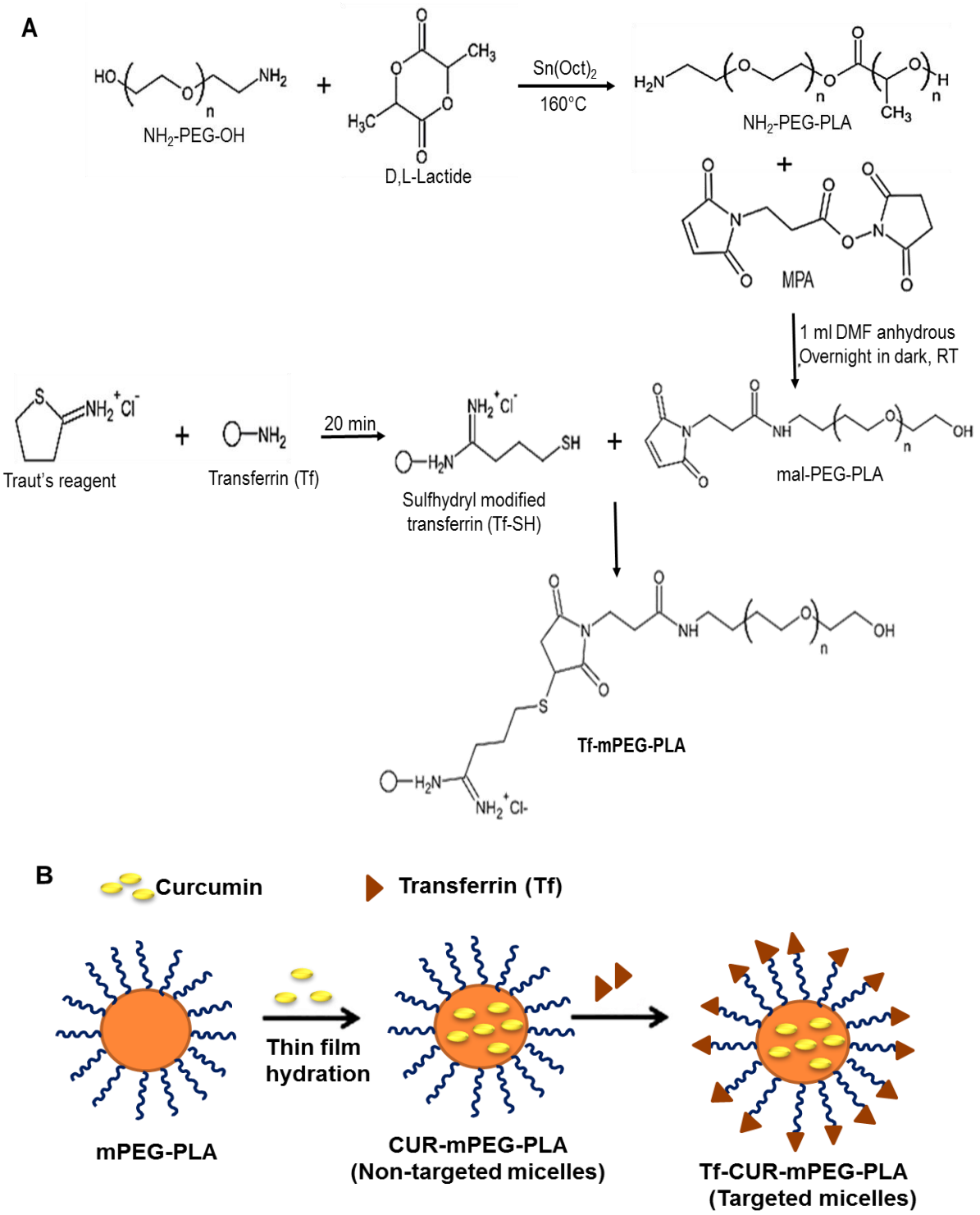

Figure. 2B.1. (A) Scheme for the synthesis of Tf-mPEG-PLA; (B) Schematic illustration of the preparation of Tf-CUR-mPEG-PLA by thin film hydration technique.

2B.2.5. Characterization of curcumin-loaded micelles

2B.2.5.1. Particle size and zeta potential

The average particle diameter and polydispersity index of CUR-mPEG-PLA and Tf-CUR-mPEG-PLA micelles were determined by zetasizer (Nano ZS90, Malvern Instruments Ltd., UK) at 25°C. All the measurements were analyzed in triplicates and data were expressed as the mean ± standard deviation (SD).

2B.2.5.2. Determination of Drug loading and Encapsulation efficiency

The encapsulation efficiency and loading of curcumin in the micelles was analyzed by UV-Visible spectrophotometer (Spectramax™, Microplate reader, Molecular Devices, US). The calibration curve of curcumin was constructed with $R^2 = 0.999$ over a concentration range of 2-20 µg/mL. All samples were analyzed in triplicate. The encapsulation efficiency (EE) and drug loading (DL) of CUR-mPEG-PLA and Tf-CUR-mPEG-PLA micelles were determined using following equations:

$$\boldsymbol{EE}\ (\%) = \frac{\boldsymbol{We}}{\boldsymbol{Wt}}\ \boldsymbol{X}\ \boldsymbol{100} \qquad (1)$$

$$\boldsymbol{DL}\ (\%) = \frac{\boldsymbol{We}}{\boldsymbol{We + Wp}}\ \boldsymbol{X}\ \boldsymbol{100} \qquad (2)$$

W_e, is the amount of curcumin encapsulated in micelles, $W_{t,\ is}$ total amount of curcumin used, and W_p is the weight of the polymer after lyophilization.

2B.2.5.3. Stability of micelles

The stability of Tf-CUR-mPEG-PLA micelles was determined by monitoring the particle size and drug content at 4°C. The stability of Tf-CUR-mPEG-PLA micelles was also evaluated after incubating the micelles at 37°C for 24 h. At different time points, particle size was and

zeta potential were determined as described above. For drug content, aliquots of each sample withdrawn and analyzed by UV-Visible spectrophotometer.

2B.2.6. *In Vitro* release profile of curcumin from CUR-mPEG-PLA and Tf-CUR-mPEG-PLA

The *in vitro* release of curcumin from CUR-mPEG-PLA and Tf-CUR-mPEG-PLA was investigated by dialysis method under sink condition as described previously (Kumari et al. 2016). One milliliter samples (Free curcumin dissolved in propylene glycol, Tf-CUR-mPEG-PLA and CUR-mPEG-PLA at a curcumin concentration of 50 μg/mL) were added into the dialysis bags (MWCO: 3.5 KDa) and dropped in beakers containing 40 mL of phosphate buffer (PBS, pH 7.4) individually, and stirred at 150 rpm at 37˚C. At definite time points, 1 mL samples were withdrawn from the receptor medium and concentration of curcumin in the supernatant was measured by UV-Visible spectrophotometer method as described above.

2B.2.7. Cell culture

HeLa, HepG2, and NIH-3T3 cells were cultured in DMEM added with 10% fetal bovine serum (FBS) and 1% penicillin-streptomycin solution. All cell lines were maintained in an incubator with humidified atmosphere at 37˚C and 5% CO_2.

2B.2.7.1. Cellular uptake of CUR-mPEG-PLA and Tf-CUR-mPEG-PLA

The cellular uptake of targeted and non-targeted micelles were evaluated using fluorescence microscopy and flow cytometry analysis. For qualitative cellular uptake, three different cell lines (HeLa, HepG2, and NIH-3T3) were seeded onto circular cover glass placed in 12-well plates and allowed to grow until 70-80% confluency. Next, the cells were treated with free curcumin, CUR-mPEG-PLA and Tf-CUR-mPEG-PLA at a curcumin concentration of 50

μg/mL for 1 and 4 h. Following the incubation period, cells were washed thoroughly with PBS, treated with DAPI solution (1 μg/mL) for 5 min, and fixed with para-formaldehyde (4%, 500 μL/well) for 10 min at RT. The cover slips were washed again and mounted cell-side down on glass slide using mounting medium (Fluoromount-G; Sigma Aldrich). The cellular uptake of various treatments was visualized by fluorescence microscope (Leica Microsystems, Germany). The LSM image files were processed using Image J software, NIH, Rockville, MD.

For quantitative estimation of cellular uptake by flow cytometry, HeLa, HepG2, and NIH-3T3 cells were seeded in 6-well plates at 5 X 10^5/well. Next day, cells were treated with CUR-mPEG-PLA, Tf-CUR-mPEG-PLA and free curcumin for 1 and 4 h at a curcumin concentration of 50 μg/mL at 37°C. The culture media was discarded after incubation and cells were washed with PBS. Then, cells were harvested using trypsin, centrifuged and pellet was resuspended in PBS, pH 7.4 (200 μL). During sample run, 10,000 cells (gated events) were collected for each sample and analyzed using flow cytometer (Amnis Flowsight, United States). The fluorescence intensity of curcumin was detected with logarithmic settings (Intensity_MC_Ch2; Ex 488 and Em 520-530 nm).

2B.2.7.2. Assessment of internalization pathways

The HeLa cells, and HepG2 cells were first pretreated with inhibitors (30 μM chlorpromazine, CPZ) for 30 min at 37°C. Then, cells were thoroughly washed with PBS (pH 7.4) and treated with Tf-CUR-mPEG-PLA. Endocytosis studies of micelles were analyzed as described above.

2B.2.7.3. Assessment of transferrin receptor-mediated internalization of Tf-CUR-mPEG-PLA

The specificity of transferrin receptor-mediated internalization of Tf-CUR-mPEG-PLA were examined by pre-incubating the HeLa and HepG2 cells with free Tf (2 mg/mL) for 1 h before treatment with the formulation. Cellular uptake was determined as described above.

2B.2.7.4. Cytotoxicity of CUR-mPEG-PLA and Tf-CUR-mPEG-PLA

For cytotoxicity assay by MTT method, HeLa, HepG2, and NIH-3T3 cells (5 X 10^3/well) were seeded in 96-well plates. Next day, cells were incubated with free curcumin, CUR-mPEG-PLA and Tf-CUR-mPEG-PLA at curcumin concentrations (3.125-50 µg/mL) for 6 and 24 h, respectively. Subsequently, the media was removed after 6 h in one plate and incubated for further 24 h. After being incubated for 24 h, media was discarded and cells were treated with 50 µL of MTT solution (5 mg/mL in serum/phenol red free DMEM) for another 4 h. Then, the solution was discarded and 150 µL of DMSO was added to dissolve the formazan crystals. Absorbance at 570 nm was measured using microplate reader (Spectramax™, Microplate reader, Molecular Devices, US) as reference wavelength (630 nm). The cell viability percentage of cells incubated with formulation was calculated as the ratio of their absorbance at 570 nm over the control cells without any treatment.

2B.2.8. Spheroid culture

In vitro HeLa spheroid model was prepared using liquid overlay method as reported previously (Sriraman et al. 2016). To prepare spheroids, 50 µL of sterilized agar solution (1.5% w/v) was added per well in 96-well plate, and kept for drying (30 min). HeLa cells (1 X 10^4/well) were seeded in 96-well plates pre-coated with agar. Then, plates were centrifuged at

1000 rcf for 15 min. When the spheroid formation was confirmed (5 days after seeding the cells), the spheroids of size 400-500 μm were used for study.

2B.2.8.1. Inhibitory effect on HeLa spheroids

The spheroids were incubated with free curcumin, CUR-mPEG-PLA, and Tf-CUR-mPEG-PLA at a curcumin concentration of 50 μg/mL for 24 h. After 24 h, the culture media was replaced. Further, the media was replaced every other day. The growth inhibition of the HeLa spheroids was studied by measuring the dimensions of HeLa spheroids using fluorescence microscope (Leica Microsystems, Germany) with a 10X objective lens. The data is reported as the mean diameter of four spheroids ± SD.

2B.2.8.2. Penetration of micelles in spheroids

The HeLa spheroids were prepared in 8-well cell culture plate. Penetration of free curcumin, CUR-mPEG-PLA, and Tf-CUR-mPEG-PLA micelles in 3D spheroids was determined after 1 and 4 h incubation with 50 μg/mL of curcumin formulations by confocal microscopy. Photo micrographs of spheroids were captured in 8-well cell culture plates at 10X magnification. Distribution of green fluorescence in the spheroids was studied by confocal microscope (Leica Microsystems, Germany) using Z-stack imaging with 10 μm intervals.

2B.2.8.3. Spheroidal cellular internalization of curcumin-loaded micelles

Cellular internalization of micelles in spheroidal cells was analyzed using flow cytometer. 5-day old HeLa spheroids were incubated with free curcumin, CUR-mPEG-PLA, and Tf-CUR-mPEG-PLA micelles for 1 and 4 h. After the incubation period, spheroids were washed thoroughly with PBS (pH 7.4). 10 spheroids were collected into each tube to obtain sufficient cell count. Accutase™ cell detachment solution (50 μL) was added and kept for 10 min at

37°C with gentle shaking, and the cell suspension was transferred in 15 mL tubes. Accutase™ activity was inhibited by the addition of FBS (500 µL) in tubes. Then, cells were centrifuged for 5 min at 1000 rpm. The obtained cell pellet was re-suspended in PBS, pH 7.4 (200 µL). The intracellular fluorescence of curcumin was determined using flow cytometer.

2B.2.8.4. *In vitro* cytotoxicity in spheroids

In vitro cytotoxicity in spheroids was evaluated by Presto blue assay according to the manufacturer's protocol. The spheroids compact in appearance (typically 3-5 days after seeding) were treated with CUR-mPEG-PLA, Tf-CUR-mPEG-PLA micelles and free curcumin (concentration: 50 µg/mL) for 24 h. Following this, the spheroids were washed with PBS and treated with Accutase™ cell detachment solution (50 µL), incubated for 10 min at 37°C with gentle shaking, and the cell suspension was transferred in 15 mL tubes. Accutase™ activity was inhibited by the addition of FBS (500 µL) in tubes. Then, cells were centrifuged for 5 min at 1000 rpm. The obtained cell pellet was re-suspended in DMEM medium (90 µL) and Presto Blue reagent (10 µL), and kept at 37°C for 2 h. The absorbance was measured at 570 nm using 600 nm as reference. Data was generated in triplicates with each triplicate consisting of 10 spheroids.

2B.2.8.5. Apoptosis in spheroidal cells

The apoptosis assay using AnnexinV/PI fluorescence labeling kit was conducted according to the protocol supplied by manufacturer. HeLa spheroids grown in 96-well plates were incubated with free curcumin, CUR-mPEG-PLA, and Tf-CUR-mPEG-PLA micelles for 24 and 48 h at 37°C respectively. The culture media was removed, treated with Accutase™ solution and neutralized with FBS. The cells were centrifuged at 1000 rpm for 5 min. The cell pellet was collected and suspended in Annexin V binding buffer (100 µL). AnnexinV-FITC (5

μL) and PI (10 μL) were added to each sample and kept for 15 min in dark. Finally, the cell suspension was diluted with AnnexinV binding buffer to make up to 500 μL and evaluated using the flow cytometer (Amnis Flowsight, USA) in Ch02 and Ch04 representing FITC and PI channels, respectively. The untreated spheroids were analyzed in same manner.

2B.2.8.6. Live/Dead cells assay in spheroidal cells

The LIVE/DEAD viability/cytotoxicity study was performed to evaluate the live and dead cell population based on esterase activity and membrane integrity. This study involves the use of calcein blue AM (acetomethoxy derivate of calcein), commonly employed cell biomarker that hydrolyzes inside the cell by endogenous esterase resulting in the formation of a highly negative-charged blue fluorescent calcein that resides inside the cytoplasm of live cells. The red fluorescent propidium iodide (PI) enters the cell through broken membranes and attaches with the nucleic acids (Akasov et al. 2016). The Live/dead assay was a qualitative study to observe the cytotoxic effect of the Tf-CUR-mPEG-PLA and CUR-mPEG-PLA micelles compared to free curcumin. HeLa spheroids were treated with free curcumin, CUR-mPEG-PLA, and Tf-CUR-mPEG-PLA at a curcumin concentration of 50 μg/mL. After 24 h, spheroids were washed with PBS (pH 7.4), stained with the assay reagents, calcein blue AM (2 μM) and propidium iodide (4 μM). The incubation was continued for 30 min at 37◦C. The spheroids were then visualized and imaged using fluorescence microscope (Leica Microsystems, Germany). The excitation wavelengths were 488 nm for Calcein blue AM, and 543 nm for PI. The emitted fluorescence signals were collected in 500-530 nm for Calcein blue AM and 560-650 nm for PI. The confocal images were processed in Leica software.

2B.2.9. Statistical analysis

The data were assessed for statistical significance using Student's t-test, calculated with the Graph Pad prism 5 software (GraphPad Software, Inc, San Diego, CA). All numerical data *in vitro* are expressed as mean ± SD, n = 3 or 4. Any p values less than 0.05 was considered statistically significant. *, **, *** in figures indicated p values <0.05, 0.01 and 0.001, respectively.

2B.3. RESULTS AND DISCUSSION

2B.3.1. Synthesis and characterization of mPEG-PLA and mal-PEG-PLA

The mPEG-PLA copolymer was synthesized by ring opening polymerization of methoxy-polyethylene glycol and D,L-lactide. The ring opening polymerization is a reliable method to polymerize monomers with lactone ring, where hydroxyl-terminated PEG acts as an initiator. Mono-hydroxylated PEG was used to obtain polymerization in one terminal point in PEG. mal-PEG-PLA was synthesized by using MPA as cross-linking agent, which readily reacted with amine-terminated PEG-PLA. The thiolated transferrin (Tf-SH) was reacted with the mal-PEG-PLA to yield Tf-mPEG-PLA. The reaction between thiol group and maleimide functionalized polymer is rapid with a high percentage yield in corroboration with previous report (Gijsens et al. 2002). The amount of transferrin present in targeted micelles was determined using bicinchoninic acid (BCA) protein assay with pure transferrin as standard (Anabousi et al. 2005). The conjugation efficiency of Tf to mPEG-PLA was found to be ~ 67% by BCA assay.

2B.3.2. Physico-chemical characterization of CUR-mPEG-PLA and Tf-CUR-mPEG-PLA

The size distributions of CUR-mPEG-PLA and Tf-CUR-mPEG-PLA micelles were measured by DLS (Figure. 2B.2). The average diameter and polydispersity index (PDI) of CUR-mPEG-PLA was 106.05 ± 0.93 nm and 0.209, respectively. The size of the micelles was increased to 132.16 ± 1.37 nm after conjugation with transferrin (Table 1). This observation is in corroboration with previous report, where conjugation of ligands on the nanocarrier surface resulted in increase of the particle size (Tavano et al. 2013). The zeta potentials of CUR-mPEG-PLA and Tf-CUR-mPEG-PLA were -8.32 ± 1.71 mV and -21.39 ± 0.64 mV, respectively. Due to the conjugation of negatively charged transferrin to surface of micelles, there is a decrease in the zeta potential (Vesterberg and Breig 1981). The EE and DL of CUR-mPEG-PLA and Tf-CUR-mPEG-PLA were 91.89 ± 1.26%, 17.18 ± 1.62%, and 88.27 ± 2.53%, 14.94 ± 0.95%, respectively (Table 1).

Tf-CUR-mPEG-PLA micelles were stable and did not show any signs of drug precipitation when stored at 4°C. There was no significant change in particle size and drug content of micelles during the period of study. Tf-CUR-mPEG-PLA micelles showed no change in particle size and drug content after incubation at 37°C for 24h. The stability of the micelles with high encapsulation efficiency is might be due to the effectiveness of mPEG-PLA micelles in solubilizing such lipophilic drugs.

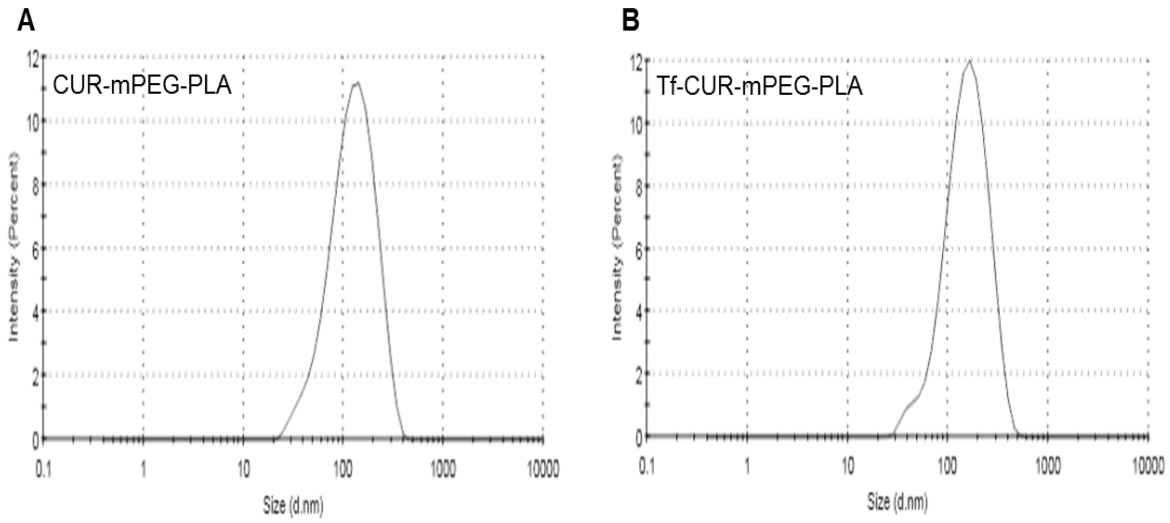

Figure. 2B.2. Particle size distribution of (A) CUR-mPEG-PLA and (B) Tf-CUR-mPEG-PLA micelles.

Table 2B.1. Particle size, polydispersity, zeta potential, encapsulation efficiency and curcumin-loading of the Tf-CUR-mPEG-PLA and CUR-mPEG-PLA micelles**.**

Micelles	**Particle Size (nm)**	**Poly dispersity**	**Zeta potential (mV)**	**Encapsulation efficiency (%)**	**Drug Loading (%)**
Targeted micelles (Tf-CUR-mPEG-PLA)	132.16 ± 1.37	0.205	-21.39 ± 0.64	88.27 ± 2.53	14.94 ± 0.95
Non targeted micelles (CUR-mPEG-PLA)	106.05 ± 0.93	0.239	-8.32 ± 1.71	91.89 ± 1.26	17.18 ± 1.62

2B.3.3. *In Vitro* release of curcumin

The release behavior of curcumin from CUR-mPEG-PLA and Tf-CUR-mPEG-PLA were measured by dialysis method in PBS (pH 7.4) at 37˚C. The medium was refreshed after every

time point to maintain a sink condition. As shown in Figure. 2B.3. curcumin showed sustained release behavior from CUR-mPEG-PLA and Tf-CUR-mPEG-PLA. More than 90% curcumin was released from free curcumin within 12 h, while the release of curcumin from CUR-mPEG-PLA and Tf-CUR-mPEG-PLA was sustained up to 72 h. Due to the insolubility of curcumin in water, free curcumin solution was prepared by dissolving curcumin in propylene glycol. The result clearly indicated that poly(Lactide) core stably accommodated the hydrophobic drug resulting in controlled drug release.

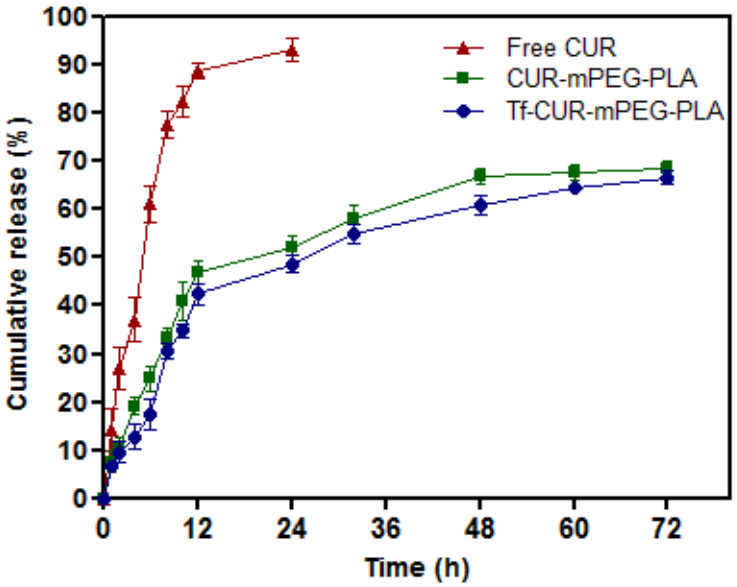

Figure. 2B.3. Curcumin release kinetics from free curcumin in propylene glycol, CUR-mPEG-PLA and Tf-CUR-mPEG-PLA in PBS (pH 7.4) at 37°C. Data represents mean ± S.D (n=3).

2B.3.4. *In Vitro* Cellular Uptake

The cellular uptake of CUR-mPEG-PLA and Tf-CUR-mPEG-PLA by HeLa, HepG2, and NIH-3T3 was evaluated using fluorescence microscopy and flow cytometry. As shown in

Figure. 2B.4A and B, Tf-CUR-mPEG-PLA treated HeLa and HepG2 cells displayed higher fluorescence compared to CUR-mPEG-PLA treated cells, whereas the fluorescence intensity were not so different in NIH-3T3 cells (Figure. 2B.4C). This implies that the higher internalization of Tf-CUR-mPEG-PLA micelles by HeLa and HepG2 cells was through the over-expressed transferrin receptors on their surface, which captured Tf-anchored, Tf-CUR-mPEG-PLA and caused TfR-mediated endocytosis. Owing to the normal expression of TfR, NIH-3T3 cells did not display drastic preferential cellular accumulation for Tf-CUR-mPEG-PLA. However, slight preference in accumulation for Tf-CUR-mPEG-PLA was observed in NIH-3T3 cells compared to CUR-mPEG-PLA. This could be due to the presence of protein on the surface, which causes non-specific interaction with the receptors on cellular surface. On the other hand, presence of non-ionic PEG on CUR-mPEG-PLA surface hinders cellular attachment resulting in less cellular internalization compared to Tf-CUR-mPEG-PLA. The geometric mean fluorescence of HeLa cells incubated with Free curcumin, CUR-mPEG-PLA and Tf-CUR-mPEG-PLA were 8721.72 ± 1.08, 33135.81 ± 0.93, 76324.44 ± 1.63 for 1 h and 7829.74 ± 0.86, 42368.65 ± 0.98, 91472.73 ± 1.82 for 4 h, respectively (Figure. 2B.5A). The geometric mean fluorescence in HepG2 cells treated with Free curcumin, CUR-mPEG-PLA and Tf-CUR-mPEG-PLA were 7865.17 ± 1.38, 16074.03 ± 0.68, 62474.87 ± 1.04 for 1 h and 14174.35 ± 1.46, 55952.61 ± 0.91, 75542.48 ± 1.97 for 4 h, respectively (Figure. 2B.5B). A decrease in geometric mean fluorescence was seen in NIH3T3 cells treated with Tf-CUR-mPEG-PLA. The geo mean values for the treatments of Free curcumin, CUR-mPEG-PLA and Tf-CUR-mPEG-PLA was 1333.32 ± 2.31, 2686.55 ± 1.65, 4228.33 ± 2.06 for 1 h, and 3147.54 ± 1.75, 5564.65 ± 1.03, 7542.45 ± 2.49 for 4 h, respectively (Figure. 2B.5C). The competitive inhibition study was performed using excess free Tf pre-treatment, which blocked

the TfR. The cellular fluorescence intensity following Tf-CUR-mPEG-PLA treatment was decreased after pre-incubation with excess free Tf. The above results confirmed the TfR mediated uptake of targeted Tf-CUR-mPEG-PLA micelles. Further, the uptake of Tf-CUR-mPEG-PLA was inhibited by CPZ, a clathrin-mediated endocytosis pathway inhibitor as shown in Figure. 2B.4D, which displayed fluorescence images of HeLa and HepG2 cells after incubation with Tf-CUR-mPEG-PLA micelles with, or without, endocytosis inhibitor CPZ. The results from flow cytometer showed the same internalization mechanism.

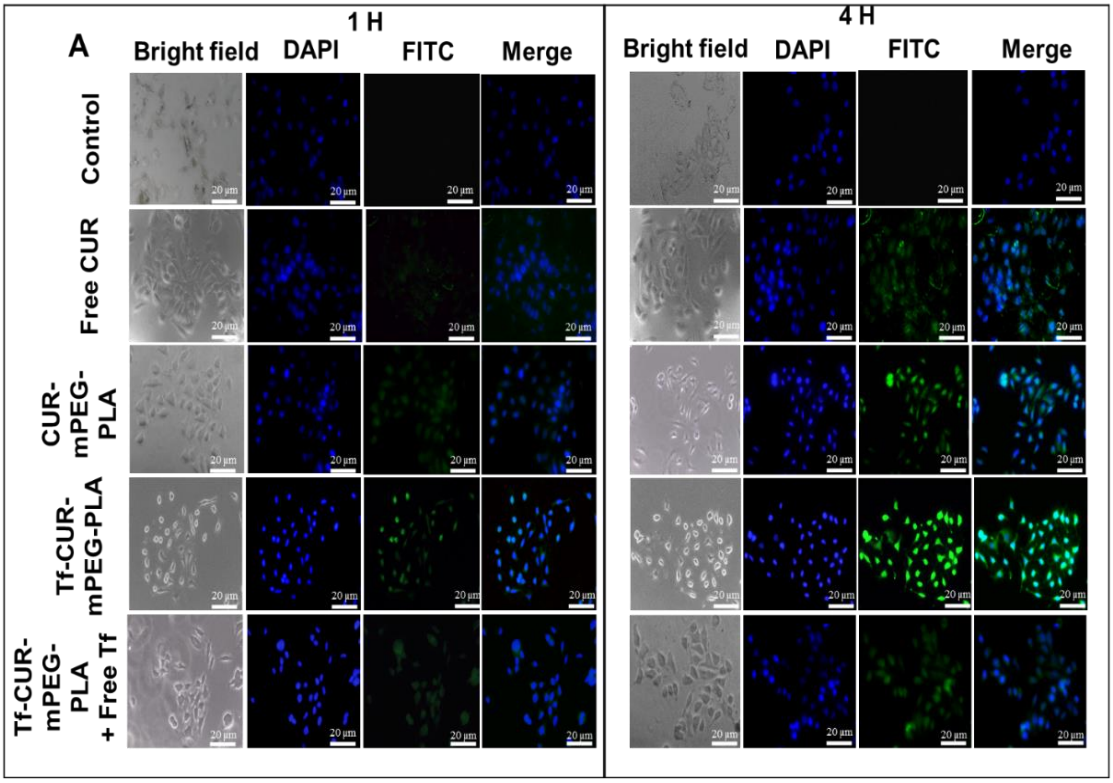

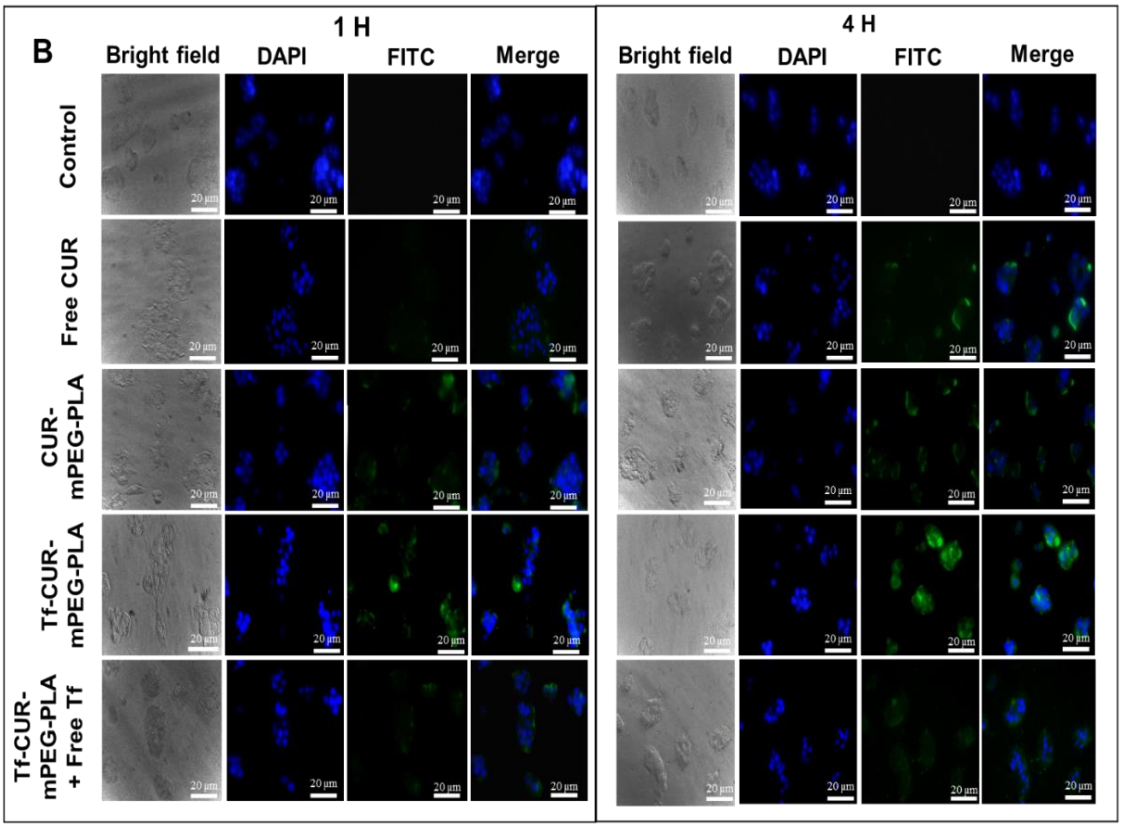
B
1 H
4 H
Bright field
DAPI
FITC
Merge
Control
Free CUR
CUR-mPEG-PLA
Tf-CUR-mPEG-PLA
Tf-CUR-mPEG-PLA + Free Tf
20 μm

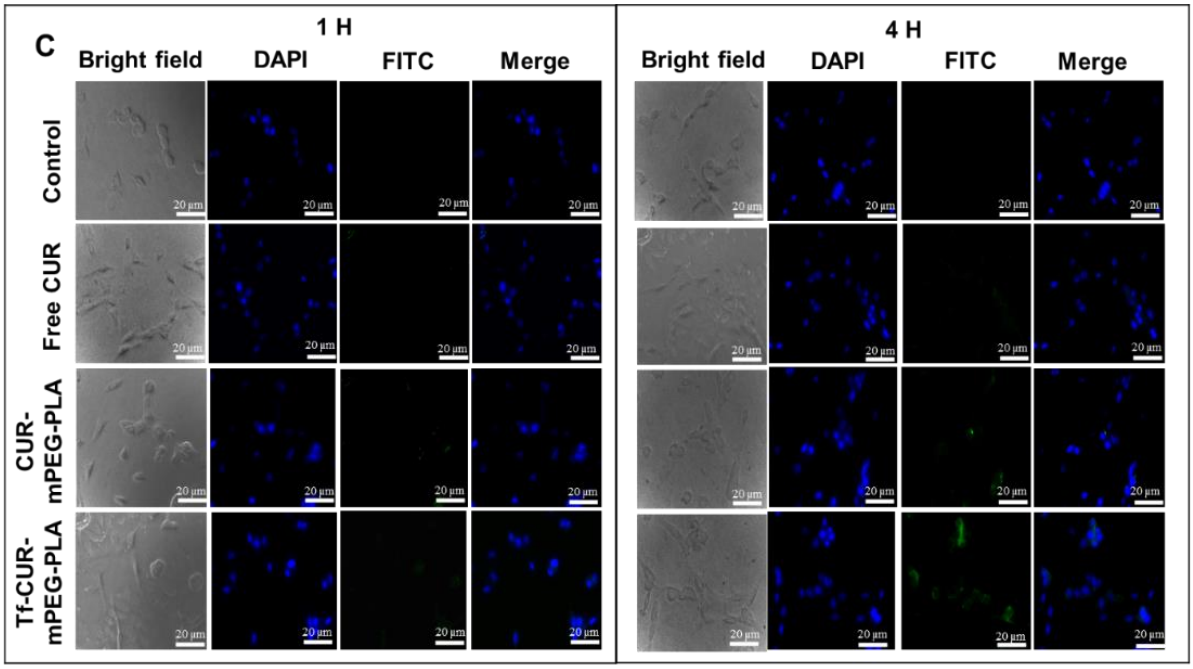
C
1 H
4 H
Bright field
DAPI
FITC
Merge
Control
Free CUR
CUR-mPEG-PLA
Tf-CUR-mPEG-PLA
20 μm

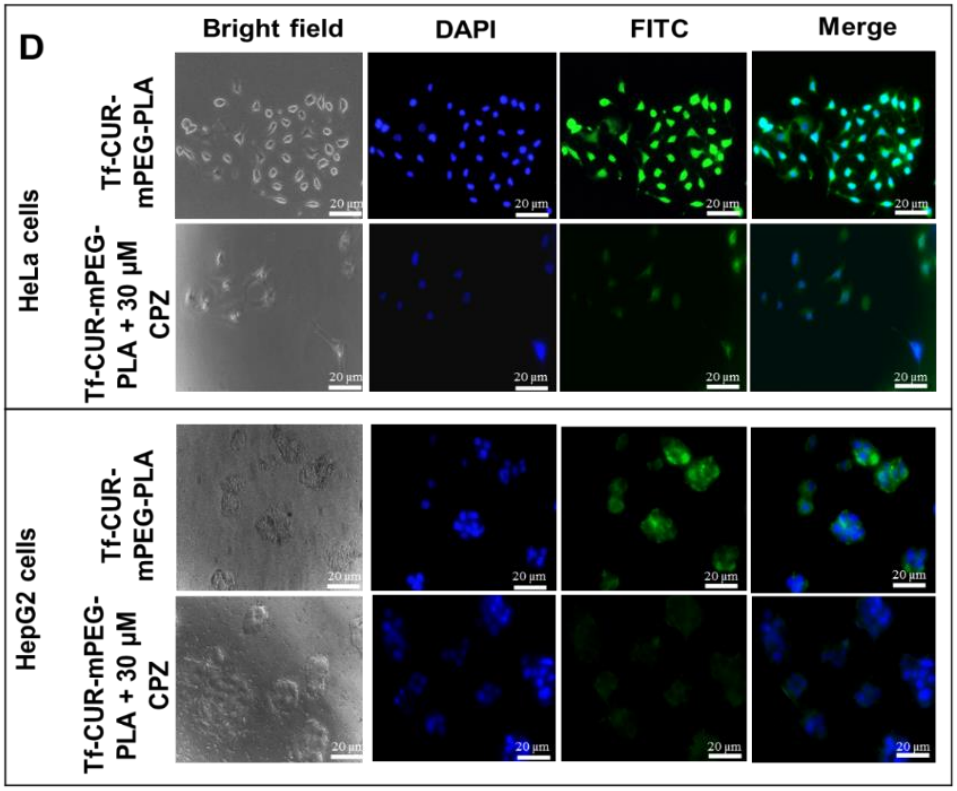

Figure. 2B.4. Fluorescence micrographs of HeLa (A), HepG2 (B), and NIH3T3 (C) cells following 1 h and 4 h incubation with free curcumin (Row 2), CUR-mPEG-PLA (Row 3), and Tf-CUR-mPEG-PLA (Row 4). Row 5 showed similar treatment as Row 4 in HeLa and HepG2 cells but with 1 h pre-incubation with free Tf. (D) Assessment of endocytosis pathway for Tf-CUR-mPEG-PLA by pre-incubation of cells with endocytosis inhibitor, chlorpromazine (CPZ, 30 µM).

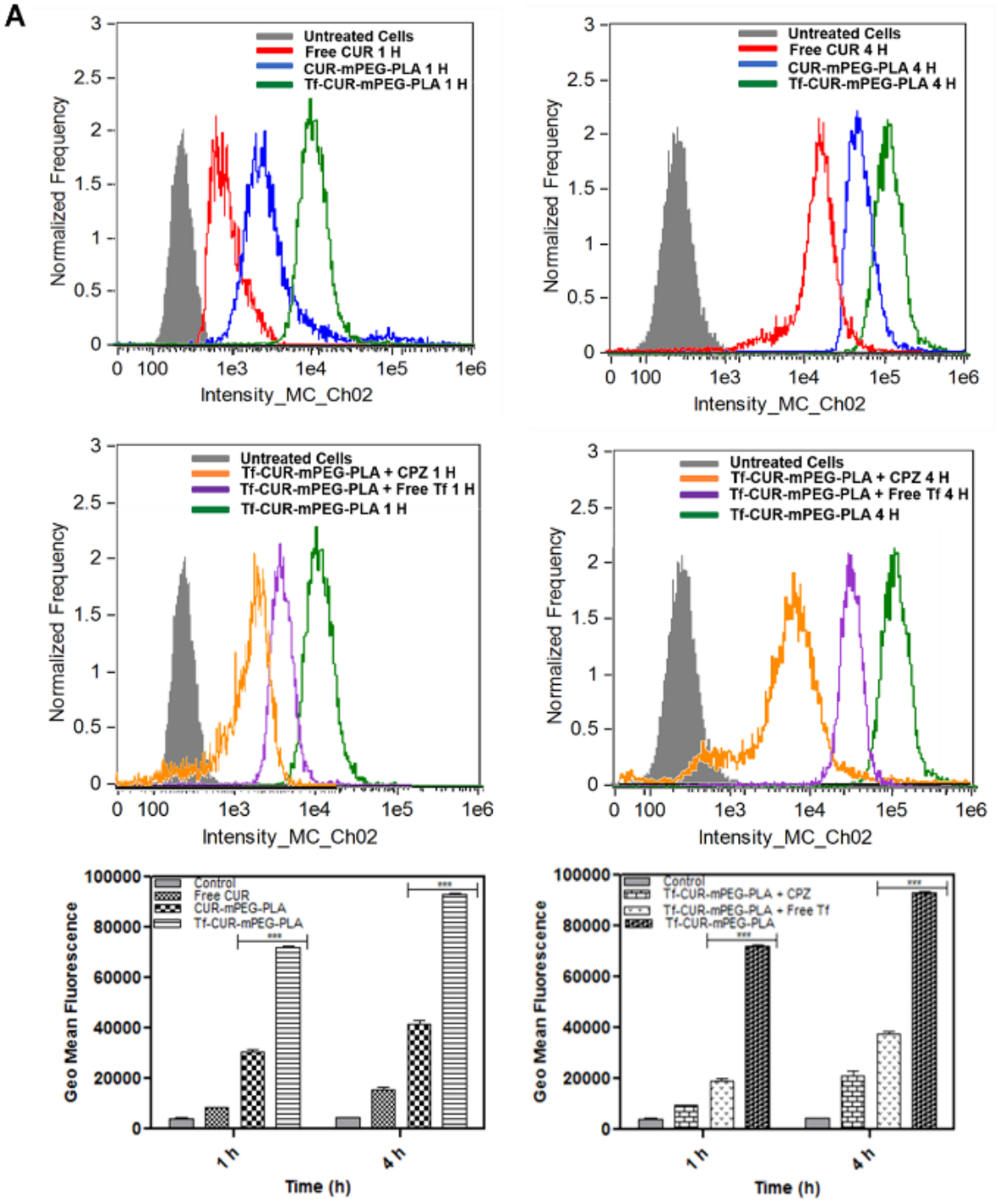
A
Untreated Cells
Free CUR 1 H
CUR-mPEG-PLA 1 H
Tf-CUR-mPEG-PLA 1 H
Normalized Frequency
Intensity_MC_Ch02
Untreated Cells
Free CUR 4 H
CUR-mPEG-PLA 4 H
Tf-CUR-mPEG-PLA 4 H
Normalized Frequency
Intensity_MC_Ch02
Untreated Cells
Tf-CUR-mPEG-PLA + CPZ 1 H
Tf-CUR-mPEG-PLA + Free Tf 1 H
Tf-CUR-mPEG-PLA 1 H
Normalized Frequency
Intensity_MC_Ch02
Untreated Cells
Tf-CUR-mPEG-PLA + CPZ 4 H
Tf-CUR-mPEG-PLA + Free Tf 4 H
Tf-CUR-mPEG-PLA 4 H
Normalized Frequency
Intensity_MC_Ch02
Control
Free CUR
CUR-mPEG-PLA
Tf-CUR-mPEG-PLA
Geo Mean Fluorescence
Time (h)
Control
Tf-CUR-mPEG-PLA + CPZ
Tf-CUR-mPEG-PLA + Free Tf
Tf-CUR-mPEG-PLA
Geo Mean Fluorescence
Time (h)

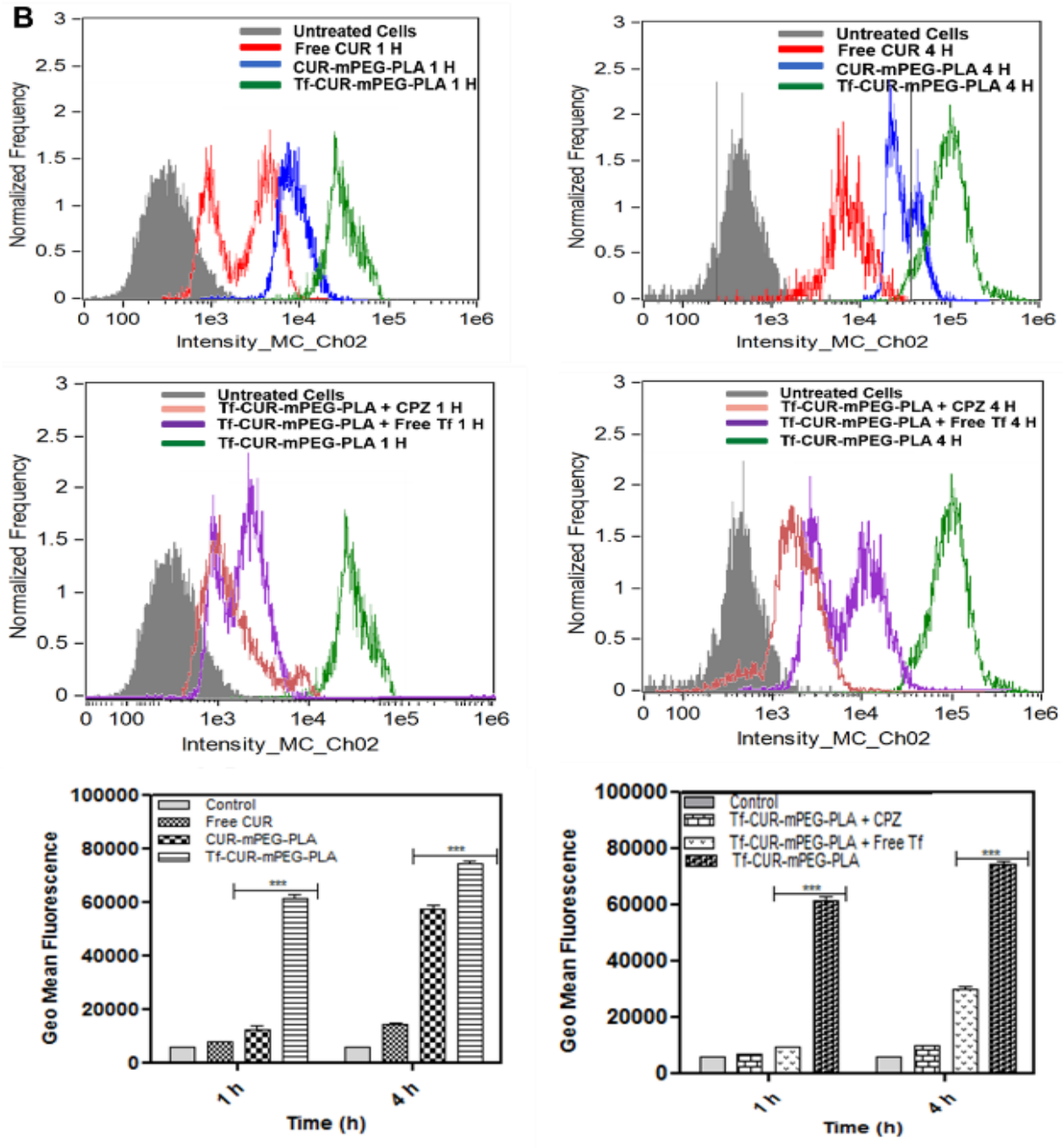
B
Untreated Cells
Free CUR 1 H
CUR-mPEG-PLA 1 H
Tf-CUR-mPEG-PLA 1 H
Normalized Frequency
Intensity_MC_Ch02
Untreated Cells
Free CUR 4 H
CUR-mPEG-PLA 4 H
Tf-CUR-mPEG-PLA 4 H
Normalized Frequency
Intensity_MC_Ch02
Untreated Cells
Tf-CUR-mPEG-PLA + CPZ 1 H
Tf-CUR-mPEG-PLA + Free Tf 1 H
Tf-CUR-mPEG-PLA 1 H
Normalized Frequency
Intensity_MC_Ch02
Untreated Cells
Tf-CUR-mPEG-PLA + CPZ 4 H
Tf-CUR-mPEG-PLA + Free Tf 4 H
Tf-CUR-mPEG-PLA 4 H
Normalized Frequency
Intensity_MC_Ch02
Control
Free CUR
CUR-mPEG-PLA
Tf-CUR-mPEG-PLA
Geo Mean Fluorescence
Time (h)
Control
Tf-CUR-mPEG-PLA + CPZ
Tf-CUR-mPEG-PLA + Free Tf
Tf-CUR-mPEG-PLA
Geo Mean Fluorescence
Time (h)

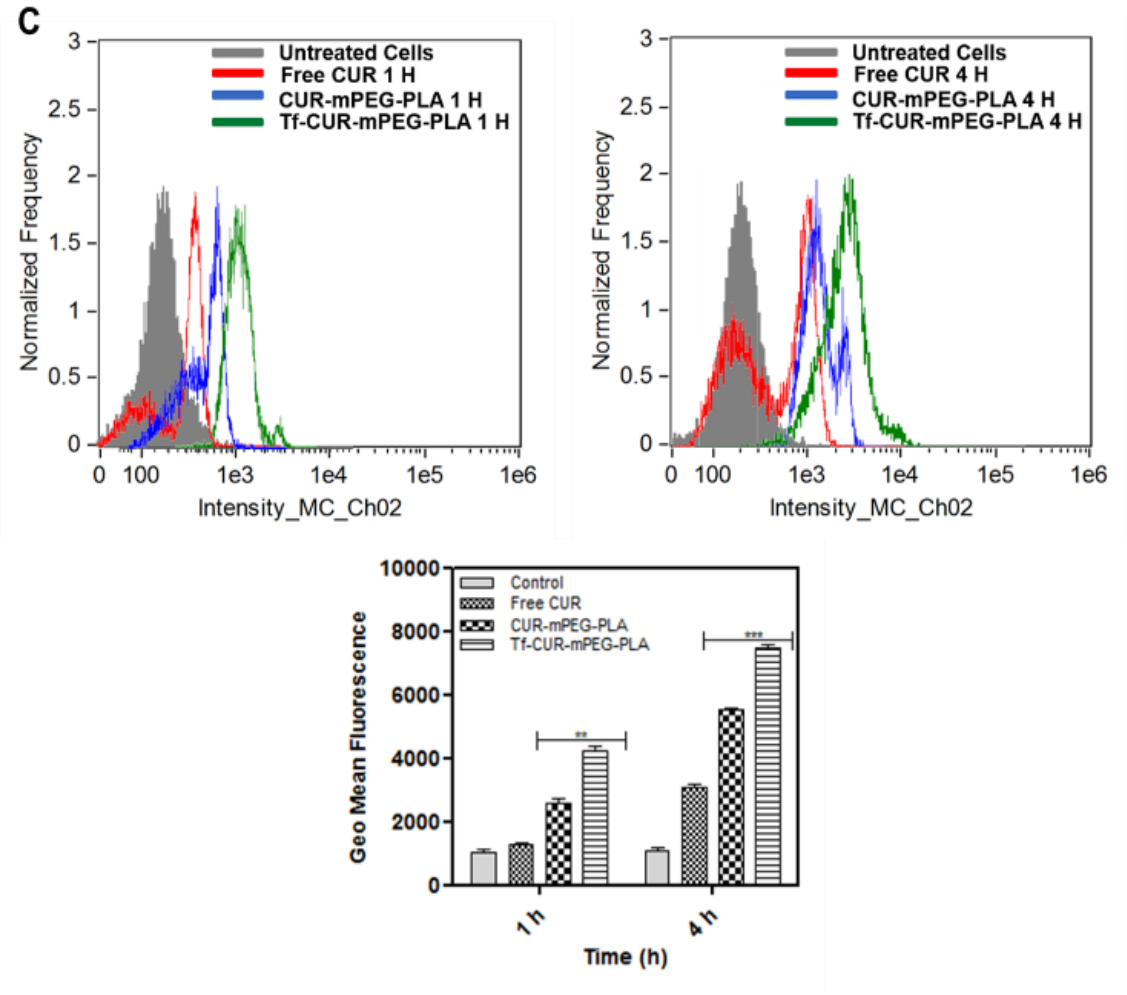

Figure. 2B.5. Flow cytometry histograms and geometric mean fluorescence graphs of the cells incubated with free curcumin, CUR-mPEG-PLA, and Tf-CUR-mPEG-PLA on HeLa (A), HepG2 (B) and NIH3T3 (C) cells after 1and 4 h incubation. Data represents the mean ± SD (n=3). (***P < 0.001, **P < 0.01). Effect of free Tf and CPZ inhibitor pre-incubation on Tf-CUR-mPEG-PLA in HeLa and HepG2 cells (A & B).

As shown in Figure. 2B.4A and B histograms, the cellular internalization of Tf-CUR-mPEG-PLA micelles decreased significantly when treated with CPZ. The inhibition of internalization with CPZ indicated that the pathways for the cellular uptake of Tf-CUR-mPEG-PLA was clathrin-mediated endocytosis (Figure. 2B.4D). Overall, above studies using flow cytometry

and confocal microscopy confirms that Tf-CUR-mPEG-PLA were taken up more efficiently by TfR-over-expressing HeLa and HelG2 cells by interaction with the over-expressed TfR via receptor-mediated endocytosis compared to the non-targeted CUR-mPEG-PLA and free curcumin at all the time points.

2B.3.5. *In Vitro* Cytotoxicity

The cytotoxicity of free curcumin, CUR-mPEG-PLA, and Tf-CUR-mPEG-PLA was studied on NIH-3T3, HeLa and HepG2 cells by MTT assay. As shown in Figure. 2B.6, Tf-CUR-mPEG-PLA decreased cell viability compared to CUR-mPEG-PLA at all curcumin concentrations in all three cell lines that clearly indicated targetability of Tf-CUR-mPEG-PLA and enhanced cellular internalization resulting in enhanced cytotoxicity. Incubation with free curcumin for 6 h followed by 24 h drug free incubation led drug molecules to come out of the normal cells by diffusion, which resulted in less cellular toxicity compared to continuous 24 h treatment.

As shown in Figure. 2B.6, following 24 h treatment, Tf-CUR-mPEG-PLA and CUR-mPEG-PLA micelles demonstrated 14.09 ± 0.82%, 10.52 ± 1.73% and 39.94 ± 2.61%, 52.76 ± 1.97% cell viability compared to 29.06 ± 3.02%, and 20.15 ± 1.16% cell viability for free curcumin at curcumin concentration of 50 µg/mL in HeLa and HepG2 cells, respectively. In NIH-3T3 cells, Tf-CUR-mPEG-PLA, CUR-mPEG-PLA and free curcumin showed cell viability of 62.32 ± 1.83%, 57.13 ± 2.06%, and 49.79 ± 1.21%, respectively following 24 h treatment at curcumin concentration of 50 µg/mL. The results demonstrated that Tf-CUR-mPEG-PLA showed higher cytotoxicity in TfR over-expressing HeLa and HepG2 cells compared to the control NIH-3T3 fibrobalst cells (Figure. 2B.6A, B and C). The blank

micelles were tested in NIH-3T3, HeLa and HepG2 did not show any decrease in cell viability (data not shown).

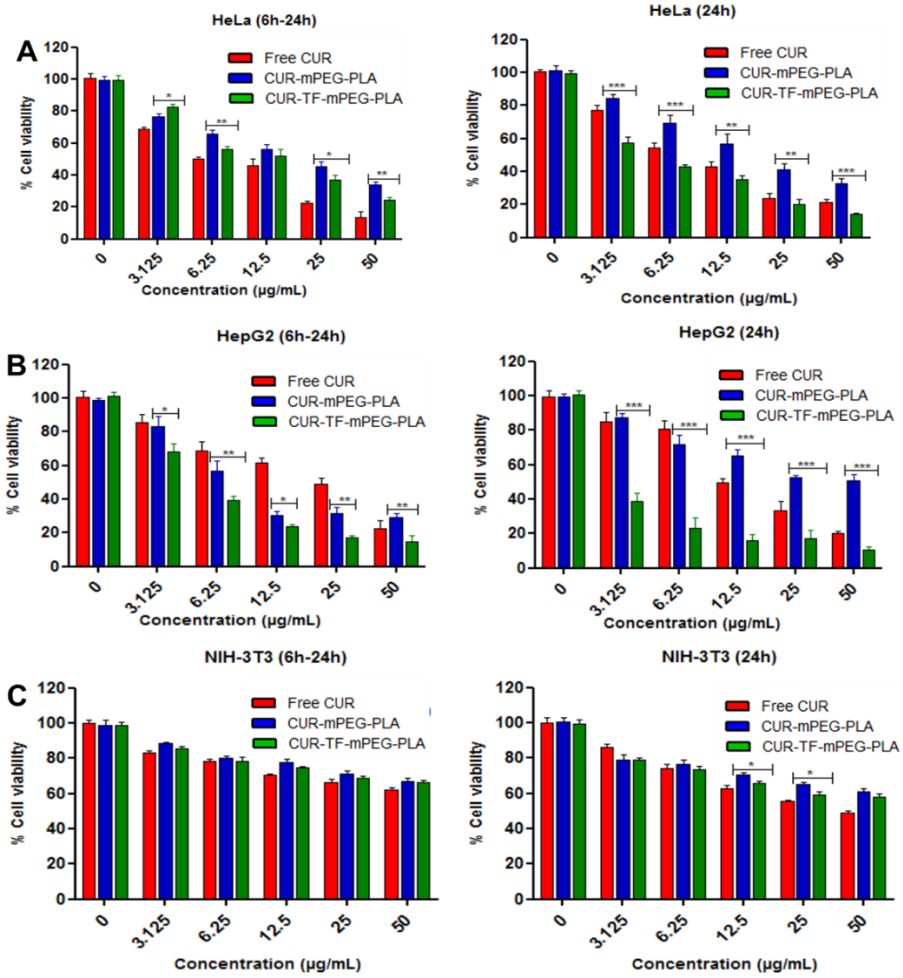

Figure. 2B.6. *In vitro* cytotoxicity of Free CUR, CUR-mPEG-PLA and Tf-CUR-mPEG-PLA on HeLa (A), HepG2 (B), and NIH-3T3 (C) cells at curcumin concentration of 3.125 to 50 µg/mL for 6 and 24 h. Data represented the mean ± S.D. n=3.

2B.3.6. Cellular uptake of CUR-mPEG-PLA and Tf-CUR-mPEG-PLA in HeLa spheroids

The uptake of Tf-CUR-mPEG-PLA by cells in HeLa spheroids was evaluated using flow cytometer. As shown in Figure. 2B.7, the fluorescence intensity of micelles enhanced with

increase in incubation time. The free curcumin showed low level of fluorescence compared to CUR-mPEG-PLA and Tf-CUR-mPEG-PLA. The fluorescence intensity of Tf-CUR-mPEG-PLA was higher with a right shift of the fluorescence intensity in the flow cytometer histogram. Multicellular spheroids is emerging as a promising tool to study cell-cell interaction, and treatment efficacy as it resembles the three dimensional tissues *in vivo* compared to the cells grown in monolayers (Zanoni et al. 2016). The enhanced uptake of Tf-CUR-mPEG-PLA by spheroidal cells compared to CUR-mPEG-PLA indicated its targeting potential, which resulted in deep tissue penetration.

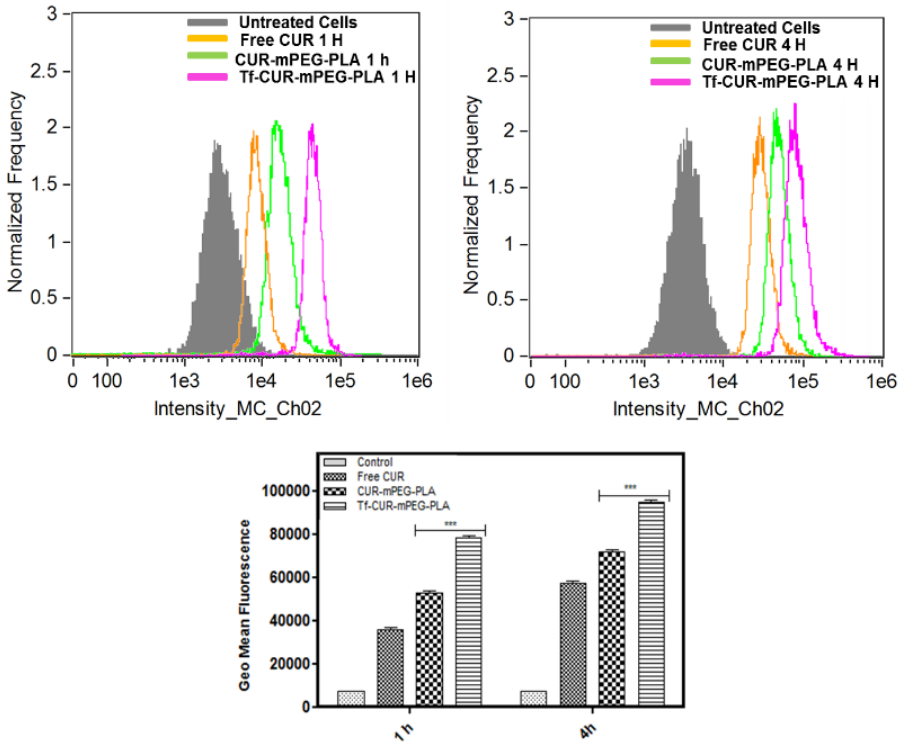

Figure. 2B.7. Quantitative spheroidal uptake of free CUR, CUR-mPEG-PLA and Tf-CUR-mPEG-PLA at 1 and 4 h by flow cytometry.

2B.3.7. Inhibition of HeLa spheroidal growth

The HeLa spheroids were treated with free CUR, CUR-mPEG-PLA and Tf-CUR-mPEG-PLA to analyze their growth inhibitory effect. Brightfield images indicated that that treatment with

CUR-mPEG-PLA and Tf-CUR-mPEG-PLA for 9 days caused reduction in spheroidal size. The spheroids lose their spherical morphology and were uneven on the surface over time (Figure. 2B.8A). The presence of debris surrounding the spheroids were seen in the spheroids incubated with Tf-CUR-mPEG-PLA. The spheroidal diameter was measured from the micrographs for 9 days and the data has been represented in Figure. 2B.8B. The diameters of spheroids gradually increased to a size of 900 µm in control wells over the treatment period of 9 days. The average diameters of tumor spheroids at the end of day 9 were estimated to be 596.84 ± 2.3 µm, 627.31 ± 1.7 µm, and 663.62 ± 2.7 µm for Tf-CUR-mPEG-PLA, CUR-mPEG-PLA and free curcumin.

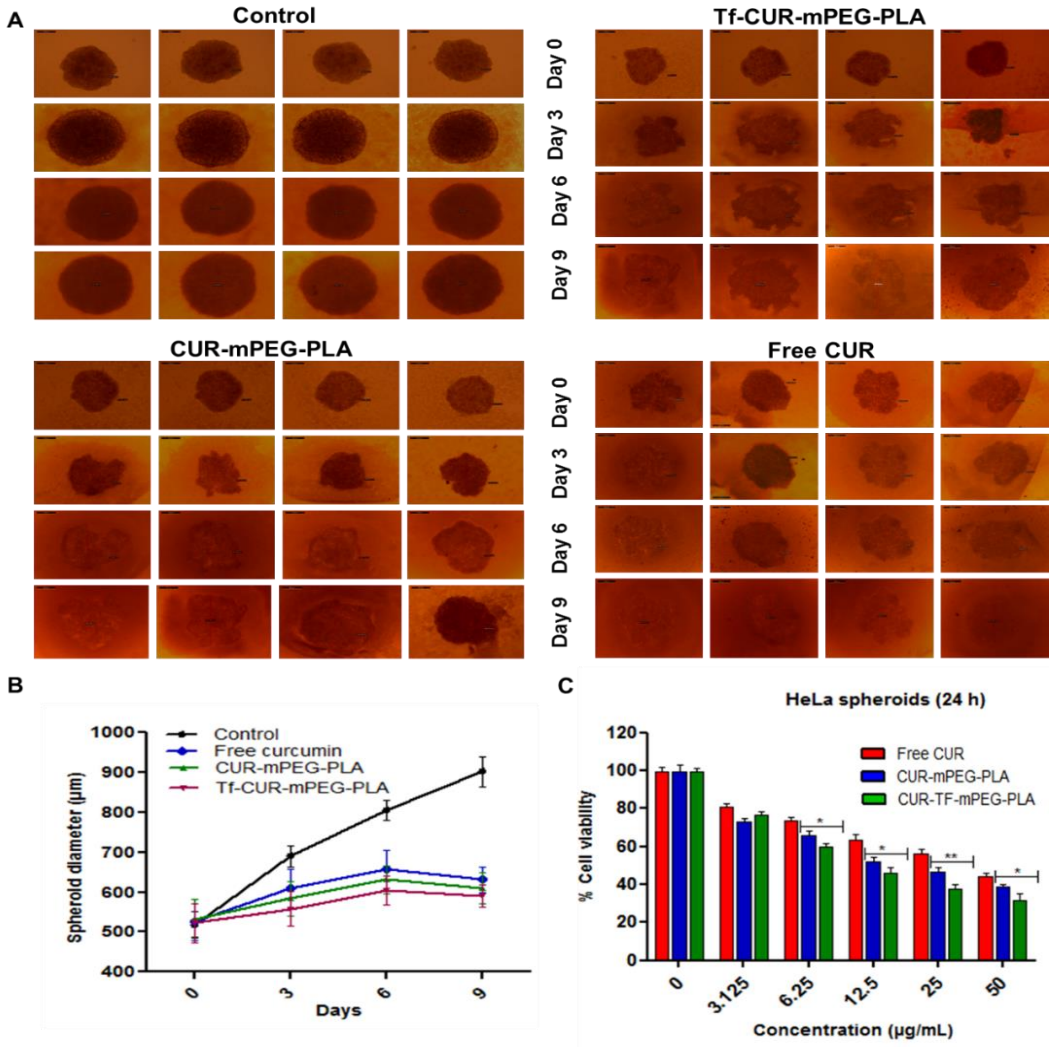

Figure. 2B.8. Bright field images of HeLa spheroids treated with free curcumin, CUR-mPEG-PLA and Tf-CUR-mPEG-PLA (A), and change in diameter of spheroids with treatment time (B), and *in vitro* cytotoxicity of spheroids (C). Untreated spheroids were set as control (n = 3). Scale bar, 200 µm.

2B.3.8. *In vitro* cytotoxicity study in HeLa spheroids

The *in vitro* cytotoxicity of targeted and non-targeted micelles in HeLa spheroids were evaluated using Presto Blue assay. As shown in Figure. 2B.8C, the cytotoxicity in 3D spheroids varied significantly compared to the monolayer cells. The Tf-CUR-mPEG-PLA accumulated more in spheroids resulting in higher cytotoxicity compared to free curcumin and CUR-mPEG-PLA. Tf-CUR-mPEG-PLA displayed lowest viability of 30.60 ± 1.97% compared to free curcumin (46.27 ± 2.04%), and CUR-mPEG-PLA (38.47 ± 2.95%).

2B.3.9. Penetration in HeLa spheroids

Spheroids were visualized under confocal microscopy and images at varied focal lengths, known as z-stacked images were captured following treatment at specific time points in order to determine the penetrability of Tf-CUR-mPEG-PLA with reference to CUR-mPEG-PLA. As shown in Figure. 2B.9, Tf-CUR-mPEG-PLA showed deeper penetration and higher distribution inside the spheroids compared to CUR-mPEG-PLA. Z-stacked images display virtually cut spheroidal sections at various depths from the surface. High resolution of the confocal microscopic pictures enables minimal interference of off-focal fluorescence. Tf-CUR-mPEG-PLA penetrated deep in the spheroids in 4 h as the bright curcumin fluorescence was observed even at a depth of 70 µm from the surface.

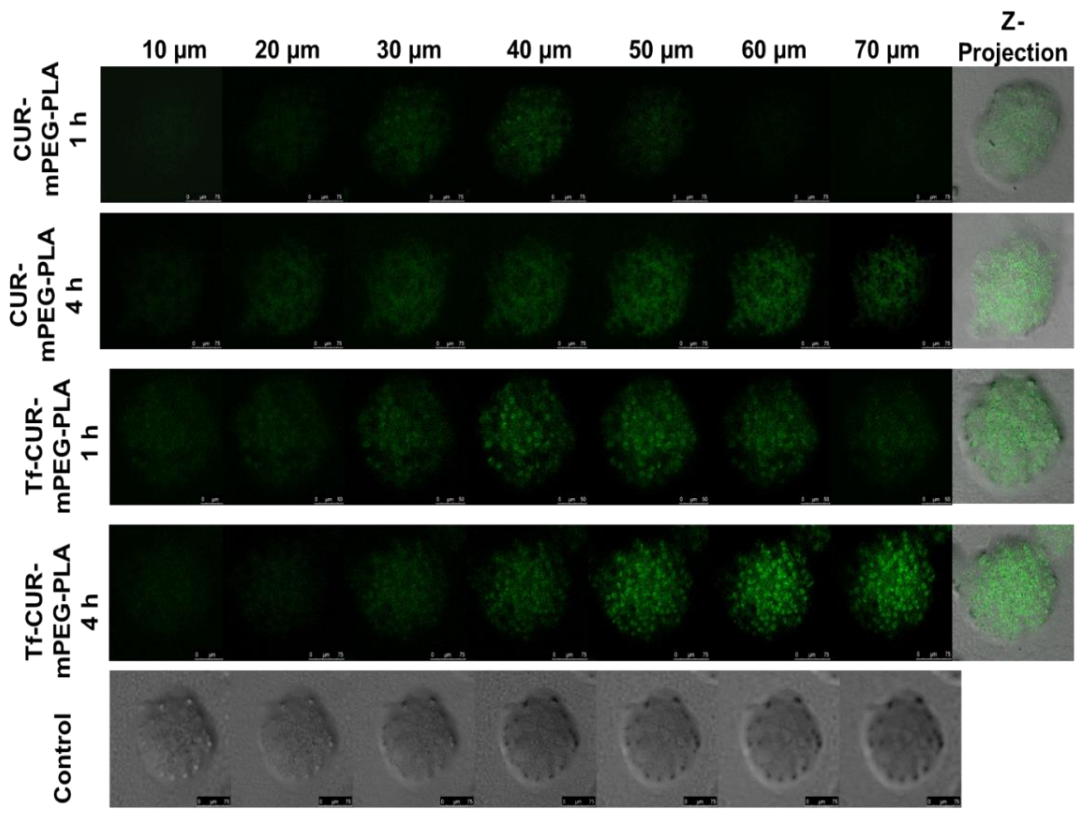

Figure. 2B.9. Z stacked images of HeLa spheroids by confocal laser scanning microscopy captured at consecutive Z-axes. The cells were treated with CUR-mPEG-PLA and Tf-CUR-mPEG-PLA for 1 and 4 h time period. Scale bar: 75 µm.

2B.3.10. Live-dead staining in 3D spheroids

Extent of cytotoxicity of the CUR-mPEG-PLA and Tf-CUR-mPEG-PLA in HeLa spheroids was visualized under microscope following live-dead assay in spheroids (Figure. 2B.10). The HeLa spheroids without any treatment internalized the Calcein Blue AM thus producing blue fluorescence. The spheroids treated with free curcumin, showed few cells with red florescence indicating the cell death. Most of the cells treated with Tf-CUR-mPEG-PLA were dead, which was evident by increase in the red fluorescence from PI staining. The increased cancer

cells targetability and delivery of loaded drug from Tf-CUR-mPEG-PLA treatment resulted in increased induction of cell death compared to CUR-mPEG-PLA.

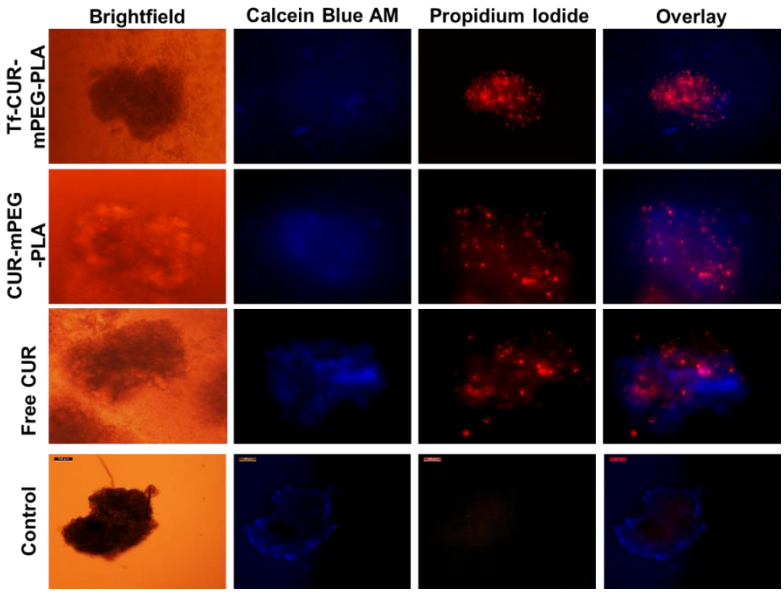

Figure. 2B.10. Brightfield and fluorescence images of HeLa spheroids stained with LIVE/DEAD reagent after incubation with free curcumin, CUR-mPEG-PLA, and Tf-CUR-mPEG-PLA at curcumin equivalent concentration of 50 µg/mL.

2B.3.11. Apoptosis in spheroidal cells

The binding of Annexin V to the outer plasma membrane phosphatidyl serine was used as an indicator of apoptosis (Waghela et al. 2015). The initiation of apoptosis by curcumin administered to the cells as CUR-mPEG-PLA, Tf-CUR-mPEG-PLA and free curcumin was evaluated using flow cytometry (Figure. 2B.11). The apoptotic cell population was seen in spheroids incubated with all the treatments, however, the percentage of apoptotic cell varied among the treatment groups.

Spheroids treated with Tf-CUR-mPEG-PLA showed 9.72% and 34.3% of early apoptotic and late apoptotic populations, respectively. The values were 10.8% and 29.4% for CUR-mPEG-

PLA and 7.81% and 25.1% for free curcumin treatments, respectively following 24 h treatment. Similarly, the early and late apoptotic populations in spheroids incubated for 48 h with Tf-CUR-mPEG-PLA, CUR-mPEG-PLA and free curcumin was found to be 9.5%, 46.9%, 8.8% and 40.1%, 11.6%, 30.3%, respectively. The data clearly indicated that targeted delivery of curcumin by Tf-CUR-mPEG-PLA resulted in time-dependent enhanced apoptotic activity in spheroids compared to free curcumin and CUR-mPEG-PLA.

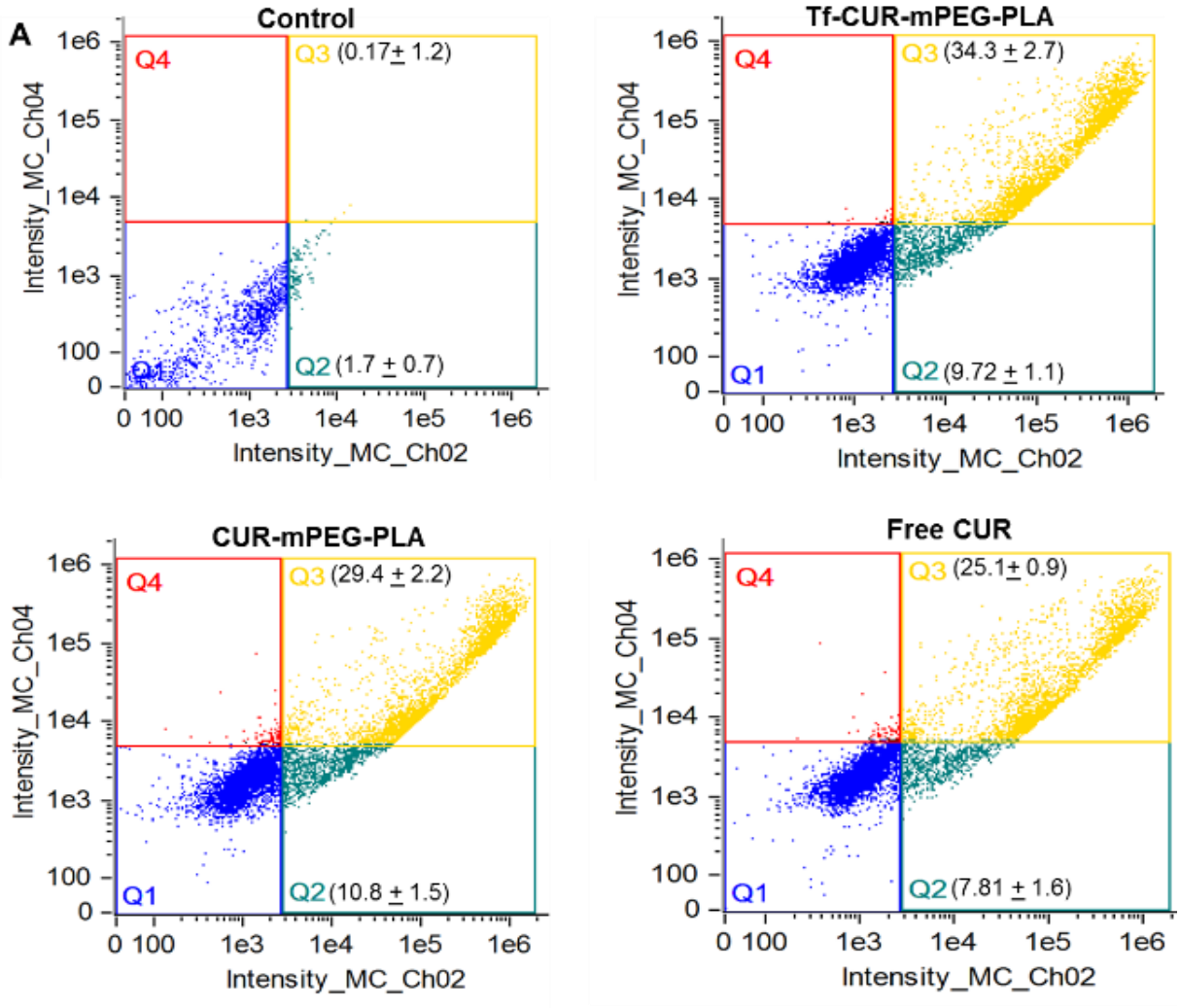

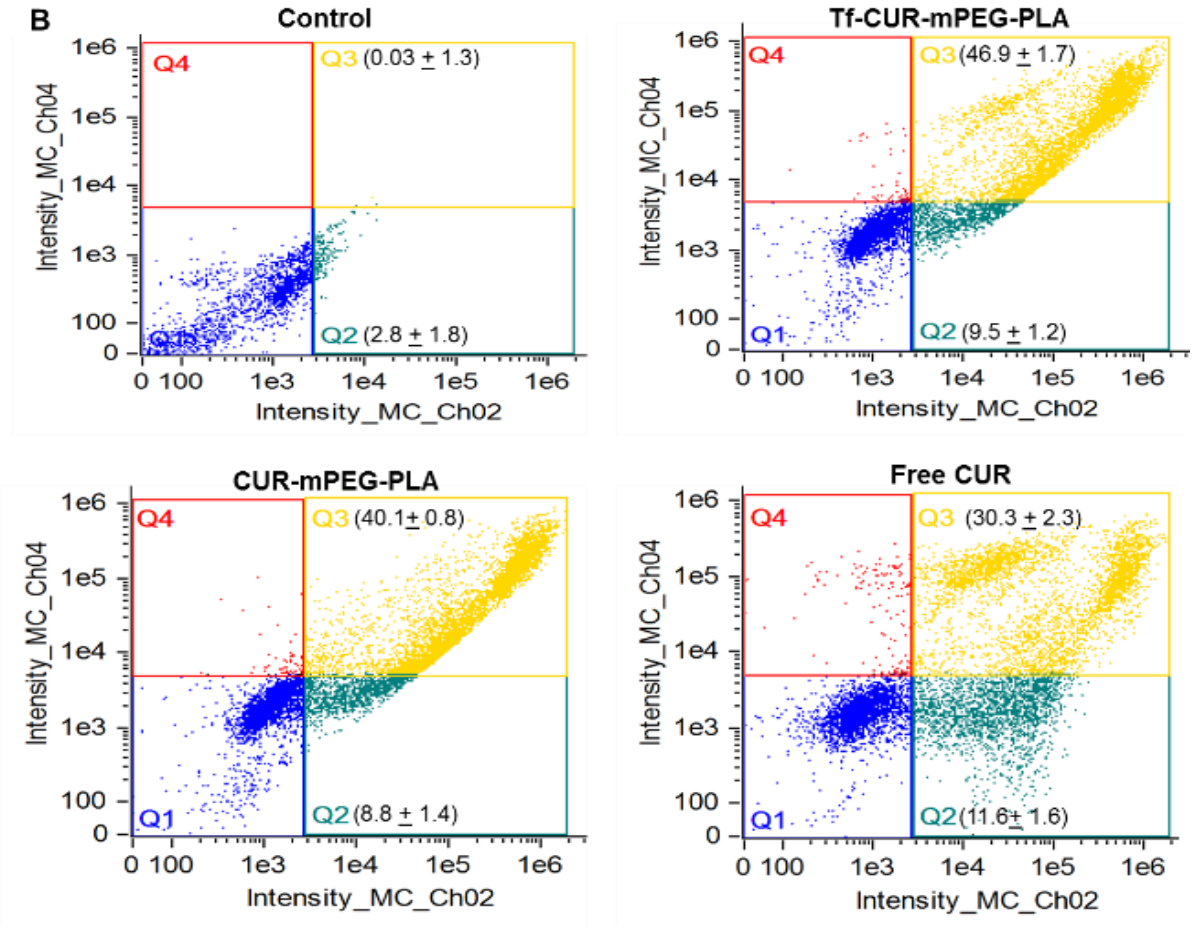

Figure. 2B.11. Apoptosis of HeLa spheroids measured by flow cytometer using AnnexinV/PI after 24 (A) and 48 h (B) incubation with free curcumin, CUR-mPEG-PLA and Tf-CUR-mPEG-PLA at curcumin concentration of 50 µg/mL.

2B.4. CONCLUSION

Here, we attempted to develop a tumor targeted nano-micellar formulation of curcumin by utilizing mPEG-PLA as amphiphilic polymer and transferrin a tumor homing ligand. Tf was conjugated to the micelles for facile recognition by the over-expressed TfR in hepatic and cervical cancer cells. The targeted micelles, Tf-CUR-mPEG-PLA were physico-chemically characterized and found to be stable with optimal loading of hydrophobic curcumin, which

released the pay load in sustained manner. The Tf-CUR-mPEG-PLA demonstrated enhanced cellular uptake in both the Tf-over-expressing cell lines that resulted in increased cytotoxicity. The cellular internalization of Tf-CUR-mPEG-PLA was Tf-dependent, and via clathrin-mediated endocytic pathway. As spheroids mimic the *in vivo* 3D representation of tumor, HeLa spheroids were used in the study to assess the therapeutic efficacy of the Tf-CUR-mPEG-PLA. The result demonstrated that the Tf-CUR-mPEG-PLA penetrated deep in spheroids compared to CUR-mPEG-PLA and free curcumin, and resulted in improved growth inhibition. The Tf-CUR-mPEG-PLA induced higher rate of apoptosis, which led to the increased dead cell population in spheroids compared to other treatments. Therefore, the study provides strong rationale for the use of this developed nano micellar system, Tf-mPEG-PLA for targeted delivery of hydrophobic chemotherapeutic agents to Tf-over-expressing cancers. The Tf-CUR-mPEG-PLA could be utilized as an effective chemotherapeutic agent for the treatment of TfR-over-expressing hepatic and cervical cancers.

Chapter 3

Cholesterol-conjugated poly(Lactide) based micelles as a nanocarrier system for effective delivery of curcumin in cancer therapy

ABSTRACT

Polymeric micelles have been widely explored pre-clinically as suitable delivery systems for poorly soluble chemotherapeutic drugs in cancer therapy. The present study reported the development of cholesterol (Ch)-conjugated poly(D,L-Lactide) (PLA)-based polymeric micelles (mPEG-PLA-Ch) for effective encapsulation and delivery of curcumin (CUR) at the tumor site. Cholesterol conjugation dramatically affected the particle size, and improved drug loading (DL) and encapsulation efficiency (EE). CUR-mPEG-PLA-Ch showed bigger hydrodynamic diameter (104.65 ± 2.14 nm, and 169.35 ± 1.52 nm for mPEG-PLA, and mPEG-PLA-Ch, respectively) due to increased size of the hydrophobic core. The newly developed polymer exhibited low critical micelles concentration (CMC) (25 µg/mL) which is close to lipid-based polymer, PEG-phosphatidyl ethanolamine (12.5 µg/mL) compared to mPEG-PLA (50 µg/mL). mPEG-PLA-Ch micelles exhibited relatively higher EE and DL (93.74 ± 1.62% and 13.86 ± 0.95%) compared to mPEG-PLA micelles (EE - 91.89 ± 1.27% and DL - 11.06 ± 0.83%,). mPEG-PLA-Ch micelles were internalized by the cancer cells effectively and exhibited higher cytotoxicity compared to free CUR in both, murine melanoma (B16F10), and human breast cancer (MDA-MB-231) cells. mPEG-PLA-Ch exhibited satisfactory hemocompatibility indicating their potential for systemic application. Further, CUR-mPEG-PLA-Ch demonstrated higher rate of reduction of tumor volume in B16F10-xenografted tumor-bearing mice compared to free CUR. At the end of 22 days, the tumor reduced to 1.87 fold (627.72 ± 0.9 mm^3 vs. 1174.68 ± 1.64 mm^3) compared to the treatment with free CUR. In conclusion, the experimental data *in vitro* and *in vivo* indicated that the newly developed CUR-mPEG-PLA-Ch micelles may have promising applications in solid tumors.

3.1. INTRODUCTION

Cancer is a deadly disease faced by humanity which, according to the report published by World Health Organization (WHO) took a toll of 8.2 million cancer-related deaths in 2012. Anticipated rise of new cancer cases is from 14 million in 2012 to 22 million within the next two decades. As a result of intensive research in the area of anticancer drug discovery in past few decades, various potent molecules with high cytotoxic potential have been discovered. However, these drugs face challenge to be an effective treatment modality as these drugs are cytotoxic toward normal cells as well. Therefore, there is an unmet need to improvise strategies to deliver anticancer drugs effectively and specifically to the tumor region.

In recent years, advancement in nanotechnology directed development of nanomedicines, in which drug is encapsulated in nano-sized drug delivery system (Alexis et al. 2010). Nanocarriers possess distinct advantage over conventional free drug administration as they eventually accumulate in the tumor area by a passive targeting phenomena, commonly referred to as Enhanced Permeability and Retention (EPR) effect (Torchilin 2011). The nanocarriers take advantage of the leaky tumor vasculature that allows nano-sized carriers to escape the circulation and accumulate in the tumor micro-environment (Biswas and Torchilin 2014). Various biocompatible self-assembled polymeric systems including liposomes, micelles; polymers of defined architectures including dendrimers; and inorganic nanoparticles including gold, silver, iron oxide, and silica have been developed where poorly soluble chemotherapeutic drugs are either loaded or conjugated for their delivery to the tumor site (Kumari, Ghosh, and Biswas 2016). Nanocarriers promote solubilization, impart stability to the poorly aqueous soluble drugs, and thereby improve their biopharmaceutical properties. Even though, the benefit of using nanoparticles as drug delivery system for cancer therapy is

obvious, the nanocarriers have to be biocompatible, biodegradable and less immunogenic to obtain maximum therapeutic benefit.

Among many other drug delivery systems, polymeric micelles (PMs) prepared from amphiphilic block copolymers received considerable attention in drug delivery research and have been applied extensively to solubilize various poorly soluble anticancer drugs, including doxorubicin (Yokoyama et al. 1998), paclitaxel (Lee et al. 2012), cisplatin (Nishiyama et al. 2003), and methotrexate (Li and Kwon 2000). Polyethylene glycol (PEG), a hydrophilic polymer is widely used as the outer shell for hydrophobic core in many self-assembled polymeric systems (Endres et al. 2011; Shuai et al. 2004). PEG is a bio-compatible, biodegradable, and non-toxic polymer with the ability to provide a stabilizing interface between the micellar core and the aqueous phase. Importantly, PEG reduces the nanoparticles (NPs) uptake by the mononuclear phagocytic system, sometime also referred to as the "stealth function" compared to the particles without PEG attachment (Gref et al. 2000). The opsonization-inhibiting property of PEG enables long circulation of NPs *in vivo* (Owens and Peppas 2006). Polylactic acid (PLA) is a hydrophobic, biodegradable and biocompatible polymer widely used in drug delivery and bioengineering (Nagarwal et al. 2009; Jain et al. 2009). In drug delivery, the polymeric micelles constituted by the self-assembly of PEG–PLA polymer have been used as carriers for poorly water soluble drugs (Zhang et al. 2005; Xiao et al. 2010). Genexol®-PM, developed by Samyang Genex Co. (Seoul, Korea), composed of PEG-PLA is the only clinically approved PLA-based nano-micellar chemotherapeutic, which loaded poorly soluble paclitaxel. In a recent study, we demonstrated the potential of PEG-PLA micelles to load poorly water soluble chemotherapeutic drug, curcumin and efficiently deliver it to various cancer cell lines (Kumari et al. 2016). However,

low drug loading limit their biomedical application. The slow degradation of PLA to lactic acid by the enzyme esterase is the limitation which prevents the use of high molecular weight PLA to improve hydrophobicity of the micelles (Wang et al. 2013). The inclusion of PEG in copolymer systems imparted extremely beneficial surface properties within the body because of the ability to repel proteins within aqueous environments (Andrade, Hlady, and Jeon 1993). This repulsion inhibited the adsorption of proteins to the polymer surface and, therefore, prevents many polymer-cell interactions. For example, nanoparticles made from diblock PLA-PEG copolymer have increased blood circulation times (decreased clearance) *in vivo* compared to particles made from PLA alone (Gref et al. 1994).

Among various hydrophobic moieties, cholesterol has gained considerable interest in recent years to improve hydrophobicity of drug delivery systems (Ha et al. 2011; Ma et al. 2013; Yao et al. 2014; Wang et al. 2010; Chen et al. 2013; Cheng et al. 2014). Cholesterol is an essential structural building block for cell membranes, responsible for membrane fluidity and permeability, intracellular transport, signal transduction, and cell trafficking (Yeagle 1991; Maxfield and Tabas 2005; Yeagle 1985). Due to the hydrophobicity and excellent biocompatibility, cholesterol has been extensively used to improve the hydrophobicity, biocompatibility, and bio-degradability of the drug delivery system without using slow-degrading polymers of high molecular weights (Zhou et al. 2009). In a study, a novel Ch-conjugated micelles, mPEG-block-poly(Ch-L-glutamate) was prepared that provided enlarged core space for loading poorly water soluble paclitaxel (Ma et al. 2013). It has been demonstrated that chitosan-conjugated to cholesterol has higher colloidal stability compared to chitosan conjugated to long alkyl chains (Ha et al. 2011). Cholesterol has been grafted to polysaccharide dextran to load anticancer doxorubicin (Yao et al. 2014).

Curcumin is a naturally occurring small molecule that demonstrated powerful anticancer activity in various pre-clinical studies (Naksuriya et al. 2014). CUR, bis(4-hydroxy-3-methoxyphenyl)-1,6-diene-3,5-dione is a polyphenol compound derived from the rhizome of plant *Curcuma longa*. CUR has been reported to having a wide range of pharmacological activities such as anti-microbial, anti-oxidant, anti-inflammatory, anti-parasitic, anti-mutagenic, anti-human immuno-deficiency virus, and anti-cancer with low or no intrinsic toxicity (Srivastava et al. 2011; Kawamori et al. 1999; Anand et al. 2008). Despite its pharmacological potentials, the application of CUR in clinic is limited due to its low aqueous solubility (0.6 µg/mL) and rapid degradation in physiological conditions (Wu et al. 2011). Therefore, it is necessary to improve the solubility, stability and bioavailability of CUR to utilize it as a therapeutic candidate.

In our study, we synthesized Ch-modified mPEG-PLA polymer, where cholesterol is conjugated to the free hydroxyl group of PLA (MW ~ 5970 Da). The polymer self-assembled efficiently into stable micelles with low critical micelles concentrations (CMC) and loaded hydrophobic CUR efficiently. The physicochemical characteristics of CUR-loaded mPEG-PLA-Ch micelles, including morphology, particle size, zeta potential, drug loading, and encapsulation efficiency were investigated. The association of the micelles with cancer cells and cytotoxic response following CUR-mPEG-PLA-Ch treatment were analyzed in murine melanoma cells, B16F10 and human breast cancer, MDA-MB-231 cell lines. Finally, the tumor-reducing efficacy of CUR-mPEG-PLA-Ch micelles *in vivo* was evaluated.

3.2. MATERIALS AND METHODS

3.2.1. Materials

Methoxy poly(ethylene glycol) 5000 (mPEG), D,L-Lactide, Cholesteryl Chloroformate, Curcumin, tetrahydrofuran (THF), DAPI 4′,6-Diamidino-2-phenylindole dihydrochloride (4,6- diamidino-2-phenylindole), and *para*-formaldehyde were purchased from Sigma-Aldrich Chemicals (Germany). Thiazoyl blue tetrazolium bromide (MTT), Fluoromount-G, and Trypan blue solution were obtained from Himedia (Mumbai, India). Dialysis membrane was purchased from Spectrum Laboratories, Inc. (USA).

For cell culture, Dulbecco's Modified Eagle's Medium (DMEM), Growth medium RPMI-1640, Penicillin-streptomycin, Trypsin-EDTA and fetal bovine serum (FBS) were purchased from Himedia (Mumbai, India). All reagents were used as received and the solvents were purified according to the general procedures.

3.2.2. Cell lines and animals

Murine melanoma cells, B16F10 and human breast cancer cells, MDA-MB-231 were purchased from National Center for Cell Sciences (Pune, India). Cells were grown in DMEM and RPMI-1640 medium supplemented with 10% FBS and 1% penicillin-streptomycin solution. Cells were maintained in a humidified atmosphere at 37°C and 5% CO_2.

Pathogen free female C57BL/6 mice of age 6-8 weeks were procured from National Centre for Laboratory Animal Sciences (NCLAS), National Institute of Nutrition (Hyderabad, India). All animal studies were carried out under the guidelines compiled by the Institutional Animal Ethics Committee of the BITS Pilani University. The animals were maintained in a room (23 ± 2°C and 60 ± 10% humidity) under a 12 h light/dark cycle. Food and water were given *ad libitum*.

3.2.3. Synthesis and characterization of mPEG-PLA-Ch copolymer

3.2.3.1. Synthesis of methoxy-polyethylene glycol-poly(D,L-Lactide) mPEG-PLA copolymer

The methoxy-polyethylene glycol-poly(D,L-Lactide) (mPEG-PLA) diblock copolymers were synthesized by ring opening polymerization according to our previously reported procedure (Kumari et al. 2016). In brief, mPEG (1 g) and D,L-Lactide (0.4 g) were placed in a dried polymerization tube. An appropriate amount of stannous octoate (0.008% w/w) was added as a solution in toluene. The reaction was placed in a pre-heated oil-bath at 160°C for 6 h. After cooling to the room temperature, the resultant copolymer was dissolved in tetrahydrofuran, recovered by precipitation into an excessive solvent of ice-cold diethyl ether. The precipitant was dried and redissolved in water and kept for dialysis against water by using cellulose ester membrane (MWCO 12-14,000 Da). The product was lyophilised and stored.

3.2.3.2. Synthesis of cholesterol-modified methoxy-polyethylene glycol-poly(D,L-Lactide) (mPEG-PLA-Ch) copolymer

mPEG-PLA-Ch copolymers were synthesized through a coupling reaction between the hydroxyl group at the end of mPEG-PLA and cholesteryl chloroformate. In a typical run, into the solution of mPEG-PLA (500 mg, 0.084 mmol) and triethylamine (8.5 µL, 0.084 mmol) in 4 mL of DCM at 0°C and under N_2 atmosphere, cholesteryl chloroformate (187.28 mg, 0.417 mmol) was added drop wise at 0°C. The mixture was stirred for 24 h at room temperature, concentrated, and precipitated into diethyl ether. The precipitate was dried, suspended in water and kept for dialysis against water by using cellulose ester membrane (MWCO 12-14,000 Da). The product was lyophilised to yield white fluffy solid. ^{1}H NMR spectra was

recorded on a Bruker spectrometer (AVANCE model, Germany) operating at 300 MHz at room temperature. The compound was dissolved in $CDCl_3$ at concentration of 5 mg/mL.

3.2.3.3. Critical micelle concentration (CMC)

A steady-state pyrene fluorescence method was used to determine the CMC of the copolymers (Song et al. 2011). Fluorescence spectra were recorded on a spectrophotometer (Spectramax™ M4, Multi detection Reader). Pyrene was used as a hydrophobic fluorescence probe. Aliquots of pyrene solutions (50 μL; 10 mg/mL dissolved in chloroform) were added to the micellar solutions used at the concentrations range of 3.125 to 150 μg/mL. The mixtures were stirred overnight for solubilization and incorporation of pyrene in the micelles. The following day, the solutions were filtered before spectral analysis. The emission wavelength was 390 nm and the excitation spectra were recorded ranging from 300 to 350 nm with both bandwidths set at 5 nm. A CMC value was determined from the ratios of pyrene intensities at 337 (I337) and 334 (I334) nm and calculated from the intersection of two tangent plots of I337/I334 versus log concentrations of copolymers.

3.2.4. Preparation and characterization of CUR-loaded polymeric micelles

CUR-loaded micelles were prepared by a thin film hydration method (Wei et al. 2009). Briefly, the co-polymer, mPEG-PLA-Ch was dissolved in 1 mL of chloroform. A certain amount of CUR from the CUR-solution (0.1% acetic acid methanol solution) was then added. The mixture was rotary evaporated resulting in the formation of yellowish thin layer of uniform film on the wall of the flask. The thin film was hydrated using PBS, pH 7.4. The solution was centrifuged (13,500 g, 4°C) to remove the unincorporated drug. Bank micelles were prepared following similar approach (Figure 3.1).

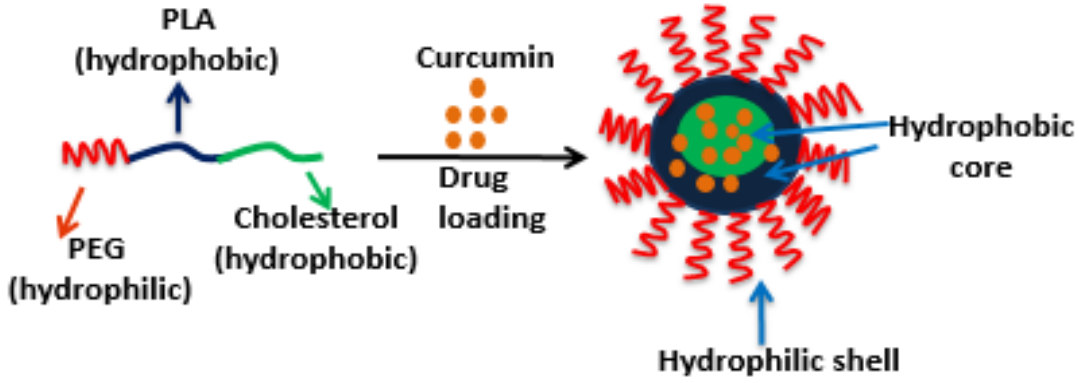

Figure 3.1. Schematic representation of CUR-mPEG-PLA-Ch micelles formation.

The drug-loaded micelles solution was added to 80% (v/v) ethanol to disrupt the micelles core-shell structure and to dissolve CUR released from the micelles. Through stepwise dilution, a solution of CUR with UV absorbance at a range of 0.2-0.8 at 420 nm was prepared. The CUR content in the drug-loaded micelles was determined using the UV–Vis spectrophotometer (Spectramax™, microplate reader, Molecular Devices, US) at 420 nm. The drug loading content (DL) and drug encapsulation efficiency (EE) were calculated based on the following formula,

$$EE\ \% = \frac{\text{Weight of the drug in micelles}}{\text{Weight of the feeding polymer and drug}} \text{ X } 100$$

$$DL\ \% = \frac{\text{Weight of the drug in micelles}}{\text{Weight of the feeding drug}} \text{ X } 100$$

3.2.4.1. Particle size and zeta potential analysis

Particle size, zeta potential and polydispersity index (PDI) of blank and CUR-loaded mPEG-PLA-Ch micelles were determined by dynamic light scattering using zetasizer (Nano ZS90, Malvern Instruments Ltd., UK) at 25°C. Results were expressed as mean ± standard deviation (SD). All the measurements were analyzed in triplicates.

3.2.4.2. Storage stability

The stability of CUR-mPEG-PLA-Ch micelles was examined by monitoring the changes in particle size and drug content stored at 4°C and 25°C for upto two months. At pre-determined time point (10, 20, 30 and 60 days), the samples were analyzed in terms of particle size, zeta potential, and curcumin content.

3.2.4.3. Transmission electron microscopy (TEM) studies

Transmission electron microscope (TEM, JEM-1200EX, JEOL, Tokyo, Japan) was used for morphological observation. One drop of micelles solution was placed on a carbon film-coated copper grid. After negative staining with 2% w/v uranyl acetate for 20 s, the excess solution was absorbed by filter paper and dried in air before analysis.

3.2.4.4. Differential Scanning Calorimetry (DSC)

mPEG-PLA-Ch, free curcumin, and curcumin encapsulated in mPEG-PLA-Ch micelles were analyzed using DSC (DSC 60, Shimadzu, Japan). About 1 mg of each sample was put in the aluminium pan and the lid of the pan was penetrated to form a small hole. Samples were heated from room temperature to 250°C at the rate of 10°C per minute under nitrogen atmosphere at a flow rate of 20 mL per minute.

3.2.5. Hemocompatibility and release profile of the mPEG-PLA-Ch micelles

The hemolysis assay procedure was modified from previously described method (Meng et al. 2011). Heparinized rat erythrocytes were separated from 5 mL of rat blood by centrifugation at 3000 rpm for 30 min and washed with physiological saline to achromatic colour for supernatant solution. After centrifugation, cells were mixed with normal saline to prepare 5% RBC solution. Further, 100 µL of purified 5% RBC solution was incubated with 900 µL of

mPEG-PLA-Ch in PBS at various concentrations for 1 h at 37°C. The copolymer concentration range was set from 0.5-10 mg/mL. Physiological saline and Triton-X 100 (1% solution) were used as negative and positive control, respectively. Samples were centrifuged and hemolysis was quantified by measuring released hemoglobin (Hb). The absorbance of Hb in the supernatant at 576 nm was measured by UV-Vis spectrophotometer (Spectramax™, microplate reader, Molecular Devices, US).

The degree of hemolysis was determined on the basis of absorbance at 576 nm and calculated from the following formula (Dutta and Dey 2011):

$$\text{Hemolysis (\%)} = \frac{\text{Abs}_{\text{sample}} - \text{Abs}_{\text{negative control}}}{\text{Abs}_{\text{positive control}} - \text{Abs}_{\text{negative control}}} \text{ X100}$$

where $\text{Abs}_{\text{sample}}$, $\text{Abs}_{\text{negative}}$, and $\text{Abs}_{\text{positive}}$ were the absorbance of copolymer sample, physiological saline (0% hemolysis) and Triton-X 100 (100% hemolysis). Data were taken from three independent experiments.

In vitro drug release profile of CUR from CUR-mPEG-PLA-Ch micelles was done by dynamic dialysis method (Wu, Zhu, and Torchilin 2013). 1 mL of CUR solution (100 μg/mL in propylene glycol) and 1 mL of CUR-mPEG-PLA-Ch micelles solution were put into dialysis bags (Spectrum Laboratories, Inc. USA) of MWCO 2000 Da. The bags were placed into 40 mL of phosphate buffer solution (pH 7.4) containing 0.1% (w/v) Tween 80 to maintain a constant sink condition. This was kept shaking on an orbital shaker at 100 rpm at 37 ± 0.5°C. At definite time intervals, 1 mL of the released medium was withdrawn. The same volume of fresh release mediums was supplemented to maintain a constant volume. The release amount of drug was quantified spectrophotometrically at a wavelength of 420 nm. All

experiments were performed in triplicates. The release rate was calculated, and the results were expressed as mean ± SD.

3.2.6. *In vitro* cellular uptake

The cellular uptake of CUR-loaded micelles was evaluated by using flow cytometry and fluorescence microscopy. For flow cytometry experiments, B16F10 and MDA-MB-231 cells were seeded on 6-well plates at 4 X 10^5 cells/well and incubated for 24 h. Prior to adding the micelles solution, the culture medium (1 mL) was replaced with fresh medium. Then, the cells were treated with free CUR and CUR-mPEG-PLA-Ch micelles (CUR 50 and 100µg/mL) for 1 and 4 h, respectively. After incubation, the cells were washed twice with PBS, detached with trypsin-EDTA and resuspended in PBS, pH 7.4 (200 µL) for flow cytometer analysis (Amnis Flowsight, United States). The data presented are the mean fluorescent signals for 10,000 cells.

For fluorescence microscopy experiments, the cells were first seeded on microscope slides and incubated with free CUR and CUR-loaded micelles in the same way as that in the flow cytometry experiments. After incubation, the culture medium was removed and the cells on microscope slides were washed with PBS, fixed with 4% paraformaldehyde, stained with DAPI and mounted cell side down on superfrost microscope slides with fluorescence-free glycerol-based mounting medium (Fluoromount-G; Sigma Aldrich, USA). Fluorescence images of cells were obtained with an Inverted Fluorescence microscope (Leica Microsystems, Germany). The images of the cells were taken using FITC filter (λex 495 and λem 520 nm). The LSM picture files were analyzed by using Image J software.

3.2.7. *In vitro* cytotoxicity

Cytotoxicity of CUR-mPEG-PLA-Ch micelles was investigated by the MTT assay. 100 µL of B16F10 and MDA-MB-231 cell lines were seeded in 96 well plates at the density of 1 X 10^4 cells/well and 5 X 10^3 cells/well with DMEM and RPMI-1640, respectively and incubated overnight to allow cell attachment. The old media was discarded and the cells were incubated with CUR-mPEG-PLA-Ch micelles, blank micelles, and free curcumin for 6 h in serum free media and 24 h in complete growth media, respectively. After 6 h, the medium was removed and the wells were incubated for additional 24 h with fresh medium. The following day, 50 µL of MTT solution (5 mg/mL) prepared in the serum/phenol red-free DMEM and RPMI-1640 was added to each well. The plates were further incubated for 4 h. Finally, MTT in medium was removed and 150 µL of DMSO was then added to each well to dissolve the formazan crystals. Each sample was tested in six replicates per plate and assayed at 570 nm wavelength using a microplate reader (Spectramax™, microplate reader, Molecular Devices, US) with a reference wavelength of 630 nm. Cell viability was calculated by the followed equation:

$$\text{Cell viability (\%)} = \frac{\text{Abs}_{\text{sample}}}{\text{Abs}_{\text{control}}} \text{ X100}$$

where, $\text{Abs}_{\text{sample}}$ is the absorbance of the transformed MTT in cells incubated with the formulations while the $\text{Abs}_{\text{control}}$ is the absorbance of transformed MTT in cells incubated with the culture medium only (positive control).

3.2.8. Anti-tumor activity assay

C57BL/6 mice were inoculated subcutaneously with murine melanoma cells, B16F10 (5 X 10^5 cells in 100 µL of PBS). Tumors were allowed to grow for 2-3 weeks to reach

proliferative phase (approximately 50-100 $mm^{3)}$. Subsequently, CUR-mPEG-PLA-Ch and CUR-mPEG-PLA micelles in PBS buffer (pH 7.4) were injected intraperitoneally once at 2-day intervals (CUR dose. 25 mg/Kg). The micelles were diluted to a concentration of 10 mg of total copolymer or 500 μg of CUR/mL of micelle solution so that the mice (approximately 20 g) received ~200 μL of micelle preparation intraperitoneally. Groups of mice were as follows: (i) Saline (the control group); (ii) Free Curcumin; (iii) CUR-mPEG-PLA and (iv) CUR-mPEG-PLA-Ch (n = 6 in each group). Each sample was intraperitoneally injected every two days for 22 days (5 times). Tumor size and animal body weight were measured every two days during the study. The tumor volume and body weight were recorded for all tumor-bearing mice for 22 days until the tumor size of animals in the control groups reached 1500 mm^3, after which animals were sacrificed in CO_2 chamber. The length and width of the tumors were measured by vernier calliper and the tumor volume was calculated using the following formula:

$V = a \times b^2/2$

where, a and b denote the long and short diameters of the tumor, respectively.

The post-mortem tumor weight was taken after washing the tumors with PBS. The tumors were embedded in tissue freezing media and stored at -80°C. For tumor histology, tumor slices (5 μM) were cryo-sectioned and stained with the Terminal Deoxynucleotidyl Transferase Biotin-dUTP Nick End Labeling (TUNEL) assay following the manufacturer's protocol and examined under a fluorescence microscope equipped with green filter.

3.2.10. Statistical analysis

The data were tested for statistical significance using Student's t-test. *p* values, calculated with the Graph Pad prism 5 software (GraphPad Software, Inc, San Diego, CA). All

numerical data are expressed as mean ± SD, n = 3 or 4, from 3 different experiments. Any *p* values less than 0.05 was considered statistically significant. *, **, *** in figures indicated *p* values <0.05, 0.01 and 0.001, respectively.

3.3. RESULT AND DISCUSSION

3.3.1. Synthesis and characterization of mPEG-PLA-Ch copolymers

mPEG-PLA-Ch block copolymers were prepared through two reaction steps. In the first step mPEG-PLA diblock copolymer was prepared by ring opening polymerization reaction of mPEG and D,L-Lactide by using stannous octoate as the catalyst followed by modifying the terminal hydroxyl group of mPEG-PLA with cholesteryl chloroformate (Figure 3.2). The final cholesterol-conjugated mPEG-PLA polymer was purified by precipitation and subsequent membrane dialysis to completely remove the unreacted cholesteryl chloroformate. The final polymer was obtained as a fine white powder as 71% yield.

The ^{1}H HMR spectrum of mPEG-PLA-Ch copolymer is shown in Figure. 3.3. The peaks at 1.6 and 5.1 ppm were assigned to CH_3-O- and multiplet of -CH of PLA, respectively. Moreover, the peak at 3.6 ppm from the methylene protons of PEG (-OCH_2-CH_2-) can also be observed. After conjugation with cholesteryl chloroformate, ^{1}H NMR spectrum of the polymer exhibited two singlets at 0.68 and 1.02 ppm, and two doublets at 0.85 and 0.91 ppm, which are assigned to four kinds of methyl groups of the cholesteryl moieties. The graph and the detail analysis of the IR of mPEG-PLA-Ch were reported in the supplementary section.

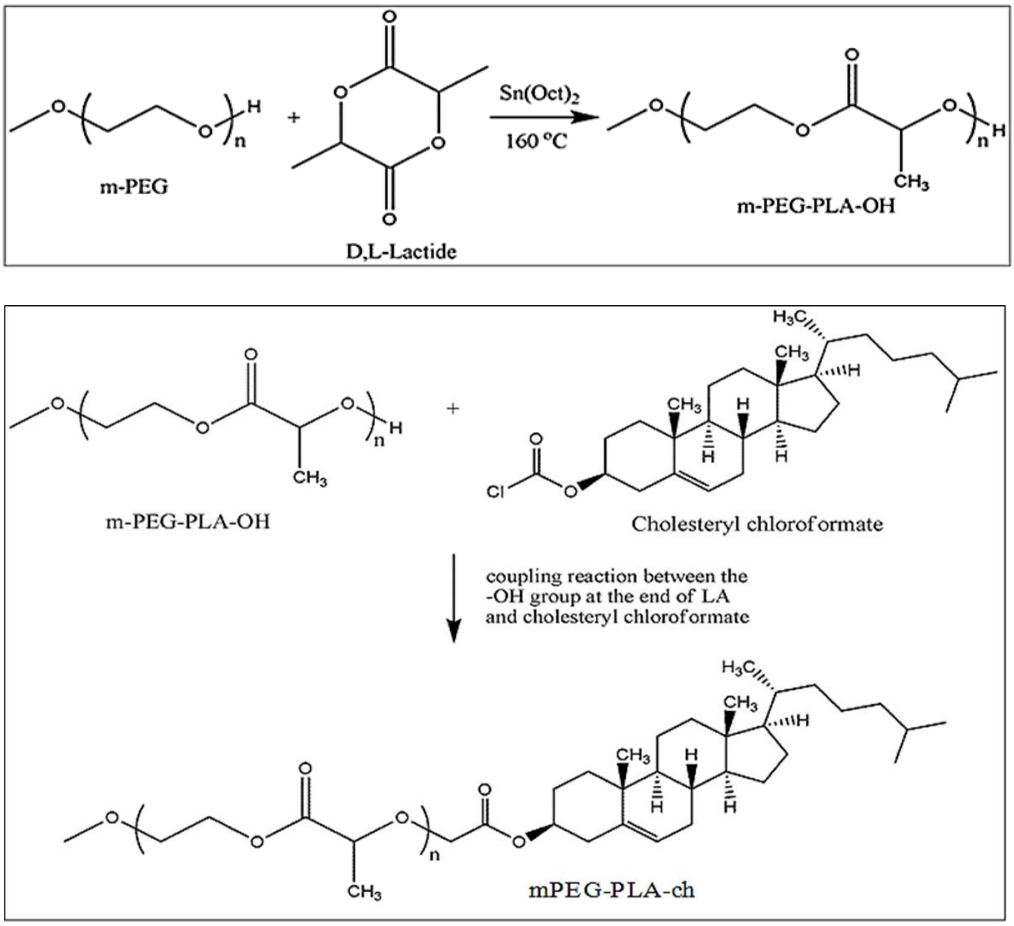

Figure 3.2. Detailed synthetic route of mPEG-PLA-Ch copolymer.

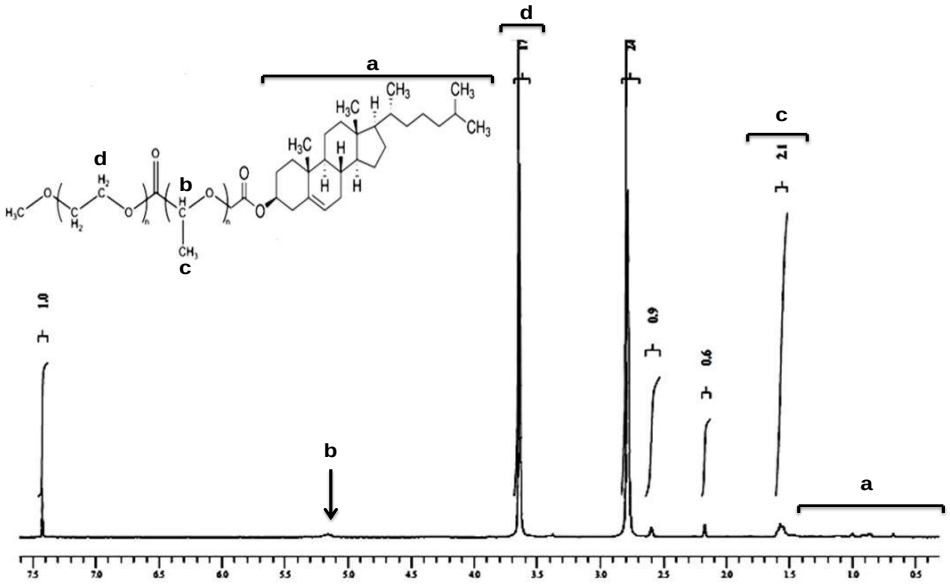

Figure 3.3. ^{1}H NMR spectrum of mPEG-PLA-Ch copolymer.

3.3.2. Preparation and characterization of CUR-loaded polymeric micelles

For the efficient encapsulation of curcumin (CUR), mPEG-PLA-Ch copolymer was used based on its solid state solubility and compatibility. We adopted the thin film hydration method to prepare curcumin loaded mPEG-PLA-Ch micelles. Solubilization of hydrophobic anticancer drugs and development of biocompatible drug delivery systems are the prime aim of drug delivery research (Shaikh et al. 2009). Thin film hydration method is most often used due to its simplicity and practicability, and its ability to yield small and uniform particles.

Curcumin loaded mPEG-PLA micelles (CUR-mPEG-PLA-Ch) was prepared using the thin film hydration technique. To optimize the process parameters, we investigated the effect of copolymer to drug ratio on the properties of the resulting micelles, shown in Table 3.1.

Table 3.1. Characteristics of curcumin-loaded mPEG-PLA-Ch micelles.

Sample	mPEG-PLA-Ch/ CUR[a]	Particle Size (mean ± SD)	PDI (mean ± SD)	Zeta Potential (mV) (mean ± SD)	DL (%) (mean ± SD)	EE (%) (mean ± SD)
CH1	12:0.5	167.02 ± 2.71	0.392 ± 0.61	-20.12 ± 1.69	9.44 ± 0.62	82.37 ± 1.02
CH2	11.5:1	175.03 ± 1.85	0.439 ± 0.97	-19.28 ± 0.88	9.83 ± 1.07	84.71 ± 1.55
CH3	11:1.5	180.17 ± 2.97	0.516 ± 0.57	-19.05 ± 1.39	10.65 ± 1.84	88.32 ± 0.91
CH4	10.5:2	183.36 ± 1.72	0.463 ± 0.38	-20.86 ± 0.86	11.68 ± 1.57	89.83 ± 1.91
CH5	10:2.5	189.91 ± 0.36	0.488 ± 0.017	-18.23 ± 0.72	13.86 ± 0.95	93.74 ± 1.62
CH6	9.5:3	b	b	b	b	b

a In feed

b Cannot be determined

The drug loading, and particle size increased with increase in CUR to mPEG-PLA-Ch ratio in the feed. When the mPEG-PLA-Ch/CUR mass ratio in the feed was 9.5:3, the resulting micelles were not stable *in vitro* (formed aggregates). However, DL was increased with enhanced drug feeding, and the DL reached 13.86 ± 0.95 at a feed weight ratio of 10:2.5 (CH

5). The composition of optimum formulation was determined as 10 mg of copolymer and 2.5 mg of CUR, which fulfilled the requirements of optimization. The mean particle size of blank and CUR-loaded mPEG-PLA-Ch micelles measured from the dynamic light scattering were 169.35 ± 1.52 and 189.91 ± 0.36 nm with polydispersity index of 0.300 ± 0.021 and 0.488 ± 0.017, respectively as shown in Figure. 3.4A. The drug was loaded into micelles, resulting in an increase in the mean particle diameter. Zeta potentials of blank and CUR loaded mPEG-PLA-Ch micelles were -12.37 ± 0.59 mV and -18.23 ± 0.72 mV, respectively. The samples were analyzed spectrophotometrically to determine CUR-fluorescence at 420 nm. The blank sample had no absorbance at this wavelength in the CUR-concentration range of 2–20 µg/mL, the following standard regression equation was obtained, A = 0.1473B + 0.0086, R2 = 0.9998 (n = 3). The average EE and DL of the optimized CUR-mPEG-PLA-Ch formulation were 93.74 ± 1.62% and 13.86 ± 0.95%, respectively compared to mPEG-PLA micelles (EE 91.89 ± 1.27% and DL 11.06 ± 0.83%) (Kumari et al. 2016).

Surface morphology of the CUR- loaded mPEG-PLA-Ch micelles was visualized by TEM (Figure. 3.4B). Characterization by DSC gives an insight into the melting and re-crystallization behaviour of the crystalline materials loaded in the micelles. Figure. 3.4C showed DSC curves of curcumin, mPEG-PLA-Ch copolymer, and CUR loaded mPEG-PLA-Ch micelles. The pure curcumin displayed a single sharp endothermic peak at 171.93°C. However no such peak depression was observed in CUR loaded micelles, suggesting a high distribution of CUR throughout the polymer matrix in micelles. This data also indicated that the CUR was present in amorphous stage in the mPEG-PLA-Ch micelles.

The ability of the polymer to form stable polymeric micelles was assessed by determining CMC. Pyrene method was used to measure the CMC of the micelles (Song et al. 2011). With

the logarithm of concentration of micelles as the abscissa and the fluorescence intensity as the ordinate, the CMC of the mPEG-PLA-Ch micelles was 25 µg/mL gained from intersection of the two tangents to scatter diagram (Figure. 3.4D). The CMC of novel micellar system was comparable to standard micelle-forming polymer, PEG-DSPE (CMC for PEG-PE 12.5 µg/mL in the assay system). Modification with cholesterol improved the hydrophobicity of the core in mPEG-PLA micelles resulting in superior micellization ability as judged by their low CMC value compared to mPEG-PLA micelles (reported CMC of mPEG-PLA 50 µg/mL based on our previous data) (Kumari et al. 2016). Because of the low CMC, the micelles had high stability and ability to maintain integrity even after extreme dilution in the systemic circulation.

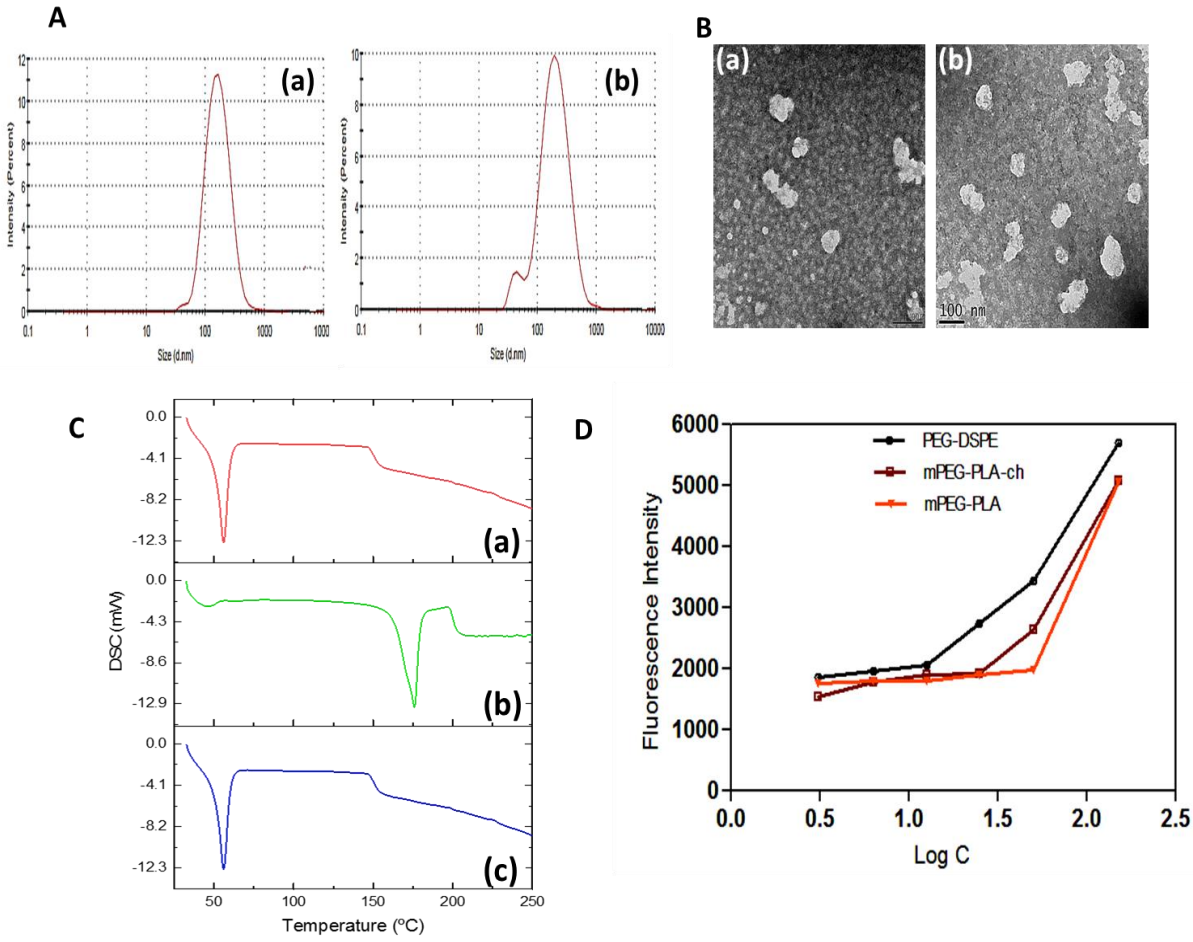

Figure. 3.4. Physico-chemical characterization of polymeric micelles. A. Particle size distribution of mPEG-PLA-Ch (a) and CUR-mPEG-PLA-Ch micelles (b) measured by light scattering method; B. Transmission electron micrograph of the mPEG-PLA-Ch (a) and CUR-mPEG-PLA-Ch micelles (b); C. Differential scanning calorimetry thermograms of the CUR-mPEG-PLA-Ch (a), free CUR (b), and mPEG-PLA-Ch (c); D. Determination of critical micelles concentrations of mPEG-PLA-Ch compared to PEG-DSPE.

The stability was checked over a two months. The variation of the sizes of mPEG-PLA-Ch micelles as a function of incubation time is shown in Table 3.1. It can be seen, the particle size of micelles was increased slightly at 4°C. The curcumin was retained inside the micelles upto two months at 4°C, and 25°C. The high encapsulation efficiency and stability is due to the hydrophobicity of the curcumin and the effectiveness of mPEG-PLA-Ch micelles in solubilizing such poorly soluble drug.

Table 3.1. Stability of curcumin-mPEG-PLA-Ch micelles at 4°C and 25°C.

Micelles	Day	Particle Size (mean ± SD)	PDI (mean ± SD)	Zeta Potential (mV) (mean ± SD)	DL (%) (mean ± SD)	EE (%) (mean ± SD)
CUR-mPEG-PLA-Ch 4°C	0	189.91 ± 0.36	0.488 ± 0.017	-18.23 ± 0.72	13.86 ± 0.95	93.74 ± 1.62
	10	190.07 ± 1.83	0.451 ± 0.028	-21.29 ± 1.06	13.21 ± 1.59	93.04 ± 2.73
	20	191.39 ± 1.69	0.385 ± 0.091	-19.04 ± 1.76	12.84 ± 0.75	92.77 ± 1.15
	30	195.42 ± 2.05	0.410 ± 0.051	-19.73 ± 1.82	12.39 ± 1.67	92.16 ± 1.55
	60	203.85 ± 1.38	0.396 ± 0.074	-20.24 ± 0.93	12.81 ± 1.55	91.73 ± 1.80
CUR-mPEG-PLA-Ch 25°C	0	189.91 ± 0.36	0.488 ± 0.017	-18.23 ± 0.72	13.86 ± 0.95	93.74 ± 1.62
	10	550.59 ± 1.71	0.708 ± 0.083	-10.82 ± 1.57	4.09 ± 2.89	49.65 ± 3.43
	20	-	-	-	-	-
	30	-	-	-	-	-
	60	-	-	-	-	-

3.3.3. Hemocompatibility and release profile of the mPEG-PLA-Ch micelles

To explore the compatibility of the copolymers with blood components, hemolytic assays were performed for the polymer, mPEG-PLA-Ch in PBS pH 7.4. Freshly isolated rat red blood cell (RBC) suspension (5% v/v) was added to PBS, 1% Triton X-100 and polymers with a final concentration of 0.5, 2, 6, and 10 mg/mL, and incubated for 60 min at 37°C. The pictures associated to the hemolytic experiments are presented in inset of Figure. 3.5A. As seen, clearly none of the samples exhibited any hemolysis. To quantify the hemolytic activity of polymer samples for each treatment, the percentage of cell lysis relative to the untreated cell (% control) was determined by measuring the absorbance (576 nm) of the supernatant. Hemolytic activity (in %) of the copolymer along with the positive and negative control is presented in Figure. 3.5B. Based on the previous studies, any sample with less than 5% hemolysis ratio is regarded as nontoxic (Rao and Sharma 1997). In the present investigation, it is observed that the copolymer mPEG-PLA-Ch at a concentration of 0.5, 2, 6, and 10 mg/mL exhibited 3.24 ± 1.07, 3.59 ± 0.96, 3.98 ± 0.64, and 4.74 ± 0.21% hemolysis, respectively whereas mPEG-PLA copolymer showed 4.86 ± 0.92% hemolysis at highest concentration of 10 mg/mL. Therefore, with cholesterol modification in side chain of copolymers did not exhibit any significant lysis to RBC membrane and hemolytic activity of the copolymers was independent on the hydrophobic composition or hydrophobic chain length to mPEG-PLA-Ch.

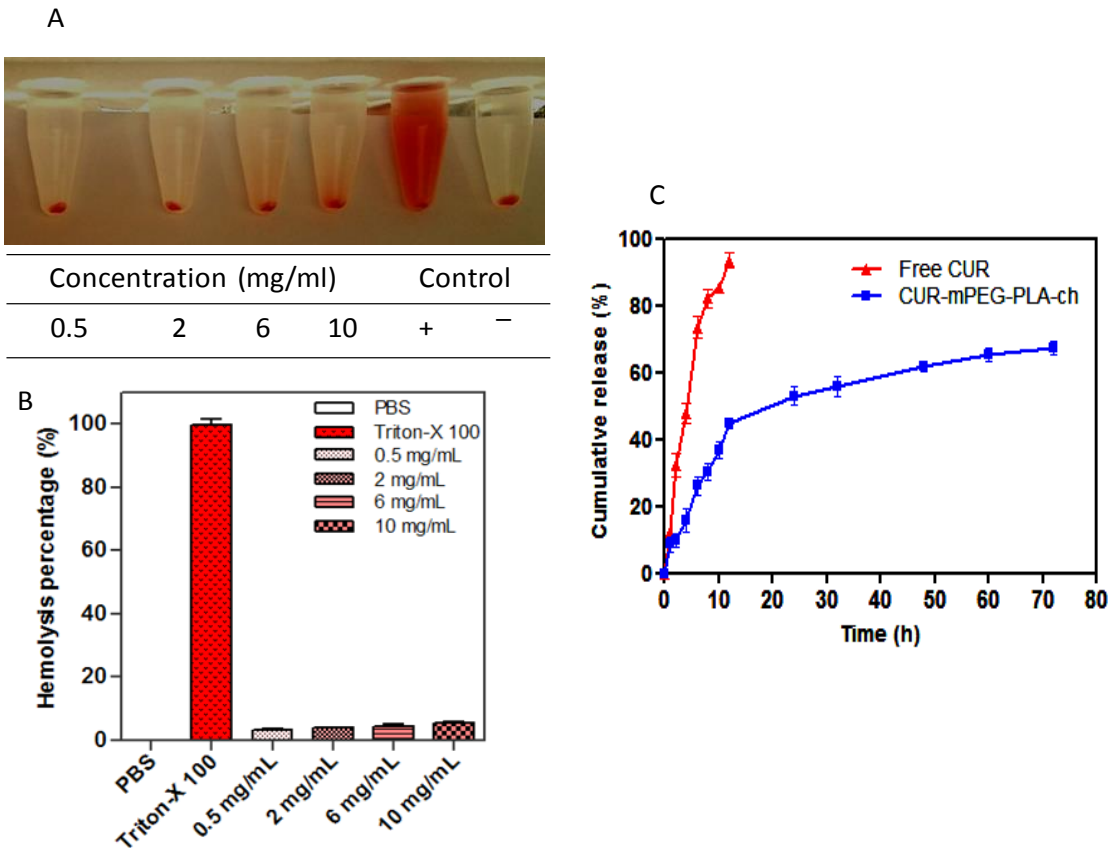

Figure. 3.5. Assessment of hemo-compatibility of the polymer (A and B) and the release of loaded CUR (C). A and B. Percentage of hemolysis of mPEG-PLA-Ch at 0.5, 2, 6, and 10 mg/mL concentration at pH 7.4; C. *In vitro* CUR-release profile from free CUR and CUR-mPEG-PLA-Ch micelles in media (PBS, pH 7.4) (data are presented as mean ± SD (n = 3)).

The release of curcumin from the mPEG-PLA-Ch micelles was investigated in PBS at 37°C. The drug release was determined at pre-determined intervals of up to 72 h. The cumulative percentage release of CUR was shown in Figure. 3.5C. Initial release of curcumin from the formulations is considered to be a burst release of deposited or weakly bound drug on the surface of the micelles (Mittal et al. 2007). The drug release percentage from the CUR propylene glycol solution and CUR-mPEG-PLA-Ch micelles was 80.16% and 47.42% of the

encapsulated drug during the first 12 h, respectively. The release percentage of CUR reached 91.69% and 69.83% within following 12 h, respectively. However, only 9.73% of CUR was released from the CUR-mPEG-PLA micelles within the first 6 h, while about 64.24% of CUR was released from the propylene glycol solution during the same time period (Kumari et al. 2016). Therefore, most of the CUR was embedded in the hydrophobic core by hydrophobic interaction, and the amount of CUR in the surface of the nanoparticles was insignificant. The released mechanism of CUR from micelles might be related to the drug diffusion and the disintegration of polymer material (Liu et al. 2001; Ruan and Feng 2003). The drug release process was mainly as follows, firstly, the media gradually got into the micellar interior to dissolve CUR, and the dissolved drug spread to the media slowly. Then, the carrier material was corroded and degraded, and the CUR was released with a slow rate.

3.3.4. Cellular uptake of CUR micelles

Free CUR and CUR-loaded micelles-treated cancer cells were visualized under fluorescence microscope to assess cellular uptake of the nanocarriers (Figure. 3.6). The result demonstrated that these micelles were actively taken up by B16F10 (Figure. 3.4A) and MDA-MB-231cells (Figure. 3.6B) as seen by green fluorescence within the cells. No fluorescence was observed in cells treated with blank micelles. CUR-loaded micelles could rapidly accumulate in the cytosol of cells in 1 h revealed by bright green fluorescence compared to the treatment with free CUR which resulted in less intense fluorescence in the cytosol. Further, intensity of green fluorescence in cytosol after micelles treatment was much brighter after 4 h compared to 1 h treatment.

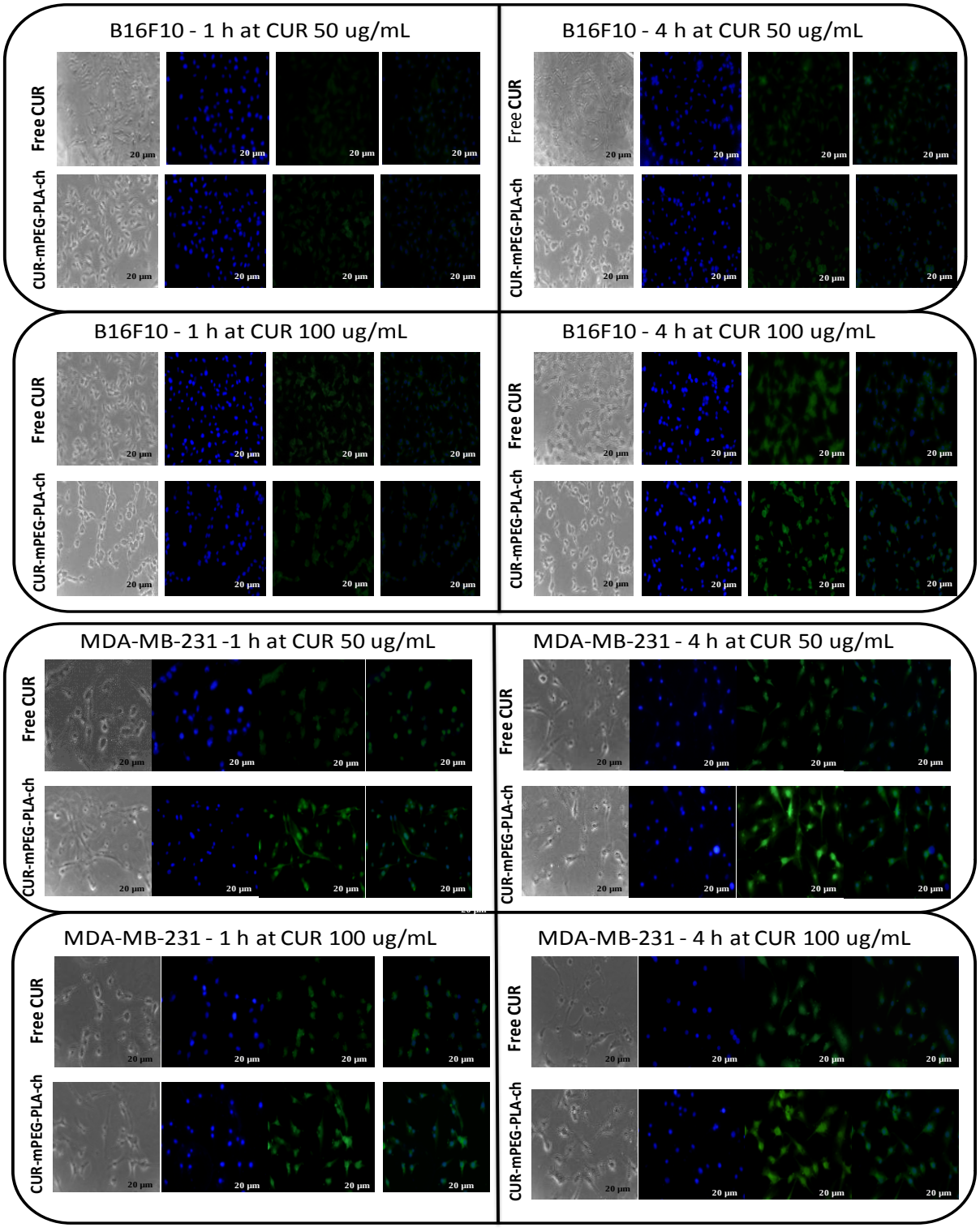

Figure. 3.6. Fluorescence microscopy images of cancer cells (B16F10, and MDA-MB-231) to assess cellular uptake of CUR-loaded polymeric micelles. A. B16F10 cells treated with free

CUR and CUR-mPEG-PLA-Ch at CUR concentration of 50 and 100 µg/mL; B. fluorescence micrograph of MDA-MB-231 cells following the same treatment as B16F10 cells. Blue and green signals present cell stained by DAPI and CUR fluorescence in cells, respectively (Scale bar = 20 µm).

The intensity of fluorescence was quantified by flow cytometry analysis. The study was performed on both the cell lines in dose (50 and 100 µg/mL) and time (1 and 4 h) dependent manner (Figure 3.7A and B). Time and dose dependent cellular association of nanocarriers were observed. Intensity of fluorescence (represented as the geometric mean of fluorescence) was much stronger for the cells treated with CUR-loaded mPEG-PLA-Ch micelles compared to the free CUR treatment and CUR-mPEG-PLA micelles (Kumari et al. 2016). Significantly lower intensity of cellular fluorescence following free CUR treatment could be due to the absence of a carrier system as well as the instability of the free CUR.

A

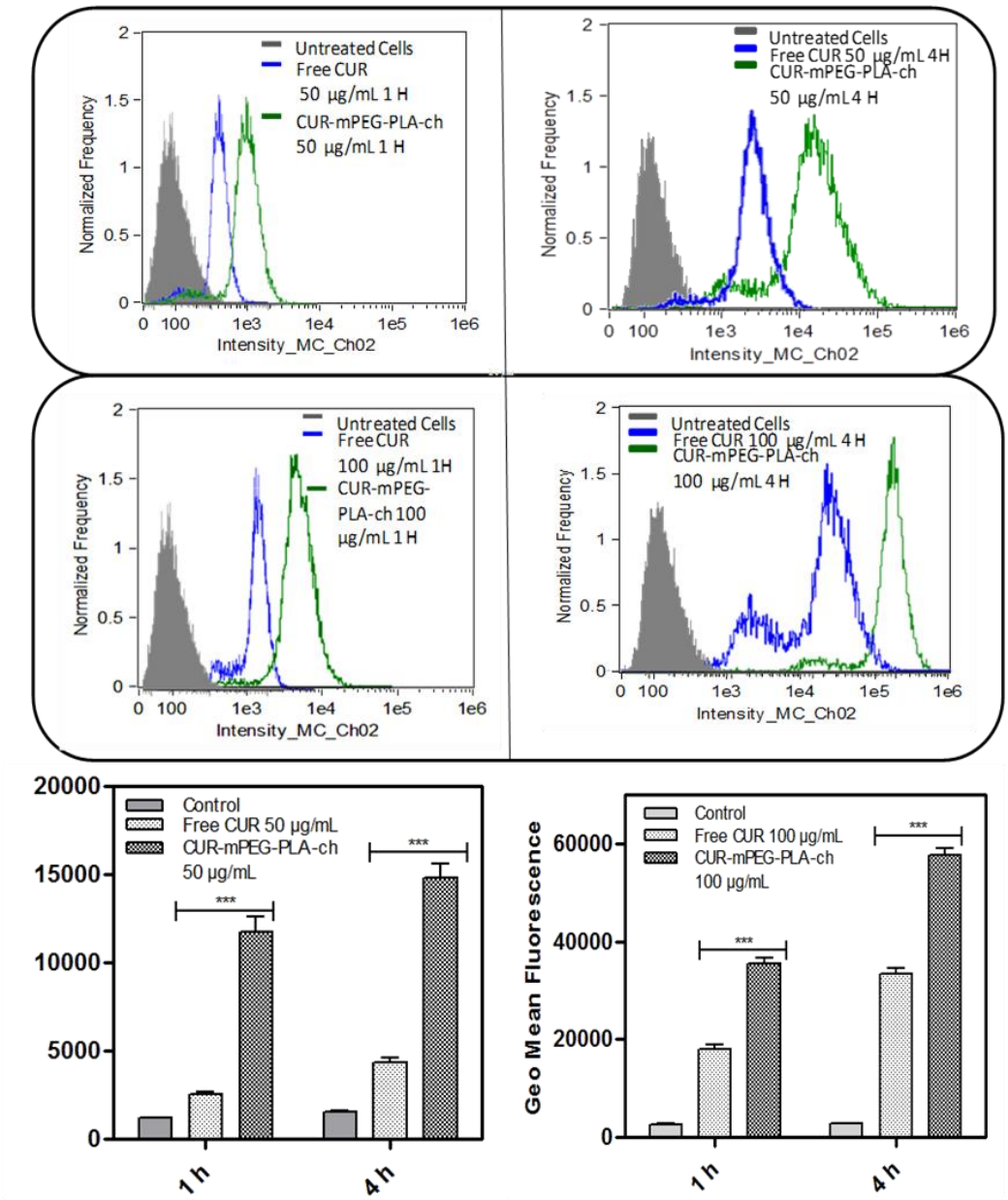
Untreated Cells
Free CUR
50 µg/mL 1 H
CUR-mPEG-PLA-ch
50 µg/mL 1 H
Normalized Frequency
Intensity_MC_Ch02
Untreated Cells
Free CUR 50 µg/mL 4H
CUR-mPEG-PLA-ch
50 µg/mL 4 H
Untreated Cells
Free CUR
100 µg/mL 1H
CUR-mPEG-
PLA-ch 100
µg/mL 1 H
Untreated Cells
Free CUR 100 µg/mL 4 H
CUR-mPEG-PLA-ch
100 µg/mL 4 H
Control
Free CUR 50 µg/mL
CUR-mPEG-PLA-ch
50 µg/mL
Control
Free CUR 100 µg/mL
CUR-mPEG-PLA-ch
100 µg/mL
Geo Mean Fluorescence
1 h
4 h

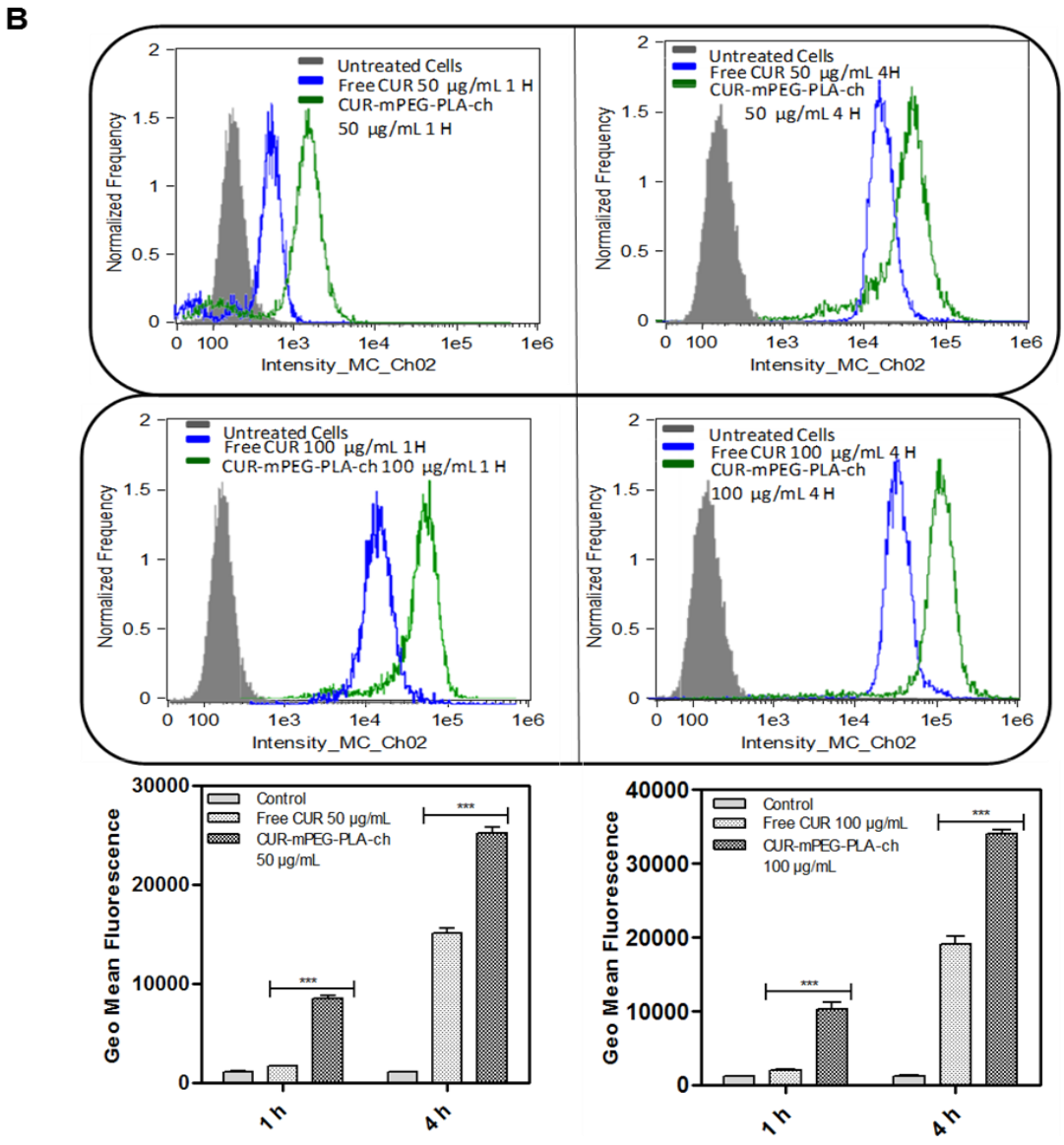

Figure. 3.7. Quantification of cellular association of Free CUR and CUR-mPEG-PLA-Ch micelles by flow cytometry in B16F10 (A) and MDA-MB-231 (B) cells. The cell-associated CUR fluorescence was measured. The figure represents the histogram plots and comparison of the geometric mean of fluorescence of the cells following 1 and 4 h treatment with Free CUR or CUR-mPEG-PLA-Ch. The data are mean ± SD, averaged from three separate experiments. The significance of difference between the mean was analyzed by Student's t-test, *, **, *** indicates <0.05, 0.01 and 0.001, respectively

3.3.5. Cytotoxicity studies

The *in vitro* cytotoxicity of both the murine and human cancer cells following treatment with CUR, either free or in micellar form was investigated by MTT assay. Blank micelles exhibited no cytotoxicity as the cellular viability was above 90% at all concentrations used during experiment (Figure. 3.8). These results indicated that the cytotoxicity following CUR-mPEG-PLA-Ch treatment was solely due to the efficient delivery of CUR. As stated earlier, two treatment protocols were followed: (i) treatment for 6 h followed by 24 h incubation before measurement of cell viability; (ii) treatment for 24 h before measurement of cell viability. The result demonstrated that the free CUR decreased the viability of B16F10 cells significantly when incubated for 24 h compared to 6 h treatment (Figure. 3.8), however, the same treatment with free CUR showed no time dependent cytotoxicity in MDA-MB-231 cell lines (Figure. 3.8). The cytotoxic effect of CUR was more prominent in B16F10 cells compared to MDA-MB-231 cell line. CUR-mPEG-PLA-Ch micelles demonstrated higher cellular toxicity compared to free CUR at the highest tested CUR dose of 50 µg/mL following the incubation period of 6 h (30.11 ± 2.3% vs. 73.13 ± 3.7% cell viability for CUR-mPEG-PLA-Ch vs. free CUR, respectively). However, no such significance in difference in cell viability was observed in B16F10 cell lines following 24 h incubation with the same dose of 50 µg/mL. Following 6 h incubation, at CUR-concentration of 50 µg/mL, CUR-micelles produced significantly higher cellular toxicity compared to free CUR (cell viability of 55.26 ± 3.7% vs. 66.84 ± 2.4%, for CUR-micelles and free CUR, respectively). Similar trend in cell viability was observed following 24 h incubation with cell viability of 35.46 ± 4.3% for CUR-mPEG-PLA-Ch compared to 62.75 ± 0.9% for free CUR at CUR concentration of 50 µg/mL.

As shown in Figure. 3.8, CUR-mPEG-PLA-Ch treatment was more effective in killing cancer cells except at 24 h time point in B16F10 cell line. This could be due to incomplete release of the loaded drug from the formulation. Further, previous studies by other groups indicated that the IC50 value varied in different cell lines with the same treatment (Wichitnithad et al. 2011). Concerning B16F10 cell line, similar result was reported by Anuchapreeda *et al* where they have shown that the encapsulation of CUR in nano-emulsion could not reduce the IC50 value compared to the administration of free CUR to B16F10 cells (Anuchapreeda et al. 2011). Variability in IC50 values following CUR administration in different leukemic and B16F10 cell lines was demonstrated by this study. Therefore, *in vitro* cytotoxicity result might not be a true prediction of the *in vivo* therapeutic activity.

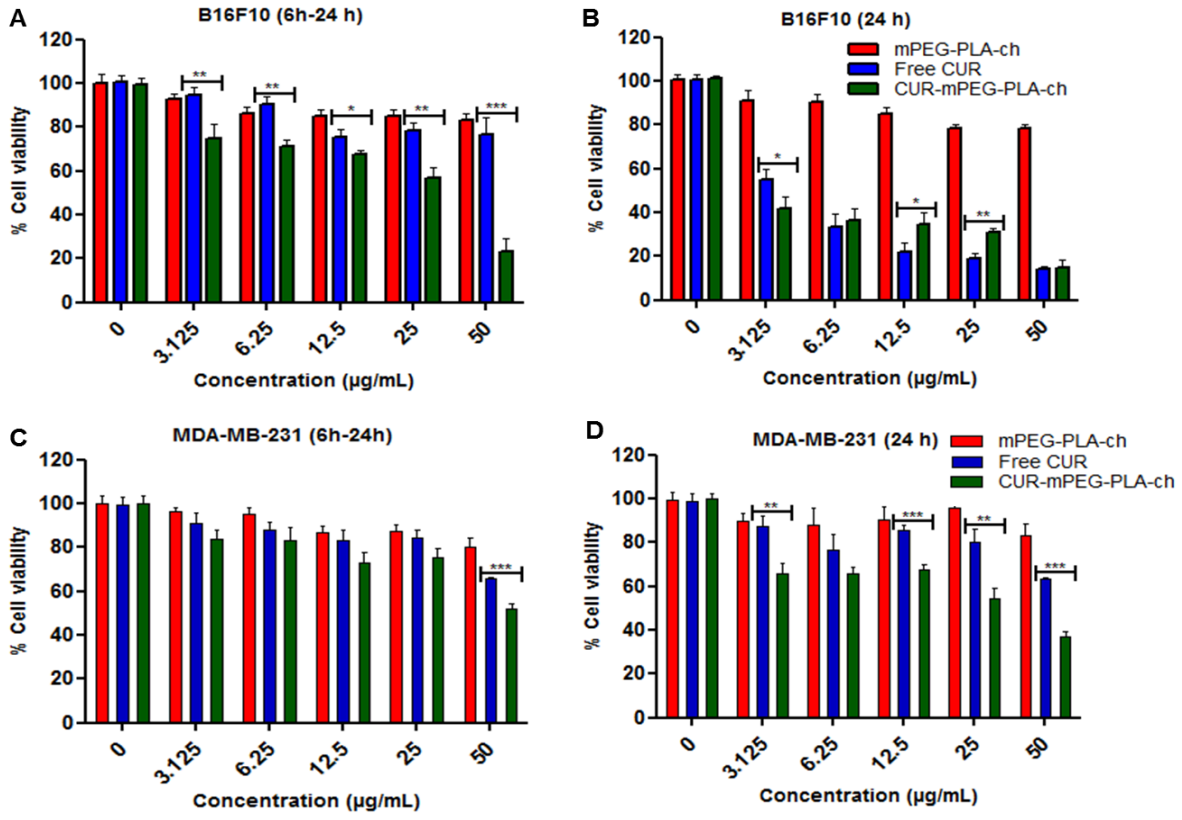

Figure. 3.8. Measurement of *in vitro* cytotoxicity of blank micelles, free CUR, and CUR-mPEG-PLA-Ch micelles by MTT assay against B16F10 and MDA-MB-231 cell lines. The

CUR concentration range was 0-50 µg/mL, and the period of incubation was 6 and 24 h. The cells undergoing 6 h treatment were incubated for additional 24 h before performing MTT assay to determine cell viability. The significance of difference between the mean was analyzed by Student's t-test, *, **, *** indicates <0.05, 0.01 and 0.001, respectively (data are presented as mean ± SD (n = 3).

3.3.7. Assessment of *in vivo* therapeutic efficacy

C57BL/6 mice bearing ~50-100 mm^3 of B16F10-xenografted tumors were treated with CUR dose of 25 mg/kg every 2 days for five times. The intraperitoneal injection volume was maintained at ~200 µL (below 500 µL) to reduce the stress on the animals. Formulations were prepared at CUR concentration of 500 µg/mL to maintain an injection volume of 200 µL and the dose of CUR at 25 mg/kg. The results obtained from the *in vivo* experiments have been represented in Figure. 3.9. The graphical representation of tumor volumes vs. time post-injection (over the course of treatment for 22 days) indicated that the treatment with CUR-mPEG-PLA-Ch suppressed the tumor growth at significantly higher rate compared to free CUR-treatment (Figure. 3.9A). Over the 22-day period, the tumor volume increased from 74.12 ± 6.72 to 589.77 ± 24.21 mm^3 for CUR-mPEG-PLA-Ch, 75.5 ± 5.89 to 732.58 ± 37.46 mm^3 for CUR-mPEG-PLA, whereas for free CUR, the volume increased from 72.73 ± 8.74 to 985.67 ± 28.96 mm^3. The tumor weight after isolation was 1.76 ± 0.04, 1.23 ± 0.05, 0.61 ± 0.07, and 0.79 ± 0.03 g for PBS, free CUR, CUR-mPEG-PLA-Ch, and CUR-mPEG-PLA treatment, respectively (Figure. 3.9B). Further, the treated animals showed no reduction in body weight over the treatment period that indicated that no formulation exhibited marked *in vivo* toxicity (Figure. 3.9C). To determine the extent of apoptosis in the tumor after the treatment, TUNEL assay was performed. Figure. 3.9D represented the fluorescence

micrograph of tumor tissue sections following TUNEL assay. As visualized under fluorescence microscope, the CUR micelles-treated group showed significantly higher amounts of green dots representative of apoptotic nuclei attributed to FITC-labeled TdT compared to the tumor section from free CUR treatment group. The cell-nuclei of tumors treated with PBS exhibited no green fluorescence attributable to FITC-labeled TdT indicating no sign of apoptosis.

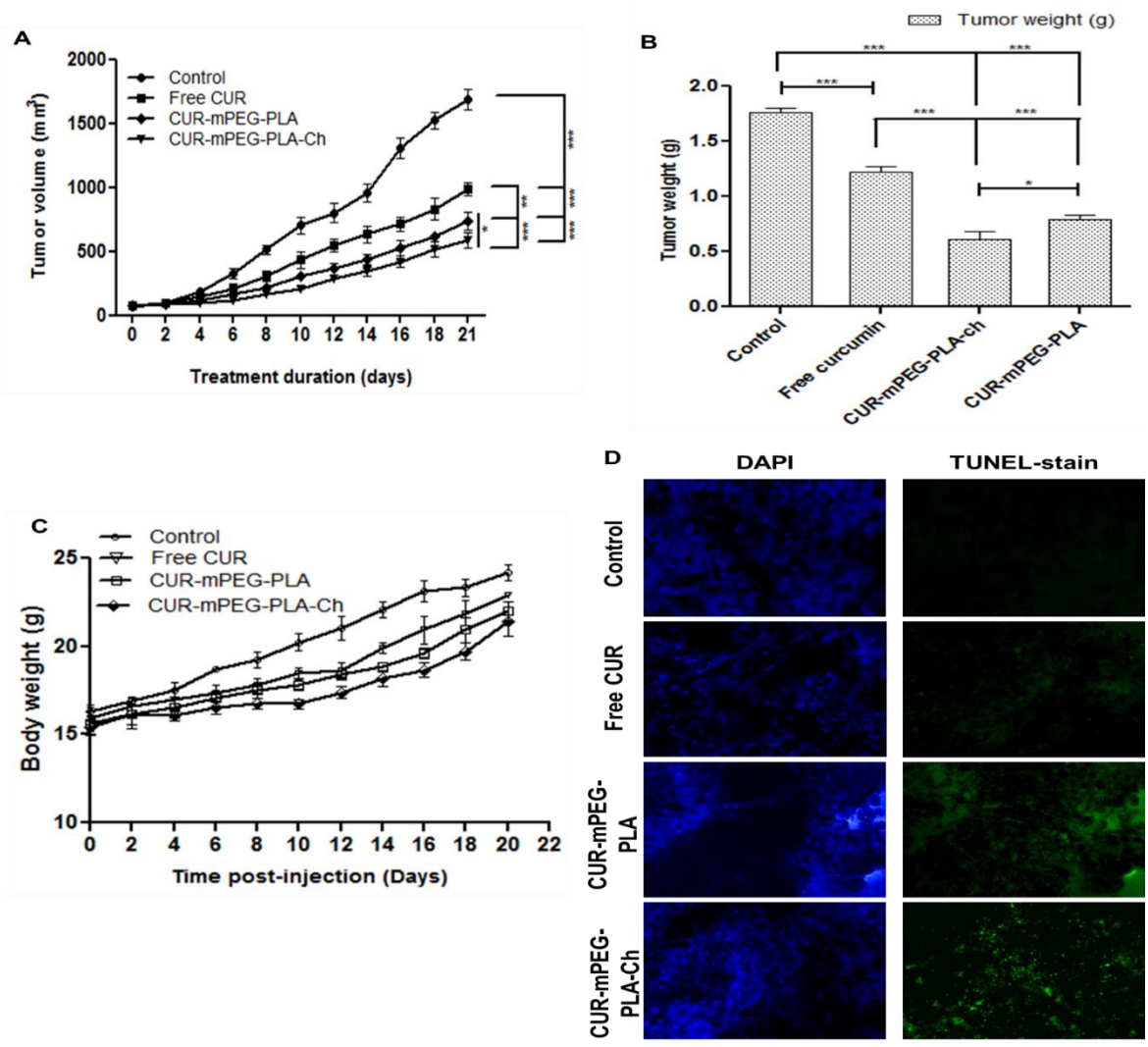

Figure. 3.9. Assessment of *in vivo* therapeutic efficacy of CUR-mPEG-PLA-Ch micelles compared to free CUR and CUR-mPEG-PLA administered intraperitoneally in B16F10-tumor

bearing mice. (A and B). A graphical representation of measured tumor volume vs. time post-injection, and the weight of the tumor isolated after sacrificing the animal post treatment; (C) The body weight of mice of different treatment groups plotted against the duration of treatment (D) Apoptosis analysis. Apoptotic cells were detected in frozen tumor sections, determined by TUNEL assay and visualized by fluorescence microscopy. The left panel shows the sections stained with DAPI and the right panel shows the TUNEL staining. Magnifications - 20 X objective.

3.4. CONCLUSION

The study has identified a novel polymeric micellar drug delivery system, cholesterol-modified mPEG-PLA micelles, mPEG-PLA-Ch for improved delivery of CUR in cancer. Modification with cholesterol improved the hydrophobicity of the core in mPEG-PLA micelles resulting in superior micellization ability. The newly developed polymeric micelles encapsulated and delivered CUR efficiently in various cancer cell lines *in vitro* and into the tumor *in vivo* that resulted in improved therapeutic efficacy of CUR compared to the treatment with free CUR. The mPEG-PLA-Ch micelles could potentially be utilized to deliver any hydrophobic chemotherapeutic agents, including CUR in cancer. In addition, the study provides a strong rationale for potential utilization of the newly developed CUR-mPEG-PLA-Ch micellar system as a promising anticancer therapy.

Chapter 4

Poly(Lactide)-based polymeric micelles loaded with chlorin e6 for photodynamic therapy: *In vitro* evaluation in monolayer and 3D spheroid models

ABSTRACT

Recently, photodynamic therapy (PDT) has found wide application as a non-invasive treatment modality for several cancers. However, the suboptimal delivery of photosensitizers (PSs) to the tumor site is a drawback, which inhibits the effectiveness of PDT. Hydrophobicity, strong oxygen and light dependence, and limited tissue penetrability of photosensitizers represent the major barriers to the clinical application of PDT. In order to improve biopharmaceutical properties of a clinically approved photosensitizer Chlorin e6 (Ce6), we developed a nano-formulation encapsulating Ce6 in methoxy-poly(ethylene glycol)-poly(D,L-Lactide) (mPEG-PLA) co-polymeric micelles. The physicochemical properties, including particle size, zeta potential, encapsulation efficiency, drug loading, generation of reactive oxygen species following near-infrared light illumination (633 nm), and *in vitro* drug release were determined. The therapeutic efficacy of Ce6-mPEG-PLA micelles following illumination were evaluated *in vitro* in both two and three-dimensional cell culture systems by using human alveolar adenocarcinoma (A549) cells in monolayers, and in A549 spheroids, respectively. The Ce6-mPEG-PLA micelles were stable with a particle size of 189.6 ± 14.32 nm and encapsulation efficiency of 75.12 ± 2.75%. Ce6-mPEG-PLA micelles mediated PDT showed improved cellular internalization in both the cell lines resulting in enhanced cytotoxicity compared to free Ce6. In contrast, the Ce6-loaded micelles did not show any cytotoxicity in the absence of irradiation. The Ce6-loaded micelles exhibited deep penetration in the spheroids leading to phototoxicity and cellular apoptosis in A549 spheroidal model. Results from this study indicated that the newly developed nano-formulation of Ce6 could be utilized in PDT as an effective treatment modality for solid tumors.

4.1. INTRODUCTION

Recently, photodynamic therapy (PDT) have found potential application as a non-invasive treatment modality for various cancers. Photosensitizers (PSs), used in PDT are activated by specific wavelength of light to generate reactive oxygen species (ROS). ROS enters the surrounding area only few tens of nanometers from their site of formation, thus limiting the phototoxicity to the illuminated tumor region (Agostinis et al. 2011; Hopper 2000; Oleinick and Evans 1998). PDT has limited side effects apart from photosensitivity to the skin compared to the conventional treatments (Hopper 2000). However, the therapeutic efficacy of PDT in clinic is limited due to poor aqueous solubility of PSs instability due to aggregation, sub-optimal tumor specificity, and low cellular internalization (Chen et al. 2009; Bechet et al. 2008; Lee, Koo, Lee, et al. 2011; Lukyanov and Torchilin 2004).

To overcome these problems of conventional PSs, several nanoparticles (NPs) including liposomes, solid lipid nanoparticles, biodegradable polymers including poly(lactic-co-glycolide) (PLGA), poly(Ɛ-caprolactone) (PCL), polylactide (PLA), graphene oxide, dendrimers and human serum albumin NPs have been investigated as PS carriers, which improve the aqueous solubility, decrease aggregation, increase cellular internalization and enhance tumor specificity through a passive phenomenon of tumor targeting of NPs called the enhanced permeation and retention (EPR) effect (Derycke and de Witte 2004; Lima et al. 2013; Li et al. 2015; Jeong et al. 2011; Lee and Kopelman 2011; Kumari, Yadav, and Yadav 2010). Recently, amphiphilic self-quenchable polymer conjugates of photosensitizers and nanocomplexes of photosensitizer-polymer-conjugate/quencher have been utilized for the delivery of photosensitizers (Penjweini et al. 2013; Isakau et al. 2008; Chin et al. 2008; Park and Na 2013; Py-Daniel et al. 2016). NPs offer great advantages for the delivery of PS in PDT

by overcoming the aforementioned limitations. However, proper choice of NPs has to be made to obtain high drug loading, thermodynamic and kinetic stability of the cargo, increased structural stability of the NPs to avoid degradation and burst release of cargo during systemic circulation (Avci, Erdem, and Hamblin 2014).

Among various PSs, a second-generation photosensitizer Chlorin e6 (Ce6) has a basic structure similar to porphyrins and absorbs energy in near-infrared region (NIR) of light. Ce6 could be readily synthesized from chlorophyll (Brandis, Salomon, and Scherz 2006). Ce6 offers a potential clinical advantage due to its ability to get activated by near infrared wavelengths (Ex.405/Em.670), which opens up the possibility of its successful utilization in treating deeply seated tumors by exciting it using NIR electromagnetic irradiation. Moreover, Ce6 has demonstrated potency against various cancers including melanoma, bladder, and nasopharyngeal cancers (Orenstein et al. 1996; Sheleg et al. 2004; Lee et al. 2010; Kostenich, Zhuravkin, and Zhavrid 1994).

Recently, polymeric micelles received a noteworthy attention as a promising photosensitizers delivery systems (Kataoka, Harada, and Nagasaki 2001). Li *et al.* has developed hydrophobic protoporphyrin IX (PpIX) encapsulated amphiphilic PEG-b-poly(caprolactone) (PEG-PCL) micelles (Li et al. 2007). Meta-tetra(hydroxyphenyl) chlorin (mTHPC) loaded in Poly(2-ethyl-2-oxazoline)-b-PLA diblock copolymer micelles exhibited enhanced PDT effect *in vivo (Shieh et al. 2010).* Polymeric micelles consist of an outer hydrophilic shell and an inner hydrophobic core which encapsulate various drugs by physical entrapment or chemical conjugation (Nishiyama and Kataoka 2006; Lavasanifar, Samuel, and Kwon 2002). Polyethylene glycol (PEG) is widely utilized in drug delivery systems as a hydrophilic outer shell. PEG surpasses other hydrophilic polymeric shells due to its extreme hydrophilicity,

excellent biocompatibility, solubility in aqueous and organic systems, bio-degradability, non-toxicity, non-immunogenicity, and ability to form stable interface between the inner hydrophobic core and the surrounding aqueous layer. Moreover, nonionic PEG shell avoids opsonin adsorption and subsequent clearance by the reticuloendothelial system following intravenous injection, which consequently enhanced the circulation time, and improved the biodistribution of nanocarriers (Layre et al. 2006; Otsuka, Nagasaki, and Kataoka 2001). As one of the most prominent biodegradable, non-toxic, and biocompatible polymers, polylactic acid (PLA) has been explored as a carrier for various hydrophobic drugs (Zhang and Feng 2006; Lucke et al. 2000; Garlotta 2001). mPEG-PLA micelles have been intensely utilized as nanocarriers to improve the stability, aqueous dispersibility and loading capacity of hydrophobic drugs (Nishiyama and Kataoka 2006).

Since, the final degradation products of the block copolymers (PEG and PLA) are safe and non-toxic, the PEG-PLA polymeric micellar system could be an attractive platform for the delivery of hydrophobic photosensitizers to the tumor tissue. Therefore, the objective of present study was to develop Ce6-loaded mPEG-PLA (Ce6-mPEG-PLA) micelles to improve the solubility, stability and permeability of Ce6, and passively target the photosensitizer to the tumor site leading to improved therapeutic efficacy. The physicochemical properties of Ce6-mPEG-PLA including size distribution, zeta potential, loading capacity, encapsulation efficiency, singlet oxygen generation, and *in vitro* rate of drug release were determined. Then, phototoxicity, and cellular uptake of micellar Ce6 in human alveolar adenocarcinoma (A549) were evaluated compared to free Ce6. Further, penetration, phototoxicity and therapeutic efficacy of micellar Ce6 were evaluated in the 3D model of A549 lung cancer spheroids.

4.2. MATERIALS AND METHODS

4.2.1. Materials

Methoxy poly(ethylene glycol) 5000, D,L-Lactide, DAPI (4,6- diamidino-2-phenylindole), and *para*-formaldehyde were obtained from Sigma-Aldrich Chemicals (Germany). Chlorin e6 (Ce6) was purchased from Frontier Scientific, Inc. (USA). Annexin V-FITC Apoptosis Detection kit and Apoptosis analysis Kit were purchased from Invitrogen Co. (USA). Spectra/Por dialysis membranes were purchased from Spectrum Laboratories, Inc. (USA). *N*,*N*-Dimethyl-4-nitrosoaniline (RNO), anhydrous dimethyl sulfoxide (DMSO), and 9,10-dimethylanthracene (DMA), propidium iodide were obtained from Sigma-Aldrich Chemicals (Germany). Singlet oxygen sensor green (SOSG), and Calcein Blue AM was purchased from Thermo Fisher Scientific (USA). Accutase^{TM}, Trypan blue solution, and Fluoromount-G were purchased from Himedia Labs (India).

Dulbecco's Modified Eagle's Medium (DMEM) and heat-inactivated fetal bovine serum (FBS), Penicillin-Streptomycin, trypsin-EDTA were obtained from Himedia Labs (India).

4.2.2. Cell Culture

Human alveolar adenocarcinoma (A549) cells were obtained from National Center for Cell Sciences (Pune, India). All media were supplemented with 10% heat-inactivated fetal bovine serum and 1% penicillin-streptomycin solution. Cells were maintained in a humidified atmosphere at 37°C with 5% CO_2.

4.2.3. Synthesis and characterization of methoxy-poly(ethylene glycol)-poly(D,L-Lactide) mPEG-PLA copolymer

The diblock copolymer methoxy-poly(ethylene glycol)-poly(D,L-Lactide) (mPEG-PLA) were synthesized by ring opening polymerization according to our previously reported procedure

(Kumari et al. 2015). Briefly, mPEG (1 g), D,L-Lactide (0.4 g) and stannous octoate (0.008% w/w) were added into a polymerization tube and stirred for 6 h at 160°C by using magnetic stirrer. The product was dissolved in tetrahydrofuran and precipitated by adding excess volume of ice-cold diethyl ether. The precipitant was dried, re-dissolved in water and dialyzed against water using cellulose ester membrane (MWCO 12-14,000 Da, Spectrum Laboratories, USA) for 24 h. The final product was lyophilized to obtain while fluffy polymer.

4.2.4. Preparation and characterization of Ce6-mPEG-PLA micelles

Polymer mPEG-PLA (10.0 mg/mL in DMSO, 1.0 mL) and photosensitizer Ce6 (2.0 mg/mL in DMSO, 0.1 mL) were mixed and stirred for 20 minutes. Then, the water (5.0 mL) was added dropwise and continually stirred for an additional 4 h. Finally, the solution was dialyzed using dialysis bag (MWCO 3500 Da, Spectrum Laboratories, USA) against distilled water for 2 days. The dialysate was dried using lyophilizer (Labconco, USA) and weighed. The product was re-dissolved in DMSO to determine loading and encapsulation efficiency. The concentration of Ce6 was determined from standard curve of free Ce6 concentrations in DMSO by UV-Vis spectrophotometer (Spectramax™, Microplate reader, Molecular Devices, US) at 405 nm wavelength. The encapsulation efficiency (EE) and drug loading (DL) were calculated by the following equations:

$$\% \text{ DL} = \frac{\text{Weight of the drug in micelles}}{\text{Weight of the feeding polymer and drug}} \text{ X } 100$$

$$\% \text{ EE} = \frac{\text{Weight of the drug in micelles}}{\text{Weight of the feeding drug}} \text{ X } 100$$

The freeze dried Ce6 micelles were dissolved in water at Ce6 concentration of 780 µg/mL and kept at 4°C for subsequent studies.

The particle size and zeta potential Ce6-loaded and blank micelles were determined in triplicate by zetasizer (Nano ZS90, Malvern Instruments Ltd., UK) at 25°C. The morphology of Ce6-mPEG-PLA was visualized by transmission electron microscopy (TEM) (JEM-2010, JEOL, Japan). 1 mg/mL of Ce6-mPEG-PLA solution was dropped onto a surface of carbon-coated copper grid and uranyl acetate (1% w/v) was added for negative staining, and dried at room temperature prior to observation under microscope.

4.2.5. Evaluation of singlet oxygen generation (SOG)

9,10-dimethylanthracene (DMA), highly selective for singlet oxygen ($^1O_2$) was used to determine the $^1O_2$ generation by Ce6-mPEG-PLA in DMSO and in distilled water. The change in the DMA fluorescence intensity was measured by fluorescent spectroscopy as reported previously (Li et al. 2011). Briefly, DMA (20 mM) was mixed with Ce6-mPEG-PLA at a Ce6 concentration of 1.5 mg/mL in DMSO, kept for 10 minutes equilibration. The solution mixture was irradiated at a laser intensity of 50 mW/cm^2 using a 633 nm laser source (Raman Spectroscopy, UniRAM Micro Raman Systems, Spectrolab Systems Limited, UK). After irradiation, fluorescence intensity of DMA (Ex. 360 nm; Em. 380-550 nm) was decreased due to the formation of non-fluorescent product, 9,10 endoperoxide. The intensity of fluorescence was recorded every 10 seconds using a spectrofluorophotometer (Spectramax™, microplate reader, Molecular Devices, US) (Hoebeke and Damoiseau 2002). The experiment was conducted in water as well following the described method.

To evaluate the SOG by Ce6-mPEG-PLA, *N*,*N*-Dimethyl-4-nitrosoaniline (RNO), a singlet oxygen indicator was used in presence of histidine, which helps in the trapping of $^1O_2$ (Lee, Koo, Jeong, et al. 2011). Aqueous solutions of free Ce6, and Ce6-mPEG-PLA micelles (1 mL) were mixed with aqueous RNO (100 µL, 250 mM) and histidine (300 µL, 30 mM)

solution. The mixture (200 µL) was added to a 96-well plate and irradiated at a laser intensity of 50 mW/cm^2 using a 633 nm laser source. RNO absorbance was determined at 440 nm (λ max of RNO) using UV-Vis spectrophotometer (Spectramax™, microplate reader, Molecular Devices, US) after irradiation for specific time interval.

Singlet oxygen sensor green (SOSG) was used to evaluate the generation of $^1O_2$ by Ce6-mPEG-PLA in distilled water following a previously reported protocol (Huang et al. 2011). Briefly, SOSG (2.5 mM) was introduced to measure the $^1O_2$ generation of Ce6 (0.25 mM) loaded mPEG-PLA micelles upon irradiation at 633 nm wavelength. The control groups included free SOSG, free Ce6, and blank mPEG-PLA. After irradiation, the extent of SOG in the samples were determined by measuring the absorbance of SOSG (Ex. 494/Em. 534 nm). The yield of SOG was evaluated by increased fluorescence intensity of SOSG compared to background or the control samples.

4.2.6. *In vitro* release profile of Ce6 from Ce6-mPEG-PLA micelles

The *in vitro* drug release profile of Ce6-mPEG-PLA micelles was evaluated by dialysis method (Yang et al. 2014). The Ce6-loaded micelles solution at a Ce6 concentration of 30 µg/mL (1 mL) was placed into a dialysis bag (MWCO 3500 Da; Spectrum Laboratories, USA), immersed in the phosphate buffered saline (40 mL, PBS; pH 7.4) containing 0.2% Tween 80. The solution was stirred at 100 rpm at 37 ± 0.5°C. The aliquots (1 mL) were drawn at 0.5, 1, 2, 4, 8, 10, 12, 24, 36, and 48 h during incubation. The same volume of withdrawn aliquots were replaced with fresh dissolution media. The cumulative release of drug from Ce6-mPEG-PLA micelles was determined using UV-Vis spectrophotometer (Spectramax™, Microplate reader, Molecular Devices, US).

4.3. Cell culture

Human alveolar adenocarcinoma (A549) cells were grown in DMEM medium supplemented with 10% heat-activated fetal bovine serum (FBS) and 1% penicillin-streptomycin. Cultures were maintained at 37°C in a humidified atmosphere with 5% CO_2 and subcultured every 2-3 days. The Ce6-mPEG-PLA, and free Ce6 (DMSO concentration <0.1%) were dissolved in serum-free DMEM medium. The untreated cells incubated in dark was used as reference control.

4.3.1. Cellular uptake of Ce6-mPEG-PLA

For flow cytometer analysis, 5 X 10^5 A549 cells were seeded separately in a 6-well tissue culture plates in complete media and allowed to grow overnight. The following day, cells were incubated with free Ce6, and mPPEG-PLA-Ce6 (the equivalent concentration of Ce6 was 5 µg/mL). After 1 and 4 h incubation period, cells were washed several times, trypsinized, and re-suspended in PBS, pH 7.4 (200 µL). The intracellular fluorescence of Ce6 was detected by flow cytometer (Amnis Flowsight, United States). The Ce6 fluorescence was analyzed by counting 10,000 cells (gated events) after irradiation using 488 nm laser. The fluorescence emissions at 630-670 nm were collected, amplified and plotted to produce single peak histogram. The intensity of the cells without any treatment was considered as threshold, cell samples with fluorescence intensity higher than threshold was designated to be positive.

To observe the subcellular localizations of the Ce6-mPEG-PLA, A549 cells were first seeded on microscope slides and were incubated in serum-free medium containing Ce6-mPEG-PLA and free Ce6 at a Ce6 concentration of 5 µg/mL for 1 and 4 h at 37°C. The old media was removed; cells were washed thoroughly with PBS, fixed with 4% *para*-formaldehyde, stained with DAPI and mounted on microscope slides using fluorescence-free glycerol-based

mounting medium (Fluoromount-G; Sigma Aldrich) and observed on a confocal laser scanning microscope (Leica Microsystems, Germany). A 358 nm and He-Ne lasers were used for the excitation of DAPI and Ce6, respectively. A 650 nm emission long-pass filter was used for the detection of Ce6. Confocal images were analyzed by using *Image J* software.

4.3.2. Phototoxicity of Ce6-mPEG-PLA

A549 cells (4 X 10^3 cells/well) were seeded into 96-well plates and incubated overnight. On following day, medium was replaced with 100 µL of free Ce6 and Ce6-mPEG-PLA in serum-free medium and incubated for 12 h. Free Ce6, and Ce6-mPEG-PLA treated cells were irradiated at laser intensity of 50 mW/cm^2 using a 633 nm laser source for 2 min using Raman spectroscopy. Further, the irradiated cells were incubated at 37°C for 12 h in dark. After incubation, old media were removed and the cells were treated with 3-[4,5-Dimethylthiazol-2-yl]- 2,5-diphenyltetrazolium bromide (MTT) solution, (50 µL; 5 mg/mL MTT solution in serum/phenol red-free DMEM) for 3 h, followed by replacement of the medium with DMSO (150 µL). The absorbance was measured at 570 nm and subtracted from the absorbance 630 nm as background.

4.3.3. Avascular A549 spheroids experiments

4.3.3.1. Formation of Avascular A549 spheroids

Avascular A549 cancer cell spheroids were prepared by liquid overlay method (Perche, Patel, and Torchilin 2012). The A549 cells grown in monolayers were trypsinized, counted and seeded at a density of 10,000 cells/well in each well of a 96-well plate previously coated with 50 µL of 1.5% (w/v) agarose in serum free DMEM medium. Prior to use, 96-well plates were cooled down at 25°C for 45 min. Further, kept for centrifugation at 1500 rcf at 25°C for 15 min. Spheroid formation was continuously monitored using Fluorescence microscope (Leica

Microsystems, Germany). When the spheroids reached a diameter of 300-400 μm diameter and became dense (after 3-5 days), they were used for the experiment. The culture medium was replaced every 3 days.

4.3.3.2. Penetration of Ce6 into cancer cell spheroids

Spheroids were treated with free Ce6, and Ce6-mPEG-PLA at a Ce6 concentration of 5 μg/mL for 1 and 4 h at 37°C. Then, the tumor spheroids were washed with cold PBS and then viewed with a confocal laser scanning microscope (Leica Microsystems, Germany). Z-stack images of spheroids were captured from the top surface towards the equatorial plane at a thickness of 10 μm. All images were visualized using a 10X objective and analyzed using *Image J* software.

4.3.3.3. Growth inhibition of avascular A549 spheroids

To measure the inhibition effect of Ce6 on A549 spheroids, spheroids were treated with Ce6-mPEG-PLA, and free Ce6, in DMEM media at a Ce6 concentration of 3 μg/mL for 4 h. Untreated spheroids were used as the control. In all cases, irradiation was performed for 2 minutes with 633 nm wavelength laser (50 mW/cm^2). All study was performed under dark conditions. The size inhibition of the A549 spheroids were evaluated under a fluorescence microscope (Leica Microsystems, Germany) every 2 days. Twelve spheroids were examined in PDT and control groups.

4.3.3.4. Spheroidal Cellular uptake of the Ce6-mPEG-PLA

Uptake of micelles in spheroidal cells was analyzed by flow cytometer. 5-day old A549 spheroids were incubated with Ce6-mPEG-PLA, and free Ce6 for 1 and 4 h. After the incubation period, spheroids were washed thoroughly with PBS (pH 7.4). 10 spheroids were

collected into each tube to obtain sufficient cell count. Accutase™ cell detachment solution (50 µL) was added and incubated for 10 min at 37°C with gentle shaking, and the cell suspension was transferred in 15 mL tubes. Accutase™ activity was inhibited by the addition of FBS (500 µL) in tubes. Then, cells were centrifuged at 1000 rpm for 5 min. Pellets were re-suspended in PBS, pH 7.4 (200 µL). The intracellular Ce6 fluorescence was analyzed using flow cytometer as described above.

4.3.3.5. Apoptosis in spheroidal cells after photo-irradiation

The apoptosis study was carried out by using Annexin V assay following the manufacturer's protocol. After the cultured A549 spheroids reached to a size of 300-400 µm (day 4/5), spheroids were incubated with Ce6-mPEG-PLA, and free Ce6 at a Ce6 concentration of 50 nM for 12 h. The media on spheroids were replaced by fresh culture media and irradiated at a laser intensity of 50 mW/cm^2 using 633 nm laser source for 30 min. Spheroids were incubated for an additional 12 and 36 h, trypsinized, washed with cold binding buffer, treated with 100 µL of Accutase™ solution (Himedia Labs, India) in 1 mL on 10 spheroids. The spheroidal suspension was centrifuged, re-suspended in binding buffer and stained with or without Alexa Fluor® 488 Annexin V/PI (Invitrogen Co., USA). The spheroids were diluted with cold binding buffer and analyzed by flow cytometer.

4.3.3.6. Live/Dead Staining of spheroids after treatment with Ce6

For the live/dead cell assay, free Ce6, and Ce6-mPEG-PLA treated spheroids were mixed with Calcein Blue AM and PI solutions for staining live cells as blue, and dead cells as red, respectively (5 mM of each dye in PBS, pH 7.4). A549 spheroids in 8-well glass chamber slides were incubated with free Ce6, and Ce6-mPEG-PLA at a Ce6 concentration of 3 µg/mL in serum-free DMEM medium for 4 h. The spheroids were irradiated at laser intensity of 50

mW/cm^2 with a 633 nm laser source for 15 min. After incubation, medium was discarded and spheroids were rinsed thoroughly with PBS (pH 7.4). Further, spheroids were incubated for an additional 4 h in complete medium and then, visualized using confocal laser scanning microscope (Leica Microsystems, Germany).

4.3.4. Statistical analysis

The data were tested for statistical significance using Student's t-tests. p values, calculated with the Graph Pad prism 5 software (GraphPad Software, Inc, San Diego, CA). All numerical data are expressed as mean ± SD, n = 3 or 4, from 3 different experiments. Any p values less than 0.05 was considered statistically significant. *, **, *** in figures indicated p values <0.05, 0.01 and 0.001, respectively.

4.4. RESULTS AND DISCUSSION

4.4.1. Synthesis and characterization of the Ce6-mPEG-PLA micelles

mPEG-PLA was synthesized by the ring opening polymerization reaction of mPEG and D,L-Lactide using stannous octoate as the catalyst (Kumari et al. 2015). The TEM image of mPEG-PLA and Ce6-mPEG-PLA showed well dispersed spherical morphology (Figure. 4.1A and B). The amount of Ce6 encapsulated in mPEG-PLA micelles was analyzed by UV-Vis spectrophotometer at 405 nm. The average encapsulation efficiency and drug loading were 75.12 ± 2.75%, and 12.95 ± 1.92% (w/w), respectively. The average hydrodynamic diameter of mPEG-PLA and Ce6-mPEG-PLA were 166.4 ± 50.68 nm, and 189.6 ± 14.32 nm, respectively (Figure. 4.1C and D). The average zeta potential values of blank mPEG-PLA and Ce6-loaded mPEG-PLA were -23.5 ± 3.68 mV, and -20.2 ± 4.73 mV, respectively. After drug loading there was increase in the size of the micelles compared to unloaded mPEG-PLA

micelles, this is usual in micellar systems following drug loading, as incorporation of cargo in the hydrophobic core leads to enhancement of the size of the compartment.

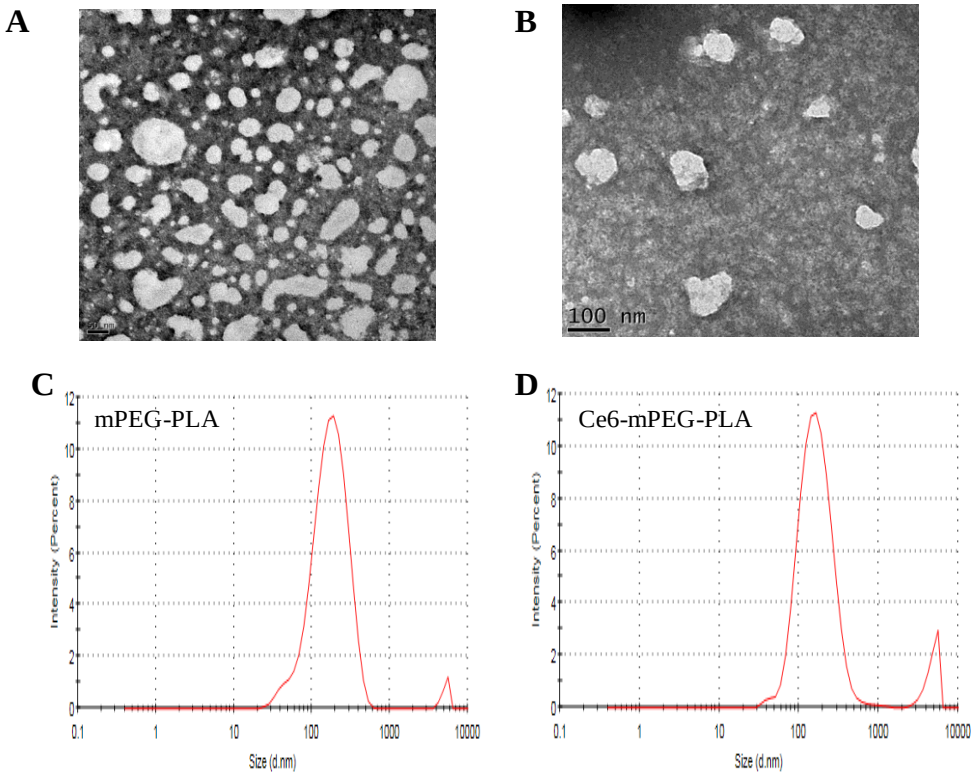

Figure. 4.1. TEM images (A-B) and graphs (C-D) representing size distribution determined by zetasizer. Figure 4.1 A, and C represents the data from mPEG-PLA; B and D for Ce6-mPEG-PLA.

4.4.2. Evaluation of the photo-activity and singlet oxygen generation

To investigate the photo-activity of Ce6-mPEG-PLA, the emission spectrum was determined by fluorescence spectrophotometry in aqueous medium. Figure. 4.2 shows the singlet oxygen generation from Ce6 loaded mPEG-PLA following irradiation. Here, 9,10-dimethylanthracene (DMA) traps the singlet oxygen generated by the photosensitizer to form non-fluorescent 9,10-endoperoxide in many organic solvents and water (Gomes, Fernandes, and Lima 2005). Herein, Ce6-mPEG-PLA, and free Ce6 were irradiated at a laser intensity of 50 mW/cm^2

using a 633 nm laser source for 10 min. Ce6 has absorption maxima at 405 and 640 nm in UV and NIR region, respectively. Here, Ce6 was excited using 633 nm laser source due to the non-vanishing absorption of Ce6 in that region as previously reported (Hou et al. 2016) (Zhang et al. 2015). The singlet oxygen generated from free Ce6 or Ce6-loaded micelles were monitored with the change in fluorescence intensity of DMA. The DMA fluorescence intensity of samples (decrease in the fluorescence due to formation of $^1O_2$ were plotted after subtracting from the untreated DMA samples. The decrease in the fluorescence intensity of DMA indicated the increase in the generation of singlet oxygen. As shown in Figure. 4.2A, Ce6-mPEG-PLA generated higher $^1O_2$ compared to free Ce6. Due to the aggregation of free Ce6 in water, decrease in the generation of singlet oxygen was observed. However, the $^1O_2$ generation in Ce6-mPEG-PLA, and free Ce6 dissolved in DMSO showed insignificant difference (Figure. 4.2B).

Next, singlet oxygen generation was evaluated using RNO in presence of histidine. The generated $^1O_2$ undergoes bleaching following reaction with histidine and RNO (Lee, Koo, Jeong, et al. 2011). The capture of $^1O_2$ by the imidazole ring of histidine forms trans-annular peroxide intermediate. Further reaction with RNO results in photobleaching. The rate of generation of singlet oxygen was determined by the change in the photobleaching. The Ce6-mPEG-PLA, and free Ce6 were irradiated at a laser intensity of 50 mW/cm^2 using a 633 nm laser source for different time intervals. RNO absorbance at 440 nm was measured. No change was observed in RNO absorbance of the blank mPEG-PLA after the irradiation (Figure. 4.2C). The free Ce6 generated singlet oxygen at a higher rate compared to mPEG-PLA-Ce6 with increasing time of irradiation, measured by the sharp decrease in RNO absorbance. The presence of hydrophobic core in the mPEG-PLA inhibited the entry of

histidine, which resulted in complication of interactions in the singlet oxygen-histidine-RNO chain causing ineffective detection of $^1O_2$.

The SOG by Ce6-mPEG-PLA, and free Ce6 in distilled water were determined by measuring the change in SOSG fluorescence intensity, depicted in Figure. 4.2D. The yield of $^1O_2$ generated by Ce6-mPEG-PLA was approximately three-fold higher in comparison to free Ce6 due to the enhanced Ce6 aqueous solubility in micellar form. The free Ce6 photo-activity was disappeared in aqueous media due to aggregation caused by π-π interactions amongst adjacent aromatic rings of free Ce6 resulted in self-quenching. Photo-activity of Ce6-mPEG-PLA was retained as the chance of aggregation was reduced in the micellar system.

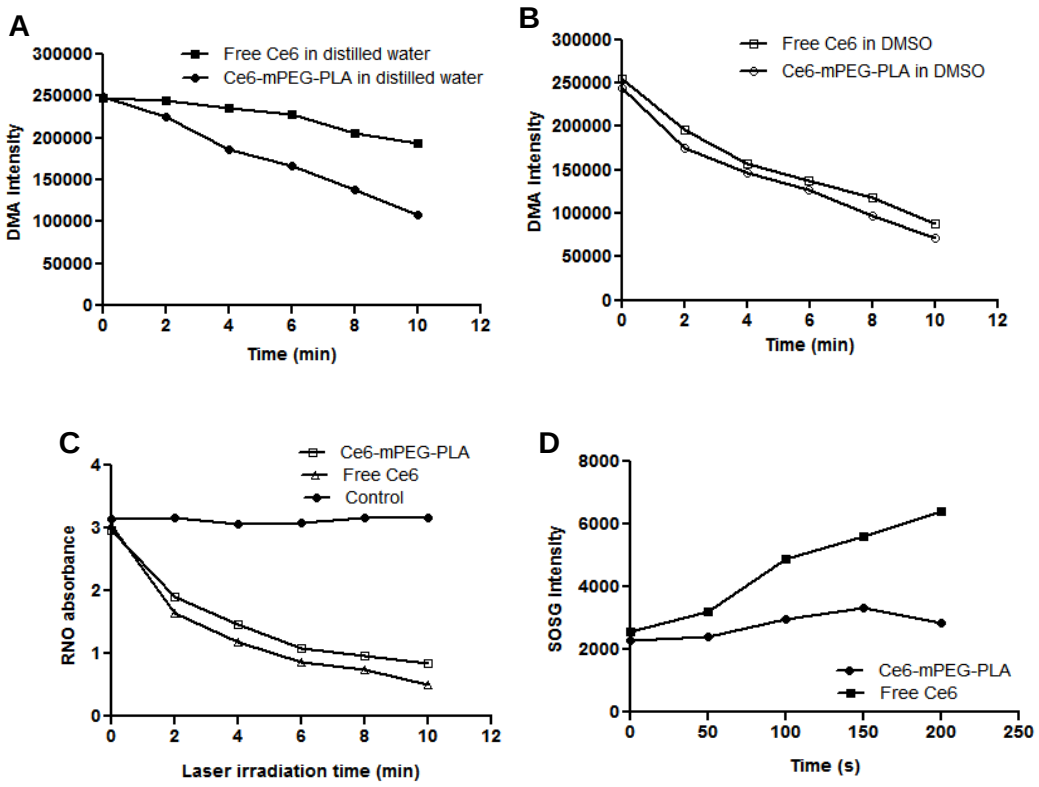

Figure.4.2. (A and B) Change in the fluorescence intensity of DMA (Ex. 360 nm; Em. 436 nm) with respect to time in presence of SOG by Ce6-mPEG-PLA, and free Ce6 in distilled water and DMSO, respectively. (C) Time-dependent photobleaching of RNO by free Ce6, and

Ce6-mPEG-PLA. (D) Changes in fluorescence intensity of SOSG in presence of free Ce6, and Ce6-mPEG-PLA in distilled water.

4.4.3. *In vitro* release profile of Ce6 from Ce6-mPEG-PLA micelles

The drug release behavior of the Ce6-loaded micelles was tested at pH 7.4. At pH 7.4, less than 60% of the incorporated Ce6 was released within 48 h, while for free Ce6 over the same time period, more than 88% of the loaded drug was released. A rapid drug release occurred with the release of more than 70% of the entrapped Ce6 within 10 h. Ce6-mPEG-PLA showed 85% release in 48 h (Figure. 4.3). The result indicated that the drug was released in sustained manner, which is beneficial in the administration of photosensitizer to avoid toxicity or untoward side effects resulting from burst release of PS from nanocarriers. The *in vitro* release profile showed that Ce6 was incorporated firmly in the micellar core rather than association with the hydrophilic outer compartment as there was no rapid release of drug.

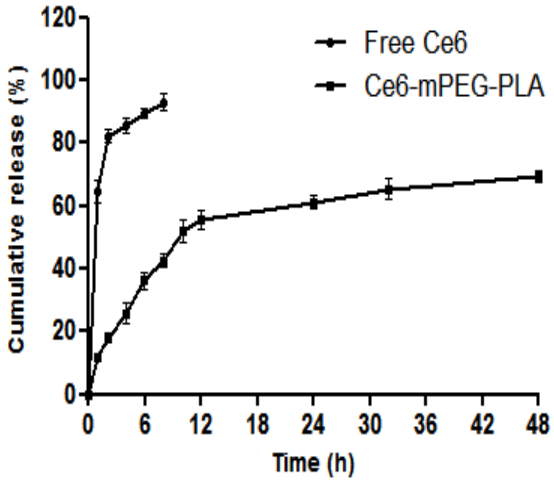

Figure. 4.3. *In vitro* release profiles of Ce6 release from Ce6-mPEG-PLA (■) and free Ce6 (●) in PBS (pH 7.4) under sink condition at 37°C. Data are represented as mean (%) ± SD (n=3).

4.4.4. Cellular uptake of Ce6-mPEG-PLA

The photosensitizers on photo-activation generates singlet oxygen which has short lifetime of <200 ns and penetrates to a depth of approximately 20 nm (Ling et al. 2012). Therefore, the cellular internalization of PS plays major role for the effective treatment of photodynamic therapy. Cellular internalization of micelles in A549 cells, was evaluated by flow cytometry and confocal microscopy studies (Figure. 4.4A and B). From the flow cytometry histogram (Figure. 4.4A), it was observed that the fluorescence peak of Ce6-mPEG-PLA was shifted to right with increase in incubation time, indicating the internalization of Ce6-mPEG-PLA more readily compared to free Ce6 in both the time points (Geo mean of fluorescence 10785 ± 8.3, and 19164 ± 6.8 in 4 h for free Ce6, and Ce6-PEG-PLA, respectively). The result was corroborated by confocal micrographs of cells treated with the formulations (Figure. 4.4B). After 1 h incubation, free Ce6 exhibited weak intensity of red signal indicating low internalization. Ce6-mPEG-PLA micelles treated cells demonstrated significantly higher intensity of red signal after 4 h treatment.

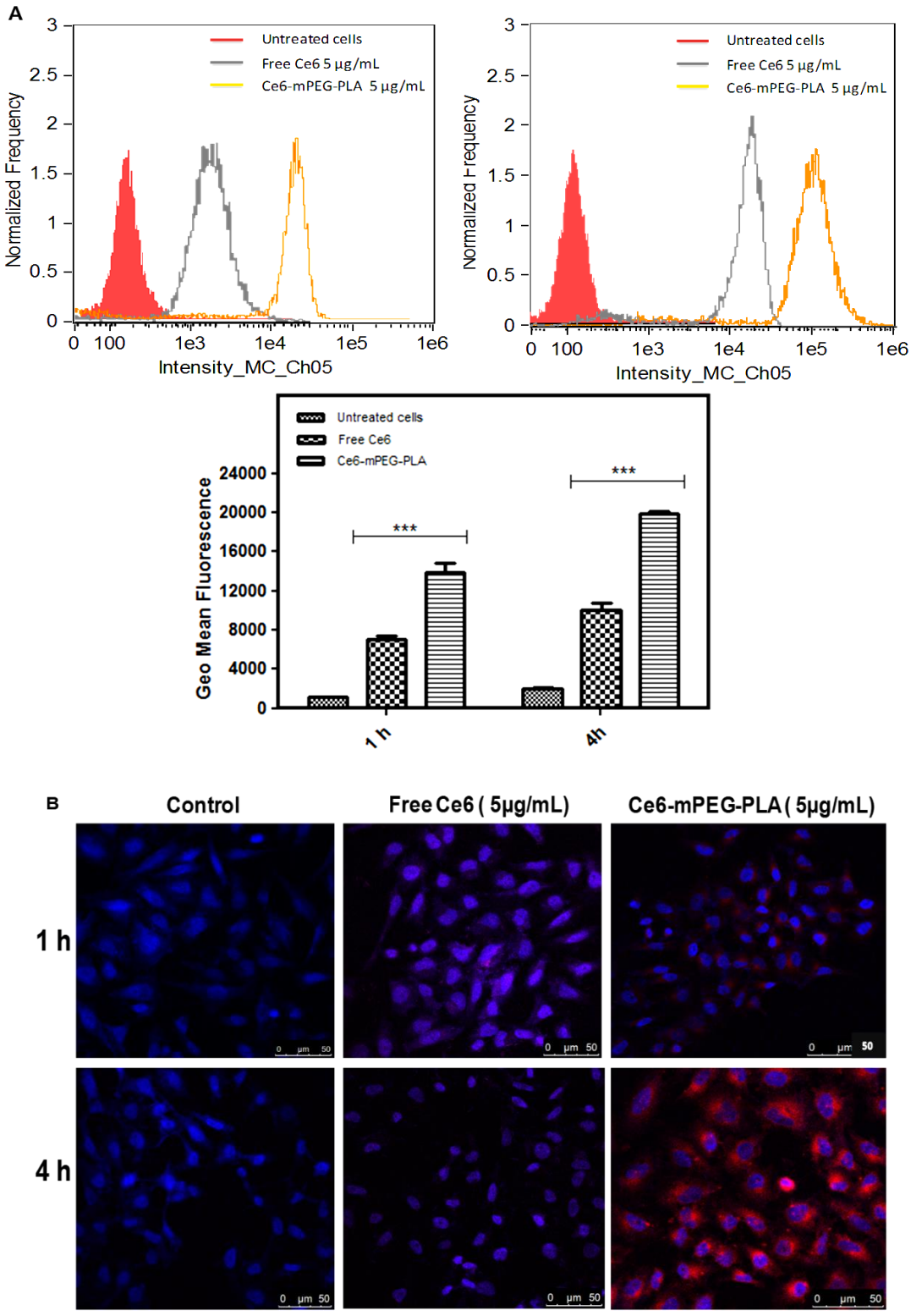

Figure. 4.4. Uptake of Ce6-mPEG-PLA, and free Ce6 in A549 cells. A) Flow cytometry histograms representing cellular uptake of free Ce6, and Ce6-mPEG-PLA in A549 cells

incubated for 1 and 4 h. The significance of difference between the mean was analyzed by Student's t-test, ***$p < 0.001$. B) Confocal microscopy images of cells treated with Ce6-mPEG-PLA, and free Ce6 at incubation times 1 and 4 h. The scale bar is 50 µm. Blue color: cell nuclei stained with DAPI. Red color: intracellular Ce6.

4.4.5. Phototoxicity of Ce6-mPEG-PLA

To confirm the photo-toxicity of Ce6-mPEG-PLA, MTT assay following irradiation and under dark condition was performed. The free Ce6, and Ce6-mPEG-PLA treatment was performed in A549 cells. The cells receiving irradiation was subjected to laser treatment at a dose of 50 mW/cm^2 at 633 nm for 2 min after 12 h during 24 h incubation time. After incubation for 12 h further, MTT assay was performed. The data has been represented graphically in Figure. 4.5. No cytotoxicity was observed in blank mPEG-PLA in the presence of light. Cells treated with free Ce6, and Ce6-mPEG-PLA were mostly viable without irradiation (Figure. 4.5A). However, Ce6-mPEG-PLA, and free Ce6 treated cells irradiated with 633 nm laser source, showed remarkable and concentration-dependent phototoxicity (Figure. 4.5B). The cytotoxicity was significantly higher in Ce6-mPEG-PLA compared to free Ce6 under stated irradiation condition. Since the blank mPEG-PLA demonstrated no phototoxicity, the improved PDT potency of Ce6-mPEG-PLA over free Ce6 could be due to the enhanced internalization of Ce6 encapsulated in mPEG-PLA micelles.

4.4.6. Penetration efficiency in the avascular A549 spheroids

The studies performed on *in vitro* monolayer cells showed erroneous results as they differ in pathophysiological conditions of solid tumors (Minchinton and Tannock 2006; Cairns, Papandreou, and Denko 2006). 3D tumor spheroids mimics the complexities of solid tumors due to the acidic pH, diverse tumor perfusion, increased cell density, and enhanced interstitial

pressure (Shirinifard et al. 2009; Hirschhaeuser et al. 2010). Therefore, avascular A549 spheroids were used to study the penetration efficiency of the Ce6-mPEG-PLA.

To study penetration and intracellular accumulation of Ce6 into the spheroids, A549 spheroids were incubated with Ce6-mPEG-PLA, and free Ce6, and observed using confocal microscopy. As seen in Figure. 4.6, Ce6 accumulated into the outer cellular layer of spheroids after 1 h of incubation in case of free Ce6, whereas Ce6-mPEG-PLA penetrated inside the spheroids as evidenced by the increased fluorescence in the deeper spheroidal sections. The fluorescence was significantly increased on treating the cells with both the formulations for 4 h. Free Ce6 could not penetrate much inside the spheroids. However, time-dependent increase in spheroidal penetration of Ce6-mPEG-PLA was observed. Low molecular weight Ce6 could translocate in and out through the cells by diffusion. However, internalization of micelles happens by energy dependent endocytosis process (Torchilin 2007). Therefore, drugs encapsulated in the micelles once gets translocated inside, could not be released out as free Ce6. Strong hydrophobicity and presence of large delocalized π-electron system in Ce6 could retard its successful internalization.

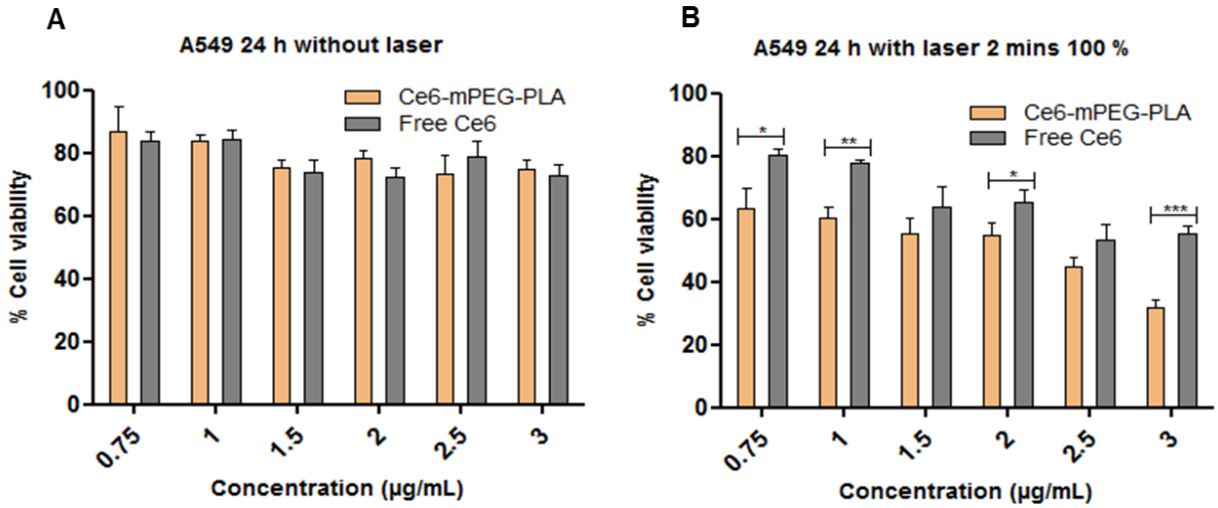

Figure. 4.5. Assessment of cell viability of A549 cells incubated with free Ce6, and Ce6-mPEG-PLA. The concentration range of Ce6 and the time of incubation was 0-3 µg/mL and 24 h, respectively. Data represents mean ± SD, averaged from three independent experiments. The significance of difference between the mean was analyzed by Student's t-test, *, **, *** indicates <0.05, 0.01 and 0.001, respectively.

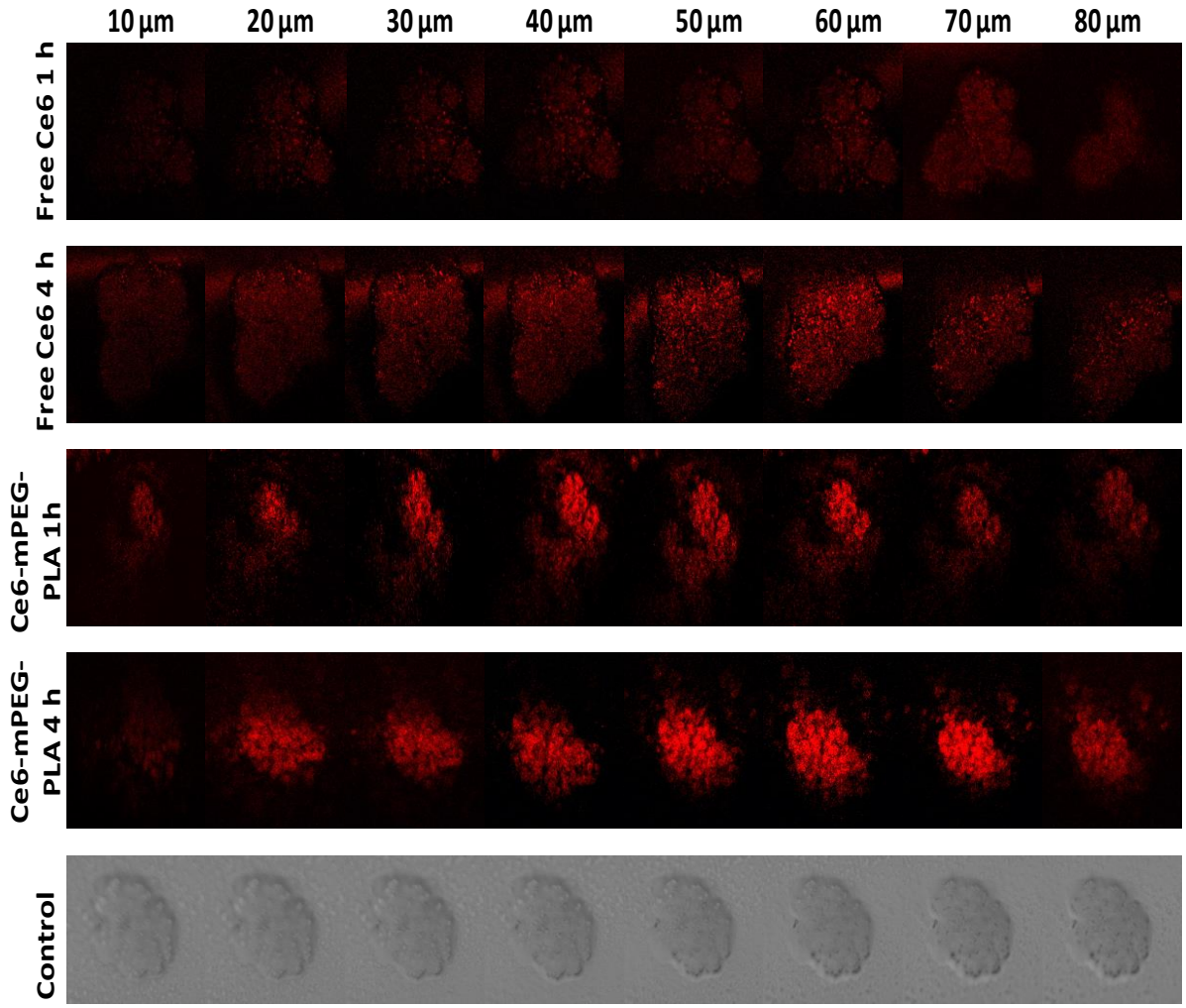

Figure. 4.6. Penetration of free Ce6, and Ce6-mPEG-PLA throughout A549 spheroids. The accumulation of Ce6-mPEG-PLA, and free Ce6 at 1 and 4 h, were observed under confocal laser scanning microscope at various focal planes from the surface to inside the spheroids at 10 µm intervals. Scale bar: 100 µm.

4.4.7. Growth inhibition of avascular A549 spheroids

To determine the growth inhibition, avascular A549 spheroids were incubated with DMEM medium, free Ce6, and Ce6-mPEG-PLA. The A549 spheroids treated with Ce6-mPEG-PLA demonstrated significant growth inhibition compared to control. The fluorescence microscope images of untreated A549 spheroids demonstrated fast growth, round and dense structure from day 0 to day 6 (Figure. 4.7). The average diameter of untreated spheroids at day 3 was 674.05 ± 16 µm, which reached a maximum of 717.15 ± 13 µm at day 6 at end of the study and appeared compact. The Ce6-mPEG-PLA, and free Ce6 demonstrated slower growth rate after irradiation with 633 nm laser source. The size of spheroids treated with Ce6-mPEG-PLA, and free Ce6 after irradiation at day 6 were 605.19 ± 23 µm, and 630.72 ± 19 µm, respectively (Figure. 4.7B). The spheroids were observed under microscope at 10X magnification and bright field images were captured (Figure. 4.7A).

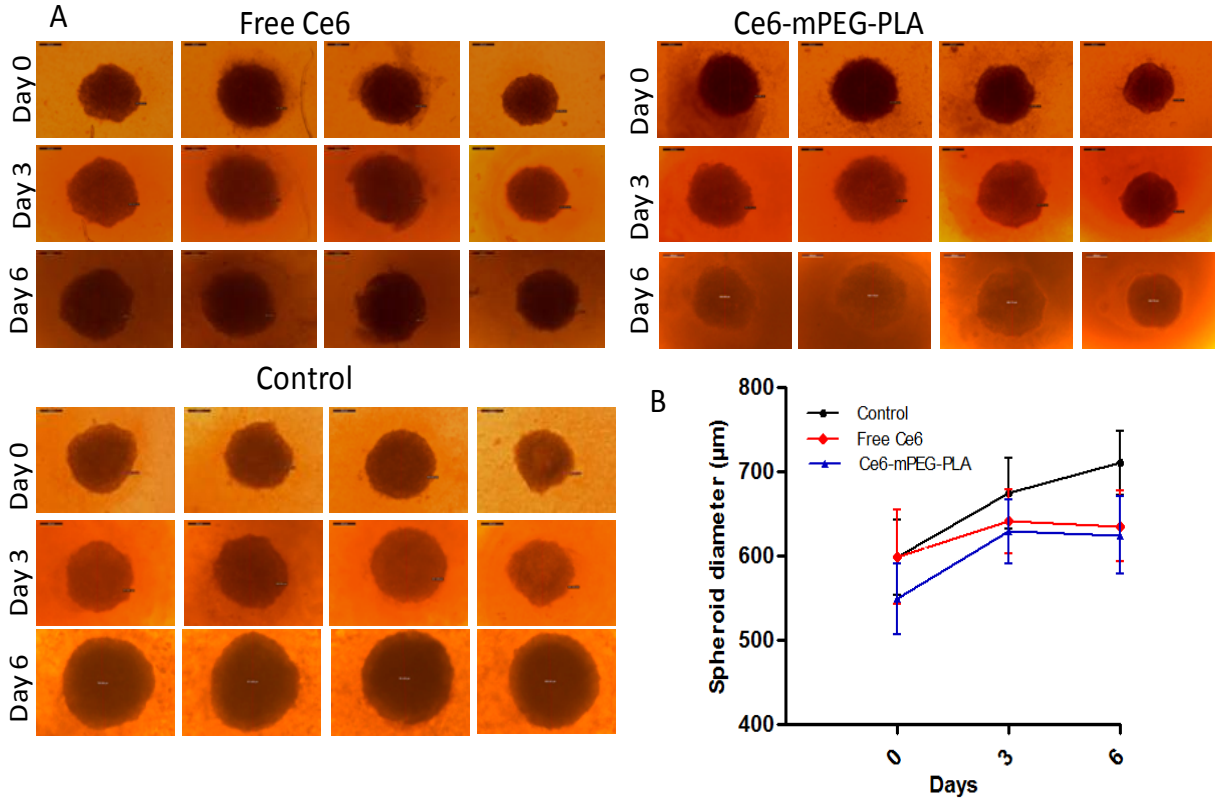

Figure. 4.7. Morphology of A549 spheroids treated with Ce6-mPEG-PLA, free Ce6, and serum-free DMEM on day 0, 3, and 6, respectively, at Ce6 concentration equivalent to 0.2 µg/mL (A), changes in diameter of spheroids subjected to different treatments (B).

4.4.8. Spheroidal cellular uptake

Spheroidal cellular uptake study was performed by preparing single cell suspension following the treatment of spheroids with Ce6, and Ce6-mPEG-PLA and analyzed by flow cytometry. The result has been represented in Figure. 4.8. Similar to monolayer cellular uptake study represented in Figure. 4.4, the shift in fluorescence peak to the right in the histogram at both the tested time points compared to cells treated with PBS or free Ce6 indicated time-dependent enhanced cell association of Ce6 into spheroids. The histogram plots showed higher cellular association of Ce6-loaded micelles compared to free Ce6 at 1 and 4 h, respectively. Flow cytometry histogram displayed presence of distinct two fluorescently labeled population of cells. This could be due to the heterogenecity in spheroidal cells as outer region of spheroids internalized formulations much quicker compared to the cell populations in the core due to their inaccessibility. The results obtained by flow cytometry (Figure. 4.8) and confocal microscopy (Figure. 4.6) demonstrated that mPEG-PLA micellar system are able to penetrate into the A549 spheroids due to their small size, as reported previously (Kim et al. 2010).

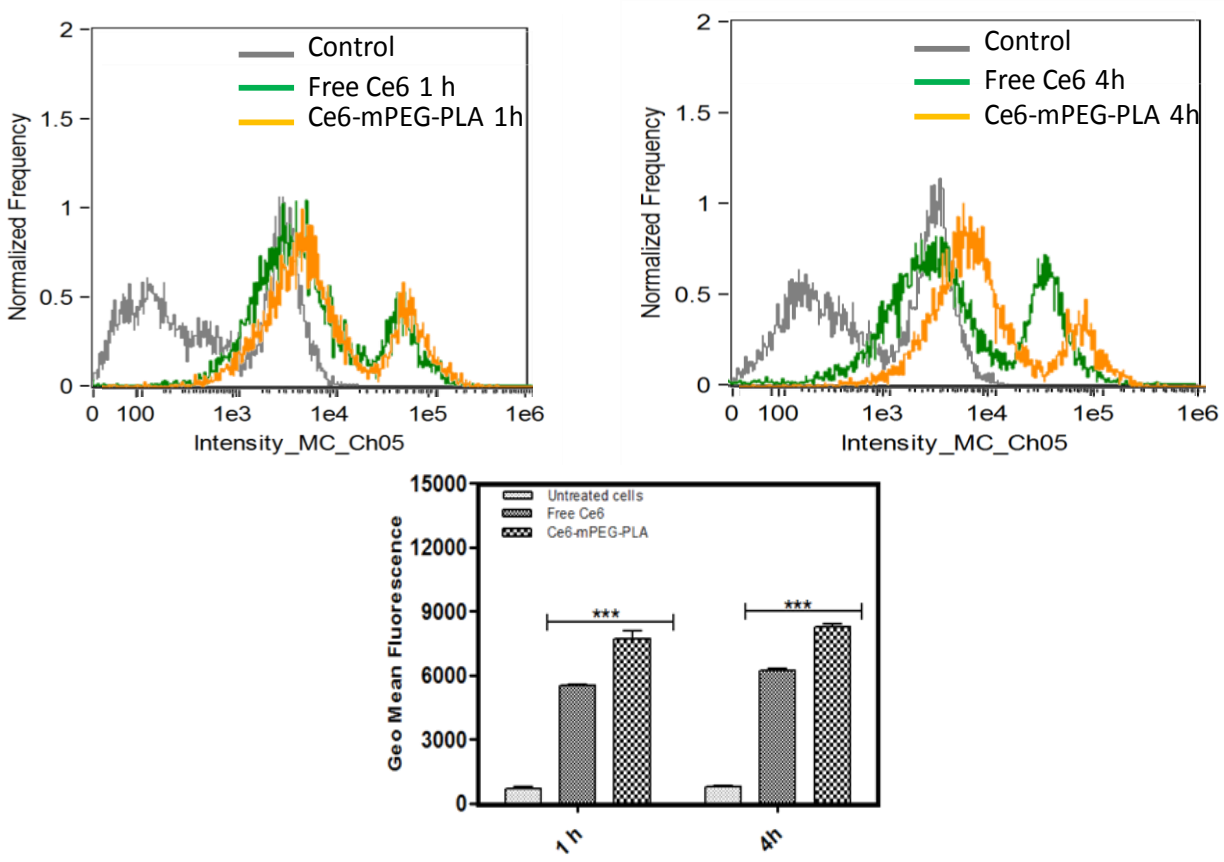

Figure. 4.8. Spheroidal cellular internalization of Ce6-mPEG-PLA, and free Ce6 analyzed by flow cytometer. The A549 spheroids were treated with Ce6-mPEG-PLA, and free Ce6 at Ce6 concentration of 3 μg/mL for 1 and 4 h. Histogram plots represented the fluorescence intensity of the cell population. The significance of difference between the mean was analyzed by Student's t-test, ***$p < 0.001$.

4.4.9. Apoptosis in spheroidal cells after photo-irradiation

Cellular apoptosis induced by Ce6-mPEG-PLA mediated PDT treatment was analyzed by using flow cytometer and compared against the treatment using free Ce6. FITC-labeled Annexin V and the PI detected the viable and dead cells, respectively. Over 97% of the cells treated with laser or blank micelles were viable indicating non-toxicity of these applications. However, free Ce6, and Ce6-mPEG-PLA treated cells demonstrated higher late apoptotic cell

population (upper right quadrant in Figure. 4.9) compared to control cell populations.

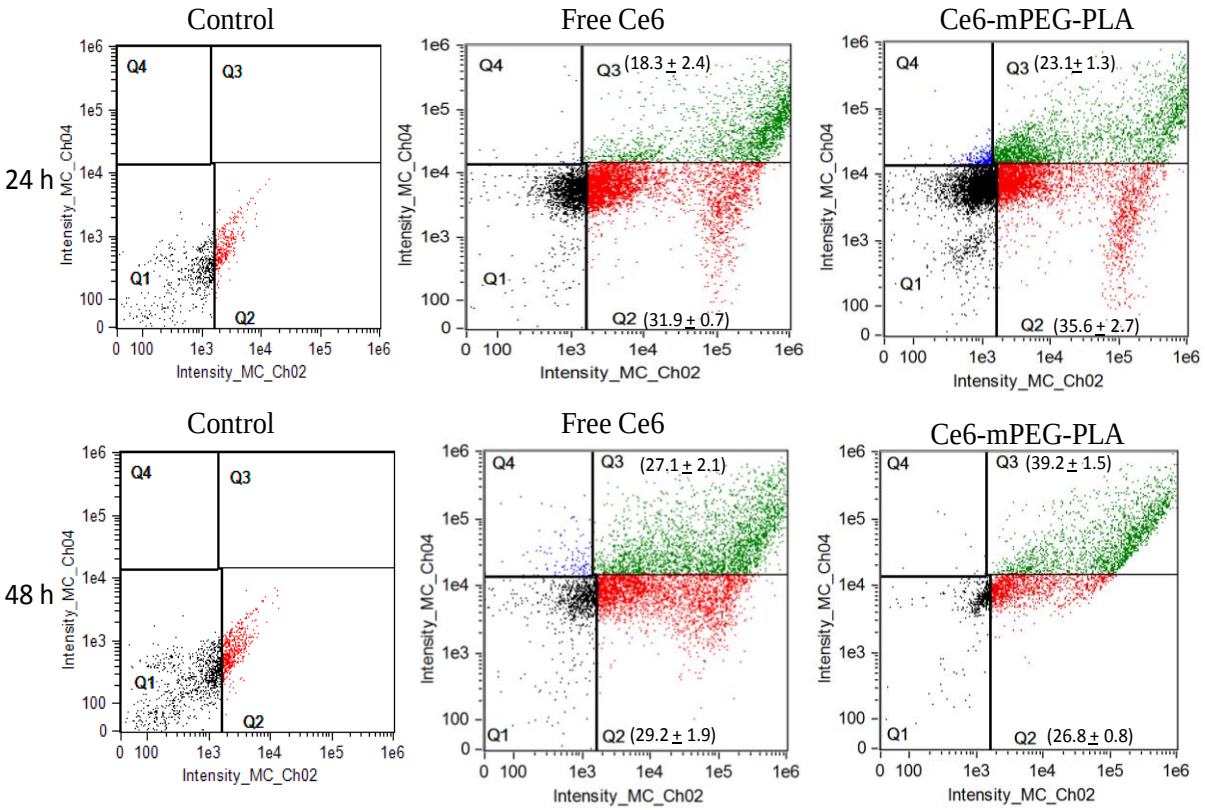

Figure. 4.9. Effect of Ce6-loaded micelles on apoptosis of A549 spheroids *in vitro*. The cells were treated with Annexin V-FITC and PI, their fluorescence was analyzed to determine the apoptotic cell population by flow cytometry. A549 spheroids were incubated with free Ce6, and Ce6-mPEG-PLA and complete medium served as the control.

Ce6-mPEG-PLA mediated PDT enhanced the late apoptotic cell population to a much higher extent compared to the PDT mediated by free ce6 (23.1 ± 1.3 vs 18.3 ± 2.4; and 39.2 ± 1.5 vs 27.1 ± 2.1 for Ce6-mPEG-PLA vs free Ce6-mediated PDT at 24 and 48 h, respectively). Irradiated spheroids treated with Ce6-mPEG-PLA at 48 h demonstrated maximum shift in the cell population to the late apoptotic quadrant compared to other treatments. The data indicates that the PDT by using mPEG-PLA-micelles incorporated Ce6 is efficacious and the cytotoxicity occurs by the induction of apoptosis.

4.4.10. Live/Dead Staining of spheroids after treatment with Ce6

The cytotoxic effect of Ce6-mPEG-PLA on A549 spheroids was further verified by co-staining the spheroids with Calcein Blue AM and PI, staining cytoplasm of viable cells (blue) and dead cells (red), respectively. The control spheroids displayed blue fluorescence under laser irradiation suggesting that the laser alone cannot kill the cancer cells. As shown in Figure. 4.10, spheroids in the Ce6-mPEG-PLA treatment group with laser exposure were killed and exhibited bright red fluorescence as visualized under fluorescence microscope, whereas the free Ce6 treatment exhibited lower extent of cells death leading to display of red fluorescence with less intensity. The live-dead cell assay corroborated the previous spheroidal apoptotic data, and proved the potential of the Ce6-nano-formulation as an effective PDT, which can penetrate the spheroids efficiently, and demonstrated enhanced cell killing compared to free Ce6.

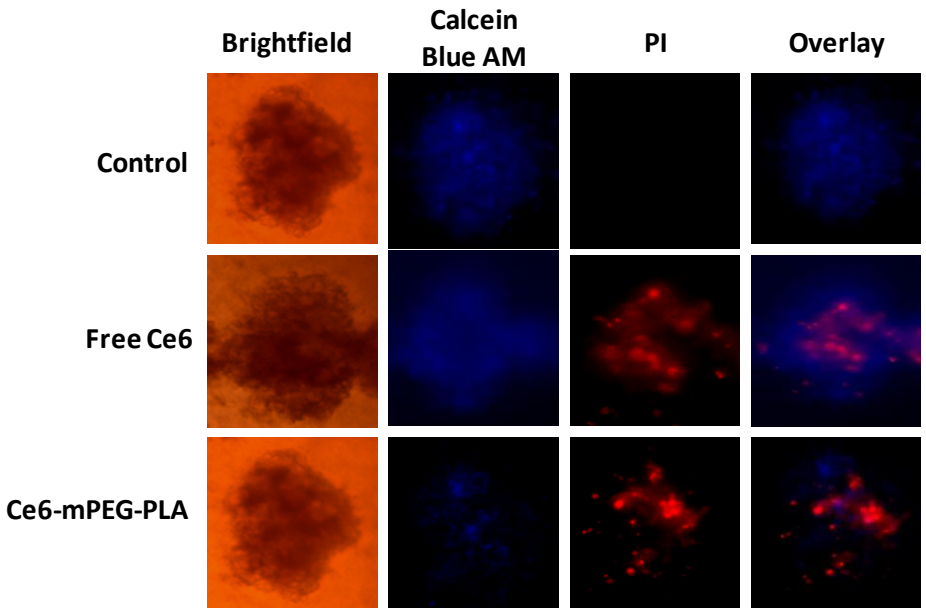

Figure. 4.10. Confocal images of live-dead stained spheroids. Calcein Blue AM and PI co-stained spheroids after light irradiation (633 nm, 50 mW/cm^2, 15 min) were captured. Blue and red represent live and dead cells, respectively.

4.5. CONCLUSION

Even though photodynamic therapy has shown potential clinical application as a non-invasive treatment modality for several cancers, but strong hydrophobicity as well as less tissue penetration ability of the photosensitizers (PSs) along with their excitability majorly in the UV-Vis range limit the application of PDT in deep-seated tumors. In our study, we have utilized Ce6 as the PS, which demonstrates excitability at NIR wavelength of light (633 nm). Ce6 was successfully encapsulated in the poly(Lactide)-based, biocompatible mPEG-PLA micelles, which significantly improved the poor biopharmaceutical properties of Ce6 resulting in the superior therapeutic efficacy in the *in vitro* cell studies compared to free Ce6. Ce6 loaded micelles exhibited higher cellular uptake and improved photo mediated cell killing potency compared to free drug without displaying noticeable dark toxicity. Further, the Ce6-loaded micelles exhibited facile penetration into 3D tumor spheroids due to their small size. Upon photo-irradiation, the Ce6-mPEG-PLA micelles generated singlet oxygen species rapidly that led to the cellular apoptosis resulting in cell death in both, monolayers and spheroidal cells. The photo-cytotoxicity induced by the Ce6-mPEG-PLA was more pronounced compared to free Ce6 indicating the potential of encapsulation in improving the biological activity of Ce6. Therefore, the newly developed poly(Lactide) nano-micellar formulation of Ce6 has great potential to be utilized successfully in PDT for the treatment of deep-seated solid tumors.

Chapter 5

Summary and Conclusion

5. SUMMARY AND CONCLUSION

As there is an urgent need for the effective treatment of advanced forms of cancer for current global population, development of appropriate drug delivery systems to overcome the limitations of cancer's resistance to chemotherapy, biologics, and radiotherapy is of main importance. Recent studies show that polymeric micelles is one of the most attractive alternatives for hydrophobic drugs to improve their bioavailability. Thus, the present study focused on the development of polymeric micelles for delivery of poorly soluble drugs used in the treatment of cancer.

As a potential anticancer agent, curcumin (CUR) has been reported for its chemopreventive and chemotherapeutic activity in a series of cancers through influencing cell cycle arrest, differentiation, apoptosis, etc. Therefore, the potential activity against various cancers of CUR raises the possibility of its application as a novel model drug in polymer-based drug delivery systems. The present investigation reported the development of curcumin loaded mPEG-PLA micelles. Characterization tests indicated that CUR was encapsulated with high drug loading and encapsulation efficiency. The incorporated CUR released from CUR-mPEG-PLA in sustained manner. CUR was effectively transported into the cells by micelles through endocytosis and localized around the nuclei in the cytoplasm. *In vitro* studies proved that the cytotoxicity of CUR-mPEG-PLA against B16F10 and MDA-MB-231 cell line in a dose-dependent manner. Many studies have indicated that the expression level of TfR on tumor cells is much higher than that on normal cells which has been widely utilized for targeting drug delivery systems as a novel potential approach. Thus, we constructed Tf-targeted mPEG-PLA micelles to improve the cellular uptake efficiency. The Tf-CUR-mPEG-PLA micelles showed the enhanced internalization by HeLa and HepG2 overexpressing TfR.

The results of *in vitro* cytotoxicity studies confirmed the enhanced efficacy of Tf-modified mPEG-PLA micelles compared to non-targeted micelles. The spheroids somewhat mimic the solid tumors *in vivo* and thus provide an advantage for study of the effects of a targeted delivery system with the encapsulated CUR in a simulated tumor micro-environment. The spheroid penetration studies indicated that targeting enhanced the delivery of micelles to the spheroids.

In continuation, we investigated the possible polymeric system consisting of cholesterol (Ch), being more lipophilic than the hydrocarbon chain of a fatty acid the micelles produced by the copolymer are expected to greatly enhance the solubility of CUR. Also, cholesterol is an important component of animal cellular membrane and responsible for membrane fluidity and permeability, intracellular transport, signal transduction, and cell trafficking. Since cholesterol is associated with so many membrane-related bioprocess, so incorporation of cholesterol may be helpful for any delivery system to cross the cellular membrane more easily. In this context, we have developed cholesterol-conjugated mPEG-PLA micelles for cancer therapy to improve the biocompatibility of the polymeric system. Our result demonstrated that the newly developed polymeric micelles loaded curcumin effectively, delivered it to the B16F10 and MDA-MB-231 cancer cells leading to decreased dose-dependent cell viability, and increased rate of tumor volume of reduction when administered *in vivo* in B16F10-tumor xenografted mice.

In the later part of this work, mPEG-PLA micelles has been utilized to specifically deliver photosensitizers to targeted tumor regions. The Chlorin e6 (Ce6) loaded mPEG-PLA micelles demonstrated enhanced cellular uptake in A549 cancer cells. Further, Ce6-loaded micelles also showed efficient penetration and growth inhibition in A549 tumor spheroids. Upon

irradiation, the Ce6-mPEG-PLA micelles generated high yield of singlet oxygen to induce cell apoptosis in both cancer cells monolayer and 3-D spheroids.

Overall, the results demonstrate that mPEG-PLA could be a potential carrier in tumor therapy and can be utilized to improve the solubility, stability, and cellular uptake of hydrophobic drug like paclitaxel, camptothecin, and docetaxel, for treatment of various types of cancers including breast cancer, ovarian cancer, non-small cell lung cancer, colon cancer, prostate cancer etc.

FUTURE PERSPECTIVES

Polymeric micelles delivery system has been recognized as a promising strategy for clinical translation of water insoluble new drugs. These polymeric micelles has the advantages of solubilization, selective tumor targeting, decreasing systemic side effect and hypersensitization towards multidrug resistance cells, which have been verified by those preclinical and clinical trials.

The developed nanocarriers incorporating combination therapeutics with molecularly targeted biologics and conventional small molecule anti-cancer drugs can be explored. However, development of combination therapies is significantly more challenging than mono-therapies and requires sophisticated optimization strategies to arrive at the best choice of cargoes to include (targeting of multiple cancer targets), the ratios of the co-loaded therapeutics to achieve synergy, and the relative safety and stability of the combination within a nanoformulation.

To date, most photosensitizers development for cancer treatment seems to have been driven chemically, rather than biologically or clinically, with a focus on improved optical properties: focus is needed on solving the problems of early photosensitizers i.e., sustained skin photosensitivity, low selectivity, and inconveniently long drug-to-light intervals. Modification of the photosensitizing moiety through its physicochemical properties or improved targeting by conjugation of the photosensitizer to moieties such as antibodies, polymers, and peptide scaffolds, might overcome the present difficulties.

BIBLIOGRAPHY

Adams, Monica L, Afsaneh Lavasanifar, and Glen S Kwon. 2003. 'Amphiphilic block copolymers for drug delivery', Journal of pharmaceutical sciences, 92: 1343-55.

Aggarwal, B. B., and B. Sung. 2009. 'Pharmacological basis for the role of curcumin in chronic diseases: an age-old spice with modern targets', Trends Pharmacol Sci, 30: 85-94.

Aggarwal, Bharat B, Anushree Kumar, and Alok C Bharti. 2003. 'Anticancer potential of curcumin: preclinical and clinical studies', Anticancer res, 23: 363-98.

Aggarwal, Bharat B, Lokesh Deb, and Sahdeo Prasad. 2014. 'Curcumin differs from tetrahydrocurcumin for molecular targets, signaling pathways and cellular responses', Molecules, 20: 185-205.

Agostinis, Patrizia, Kristian Berg, Keith A Cengel, Thomas H Foster, Albert W Girotti, Sandra O Gollnick, Stephen M Hahn, Michael R Hamblin, Asta Juzeniene, and David Kessel. 2011. 'Photodynamic therapy of cancer: an update', CA: a cancer journal for clinicians, 61: 250-81.

Akasov, Roman, Daria Zaytseva-Zotova, Sergey Burov, Maria Leko, Monique Dontenwill, Manuela Chiper, Thierry Vandamme, and Elena Markvicheva. 2016. 'Formation of multicellular tumor spheroids induced by cyclic RGD-peptides and use for anticancer drug testing in vitro', International journal of pharmaceutics, 506: 148-57.

Alexis, Frank, Eric M Pridgen, Robert Langer, and Omid C Farokhzad. 2010. 'Nanoparticle technologies for cancer therapy.' in, Drug delivery (Springer).

Ali, Imran, K Salim, M A Rather, W A Wani, and Ashanul Haque. 2011. 'Advances in nano drugs for cancer chemotherapy', Current cancer drug targets, 11: 135-46.

Allen, Theresa M. 2002. 'Ligand-targeted therapeutics in anticancer therapy', Nature Reviews Cancer, 2: 750-63.

Anabousi, Samah, Michael Laue, Claus-Michael Lehr, Udo Bakowsky, and Carsten Ehrhardt. 2005. 'Assessing transferrin modification of liposomes by atomic force microscopy and transmission electron microscopy', European journal of pharmaceutics and biopharmaceutics, 60: 295-303.

Anand, P, C Sundaram, S Jhurani, AB Kunnumakkara, and BB Aggarwal. 2008. 'Curcumin and cancer: an "old-age" disease with an "age-old" solution', Cancer Lett, 267: 133 - 64.

Anand, Preetha, Ajaikumar B Kunnumakkara, Robert A Newman, and Bharat B Aggarwal. 2007. 'Bioavailability of curcumin: problems and promises', Molecular pharmaceutics, 4: 807-18.

Anand, Preetha, Chitra Sundaram, Sonia Jhurani, Ajaikumar B Kunnumakkara, and Bharat B Aggarwal. 2008. 'Curcumin and cancer: an “old-age” disease with an “age-old” solution', Cancer letters, 267: 133-64.

Anand, Preetha, Hareesh B Nair, Bokyung Sung, Ajaikumar B Kunnumakkara, Vivek R Yadav, Rajeshwar R Tekmal, and Bharat B Aggarwal. 2010. 'Design of curcumin-loaded PLGA nanoparticles formulation with enhanced cellular uptake, and increased bioactivity in vitro and superior bioavailability in vivo', Biochemical pharmacology, 79: 330-38.

Andrade, JD, Vladimir Hlady, and SI Jeon. 1993. "Polyethylene oxide and protein resistance." In Publ by ACS.

Anuchapreeda, Songyot, Yoshinobu Fukumori, Siriporn Okonogi, and Hideki Ichikawa. 2011. 'Preparation of lipid nanoemulsions incorporating curcumin for cancer therapy', Journal of Nanotechnology, 2012.

Aryal, Santosh, Che-Ming Jack Hu, and Liangfang Zhang. 2011. 'Polymeric nanoparticles with precise ratiometric control over drug loading for combination therapy', Molecular pharmaceutics, 8: 1401-07.

Avci, Pinar, S Sibel Erdem, and Michael R Hamblin. 2014. 'Photodynamic therapy: one step ahead with self-assembled nanoparticles', Journal of biomedical nanotechnology, 10: 1937-52.

Barenholz, Yechezkel. 2012. 'Doxil® — The first FDA-approved nano-drug: Lessons learned', Journal of Controlled Release, 160: 117-34.

Bechet, Denise, Pierre Couleaud, Céline Frochot, Marie-Laure Viriot, François Guillemin, and Muriel Barberi-Heyob. 2008. 'Nanoparticles as vehicles for delivery of photodynamic therapy agents', Trends in biotechnology, 26: 612-21.

Bhadra, D, S Bhadra, S Jain, and NK Jain. 2003. 'A PEGylated dendritic nanoparticulate carrier of fluorouracil', International journal of pharmaceutics, 257: 111-24.

Bisht, Savita, Georg Feldmann, Sheetal Soni, Rajani Ravi, Collins Karikar, Amarnath Maitra, and Anirban Maitra. 2007. 'Polymeric nanoparticle-encapsulated curcumin (“nanocurcumin”): a novel strategy for human cancer therapy', J Nanobiotechnology, 5: 1-18.

Biswas, Swati, and Vladimir P Torchilin. 2014. 'Nanopreparations for organelle-specific delivery in cancer', Advanced drug delivery reviews, 66: 26-41.

Brandis, Alexander S, Yoram Salomon, and Avigdor Scherz. 2006. 'Chlorophyll sensitizers in photodynamic therapy.' in, Chlorophylls and Bacteriochlorophylls (Springer).

Brannon-Peppas, Lisa, and James O Blanchette. 2012. 'Nanoparticle and targeted systems for cancer therapy', Advanced drug delivery reviews, 64: 206-12.

Brigger, Irene, Catherine Dubernet, and Patrick Couvreur. 2002. 'Nanoparticles in cancer therapy and diagnosis', Advanced drug delivery reviews, 54: 631-51.

Brody, Edward N, and Larry Gold. 2000. 'Aptamers as therapeutic and diagnostic agents', Reviews in Molecular Biotechnology, 74: 5-13.

Cairns, Rob, Ioanna Papandreou, and Nicholas Denko. 2006. 'Overcoming physiologic barriers to cancer treatment by molecularly targeting the tumor microenvironment', Molecular Cancer Research, 4: 61-70.

Calzolari, Alessia, Isabella Oliviero, Silvia Deaglio, Gualtiero Mariani, Mauro Biffoni, Nadia Maria Sposi, Fabio Malavasi, Cesare Peschle, and Ugo Testa. 2007. 'Transferrin receptor 2 is frequently expressed in human cancer cell lines', Blood Cells, Molecules, and Diseases, 39: 82-91.

Chen, C. J., J. C. Wang, E. Y. Zhao, L. Y. Gao, Q. Feng, X. Y. Liu, Z. X. Zhao, X. F. Ma, W. J. Hou, L. R. Zhang, W. L. Lu, and Q. Zhang. 2013. 'Self-assembly cationic nanoparticles based on cholesterol-grafted bioreducible poly(amidoamine) for siRNA delivery', Biomaterials, 34: 5303-16.

Chen, J., L. Li, J. Su, B. Li, X. Zhang, and T. Chen. 2015. 'Proteomic Analysis of G2/M Arrest Triggered by Natural Borneol/Curcumin in HepG2 Cells, the Importance of the Reactive Oxygen Species-p53 Pathway', J Agric Food Chem, 63: 6440-9.

Chen, Kuan, Annegret Preuß, Steffen Hackbarth, Matthias Wacker, Klaus Langer, and Beate Röder. 2009. 'Novel photosensitizer-protein nanoparticles for photodynamic therapy: photophysical characterization and in vitro investigations', Journal of Photochemistry and Photobiology B: Biology, 96: 66-74.

Cheng, W., J. N. Kumar, Y. Zhang, and Y. Liu. 2014. 'pH- and redox-responsive poly(ethylene glycol) and cholesterol-conjugated poly(amido amine)s based micelles for controlled drug delivery', Macromol Biosci, 14: 347-58.

Chin, William Wei Lim, Paul Wan Sia Heng, Patricia Soo Ping Thong, Ramaswamy Bhuvaneswari, Werner Hirt, Sebastian Kuenzel, Khee Chee Soo, and Malini Olivo. 2008. 'Improved formulation of photosensitizer chlorin e6 polyvinylpyrrolidone for fluorescence diagnostic imaging and photodynamic therapy of human cancer', European Journal of Pharmaceutics and Biopharmaceutics, 69: 1083-93.

Cho, Kwangjae, XU Wang, Shuming Nie, and Dong M Shin. 2008. 'Therapeutic nanoparticles for drug delivery in cancer', Clinical cancer research, 14: 1310-16.

Dabholkar, Rupa D, Rishikesh M Sawant, Dimitriy A Mongayt, Padma V Devarajan, and Vladimir P Torchilin. 2006. 'Polyethylene glycol–phosphatidylethanolamine conjugate (PEG–PE)-based mixed micelles: some properties, loading with paclitaxel, and modulation of P-glycoprotein-mediated efflux', International journal of pharmaceutics, 315: 148-57.

Danhier, Fabienne, Olivier Feron, and Véronique Préat. 2010. 'To exploit the tumor microenvironment: passive and active tumor targeting of nanocarriers for anti-cancer drug delivery', Journal of Controlled Release, 148: 135-46.

Daniels, Tracy R, Tracie Delgado, Jose A Rodriguez, Gustavo Helguera, and Manuel L Penichet. 2006. 'The transferrin receptor part I: Biology and targeting with cytotoxic antibodies for the treatment of cancer', Clinical immunology, 121: 144-58.

Derycke, Annelies SL, and Peter AM de Witte. 2004. 'Liposomes for photodynamic therapy', Advanced drug delivery reviews, 56: 17-30.

Dhillon, Navneet, Bharat B Aggarwal, Robert A Newman, Robert A Wolff, Ajaikumar B Kunnumakkara, James L Abbruzzese, Chaan S Ng, Vladimir Badmaev, and Razelle Kurzrock. 2008. 'Phase II trial of curcumin in patients with advanced pancreatic cancer', Clinical Cancer Research, 14: 4491-99.

Dong, Yuancai, and Si-Shen Feng. 2004. 'Methoxy poly (ethylene glycol)-poly (lactide)(MPEG-PLA) nanoparticles for controlled delivery of anticancer drugs', Biomaterials, 25: 2843-49.

Dutta, Pranabesh, and Joykrishna Dey. 2011. 'Drug solubilization by amino acid based polymeric nanoparticles: characterization and biocompatibility studies', International journal of pharmaceutics, 421: 353-63.

Ellman, George L. 1959. 'Tissue sulfhydryl groups', Archives of biochemistry and biophysics, 82: 70-77.

Endres, Thomas K, Moritz Beck-Broichsitter, Olga Samsonova, Thomas Renette, and Thomas H Kissel. 2011. 'Self-assembled biodegradable amphiphilic PEG–PCL–lPEI triblock copolymers at

the borderline between micelles and nanoparticles designed for drug and gene delivery', Biomaterials, 32: 7721-31.

Fang, J., T. Sawa, and H. Maeda. 2003. 'Factors and mechanism of "EPR" effect and the enhanced antitumor effects of macromolecular drugs including SMANCS', Adv Exp Med Biol, 519: 29-49.

Fenart, Laurence, A Casanova, Bénédicte Dehouck, C Duhem, Stéphanie Slupek, Roméo Cecchelli, and Didier Betbeder. 1999. 'Evaluation of effect of charge and lipid coating on ability of 60-nm nanoparticles to cross an in vitro model of the blood-brain barrier', Journal of Pharmacology and Experimental Therapeutics, 291: 1017-22.

Ferrari, Mauro. 2005. 'Cancer nanotechnology: opportunities and challenges', Nature Reviews Cancer, 5: 161-71.

Floor, S. L., J. E. Dumont, C. Maenhaut, and E. Raspe. 2012. 'Hallmarks of cancer: of all cancer cells, all the time?', Trends Mol Med, 18: 509-15.

Foote, Christopher S. 1991. 'Definition of type I and type II photosensitized oxidation', Photochemistry and photobiology, 54: 659-59.

Fuchs, Jürgen, and Jens Thiele. 1998. 'The role of oxygen in cutaneous photodynamic therapy', Free Radical Biology and Medicine, 24: 835-47.

Gao, Yu, Zhihong Li, Xiaodong Xie, Chaoqun Wang, Jiali You, Fan Mo, Biyu Jin, Jianzhong Chen, Jingwei Shao, and Haijun Chen. 2015. 'Dendrimeric anticancer prodrugs for targeted delivery of ursolic acid to folate receptor-expressing cancer cells: Synthesis and biological evaluation', European Journal of Pharmaceutical Sciences, 70: 55-63.

Garlotta, Donald. 2001. 'A literature review of poly (lactic acid)', Journal of Polymers and the Environment, 9: 63-84.

Gaucher, Geneviève, Marie-Hélène Dufresne, Vinayak P Sant, Ning Kang, Dusica Maysinger, and Jean-Christophe Leroux. 2005. 'Block copolymer micelles: preparation, characterization and application in drug delivery', Journal of controlled release, 109: 169-88.

Gijsens, Antoon, Annelies Derycke, Ludwig Missiaen, Dirk De Vos, Jörg Huwyler, Alex Eberle, and Peter de Witte. 2002. 'Targeting of the photocytotoxic compound AlPcS4 to hela cells by transferrin conjugated peg-liposomes', International journal of cancer, 101: 78-85.

Giordano, Karin F, and Aminah Jatoi. 2005. 'The cancer anorexia/weight loss syndrome: therapeutic challenges', Current oncology reports, 7: 271-76.

Gomes, Ana, Eduarda Fernandes, and José LFC Lima. 2005. 'Fluorescence probes used for detection of reactive oxygen species', Journal of biochemical and biophysical methods, 65: 45-80.

Gref, R, M Lück, P Quellec, M Marchand, E Dellacherie, S Harnisch, T Blunk, and RH Müller. 2000. ''Stealth'corona-core nanoparticles surface modified by polyethylene glycol (PEG): influences of the corona (PEG chain length and surface density) and of the core composition on phagocytic uptake and plasma protein adsorption', Colloids and Surfaces B: Biointerfaces, 18: 301-13.

Gref, Ruxandra, Yoshiharu Minamitake, Maria Teresa Peracchia, Vladimir Trubetskoy, Vladimir Torchilin, and Robert Langer. 1994. 'Biodegradable long-circulating polymeric nanospheres', Science, 263: 1600-03.

Griesser, Markus, Valentina Pistis, Takashi Suzuki, Noemi Tejera, Derek A Pratt, and Claus Schneider. 2011. 'Autoxidative and cyclooxygenase-2 catalyzed transformation of the dietary chemopreventive agent curcumin', Journal of Biological Chemistry, 286: 1114-24.

Gullotti, Emily, and Yoon Yeo. 2009. 'Extracellularly activated nanocarriers: a new paradigm of tumor targeted drug delivery', Molecular pharmaceutics, 6: 1041-51.

Ha, Wei, Hao Wu, Xiao-Ling Wang, Shu-Lin Peng, Li-Sheng Ding, Sheng Zhang, and Bang-Jing Li. 2011. 'Self-aggregates of cholesterol-modified carboxymethyl konjac glucomannan conjugate: Preparation, characterization, and preliminary assessment as a carrier of etoposide', Carbohydrate Polymers, 86: 513-19.

Hassaninasab, Azam, Yoshiteru Hashimoto, Kaori Tomita-Yokotani, and Michihiko Kobayashi. 2011. 'Discovery of the curcumin metabolic pathway involving a unique enzyme in an intestinal microorganism', Proceedings of the National Academy of Sciences, 108: 6615-20.

Heath, Timothy D, John A Montgomery, James R Piper, and Demetrios Papahadjopoulos. 1983. 'Antibody-targeted liposomes: increase in specific toxicity of methotrexate-gamma-aspartate', Proceedings of the National Academy of Sciences, 80: 1377-81.

Heidel, Jeremy D, and Mark E Davis. 2011. 'Clinical developments in nanotechnology for cancer therapy', Pharmaceutical research, 28: 187-99.

Hillaireau, Hervé, and Patrick Couvreur. 2009. 'Nanocarriers' entry into the cell: relevance to drug delivery', Cellular and Molecular Life Sciences, 66: 2873-96.

Hirschhaeuser, Franziska, Heike Menne, Claudia Dittfeld, Jonathan West, Wolfgang Mueller-Klieser, and Leoni A Kunz-Schughart. 2010. 'Multicellular tumor spheroids: an underestimated tool is catching up again', Journal of biotechnology, 148: 3-15.

Hoebeke, Maryse, and Xavier Damoiseau. 2002. 'Determination of the singlet oxygen quantum yield of bacteriochlorin a: a comparative study in phosphate buffer and aqueous dispersion of dimiristoyl-L-α-phosphatidylcholine liposomes', Photochemical & Photobiological Sciences, 1: 283-87.

Hoehle, Simone I, Erika Pfeiffer, Anikó M Sólyom, and Manfred Metzler. 2006. 'Metabolism of curcuminoids in tissue slices and subcellular fractions from rat liver', Journal of agricultural and food chemistry, 54: 756-64.

Hopper, Colin. 2000. 'Photodynamic therapy: a clinical reality in the treatment of cancer', The lancet oncology, 1: 212-19.

Hou, Wenxiu, Fangfang Xia, Carla S Alves, Xiaoqing Qian, Yuming Yang, and Daxiang Cui. 2016. 'MMP2-targeting and redox-responsive PEGylated chlorin e6 nanoparticles for cancer near-infrared imaging and photodynamic therapy', ACS applied materials & interfaces, 8: 1447-57.

Huang, Peng, Zhiming Li, Jing Lin, Dapeng Yang, Guo Gao, Cheng Xu, Le Bao, Chunlei Zhang, Kan Wang, and Hua Song. 2011. 'Photosensitizer-conjugated magnetic nanoparticles for in vivo simultaneous magnetofluorescent imaging and targeting therapy', Biomaterials, 32: 3447-58.

Huynh, NT, Catherine Passirani, Patrick Saulnier, and JP Benoit. 2009. 'Lipid nanocapsules: a new platform for nanomedicine', International journal of pharmaceutics, 379: 201-09.

Ireson, Christopher R, Donald JL Jones, Samantha Orr, Michael WH Coughtrie, David J Boocock, Marion L Williams, Peter B Farmer, William P Steward, and Andreas J Gescher. 2002. 'Metabolism of the cancer chemopreventive agent curcumin in human and rat intestine', Cancer Epidemiology Biomarkers & Prevention, 11: 105-11.

Ireson, Christopher, Samantha Orr, Don JL Jones, Richard Verschoyle, Chang-Kee Lim, Jin-Li Luo, Lynne Howells, Simon Plummer, Rebekah Jukes, and Marion Williams. 2001. 'Characterization of metabolites of the chemopreventive agent curcumin in human and rat hepatocytes and in the rat in vivo, and evaluation of their ability to inhibit phorbol ester-induced prostaglandin E2 production', Cancer Research, 61: 1058-64.

Isakau, HA, MV Parkhats, VN Knyukshto, BM Dzhagarov, EP Petrov, and PT Petrov. 2008. 'Toward understanding the high PDT efficacy of chlorin e6–polyvinylpyrrolidone formulations: Photophysical and molecular aspects of photosensitizer–polymer interaction in vitro', Journal of Photochemistry and Photobiology B: Biology, 92: 165-74.

Ito, Takashi. 1978. 'Cellular and subcellular mechanisms of photodynamic action: the O2 hypothesis as a driving force in recent research', Photochemistry and photobiology, 28: 493-506.

Iyer, A. K., G. Khaled, J. Fang, and H. Maeda. 2006. 'Exploiting the enhanced permeability and retention effect for tumor targeting', Drug Discov Today, 11: 812-8.

Jain, Anekant, and Sanjay K Jain. 2008. 'In vitro and cell uptake studies for targeting of ligand anchored nanoparticles for colon tumors', european journal of pharmaceutical sciences, 35: 404-16.

Jain, Arvind K, Amit K Goyal, Prem N Gupta, Kapil Khatri, Neeraj Mishra, Abhinav Mehta, Sharad Mangal, and Suresh P Vyas. 2009. 'Synthesis, characterization and evaluation of novel triblock copolymer based nanoparticles for vaccine delivery against hepatitis B', Journal of Controlled Release, 136: 161-69.

Jain, Rakesh K. 1987. 'Transport of molecules in the tumor interstitium: a review', Cancer research, 47: 3039-51.

Jeong, Hayoung, MyungSook Huh, So Jin Lee, Heebeom Koo, Ick Chan Kwon, Seo Young Jeong, and Kwangmeyung Kim. 2011. 'Photosensitizer-conjugated human serum albumin nanoparticles for effective photodynamic therapy', Theranostics, 1: 230.

Jia, Xiao, and Lee Jia. 2012. 'Nanoparticles improve biological functions of phthalocyanine photosensitizers used for photodynamic therapy', Current drug metabolism, 13: 1119-22.

Jones, Marie-Christine, and Jean-Christophe Leroux. 1999. 'Polymeric micelles–a new generation of colloidal drug carriers', European journal of pharmaceutics and biopharmaceutics, 48: 101-11.

Juliano, RL, and D Stamp. 1976. 'Lectin-mediated attachment of glycoprotein-bearing liposomes to cells'.

Kabanov, Alexander V, Elena V Batrakova, and Valery Yu Alakhov. 2002. 'Pluronic® block copolymers as novel polymer therapeutics for drug and gene delivery', Journal of controlled release, 82: 189-212.

Kataoka, Kazunori, Atsushi Harada, and Yukio Nagasaki. 2001. 'Block copolymer micelles for drug delivery: design, characterization and biological significance', Advanced drug delivery reviews, 47: 113-31.

Kawamori, T, R Lubet, VE Steele, GJ Kelloff, RB Kaskey, CV Rao, and BS Reddy. 1999. 'Chemopreventive effect of curcumin, a naturally occurring anti-inflammatory agent, during the promotion/progression stages of colon cancer', Cancer Res, 59: 597.

Kawamori, Toshihiko, Ronald Lubet, Vernon E Steele, Gary J Kelloff, Robert B Kaskey, Chinthalapally V Rao, and Bandaru S Reddy. 1999. 'Chemopreventive effect of curcumin, a naturally occurring anti-inflammatory agent, during the promotion/progression stages of colon cancer', Cancer research, 59: 597-601.

Kim, Jong-Ho, Yoo-Shin Kim, Sungwon Kim, Jae Hyung Park, Kwangmeyung Kim, Kuiwon Choi, Hesson Chung, Seo Young Jeong, Rang-Woon Park, and In-San Kim. 2006. 'Hydrophobically modified glycol chitosan nanoparticles as carriers for paclitaxel', Journal of Controlled Release, 111: 228-34.

Kim, Tae Hyung, Hai Hua Jiang, Yu Seok Youn, Chan Woong Park, Kyung Kook Tak, Seulki Lee, Hyungjun Kim, Sangyong Jon, Xiaoyuan Chen, and Kang Choon Lee. 2011. 'Preparation and characterization of water-soluble albumin-bound curcumin nanoparticles with improved antitumor activity', International journal of pharmaceutics, 403: 285-91.

Kim, Tae-Hee, Christopher W Mount, Wayne R Gombotz, and Suzie H Pun. 2010. 'The delivery of doxorubicin to 3-D multicellular spheroids and tumors in a murine xenograft model using tumor-penetrating triblock polymeric micelles', Biomaterials, 31: 7386-97.

Konopka, KRYSTYNA, and TOMASZ Goslinski. 2007. 'Photodynamic therapy in dentistry', Journal of dental research, 86: 694-707.

Koo, Heebeom, Myung Sook Huh, In-Cheol Sun, Soon Hong Yuk, Kuiwon Choi, Kwangmeyung Kim, and Ick Chan Kwon. 2011. 'In vivo targeted delivery of nanoparticles for theranosis', Accounts of chemical research, 44: 1018-28.

Kostenich, GA, IN Zhuravkin, and EA Zhavrid. 1994. 'Experimental grounds for using chlorin ρ6 in the photodynamic therapy of malignant tumors', Journal of Photochemistry and Photobiology B: Biology, 22: 211-17.

Krishna, Rajesh, and Lawrence D Mayer. 2000. 'Multidrug resistance (MDR) in cancer: mechanisms, reversal using modulators of MDR and the role of MDR modulators in influencing the pharmacokinetics of anticancer drugs', European Journal of Pharmaceutical Sciences, 11: 265-83.

Kumar, Challa SSR. 2006. Nanomaterials for cancer therapy (Wiley-VCH Weinheim, Germany).

Kumari, Avnesh, Sudesh Kumar Yadav, and Subhash C Yadav. 2010. 'Biodegradable polymeric nanoparticles based drug delivery systems', Colloids and Surfaces B: Biointerfaces, 75: 1-18.

Kumari, Preeti, Balaram Ghosh, and Swati Biswas. 2016. 'Nanocarriers for cancer-targeted drug delivery', Journal of drug targeting, 24: 179-91.

Kumari, Preeti, Muddineti Omkara Swami, Sravan Kumar Nadipalli, Srividya Myneni, Balaram Ghosh, and Swati Biswas. 2016. 'Curcumin delivery by poly (Lactide)-based co-polymeric micelles: an in vitro anticancer study', Pharmaceutical research, 33: 826-41.

Kumari, Preeti, Muddineti Omkara Swami, Sravan Kumar Nadipalli, Srividya Myneni, Balaram Ghosh, and Swati Biswas. 2015. 'Curcumin Delivery by Poly (Lactide)-Based Co-Polymeric Micelles: An In Vitro Anticancer Study', Pharmaceutical research: 1-16.

Langer, Robert. 1998. 'Drug delivery and targeting', Nature, 392: 5-10.

LaPorte, Richard J. 1997. Hydrophilic polymer coatings for medical devices (CRC Press).

Larina, Irina V, B Mark Evers, Taras V Ashitkov, Christian Bartels, Kirill V Larin, and Rinat O Esenaliev. 2005. 'Enhancement of drug delivery in tumors by using interaction of nanoparticles with ultrasound radiation', Technology in cancer research & treatment, 4: 217-26.

Lavasanifar, Afsaneh, John Samuel, and Glen S Kwon. 2002. 'Poly (ethylene oxide)-block-poly (L-amino acid) micelles for drug delivery', Advanced drug delivery reviews, 54: 169-90.

Layre, A, P Couvreur, H Chacun, J Richard, C Passirani, D Requier, JP Benoit, and R Gref. 2006. 'Novel composite core-shell nanoparticles as busulfan carriers', Journal of controlled release, 111: 271-80.

Lee, Ashlynn LZ, Shrinivas Venkataraman, Syamilah BM Sirat, Shujun Gao, James L Hedrick, and Yi Yan Yang. 2012. 'The use of cholesterol-containing biodegradable block copolymers to exploit hydrophobic interactions for the delivery of anticancer drugs', Biomaterials, 33: 1921-28.

Lee, Chung-Sung, Wooram Park, Sin-jung Park, and Kun Na. 2013. 'Endolysosomal environment-responsive photodynamic nanocarrier to enhance cytosolic drug delivery via photosensitizer-mediated membrane disruption', Biomaterials, 34: 9227-36.

Lee, Lui Shiong, Patricia Soo Ping Thong, Malini Olivo, William Wei Lim Chin, Bhuvaneswari Ramaswamy, Kiang Wei Kho, Pei Li Lim, and Weber Kam On Lau. 2010. 'Chlorin e6-

polyvinylpyrrolidone mediated photodynamic therapy—A potential bladder sparing option for high risk non-muscle invasive bladder cancer', Photodiagnosis and photodynamic therapy, 7: 213-20.

Lee, So Jin, Heebeom Koo, Dong-Eun Lee, Solki Min, Seulki Lee, Xiaoyuan Chen, Yongseok Choi, James F Leary, Kinam Park, and Seo Young Jeong. 2011. 'Tumor-homing photosensitizer-conjugated glycol chitosan nanoparticles for synchronous photodynamic imaging and therapy based on cellular on/off system', Biomaterials, 32: 4021-29.

Lee, So Jin, Heebeom Koo, Hayoung Jeong, Myung Sook Huh, Yongseok Choi, Seo Young Jeong, Youngro Byun, Kuiwon Choi, Kwangmeyung Kim, and Ick Chan Kwon. 2011. 'Comparative study of photosensitizer loaded and conjugated glycol chitosan nanoparticles for cancer therapy', Journal of controlled release, 152: 21-29.

Lee, Yong-Eun Koo, and Raoul Kopelman. 2011. 'Polymeric nanoparticles for photodynamic therapy', Biomedical Nanotechnology: Methods and Protocols: 151-78.

Letchford, Kevin, Richard Liggins, and Helen Burt. 2008. 'Solubilization of hydrophobic drugs by methoxy poly (ethylene glycol)-block-polycaprolactone diblock copolymer micelles: Theoretical and experimental data and correlations', Journal of pharmaceutical sciences, 97: 1179-90.

Li, Buhong, Eduardo H Moriyama, Fugang Li, Mark T Jarvi, Christine Allen, and Brian C Wilson. 2007. 'Diblock copolymer micelles deliver hydrophobic protoporphyrin IX for photodynamic therapy', Photochemistry and photobiology, 83: 1505-12.

Li, Lan, Bilal Ahmed, Kapil Mehta, and Razelle Kurzrock. 2007. 'Liposomal curcumin with and without oxaliplatin: effects on cell growth, apoptosis, and angiogenesis in colorectal cancer', Molecular cancer therapeutics, 6: 1276-82.

Li, Li, Byoung-chan Bae, Thanh Huyen Tran, Kwon Hyeok Yoon, Kun Na, and Kang Moo Huh. 2011. 'Self-quenchable biofunctional nanoparticles of heparin–folate-photosensitizer conjugates for photodynamic therapy', Carbohydrate polymers, 86: 708-15.

Li, Yan, Haiqing Dong, Yongyong Li, and Donglu Shi. 2015. 'Graphene-based nanovehicles for photodynamic medical therapy', International journal of nanomedicine, 10: 2451.

Li, Yu, and Glen S Kwon. 2000. 'Methotrexate esters of poly (ethylene oxide)-block-poly (2-hydroxyethyl-L-aspartamide). Part I: Effects of the level of methotrexate conjugation on the stability of micelles and on drug release', Pharmaceutical research, 17: 607-11.

Li, Yuhua, Yalu Yu, Ling Kang, and Ying Lu. 2014. 'Effects of chlorin e6-mediated photodynamic therapy on human colon cancer SW480 cells', International journal of clinical and experimental medicine, 7: 4867.

Li, Zhiwei, Chao Wang, Liang Cheng, Hua Gong, Shengnan Yin, Qiufang Gong, Yonggang Li, and Zhuang Liu. 2013. 'PEG-functionalized iron oxide nanoclusters loaded with chlorin e6 for targeted, NIR light induced, photodynamic therapy', Biomaterials, 34: 9160-70.

Lima, Adriel M, Carine Dal Pizzol, Fabíola BF Monteiro, Tânia B Creczynski-Pasa, Gislaine P Andrade, Anderson O Ribeiro, and Janice R Perussi. 2013. 'Hypericin encapsulated in solid lipid nanoparticles: phototoxicity and photodynamic efficiency', Journal of Photochemistry and Photobiology B: Biology, 125: 146-54.

Lin, Yu-Ling, Yen-Ku Liu, Nu-Man Tsai, Jui-Hung Hsieh, Chia-Hung Chen, Ching-Min Lin, and Kuang-Wen Liao. 2012. 'A Lipo-PEG-PEI complex for encapsulating curcumin that enhances its antitumor effects on curcumin-sensitive and curcumin-resistance cells', Nanomedicine: Nanotechnology, Biology and Medicine, 8: 318-27.

Ling, Daishun, Byoung-chan Bae, Wooram Park, and Kun Na. 2012. 'Photodynamic efficacy of photosensitizers under an attenuated light dose via lipid nano-carrier-mediated nuclear targeting', Biomaterials, 33: 5478-86.

Lipinski, Christopher A, Franco Lombardo, Beryl W Dominy, and Paul J Feeney. 2012. 'Experimental and computational approaches to estimate solubility and permeability in drug discovery and development settings', Advanced drug delivery reviews, 64: 4-17.

Lipinski, Christopher A. 2000. 'Drug-like properties and the causes of poor solubility and poor permeability', Journal of pharmacological and toxicological methods, 44: 235-49.

Liu, Li, Chenxi Li, Xuechen Li, Zhi Yuan, Yingli An, and Binglin He. 2001. 'Biodegradable polylactide/poly (ethylene glycol)/polylactide triblock copolymer micelles as anticancer drug carriers', Journal of applied polymer science, 80: 1976-82.

Liu, Shi, Yubin Huang, Xuesi Chen, Liping Zhang, and Xiabin Jing. 2010. 'Lactose mediated liver-targeting effect observed by ex vivo imaging technology', Biomaterials, 31: 2646-54.

Lucke, Andrea, Jörg Teßmar, Edith Schnell, Georg Schmeer, and Achim Göpferich. 2000. 'Biodegradable poly (D, L-lactic acid)-poly (ethylene glycol)-monomethyl ether diblock copolymers: structures and surface properties relevant to their use as biomaterials', Biomaterials, 21: 2361-70.

Lukyanov, Anatoly N, and Vladimir P Torchilin. 2004. 'Micelles from lipid derivatives of water-soluble polymers as delivery systems for poorly soluble drugs', Advanced drug delivery reviews, 56: 1273-89.

Luo, Ji, Nicole L Solimini, and Stephen J Elledge. 2009. 'Principles of cancer therapy: oncogene and non-oncogene addiction', Cell, 136: 823-37.

Luo, Laibin, Joseph Tam, Dusica Maysinger, and Adi Eisenberg. 2002. 'Cellular internalization of poly (ethylene oxide)-b-poly (ε-caprolactone) diblock copolymer micelles', Bioconjugate chemistry, 13: 1259-65.

Ma, Q., B. Li, Y. Yu, Y. Zhang, Y. Wu, W. Ren, Y. Zheng, J. He, Y. Xie, X. Song, and G. He. 2013. 'Development of a novel biocompatible poly(ethylene glycol)-block-poly(gamma-cholesterol-L-glutamate) as hydrophobic drug carrier', Int J Pharm, 445: 88-92.

Ma, Zengshuan, Azita Haddadi, Ommoleila Molavi, Afsaneh Lavasanifar, Raymond Lai, and John Samuel. 2008. 'Micelles of poly (ethylene oxide)-b-poly (ε-caprolactone) as vehicles for the solubilization, stabilization, and controlled delivery of curcumin', Journal of Biomedical Materials Research Part A, 86: 300-10.

Maeda, H. 2001a. 'SMANCS and polymer-conjugated macromolecular drugs: advantages in cancer chemotherapy', Adv Drug Deliv Rev, 46: 169-85.

Maeda, H., G. Y. Bharate, and J. Daruwalla. 2009. 'Polymeric drugs for efficient tumor-targeted drug delivery based on EPR-effect', Eur J Pharm Biopharm, 71: 409-19.

Maeda, Hiroshi, Tomohiro Sawa, and Toshimitsu Konno. 2001. 'Mechanism of tumor-targeted delivery of macromolecular drugs, including the EPR effect in solid tumor and clinical overview of the prototype polymeric drug SMANCS', Journal of controlled release, 74: 47-61.

Maeda, Hiroshi. 2001b. 'The enhanced permeability and retention (EPR) effect in tumor vasculature: the key role of tumor-selective macromolecular drug targeting', Advances in enzyme regulation, 41: 189-207.

Malam, Yogeshkumar, Marilena Loizidou, and Alexander M Seifalian. 2009. 'Liposomes and nanoparticles: nanosized vehicles for drug delivery in cancer', Trends in pharmacological sciences, 30: 592-99.

Martin, Robert C. G., Erica Locatelli, Yan Li, Weizhong Zhang, Suping Li, Ilaria Monaco, and Mauro Comes Franchini. 2015. 'Gold nanorods and curcumin-loaded nanomicelles for efficient in vivo photothermal therapy of Barrett's esophagus', Nanomedicine, 10: 1723-33.

Matsumura, Yasuhiro, and Hiroshi Maeda. 1986. 'A new concept for macromolecular therapeutics in cancer chemotherapy: mechanism of tumoritropic accumulation of proteins and the antitumor agent smancs', Cancer research, 46: 6387-92.

Maxfield, F. R., and I. Tabas. 2005. 'Role of cholesterol and lipid organization in disease', Nature, 438: 612-21.

Mays, Ashley N, Neil Osheroff, Yuanyuan Xiao, Joseph L Wiemels, Carolyn A Felix, Jo Ann W Byl, Kandeepan Saravanamuttu, Andrew Peniket, Robert Corser, and Cherry Chang. 2010. 'Evidence for direct involvement of epirubicin in the formation of chromosomal translocations in t (15; 17) therapy-related acute promyelocytic leukemia', Blood, 115: 326-30.

Mehmet, HU, K Seta, S Bernhard, and BS Uwe. 2013. 'Characterization of CurcuEmulsomes: nanoformulation for enhanced solubility and delivery of curcumin', J Nanobiotechnology, 11: 37.

Meng, Huan, Min Xue, Tian Xia, Zhaoxia Ji, Derrick Y Tarn, Jeffrey I Zink, and Andre E Nel. 2011. 'Use of size and a copolymer design feature to improve the biodistribution and the enhanced permeability and retention effect of doxorubicin-loaded mesoporous silica nanoparticles in a murine xenograft tumor model', ACS nano, 5: 4131-44.

Minchinton, Andrew I, and Ian F Tannock. 2006. 'Drug penetration in solid tumours', Nature Reviews Cancer, 6: 583-92.

Mittal, G, DK Sahana, V Bhardwaj, and MNV Ravi Kumar. 2007. 'Estradiol loaded PLGA nanoparticles for oral administration: effect of polymer molecular weight and copolymer composition on release behavior in vitro and in vivo', Journal of Controlled Release, 119: 77-85.

.

Mock, Charlotta D, Brian C Jordan, and Chelliah Selvam. 2015. 'Recent advances of curcumin and its analogues in breast cancer prevention and treatment', RSC Advances, 5: 75575-88.

Moghimi, S Moein, A Christy Hunter, and J Clifford Murray. 2005. 'Nanomedicine: current status and future prospects', The FASEB journal, 19: 311-30.

Mohanty, C., S. Acharya, A. K. Mohanty, F. Dilnawaz, and S. K. Sahoo. 2010. 'Curcumin-encapsulated MePEG/PCL diblock copolymeric micelles: a novel controlled delivery vehicle for cancer therapy', Nanomedicine (Lond), 5: 433-49.

Mulik, RS, J Monkkonen, RO Juvonen, KR Mahadik, and AR Paradkar. 2012. 'ApoE3 mediated polymeric nanoparticles containing curcumin: Apoptosis induced in vitro anticancer activity against neuroblastoma cells', Int J Pharm, 437: 29 - 41.

Muthu, Madaswamy S, Rajaletchumy Veloo Kutty, Zhentao Luo, Jianping Xie, and Si-Shen Feng. 2015. 'Theranostic vitamin E TPGS micelles of transferrin conjugation for targeted co-delivery of docetaxel and ultra bright gold nanoclusters', Biomaterials, 39: 234-48.

Nagarwal, Ramesh C, Shri Kant, PN Singh, P Maiti, and JK Pandit. 2009. 'Polymeric nanoparticulate system: a potential approach for ocular drug delivery', Journal of Controlled Release, 136: 2-13.

Naksuriya, Ornchuma, Siriporn Okonogi, Raymond M Schiffelers, and Wim E Hennink. 2014. 'Curcumin nanoformulations: a review of pharmaceutical properties and preclinical studies and clinical data related to cancer treatment', Biomaterials, 35: 3365-83.

Nasongkla, Norased, Erik Bey, Jimin Ren, Hua Ai, Chalermchai Khemtong, Jagadeesh Setti Guthi, Shook-Fong Chin, A Dean Sherry, David A Boothman, and Jinming Gao. 2006. 'Multifunctional polymeric micelles as cancer-targeted, MRI-ultrasensitive drug delivery systems', Nano letters, 6: 2427-30.

Nehoff, H., N. N. Parayath, L. Domanovitch, S. Taurin, and K. Greish. 2014. 'Nanomedicine for drug targeting: strategies beyond the enhanced permeability and retention effect', Int J Nanomedicine, 9: 2539-55.

Nishiyama, Nobuhiro, and Kazunori Kataoka. 2006. 'Current state, achievements, and future prospects of polymeric micelles as nanocarriers for drug and gene delivery', Pharmacology & therapeutics, 112: 630-48.

Nishiyama, Nobuhiro, and Kazunori Kataoka. 2006. 'Nanostructured devices based on block copolymer assemblies for drug delivery: designing structures for enhanced drug function', Polymer Therapeutics II: 67-101.

Nishiyama, Nobuhiro, Souichiro Okazaki, Horacio Cabral, Masaki Miyamoto, Yukio Kato, Yuichi Sugiyama, Kazuto Nishio, Yasuhiro Matsumura, and Kazunori Kataoka. 2003. 'Novel cisplatin-incorporated polymeric micelles can eradicate solid tumors in mice', Cancer research, 63: 8977-83.

Ochsner, M. 1997. 'Photophysical and photobiological processes in the photodynamic therapy of tumours', Journal of Photochemistry and Photobiology B: Biology, 39: 1-18.

Oleinick, Nancy L, and Helen H Evans. 1998. 'The photobiology of photodynamic therapy: cellular targets and mechanisms', Radiation research, 150: S146-S56.

Orenstein, A, G Kostenich, L Roitman, Y Shechtman, Y Kopolovic, B Ehrenberg, and Z Malik. 1996. 'A comparative study of tissue distribution and photodynamic therapy selectivity of chlorin e6, Photofrin II and ALA-induced protoporphyrin IX in a colon carcinoma model', British journal of cancer, 73: 937.

Otsuka, Hidenori, Yukio Nagasaki, and Kazunori Kataoka. 2001. 'Self-assembly of poly (ethylene glycol)-based block copolymers for biomedical applications', Current Opinion in Colloid & Interface Science, 6: 3-10.

Owens III, Donald E, and Nicholas A Peppas. 2006. 'Opsonization, biodistribution, and pharmacokinetics of polymeric nanoparticles', International journal of pharmaceutics, 307: 93-102.

Ozawa, Michael G, Amado J Zurita, Emmanuel Dias-Neto, Diana N Nunes, Richard L Sidman, Juri G Gelovani, Wadih Arap, and Renata Pasqualini. 2008. 'Beyond receptor expression levels: the relevance of target accessibility in ligand-directed pharmacodelivery systems', Trends in cardiovascular medicine, 18: 126-33.

Ozcelikkale, Altug, Soham Ghosh, and Bumsoo Han. 2013. 'Multifaceted transport characteristics of nanomedicine: needs for characterization in dynamic environment', Molecular pharmaceutics, 10: 2111-26.

Pan, Min-Hsiung, Tsang-Miao Huang, and Jen-Kun Lin. 1999. 'Biotransformation of curcumin through reduction and glucuronidation in mice', Drug metabolism and disposition, 27: 486-94.

Park, Hyung, and Kun Na. 2013. 'Conjugation of the photosensitizer Chlorin e6 to pluronic F127 for enhanced cellular internalization for photodynamic therapy', Biomaterials, 34: 6992-7000.

Park, Jae Hyung, Seulki Lee, Jong-Ho Kim, Kyeongsoon Park, Kwangmeyung Kim, and Ick Chan Kwon. 2008. 'Polymeric nanomedicine for cancer therapy', Progress in Polymer Science, 33: 113-37.

Peer, Dan, Jeffrey M Karp, Seungpyo Hong, Omid C Farokhzad, Rimona Margalit, and Robert Langer. 2007. 'Nanocarriers as an emerging platform for cancer therapy', Nature nanotechnology, 2: 751-60.

Penjweini, Rozhin, Hans G Loew, Maria Eisenbauer, and Karl W Kratky. 2013. 'Modifying excitation light dose of novel photosensitizer PVP-Hypericin for photodynamic diagnosis and therapy', Journal of Photochemistry and Photobiology B: Biology, 120: 120-29.

Perche, Federico, Niravkumar R Patel, and Vladimir P Torchilin. 2012. 'Accumulation and toxicity of antibody-targeted doxorubicin-loaded PEG–PE micelles in ovarian cancer cell spheroid model', Journal of controlled release, 164: 95-102.

Perumal, Venkatesan, Shubhadeep Banerjee, Shubasis Das, RK Sen, and Mahitosh Mandal. 2011. 'Effect of liposomal celecoxib on proliferation of colon cancer cell and inhibition of DMBA-induced tumor in rat model', Cancer Nanotechnology, 2: 67-79.

Pokropivny, VV, and VV Skorokhod. 2008. 'New dimensionality classifications of nanostructures', Physica E: Low-dimensional Systems and nanostructures, 40: 2521-25.

Py-Daniel, Karen R, Joy S Namban, Laise R de Andrade, Paulo EN de Souza, Leonardo G Paterno, Ricardo B Azevedo, and Maria AG Soler. 2016. 'Highly efficient photodynamic therapy colloidal system based on chloroaluminum phthalocyanine/pluronic micelles', European Journal of Pharmaceutics and Biopharmaceutics, 103: 23-31.

Rao, S Bhaskara, and Chandra P Sharma. 1997. 'Use of chitosan as a biomaterial: studies on its safety and hemostatic potential', Journal of biomedical materials research, 34: 21-28.

Raveendran, R., G. Bhuvaneshwar, and C. P. Sharma. 2013. 'In vitro cytotoxicity and cellular uptake of curcumin-loaded Pluronic/Polycaprolactone micelles in colorectal adenocarcinoma cells', J Biomater Appl, 27: 811-27.

Rizzo, Larissa Y, Benjamin Theek, Gert Storm, Fabian Kiessling, and Twan Lammers. 2013. 'Recent progress in nanomedicine: therapeutic, diagnostic and theranostic applications', Current opinion in biotechnology, 24: 1159-66.

Rosenthal, I, and E Ben-Hur. 1995. 'Role of oxygen in the phototoxicity of phthalocyanines', International journal of radiation biology, 67: 85-91.

Ruan, Gang, and Si-Shen Feng. 2003. 'Preparation and characterization of poly (lactic acid)–poly (ethylene glycol)–poly (lactic acid)(PLA–PEG–PLA) microspheres for controlled release of paclitaxel', Biomaterials, 24: 5037-44.

Rui, Yuanjin, Susan Wang, Philip S Low, and David H Thompson. 1998. 'Diplasmenylcholine-folate liposomes: an efficient vehicle for intracellular drug delivery', Journal of the American Chemical Society, 120: 11213-18.

Ryan, J. L., C. E. Heckler, M. Ling, A. Katz, J. P. Williams, A. P. Pentland, and G. R. Morrow. 2013. 'Curcumin for radiation dermatitis: a randomized, double-blind, placebo-controlled clinical trial of thirty breast cancer patients', Radiat Res, 180: 34-43.

Safavy, Ahmad, Kevin P Raisch, Sushma Mantena, Leisa L Sanford, Simon W Sham, N Rama Krishna, and James A Bonner. 2007. 'Design and Development of Water-Soluble Curcumin Conjugates as Potential Anticancer Agents£', Journal of medicinal chemistry, 50: 6284-88.

Sahu, A., N. Kasoju, P. Goswami, and U. Bora. 2011. 'Encapsulation of curcumin in Pluronic block copolymer micelles for drug delivery applications', J Biomater Appl, 25: 619-39.

Sahu, Abhishek, Utpal Bora, Naresh Kasoju, and Pranab Goswami. 2008. 'Synthesis of novel biodegradable and self-assembling methoxy poly (ethylene glycol)–palmitate nanocarrier for curcumin delivery to cancer cells', Acta Biomaterialia, 4: 1752-61.

Savić, Radoslav, Laibin Luo, Adi Eisenberg, and Dusica Maysinger. 2003. 'Micellar nanocontainers distribute to defined cytoplasmic organelles', Science, 300: 615-18.

Schiffelers, Raymond M, Gerben A Koning, Timo LM ten Hagen, Marcel HAM Fens, Astrid J Schraa, Adriënne PCA Janssen, Robbert J Kok, Grietje Molema, and Gert Storm. 2003. 'Anti-tumor efficacy of tumor vasculature-targeted liposomal doxorubicin', Journal of Controlled Release, 91: 115-22.

Serpe, Loredana. 2006. 'Conventional chemotherapeutic drug nanoparticles for cancer treatment', Nanotechnologies for the Life Sciences.

Shaikh, J, DD Ankola, V Beniwal, D Singh, and MNV Ravi Kumar. 2009. 'Nanoparticle encapsulation improves oral bioavailability of curcumin by at least 9-fold when compared to curcumin administered with piperine as absorption enhancer', european journal of pharmaceutical sciences, 37: 223-30.

Sheleg, Sergey V, Edvard A Zhavrid, Tatsiana V Khodina, Georgy A Kochubeev, Yury P Istomin, Vadim N Chalov, and Ivan N Zhuravkin. 2004. 'Photodynamic therapy with chlorin e6 for skin metastases of melanoma', Photodermatology, photoimmunology & photomedicine, 20: 21-26.

Shieh, Ming-Jium, Cheng-Liang Peng, Wei-Lun Chiang, Chau-Hui Wang, Chia-Yen Hsu, Shian-Jy Jassy Wang, and Ping-Shan Lai. 2010. 'Reduced skin photosensitivity with meta-tetra

(hydroxyphenyl) chlorin-loaded micelles based on a poly (2-ethyl-2-oxazoline)-b-poly (d, l-lactide) diblock copolymer in vivo', Molecular pharmaceutics, 7: 1244-53.

Shirinifard, Abbas, J Scott Gens, Benjamin L Zaitlen, Nikodem J Popławski, Maciej Swat, and James A Glazier. 2009. '3D multi-cell simulation of tumor growth and angiogenesis', PloS one, 4: e7190.

Shuai, Xintao, Hua Ai, Norased Nasongkla, Saejeong Kim, and Jinming Gao. 2004. 'Micellar carriers based on block copolymers of poly (ε-caprolactone) and poly (ethylene glycol) for doxorubicin delivery', Journal of Controlled Release, 98: 415-26.

Skeel, Roland T, and Samir N Khleif. 2011. Handbook of cancer chemotherapy (Lippincott Williams & Wilkins).

Song, Lei, Yuanyuan Shen, Jingwen Hou, Lei Lei, Shengrong Guo, and Changyun Qian. 2011. 'Polymeric micelles for parenteral delivery of curcumin: preparation, characterization and in vitro evaluation', Colloids and Surfaces A: Physicochemical and Engineering Aspects, 390: 25-32.

Sou, Keitaro, Shunsuke Inenaga, Shinji Takeoka, and Eishun Tsuchida. 2008. 'Loading of curcumin into macrophages using lipid-based nanoparticles', International journal of pharmaceutics, 352: 287-93.

Sriraman, Shravan Kumar, Jiayi Pan, Can Sarisozen, Ed Luther, and Vladimir Torchilin. 2016. 'Enhanced cytotoxicity of folic acid-targeted liposomes co-loaded with C6 ceramide and doxorubicin: in vitro evaluation on HeLa, A2780-ADR, and H69-AR cells', Molecular pharmaceutics, 13: 428-37.

Srivastava, Raghvendra M, Sarvjeet Singh, Shiv K Dubey, Krishna Misra, and Ashok Khar. 2011. 'Immunomodulatory and therapeutic activity of curcumin', International immunopharmacology, 11: 331-41.

Stewart, BW, and P Kleihues. 2003. 'World cancer report. Geneva: International Agency for Research on Cancer', World Health Organization.

Stortecky, Stefan, and Thomas M Suter. 2010. 'Insights into cardiovascular side-effects of modern anticancer therapeutics', Current opinion in oncology, 22: 312-17.

Subbiah, R, M Veerapandian, and K S Yun. 2010. 'Nanoparticles: functionalization and multifunctional applications in biomedical sciences', Current medicinal chemistry, 17: 4559-77.

Sutton, Damon, Norased Nasongkla, Elvin Blanco, and Jinming Gao. 2007. 'Functionalized micellar systems for cancer targeted drug delivery', Pharmaceutical research, 24: 1029-46.

Szakács, Gergely, Jill K Paterson, Joseph A Ludwig, Catherine Booth-Genthe, and Michael M Gottesman. 2006. 'Targeting multidrug resistance in cancer', Nature reviews Drug discovery, 5: 219-34.

Talekar, Meghna, Jackie Kendall, William Denny, and Sanjay Garg. 2011. 'Targeting of nanoparticles in cancer: drug delivery and diagnostics', Anti-Cancer Drugs, 22: 949-62.

Tan, Suryani, Thusitha WT Rupasinghe, Dedreia L Tull, Berin Boughton, Christine Oliver, Chris McSweeny, Sally L Gras, and Mary Ann Augustin. 2014. 'Degradation of curcuminoids by in vitro pure culture fermentation', Journal of agricultural and food chemistry, 62: 11005-15.

Tavano, Lorena, Rita Muzzalupo, Loredana Mauro, Michele Pellegrino, Sebastiano Andò, and Nevio Picci. 2013. 'Transferrin-conjugated pluronic niosomes as a new drug delivery system for anticancer therapy', Langmuir, 29: 12638-46.

Torchilin, V. 2011. 'Tumor delivery of macromolecular drugs based on the EPR effect', Adv Drug Deliv Rev, 63: 131-5.

Torchilin, V. P. 2001. 'Structure and design of polymeric surfactant-based drug delivery systems', Journal of controlled release, 73: 137-72.

Torchilin, V. P. 2002. 'PEG-based micelles as carriers of contrast agents for different imaging modalities', Advanced drug delivery reviews, 54: 235-52.

Torchilin, V. P. 2007. 'Micellar nanocarriers: pharmaceutical perspectives', Pharmaceutical research, 24: 1.

Torchilin, V. P. 2010. 'Passive and active drug targeting: drug delivery to tumors as an example', Handb Exp Pharmacol: 3-53.

Torchilin, Vladimir P. 2000. 'Drug targeting', European Journal of Pharmaceutical Sciences, 11: S81-S91.

Torchilin, Vladimir. 2011. 'Tumor delivery of macromolecular drugs based on the EPR effect', Advanced drug delivery reviews, 63: 131-35.

Tuorkey, M. J. 2014. 'Curcumin a potent cancer preventive agent: Mechanisms of cancer cell killing', Interv Med Appl Sci, 6: 139-46.

Valenzeno, Dennis Paul. 1987. 'Photomodification of biological membranes with emphasis on singlet oxygen mechanisms', Photochemistry and photobiology, 46: 147-60.

Veerendra, Nath Reddy, Rani K Rekha, G Chandana, and Sehrawat Sangeeta. 2009. 'Photodynamic therapy', Indian Journal of Dental Advancements, 1: 46-51.

Vemula, Praveen Kumar, Jun Li, and George John. 2006. 'Enzyme catalysis: tool to make and break amygdalin hydrogelators from renewable resources: a delivery model for hydrophobic drugs', Journal of the American Chemical Society, 128: 8932-38.

Vesterberg, Olof, and Ulrik Breig. 1981. 'Quantitative analysis of multiple molecular forms of transferrin using isoelectric focusing and zone immunoelectrophoresis assay (ZIA)', Journal of Immunological Methods, 46: 53-62.

Vonarbourg, Arnaud, Catherine Passirani, Patrick Saulnier, and Jean-Pierre Benoit. 2006. 'Parameters influencing the stealthiness of colloidal drug delivery systems', Biomaterials, 27: 4356-73.

Waghela, Bhargav N, Anupama Sharma, Suhashini Dhumale, Shashibahl M Pandey, and Chandramani Pathak. 2015. 'Curcumin conjugated with PLGA potentiates sustainability, anti-proliferative activity and apoptosis in human colon carcinoma cells', PloS one, 10: e0117526.

Wang, David K, Srinivas Varanasi, Peter M Fredericks, David JT Hill, Anne L Symons, Andrew K Whittaker, and Firas Rasoul. 2013. 'FT-IR characterization and hydrolysis of PLA-PEG-PLA based copolyester hydrogels with short PLA segments and a cytocompatibility study', Journal of Polymer Science Part A: Polymer Chemistry, 51: 5163-76.

Wang, H., P. Zhao, X. Liang, X. Gong, T. Song, R. Niu, and J. Chang. 2010. 'Folate-PEG coated cationic modified chitosan--cholesterol liposomes for tumor-targeted drug delivery', Biomaterials, 31: 4129-38.

Wang, Yiguang, Tingyuan Yang, Xun Wang, Jiancheng Wang, Xuan Zhang, and Qiang Zhang. 2010. 'Targeted polymeric micelle system for delivery of combretastatin A4 to tumor vasculature in vitro', Pharmaceutical research, 27: 1861-68.

Wang, Ying-Jan, Min-Hsiung Pan, Ann-Lii Cheng, Liang-In Lin, Yuan-Soon Ho, Chang-Yao Hsieh, and Jen-Kun Lin. 1997. 'Stability of curcumin in buffer solutions and characterization of its degradation products', Journal of pharmaceutical and biomedical analysis, 15: 1867-76.

Wei, Zhang, Junguo Hao, Shi Yuan, Yajuan Li, Wu Juan, Xianyi Sha, and Xiaoling Fang. 2009. 'Paclitaxel-loaded Pluronic P123/F127 mixed polymeric micelles: formulation, optimization and in vitro characterization', International journal of pharmaceutics, 376: 176-85.

Weishaupt, Kenneth R, Charles J Gomer, and Thomas J Dougherty. 1976. 'Identification of singlet oxygen as the cytotoxic agent in photo-inactivation of a murine tumor', Cancer research, 36: 2326-29.

Wichitnithad, Wisut, Ubonthip Nimmannit, Patrick S Callery, and Pornchai Rojsitthisak. 2011. 'Effects of different carboxylic ester spacers on chemical stability, release characteristics, and anticancer activity of mono-PEGylated curcumin conjugates', Journal of pharmaceutical sciences, 100: 5206-18.

Wu, Hong, Lin Zhu, and Vladimir P Torchilin. 2013. 'pH-sensitive poly (histidine)-PEG/DSPE-PEG co-polymer micelles for cytosolic drug delivery', Biomaterials, 34: 1213-22.

Wu, Jia-Ching, Mei-Ling Tsai, Ching-Shu Lai, Ying-Jan Wang, Chi-Tang Ho, and Min-Hsiung Pan. 2014. 'Chemopreventative effects of tetrahydrocurcumin on human diseases', Food & function, 5: 12-17.

Wu, Xuemei, Jianhua Xu, Xiuwang Huang, and Caixia Wen. 2011. 'Self-microemulsifying drug delivery system improves curcumin dissolution and bioavailability', Drug development and industrial pharmacy, 37: 15-23.

Xiao, Ren Zhong, Zhao Wu Zeng, Guang Lin Zhou, Jun Jie Wang, Fan Zhu Li, and An Ming Wang. 2010. 'Recent advances in PEG–PLA block copolymer nanoparticles', International journal of nanomedicine, 5: 1057.

Xiao, Ren Zhong, Zhao Wu Zeng, Guang Lin Zhou, Jun Jie Wang, Fan Zhu Li, and An Ming Wang. 2010. 'Recent advances in PEG-PLA block copolymer nanoparticles', Int J Nanomedicine, 5: 1057-65.

Xiong, Xiao-Bing, Abdullah Mahmud, Hasan Uludağ, and Afsaneh Lavasanifar. 2008. 'Multifunctional polymeric micelles for enhanced intracellular delivery of doxorubicin to metastatic cancer cells', Pharmaceutical research, 25: 2555-66.

Yallapu, Murali M, Meena Jaggi, and Subhash C Chauhan. 2012. 'Curcumin nanoformulations: a future nanomedicine for cancer', Drug discovery today, 17: 71-80.

Yallapu, Murali Mohan, Brij K Gupta, Meena Jaggi, and Subhash C Chauhan. 2010. 'Fabrication of curcumin encapsulated PLGA nanoparticles for improved therapeutic effects in metastatic cancer cells', Journal of colloid and interface science, 351: 19-29.

Yang, C., X. Su, A. Liu, L. Zhang, A. Yu, Y. Xi, and G. Zhai. 2013. 'Advances in clinical study of curcumin', Curr Pharm Des, 19: 1966-73.

Yang, Chunfen, Hao Chen, Jie Zhao, Xin Pang, Yanwei Xi, and Guangxi Zhai. 2014. 'Development of a folate-modified curcumin loaded micelle delivery system for cancer targeting', Colloids and Surfaces B: Biointerfaces, 121: 206-13.

Yang, Xian-Zhu, Shuang Dou, Tian-Meng Sun, Cheng-Qiong Mao, Hong-Xia Wang, and Jun Wang. 2011. 'Systemic delivery of siRNA with cationic lipid assisted PEG-PLA nanoparticles for cancer therapy', Journal of Controlled Release, 156: 203-11.

Yao, X., L. Chen, X. Chen, C. He, and H. Zheng. 2014. 'Intercellular pH-responsive histidine modified dextran-g-cholesterol micelle for anticancer drug delivery', Colloids Surf B Biointerfaces, 121: 36-43.

Yeagle, P. L. 1985. 'Cholesterol and the cell membrane', Biochim Biophys Acta, 822: 267-87.

Yeagle, P. L. 1991. 'Modulation of membrane function by cholesterol', Biochimie, 73: 1303-10.

Yokoyama, Masayuki, Shigeto Fukushima, Ryuji Uehara, Kazuya Okamoto, Kazunori Kataoka, Yasuhisa Sakurai, and Teruo Okano. 1998. 'Characterization of physical entrapment and chemical conjugation of adriamycin in polymeric micelles and their design for in vivo delivery to a solid tumor', Journal of Controlled Release, 50: 79-92.

Zanoni, Michele, Filippo Piccinini, Chiara Arienti, Alice Zamagni, Spartaco Santi, Rolando Polico, Alessandro Bevilacqua, and Anna Tesei. 2016. '3D tumor spheroid models for in vitro therapeutic screening: a systematic approach to enhance the biological relevance of data obtained', Scientific reports, 6.

Zenkevich, Eduard, Evgenii Sagun, Valentin Knyukshto, Alexander Shulga, Andrei Mironov, Olga Efremova, Raymond Bonnett, S Phinda Songca, and Mohammed Kassem. 1996. 'Photophysical and photochemical properties of potential porphyrin and chlorin photosensitizers for PDT', Journal of Photochemistry and Photobiology B: Biology, 33: 171-80.

Zhan, Changyou, Bing Gu, Cao Xie, Jin Li, Yu Liu, and Weiyue Lu. 2010. 'Cyclic RGD conjugated poly (ethylene glycol)-co-poly (lactic acid) micelle enhances paclitaxel anti-glioblastoma effect', Journal of Controlled Release, 143: 136-42.

Zhang, Chunlei, Chao Li, Yanlei Liu, Jingpu Zhang, Chenchen Bao, Shujing Liang, Qing Wang, Yao Yang, Hualin Fu, and Kan Wang. 2015. 'Gold Nanoclusters-Based Nanoprobes for Simultaneous Fluorescence Imaging and Targeted Photodynamic Therapy with Superior Penetration and Retention Behavior in Tumors', Advanced Functional Materials, 25: 1314-25.

Zhang, Xuefei, Yuxin Li, Xuesi Chen, Xiuhong Wang, Xiaoyi Xu, Qizhi Liang, Junli Hu, and Xiabin Jing. 2005. 'Synthesis and characterization of the paclitaxel/MPEG-PLA block copolymer conjugate', Biomaterials, 26: 2121-28.

Zhang, Yan, Qizhi Zhang, Liusheng Zha, Wuli Yang, Changchun Wang, Xinguo Jiang, and Shoukuan Fu. 2004. 'Preparation, characterization and application of pyrene-loaded methoxy poly (ethylene glycol)–poly (lactic acid) copolymer nanoparticles', Colloid and Polymer Science, 282: 1323-28.

Zhang, Zhiping, and Si-Shen Feng. 2006. 'Nanoparticles of poly (lactide)/vitamin E TPGS copolymer for cancer chemotherapy: synthesis, formulation, characterization and in vitro drug release', Biomaterials, 27: 262-70.

Zhou, Yuxiang, Victoria A Briand, Nitin Sharma, Suk-kyun Ahn, and Rajeswari M Kasi. 2009. 'Polymers comprising cholesterol: synthesis, self-assembly, and applications', Materials, 2: 636-60.

Zhu, KJ, Lin Xiangzhou, and Yang Shilin. 1990. 'Preparation, characterization, and properties of polylactide (PLA)–poly (ethylene glycol)(PEG) copolymers: a potential drug carrier', Journal of applied polymer science, 39: 1-9.

APPENDIX

LIST OF PUBLICATIONS

From thesis work

1. Kumari P, Swami MO, Nadipalli SK, Myneni S, Ghosh B, Biswas S. Curcumin delivery by poly (Lactide)-based co-polymeric micelles: an in vitro anticancer study. *Pharmaceutical research*. 2016 Apr 1;33(4):826-41.

2. Kumari P, Muddineti OS, Rompicharla SV, Ghanta P, BBN AK, Ghosh B, Biswas S. Cholesterol-conjugated poly (D, L-lactide)-based micelles as a nanocarrier system for effective delivery of curcumin in cancer therapy. *Drug delivery*. 2017 Jan 1;24(1):209-23.

3. Kumari P, Jain S, Ghosh B, Zorin V, Biswas S. Polylactide-Based Block Copolymeric Micelles Loaded with Chlorin e6 for Photodynamic Therapy: In Vitro Evaluation in Monolayer and 3D Spheroid Models. *Molecular pharmaceutics*. 2017 Oct 9;14(11):3789-800.

4. Kumari P, Rompicharla SV, Muddineti OS, Ghosh B, Biswas S. Transferrin-anchored poly (lactide) based micelles to improve anticancer activity of curcumin in hepatic and cervical cancer cell monolayers and 3D spheroids. *International journal of biological macromolecules*. 2018 Sep 1;116:1196-213.

Other publications

1. Omkara Swami Muddineti, Preeti Kumari, Balaram Ghosh, Swati Biswas. Transferrin-Modified Vitamin-E/Lipid Based Polymeric Micelles for Improved Tumor Targeting and Anticancer Effect of Curcumin. *Pharmaceutical Research*. doi.org/10.1007/s11095-018-2382-9.

2. Muddineti OS, Vanaparthi A, Rompicharla SVK, Kumari P, Ghosh, B, Biswas S. Cholesterol and vitamin -conjugated PEGylated polymeric micelles for efficient delivery and enhanced anticancer activity of curcumin: evaluation in 2D monolayers and 3D spheroids". *Artificial Cells Nanomedicine Biotechnology*. 2018, 9: 1-14.

3. Muddineti OS, Kumari P, Ray E, Ghosh B, Biswas S. Curcumin-loaded chitosan–cholesterol micelles: evaluation in monolayers and 3D cancer spheroid model. *Nanomedicine*. 2017 Jun 2(0).

4. Omkara Swami Muddineti, Preeti Kumari, Balaram Ghosh, Vladimir Torchilin, Swati Biswas. D-α-Tocopheryl succinate/phosphatidyl ethanolamine conjugated amphiphilic polymer based nano-micellar system for the efficient delivery of curcumin and to overcome multiple drug resistance in cancer. *ACS Applied Materials & Interfaces*. 2017.

5. Rompicharla SV, Trivedi P, Kumari P, Ghanta P, Ghosh B, Biswas S. Polymeric micelles of suberoylanilide hydroxamic acid to enhance the anticancer potential in vitro and in vivo. *Nanomedicine*. 2017 Jan;12(1):43-58.

6. Muddineti OS, Kumari P, Ajjarapu S, Lakhani PM, Bahl R, Ghosh B, Biswas S. Xanthan gum stabilized PEGylated gold nanoparticles for improved delivery of curcumin in cancer. *Nanotechnology*. 2016 Jun 27;27(32):325101.

7. Kumari P, Ghosh B, Biswas S. Nanocarriers for cancer-targeted drug delivery. *Journal of drug targeting*. 2016 Mar 15;24(3):179-91.

8. Biswas S, Kumari P, Lakhani PM, Ghosh B. Recent advances in polymeric micelles for anti-cancer drug delivery. *European Journal of Pharmaceutical Sciences*. 2016 Feb 15;83:184-202.

Papers accepted/presented in conference

From thesis

1. "Photosensitizer-loaded poly(ethylene glycol)-poly(d,l-lactic acid) polymeric micelles for effective photodynamic therapy" at Ramanbhai Foundation 8th International Symposium on Current Trends in Healthcare "Advances in New Drug Discovery And Development" from February 2-4, 2017, Ahmedabad, Gujarat.

2. “Cholesterol-Modified Polylactide-Based Micelle for Effective Delivery of Curcumin” at American 2016 AAPS Annual Meeting and Exposition from November 13-17, 2016, Colorado Convention Center, Denver, Colorado, USA.

3. “Development of transferrin functionalized poly(ethylene glycol)/poly(lactic acid) copolymeric micelles as a potential delivery system” at International Conference on Nanostructured Polymeric Materials and Polymer Nanocomposites (ICNPM 2015) from 13-15 November 2015, Kerala.

4. “Transferrin modified Poly(ethylene glycol)-poly(D,L-lactic acid) copolymeric micelles for targeted delivery of chemotherapeutics: Synthesis, characterization and *in vitro* evaluation” at 2015 AAPS Annual Meeting and Exposition from October 25-29, 2015 in Orlando, USA.

BIOGRAPHY OF PREETI KUMARI

Ms. Preeti Kumari completed her Bachelor of Pharmacy from Rajiv Gandhi University of Health sciences, Bangalore, Karnataka, India. She has been awarded INSPIRE fellowship by Department of Science and Technology (DST), India for a period of five years (2013-2018) to carry out her doctoral research work under the supervision of Dr. Swati Biswas. She has received international travel support grant from Indian Council of Medical Research (ICMR) to present her research work at various international conferences. She has published 10 scientific publications in well-renowned international journals and presented papers in various conferences.

BIOGRAPHY OF Dr. SWATI BISWAS

Dr. Swati Biswas is presently working as Associate Professor, in Department of Pharmacy, Birla Institute of Technology and Science, Pilani, Hyderabad Campus. She received her B. Pharm degree (1998) and M.Pharm (2000) from Jadavpur University, India. She was awarded her Ph.D. in Pharmaceutical Sciences in the year 2008 from Wayne State University, USA. After completion of doctoral studies, she pursued her postdoctoral studies in Northeastern State University, USA (2013). She has been involved in research for the last 15 years. She has to her credit more than 40 research publications, two US patents and two Indian Patents. She has authored 3 book chapters in "Dendrimers: Synthesis, Applications and Role in Nanotechnology", "Drug Delivery Strategies for Poorly Water-Soluble Drugs" and "Handbook of Polymers for Pharmaceutical technologies, Volume 2: Processing and Applications". She has successfully completed many sponsored projects and currently handling projects sponsored by DST, DBT and DST-LVPI. She has guided one Ph.D student and currently four students are pursuing their Ph.D. work.